

# Routes to Novel Colloidal Gels

THÈSE N° 5584 (2012)

PRÉSENTÉE LE 14 DECEMBRE 2012  
À LA FACULTÉ DES SCIENCES DE BASE  
GROUPE FOFFI  
PROGRAMME DOCTORAL EN PHYSIQUE

ÉCOLE POLYTECHNIQUE FÉDÉRALE DE LAUSANNE

POUR L'OBTENTION DU GRADE DE DOCTEUR ÈS SCIENCES

PAR

Francesco VARRATO

acceptée sur proposition du jury:

Prof. H. Rønnow, président du jury  
Prof. G. Foffi, directeur de thèse  
Prof. E. Del Gado, rapporteur  
Prof. C. Likos, rapporteur  
Prof. F. Stellacci, rapporteur



ÉCOLE POLYTECHNIQUE  
FÉDÉRALE DE LAUSANNE

Suisse  
2012



For that matter, physicists themselves go around  
transforming negative entropy into information,

said Brillouin.

From observations and measurements,  
the physicist derives scientific laws;

with these laws, people create machines

never seen in nature,

with the most improbable structures.

— *James Gleick*

Ai miei genitori.



# Acknowledgements

*Lausanne, 3 December 2012*

Above all, I would like to thank Prof. Giuseppe Foffi, who gave me the opportunity to do my research in his group and for his steady, patient and enriching supervision. I am grateful to Dr. Cristiano De Michele, who introduced me to this opportunity. Thank you also to professors Christos Likos, Francesco Stellacci and Emanuela Del Gado, for showing how science can be mixed (and not demixed) with enthusiasm and curiosity.

During these years of scientific and personal development, I have enjoyed the motivating discussions, the constructive criticisms, and the support of great colleagues and friends: Davide Fiocco, Nicolas Dorsaz and Maxim Belushkin. From each one of them I still have a lot to learn. Special thanks goes to M.me Noemi Porta, our secret hero. My work has been possible also thanks to the precious collaborations with Prof. Erika Eiser, Dr. Claudio Grimaldi, Biagio Nigro and Lorenzo Di Michele.

I want to thank Prof. Paolo De Los Rios for his prompt witticisms and his suggestions. I am also very grateful to Tamas Toth, Paolo Torrielli, Carlo Maffi and Lucio Floretta, for sharing deep thoughts as well as working spacetime, caffeine and music. Warm thanks to all my friends at the <sup>3</sup>tron and all over Europe. They constitute the proof that life exists beyond a computer screen.

To Chiara goes my loving gratitude, for being the wonderful person that she is (and for being that person at all times). Last but not least, I thank my parents, to whom I dedicate this thesis. They are always with me even when thousands of kilometers separate us.

E. V.



# Abstract

**ABSTRACT (ENG).** The thesis describes how demixing of binary colloidal mixtures could be used to design new kinds of amorphous structures. We show that a rich phase behavior emerges, dependent on density (colloidal concentration) and composition (species relative populations). A simple model is adopted for the colloidal particles, which are assumed to be hard spheres interacting via an effective short-ranged attractive square-well (SW) potential. We show that *demixing* - due to composition fluctuations - can strongly interfere with typically dominating *condensation* mechanism - due to density fluctuations, - if the inter-species attraction is significantly reduced with respect to intra-species one. Thermodynamic perturbation theory (TPT) calculations and extensive numerical simulations have been performed on binary mixtures of the SW model.

In the whole range of compositions and densities, we demonstrate how the enhancement of demixing over condensation brings to distinctive properties of the arrested structures. If the population of one colloidal species largely exceeds the other (asymmetric composition), the typical condensation mechanism dominates and brings to the percolation of only the main species. Instead, demixing separation prevails approaching the symmetric composition, and results in two interpenetrating sub-gels, both percolating. We name this structure a *BiGel*.

The formation of BiGels has been analyzed in the thesis, pointing out structural differences and similarities with the usual one-component gel. In particular, we implemented a novel method that enables an explicit topological characterization. Despite the sub-gel branches of a BiGel present longer and thinner arms, we quantified the resemblance of gels and BiGels at large length-scales in light of their congruent porosities.

Furthermore, we propose an experimental exploration of the dominant demixing scenario. The possibility is offered by the fine tuning of inter-species interactions that can be achieved in DNA-coated colloids (DNACCs). Thus, the numerical investigation is complemented with experiments on symmetric mixtures of DNACCs and the proof of BiGel's actual realization.

The main result of the thesis is the demonstration that, in presence of tunable inter-particle interactions, phase separation driven by the demixing mechanism can be arrested in the same fashion as condensation. We show how to enhance the demixing and demonstrate, by simulations and experiments, the possibility of multi-component gelation. Notably, complex structures result without requiring complex architectures of the single particles, nor anisotropic potentials, as isotropic spherical colloids already constitute suitable building blocks. Hence, the results and ideas here presented may find application in the design and development of novel types of materials.

## Acknowledgements

---

**RIASSUNTO (ITA).** La tesi descrive come il *demixing* di miscele colloidali binarie possono essere utilizzate per nuovi design di strutture amorfe. Mostriamo che un ricco comportamento di fase emerge, dipendente dalla densità (concentrazione di colloid) e dalla composizione (popolazioni relative delle specie). Adottiamo un semplice modello di sfere dure interagenti tramite un potenziale efficace, *square-well* (SW, buca rettangolare) ed attrattivo a corto raggio. Mostriamo che il demixing - dovuto alle fluttuazioni in composizione - può fortemente interferire con il meccanismo tipicamente dominante di *condensazione* - dovuto alle fluttuazioni di densità,- quando l'attrazione inter-specie è significativamente ridotta rispetto a quella intra-specie. Calcoli di Teoria di perturbazioni termodinamiche (TPT) e estensive simulazioni numeriche sono state eseguite per miscele binarie del modello SW.

Dimostriamo per una vasta gamma di composizioni e densità come il prevalere del demixing sulla condensazione porta a proprietà distintive delle strutture arrestate. Se la popolazione di una specie colloidale eccede largamente l'altra (composizione asimmetrica), allora il tipico meccanismo di condensazione domina e porta alla percolazione della specie principale. Il meccanismo di demixing invece prevale per una miscela più simmetrica, la cui aggregazione risulta in sotto-gel interpenetranti ed entrambi percolanti. Chiamiamo questo tipo di struttura un *BiGel*.

Nella tesi la formazione dei BiGel è stata analizzata, chiarendo le differenze e somiglianze strutturali con l'usuale gel mono-componente. In particolare, abbiamo implementato un nuovo strumento che permette l'esplicita caratterizzazione della loro topologia: nonostante le ramificazioni dei sotto-gel costituenti un BiGel presentino braccia più lunghe e fini, noi riusciamo a quantificare la somiglianza a larga scala dei gel e dei BiGel alla luce dei loro simili valori di porosità.

Proponiamo inoltre uno studio sperimentale nel caso in cui il demixing sia dominante: la possibilità ci è offerta dalle interazioni inter-specie regolabili realizzabili con colloid funzionalizzati in superficie con DNA (*DNA-coated colloids*, DNACCs). La trattazione numerica e teorica trova quindi complemento negli esperimenti svolti su miscele binarie di DNACCs e, conseguentemente, nell'evidenza fornita dalla concreta realizzazione del BiGel.

Il principale risultato della tesi consiste nella dimostrazione che, potendo regolare le interazioni fra particelle, il processo di separazione di fase dovuto a demixing può essere arrestato allo stesso modo che nel caso di condensazione. Mostriamo come far prevalere il demixing e dimostriamo, con simulazioni e sperimentalmente, la possibilità di ottenere gel di miscele multi-componente. Considerevole è anche la realizzazione di strutture complesse che non richiedono particelle con struttura di per sé complessa, né richiedono potenziali anisotropi: colloid sferici isotropi sono già elementi sufficienti. Di conseguenza, i risultati e le idee qui presentate possono sperabilmente apportare impulso nuovo allo sviluppo, design e applicazione di nuovi tipi di materiali.

**Keywords:** COLLOID, GEL, THERMODYNAMIC PERTURBATION THEORY, DEMIXING, BIGEL, PERCOLATION, TOPOLOGY, DNA-COATED COLLOID



# Contents

<b>Acknowledgements</b>	<b>v</b>
<b>Abstract (English/Italiano)</b>	<b>vii</b>
<b>Contents</b>	<b>x</b>
<b>1 Introduction.</b>	<b>1</b>
1.1 Thesis aim and layout. . . . .	9
1.1.1 Layout. . . . .	11
<b>2 Colloidal aggregation and gelation.</b>	<b>13</b>
2.1 Phenomenology. . . . .	14
2.1.1 Gelation as non-equilibrium process . . . . .	15
2.2 From colloid-polymer mixtures to the square-well model. . . . .	17
2.2.1 Computer models. . . . .	22
2.3 Observing aggregation. . . . .	27
2.3.1 Percolation. . . . .	27
2.3.2 Characteristic length. . . . .	32
<b>3 Demixing: simulations, theory and experiments.</b>	<b>43</b>
3.1 Model and Simulation Protocol . . . . .	43
3.1.1 Molecular Dynamics . . . . .	44
3.1.2 One to more components. . . . .	51
3.2 TPT and topology . . . . .	54
3.2.1 Condensation vs. Demixing. . . . .	54
3.2.2 Porosity. . . . .	59
<b>4 Results: BiGels from arrested demixing.</b>	<b>67</b>
4.1 BiGel: numerical simulations. . . . .	68
4.1.1 Dynamics and arrest. . . . .	69
4.1.2 Percolation as fingerprint. . . . .	72
4.1.3 Arrested Structure of the BiGel. . . . .	77
4.2 Bigel: experiments. . . . .	85
4.2.1 From model to lab. . . . .	85
4.2.2 The actual BiGel. . . . .	89

## Contents

---

<b>5 Ongoing developments and perspectives.</b>	<b>93</b>
5.1 Dynamics close to the arrest. . . . .	93
5.1.1 Microscopy intensity measurements for BiGel. . . . .	98
5.2 Perspectives. . . . .	100
<b>A Appendix: Conductivity enhancement from colloidal gelation.</b>	<b>105</b>
<b>B Appendix: Imaging with Confocal Microscopy.</b>	<b>113</b>
<b>C Appendix: Growth of random configurations of hard spheres.</b>	<b>117</b>
<b>D Appendix: Physical fractals of spheres.</b>	<b>121</b>
<b>E Appendix: Materials and experimental setup.</b>	<b>131</b>
<b>Bibliography</b>	<b>166</b>
<b>Curriculum Vitae</b>	<b>167</b>

# 1 Introduction.

**SIMPLE LIQUIDS.** The study of liquids and their properties have attracted and attract the attention of researchers from different scientific and industrial domains, for both the ubiquity of the processes involved and for the fascinating, underlying physics. The theories of statistical mechanics, are readily applicable to liquid systems. In the passage from a continuous, macroscopic description to a microscopic, local interpretation, liquids have been originally based on simple model entities, the “particles”. These are general, elementary building blocks of liquids. The definition of “liquid” itself intimately depends on the kinetics and the spacial configurations taken by a vast quantity of such building blocks.

Even at densities where their movement results as slow as in solids, still the structure can present non-crystalline features. A crystal can be considered as a spatially inhomogeneous fluid that is periodically modulated, while liquids are translationally invariant fluids, similarly to gases, but can still present short- and long-range correlations between the constituent particles. When very dilute systems of particles are considered, what differentiate a liquid from a gas is the impossibility for the particles to overcome the attractive forces that hold them together. Unlike gases, liquids cannot expand indefinitely if unconstrained.

When the particles composing a liquid are considered to be identical and interacting through a radially symmetric, pairwise additive potential  $V(|\vec{r}|)$  - for each particles pair at distance  $\vec{r}$  - then the kind of system under study is named<sup>1</sup> a “simple liquid”. Examples of simple liquids are water, ethanol or metallic glasses [Greer (1995); Banerjee et al. (2009)], and typical examples for the particle models are the hard sphere or the Lennard-Jones potentials [Hansen and McDonald (2006)].

**COLLOIDAL SOLUTIONS & SOFT MATTER.** The domain of liquids and of their constituents includes a large variety of systems, whose distinctive peculiarities have been rationalized into the unified view of *soft matter* [Gompper et al. (2008)]. The Fig. 1.1 depicts the continuum of materials, classified accordingly to the components characteristics and arranged in a triangle.

---

<sup>1</sup>Despite the long history and the apparently obvious definition, nowadays is still debated if such a definition for simple liquids is sufficient or if, instead, a more quantitative definition could or should be used [Ingebrigtsen et al. (2012)].

## Chapter 1. Introduction.

---

From left to the right, it describes their amphiphilicity, while from the top to the bottom it describes their elongation. Great relevance as a soft matter have dispersions of particles called *colloids*, at the bottom-left of the triangle. In the thesis we focus on these constituent particles.

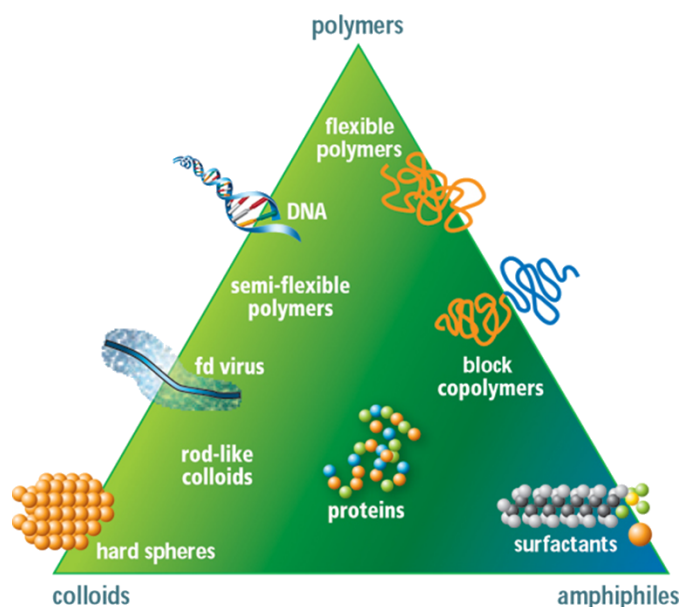


Figure 1.1: The main components of Soft Matter systems are shown arranged in a triangle, from [Gompper et al. (2008)]. This provides an ideally continuum of molecules and materials which fills the space between spherical colloids, flexible polymers, and surfactants.

For a large variety of applications, colloids can be described by means of spherical, isotropic, pairwise potentials: colloidal suspensions are then simple liquids. The term *colloidal* refers to a state of separation of matter and can be referred to a wide variety of materials. The IUPAC definition of colloidal particles reads in fact [Everett (1972)]: “*The term refers to a state of subdivision, implying that the molecules or polymolecular particles dispersed in a medium have at least in one direction a dimension roughly between 1 nm and  $\mu\text{m}$ , or that in a system discontinuities are found at distances of that order.*”

This classification includes an astonishingly vast number of systems, as illustrated in Tab.1.1. Among all these possible combinations, the colloidal solutions in which solid or semi-solid particles are suspended into a continuous liquid solvent, represent a fundamental case.

Besides their practical use, colloidal systems have been used as a model to test several theoretical predictions [Carpinetti and Giglio (1992); Poulin et al. (1999); Ramakrishnan et al. (2002); Anderson and Lekkerkerker (2002)]. In statistical mechanics, their use as benchmark has been fundamental, for example, to test the static and dynamical properties of the hard sphere model that, before the modern evolution of colloidal synthesis, may have been considered a toy model [Lancon et al. (1982); Pusey et al. (1989)].

As aggregates, colloids also represent a prototypical reference for soft matter. More than

Solute	Solvent	Notation	Technical name	Examples
Solid	Gas	S/G	Aerosol	Smoke
Liquid	Gas	L/G	Aerosol	Hairspray, mist, fog
Solid	Liquid	S/L	Dispersion or Sol	Printing ink, paint
Liquid	Liquid	L/L	Emulsion	Milk, mayonnaise
Gas	Liquid	G/L	Foam	Fire-extinguisher foam
Solid	Solid	S/S	Solid dispersion	Ruby glass, some alloys
Liquid	Solid	L/S	Solid emulsion	Road paving, ice cream
Gas	Solid	G/S	Solid foam	Insulating foam

Table 1.1: The various types of colloidal dispersions with some common examples (from [Hunter (1986)].)

from the specific nature of colloidal particles, the “softness” depends on their size. Following [Likos (2001)], the ratio of the elastic constants  $G$  (proportional to the critical shear stress) required to cleave a colloidal or an atomic crystal, is  $\frac{G_{\text{coll.}}}{G_{\text{atom.}}} \approx 10^{-12} \sim 10^{-3}$ . Their overall rigidity against mechanical deformations, orders of magnitude smaller than the atomic counterparts, mainly depend on  $G$  difference of the sizes. If  $\epsilon$  is the energy scale of the cohesive energy per particle, and  $a$  is the colloidal typical size, then the elastic constant can be written as  $G = \frac{1}{a^3} \epsilon V''(r = a; \{p\})$ , where the family of interaction potentials  $V(r = a; \{p\})$  depends on a set  $\{p\}$  of parameters. It is rather insensitive to  $\{p\}$  and so are the second derivatives  $V''$ . For atomic and colloidal systems, the energy scale  $\epsilon$  is about the same. For atomic systems, the energy scale  $\epsilon$  ranges from  $10^{-1}$  eV for the noble gases to 10 eV for the metals; for typical colloidal crystals, it ranges between  $k_B T$  and  $100 k_B T$ , the thermal energy. Since  $k_B T \cong 1/40$  eV at room temperature, colloids have  $a_{\text{coll.}} \cong 10^{-9} \sim 10^{-6}$  m, while for atoms it is  $a_{\text{atom.}} \cong 10^{-10}$  m. This argument, made for colloidal crystals, is reinforced when considering the very low densities that colloidal suspension can attain in other states.

**EFFECTIVE INTERACTIONS.** In reality, when for example a single water molecule or a single colloid are closely analyzed, they do not appear to have a structure as simple as the models. A large class of liquids exists which are mainly solutions (or suspensions) of solid particles much larger than atomic size, plus additional constituents (like polymeric coils or salt). Due to the constitutive richness and variety, such systems are called “complex fluids”. The knowledge of the microscopic description plays then a fundamental role. Despite this definition, complex fluids may be greatly simplified by adopting *effective interactions*. If only pair interactions between the large particles can be considered, then complex fluids may be rendered as simple liquids. When considering a sample of liquid at a certain scale, in space or in time, the possibility of reducing in complexity its constitutive particles relies on the possibility to retain the physical description that pertains to the scales considered.

The model colloidal systems represents a perfect example<sup>2</sup>. Mixtures of colloidal spheres in a

<sup>2</sup>Considering a spherical shape for the dispersed particles simplifies their study in terms of effective interactions, as in absence of internal degrees of freedom (for example magnetic or electric moments) the symmetry imposes a

## Chapter 1. Introduction.

---

polymeric solution, for instance, allow the definition of an effective (depletion) potential: as schematized in Fig. 1.2, the short polymer chains in solution can be modeled as little isotropic particles, and the degrees of freedom associated to these particles can be traced out [Likos (2001)]. Therefore, colloidal solutions and their model counterparts constitute an optimal playground for studying simple liquids. An example of model is the DeJaguin-Landau-Verwey-Overbeek (DLVO) potential

$$V_{\text{DLVO}}(r) = \begin{cases} \infty & \text{if } r < 2R \\ V_{\text{vdW}}(r) + V_C(r) & \text{if } r \geq 2R \end{cases},$$

where a hard core repulsion is summed to the attractive ( $V_{\text{vdW}}$ ) and repulsive ( $V_C$ ) contributions. The core radius  $R$  approximates the Born repulsion [Born (1962)], that forbids the overlaps between the colloids during the random collisions with the solvent molecules (constant Brownian motion with thermal energies of the order  $k_B T$ ). The van der Waals and the screened Coulombic interactions give an attractive and a repulsive terms,  $V_{\text{vdW}}(r)$  and  $V_C(r)$  respectively. The DLVO potential is shown in Fig. 1.2 (left). The hard core repulsion, rendered as an isotropic potential, constitutes the main reason why hard spheres are adopted as the reference model for the perturbative approaches used in soft matter.

Other commonly used models are the Asakura-Oosawa (AO) or the square-well (SW) potentials, where a colloid is described by an impenetrable, spherical core (hard sphere) plus an attractive well [Hansen and McDonald (1986); Likos (2001)]. Even if mapping complex fluids into simple liquids is not always possible<sup>3</sup>, these *coarse-grained* models constitute a powerful, indispensable tool on which not only theories can settle, but that also allow computer simulations. The first numerical simulations in the 1960s have proved their possibility to achieve the different configurations and phase transformations a liquid can attain, and have boosted the succeeding development of theories involving the crude, yet essential building blocks that define simple liquids. They also made the solution of approximate integral equations tractable, providing information about the structure of the liquids. What is more, by reason of the densities involved, perturbative approaches can be hardly applicable, but with computers they have become numerically tractable, as they are based on simple reference systems (non-interacting gas, hard spheres).

**AGGREGATION.** The phase transition of a liquid (into crystal or gas) can depend on macroscopic changes of quantities such as temperature  $T$  or density  $\phi$ . But the kinetics of the process, as for instance the speed at which  $T$  or  $\phi$  are altered, also has an important role and can bring to completely different results. Upon cooling, for example, if the temperature is lowered at enough high speed to suddenly subtract particles kinetic energy, crystallization can be avoided and particles maintain a disordered configuration proper of liquids. Unlike phase

---

dependence solely on the distance between particles.

<sup>3</sup>Polymers in solution, for example, can be considered as soft penetrable particles (with size given by their gyration radius) under certain conditions. Nonetheless, many applications admit as maximum simplification strings made up of “simple” monomers, held together by (possibly unbreakable) bonds. Even this can be an over-simplification if monomer’s structure strongly influences the description of the phenomenon.

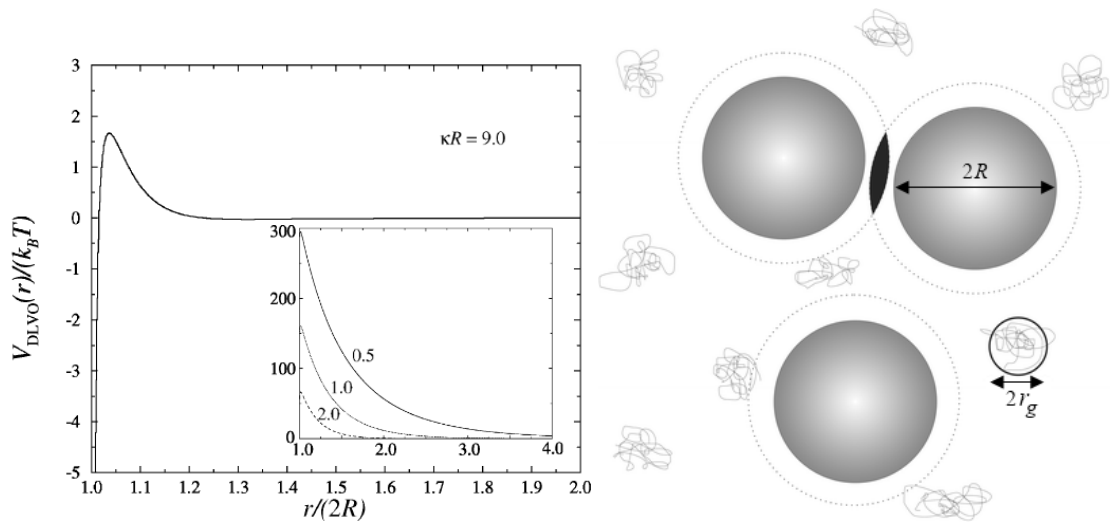


Figure 1.2: **(Left)** The sum of a hard core repulsion (for  $r/2R < 1$ ), the van der Waals attraction and the screened Coulomb repulsion for weak screening (adapted from [Likos (2001)]). The screening value is in terms of the radius times the inverse Debye length,  $\kappa = \lambda_D^{-1}$ . Inset: for high screening the electrostatic repulsion dominates over the vdW attraction. **(Right)** Schematic of colloidal spheres suspended in a polymer solution (adapted from [Mutch et al. (2007)]). The depletion layers surround the colloids - spheres of diameter  $2R$  - as indicated by dashed lines, and the excluded volume caused by overlapping layers - darkly shaded - indicates the depletion zone. The attraction range depends on the gyration radius  $r_g$  of the polymers in solution.

transitions, this *non-equilibrium* process brings frustration: macroscopic rearrangements cannot take place as a globally favorable configuration is prevented at advantage of local, more (energetically) favorable rearrangements. As the particles mobility slows down, a phase separation occurs that becomes arrested, with consequent coarsening processes responsible for the formation of a dense (solid-like) phase aggregate [Zaccarelli et al. (2004); Mattsson et al. (2009)]. We call the sudden arrest of the kinetics a *quench*. In the left panel of Figure 1.3, a schematic of the phase diagram  $(T, \phi)$  highlights the domains of the non-crystalline arrested liquids. A quench can be made not only by suddenly lowering  $T$ , but can also be triggered by means of other changes. The possible ways of quenching a system ultimately depend on the interaction potential of colloids and on external parameters<sup>4</sup>.

For keeping the colloidal suspension stable against the aggregation, some stabilization mechanisms can be put in place. Stabilization is difficult as there always exists the van der Waals attractive interaction  $V_{vdW}(r)$  between the particles<sup>5</sup>. Quantities such as density, temperature, solvent quality, etc., directly affect the Coulomb screening. Being sensitive to external

<sup>4</sup>In the phenomenological study of gels, open questions still remain. For example, whether gelation could occur coming from equilibrium states or not, or if, more generally, a unique scenario ranging from very diluted fluids up to glasses could incorporate a description of gels.

<sup>5</sup>This can be strongly suppressed by *index matching* the two materials, colloids and solvent. By setting the two optical refractive indexes like  $n_{coll.} \approx n_{solv.}$ , the Hamaker constant  $A \propto (n_{coll.} - n_{solv.})^2$  and in turn the attraction  $V_{vdW}(r) \propto A$  are suppressed. However, index matching is not always possible.

parameters, such mechanisms are used also in order to tune the interactions and thus to trigger or control the aggregation. A common method to enhance the aggregation works by adding salt in order to modify the characteristic length<sup>6</sup> of the screened Coulombic repulsion  $V_C(r)$ . For weak screening, the potential barrier is barely capable of keeping the particles apart: a further weakening would bring the system towards *irreversible aggregation*. Unlike the atomic systems, where the interactions are determined by the electronic structure, for colloidal suspensions changes in the “external” conditions (solvent quality, temperature, salt concentration, chemistry of the mixture) can involve dramatic changes in the effective interactions between the macromolecular aggregates. The colloidal density, for example, plays a crucial role in the resulting structure. A homogeneous glass emerges when the solute occupies more than 50% of the available volume, and presents an extremely large number of voids of sizes smaller than the typical colloidal size [Pham et al. (2002); Trappe and Sandkühler (2004); Mezzenga et al. (2005); Zaccarelli (2007)]. At lower densities, arrested states can occur due to pronounced heterogeneities: relatively coarse and non-uniform structures, in which the voids are larger than particle size. Short-ranged attractive colloidal systems, for example, can form crystals, two glasses of different origin, or gels.

Aggregation can be also induced for hard-sphere colloids by the presence of polymers in solution. The so-called *depletion mechanism*, carried out by adding non-adsorbing polymers, represents another example of externally controlled aggregation. A schematic colloid-polymer mixture is shown in Fig. 1.2 (right). The presence of polymer clumps in the region between two nearby particles is entropically disfavored, giving rise to an unbalanced osmotic pressure that pushes the two colloids together; this results in an attractive potential. The range and strength of this attraction are controlled by the size (molecular weight) and the concentration of polymers respectively. The aggregation of HS induced by *short-range attraction* is particularly important, as a reference model where microscopic details at the colloid scale can be neglected [Miller and Frenkel (2003)]. With just this simplification, it is possible to reproduce the rich phase behavior of colloidal suspensions of Fig. 1.3 (left). The disordered, arrested aggregates formed by quenching a colloidal solution represents the main argument of the thesis, the *colloidal gels* [Hurtado et al. (2007); Lu et al. (2008); Ronsin et al. (2009); Pineiro et al. (2009)].

**GELATION.** Gelation occurs when colloidal suspensions are driven to a state where strong inter-particle attraction dominates. When the depletion potential is deep enough, for example, non-equilibrium aggregation occurs, which can result in gelation<sup>7</sup>. The lowering in temperatures of a quench can be associated to an increase in attraction [Foffi et al. (2005b)] and the

---

<sup>6</sup>Additional counterions and coions form spontaneously into the mixture, resulting into an enhancing of the inverse Debye screening length  $\kappa^{-1} = \lambda_D = \sqrt{\epsilon_r \epsilon_0 k_B T / \sum_i n_i q_i}$  (where  $n_i$  is the mean concentration of charges of the species  $q_i$ ).

<sup>7</sup>Common examples of gels formed via depletion attraction are PMMA colloids with non-adsorbing polystyrene [Pusey et al. (1993); Poon et al. (1995)]. Systems with combined mechanisms of charge and steric tuning are also possible, like for example colloids coated with flexible chains which carry a net charge, such as gelatin [Ward and Courts (1977)] or polyelectrolytes [Pincus (1991)] or DNA [Seeman (2003); Valignat et al. (2005); Dreyfus et al. (2010); Rogers and Crocker (2011)].



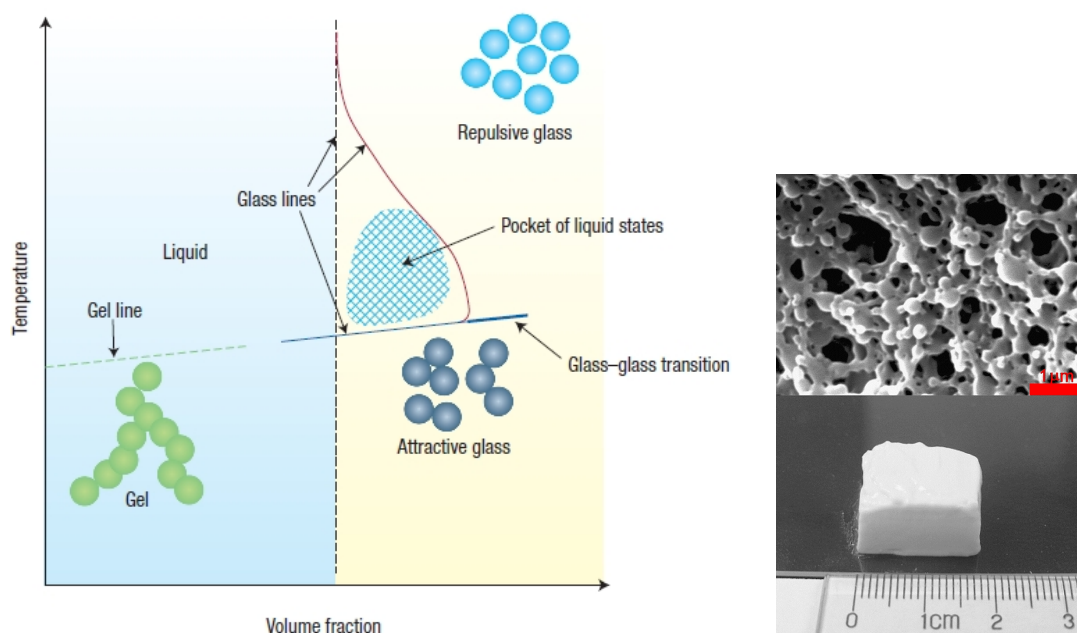


Figure 1.3: **(Left)** Temperature versus volume fraction schematic phase diagram, from [Sciortino (2002)]. The vertical black dashed line represents the hard-sphere glass line (for short-range attractive colloids the re-entrant, non-monotonic glass line - solid red and blue lines - creates a pocket of liquid states, stabilized by the short-range attraction). A lowering in temperatures is associated to an increase in attraction, from [Foffi et al. (2005b)]. **(Left)** Scanning electron micrographs of a colloidal gel (scale bar =  $1\mu m$ ) and relative macroscopic formation, from [Wang et al. (2010)].

resulting non-equilibrium mechanism of *arrested phase separation* represents the main route to colloidal gelation. At equilibrium the system in the same state point would separate in two liquids of different density so to minimize the total free energy, but in reality the bonding time among particles stretches and this causes the dynamical slowing down of the rearrangements. Fluctuations in density are arrested after an initial transient and this results in ramified amorphous structures instead of two completely separate phases [Gado et al. (2004)]. As soon as a space-spanning, percolating structure emerges that is capable of sustaining mechanical stress, a gel is observed<sup>8</sup>. It has only recently been understood the universality of colloidal gelation mechanism arising as a consequence of a dynamic arrested that interferes with phase separation [Manley et al. (2005); Foffi et al. (2005b,a); Lu et al. (2008)], and it has been observed experimentally in colloidal and protein systems [Cipelletti and Ramos (2005); Poon (2002); Cardinaux et al. (2007); Lu et al. (2008)] and by computer simulations [Soga et al. (1998); Foffi et al. (2005b); Del Gado (2010)].

Found at densities typically lower than a glass, gels are liquids rapidly frozen out of equilibrium that become unable to flow, if not over large time scales. Indeed, what characterizes a gel (or

<sup>8</sup>Examples of gels are silica aerogels [Hasmy et al. (1994)]; silica particles coated with stearyl alcohol or proteins suspensions (like lysozymes) induced to aggregate by cooling [Verduin and Dhont (1995); Piazza (1999)]; percolative networks of proteins aggregated through filaments (as for actin).

a glass) is the arrest of the kinetics<sup>9</sup>. An example of colloidal gel is shown in Fig. 1.3 (right). Colloidal gels play a fundamental role in the soft matter context [Segré et al. (2001); Trappe and Sandkühler (2004)]. When structural heterogeneities are pronounced and the arrested amorphous state occurs, we are dealing with a *gel*. Obtained by colloidal solutions, they display elastic properties close to those of solid, but possess an amorphous ramified structure that spans space. Colloidal gels find applications in synthetic porous materials [Duguet et al. (2011); Lo Verso et al. (2006)], functionalization of surfaces and films production [Miljanic et al. (2008); Wang et al. (2008)], ceramics processing [Schenker et al. (2008); Wyss et al. (2005)], protein assemblies [Cardinaux et al. (2007); van Gruijthuijsen et al. (2012)], food science [Dickinson (1992); Bergholtz et al. (2003); Mezzenga et al. (2005); Gibaud et al. (2012)] and soft matter [Zaccarelli (2007); Dorsaz et al. (2011)].

In the context of amorphous aggregation, if an attractive selectivity exists among distinct colloidal particles such that they can be identified in “species”, then a *demixing* mechanism can affect the gelation and lead to amorphous structures with different properties. We will describe how both fluctuations in the total density  $\phi$  and in the relative composition  $c$  of the species drive the thermodynamic instability leading to phase separation but, depending on whether the two phases differ more in  $\phi$  or  $c$ , the aggregation brings to *condensation* (usual gelation) or demixing, respectively. The demixing brings each species to aggregate separately from the others, with consequent segregation. The nature of the gel obtained by a 2-component mixture does not allow, *a priori*, a simple liquid description, but brings to an intrinsically irreducible complex fluid. Complexity arises in this case from the distinction between inter-species and intra-species interactions, even if the potential is radially symmetric and pairwise additive. Thus, complexity can be obtained - as we will show - even in the arrested structure of these simple constituents.

**TUNABILITY.** In recent years the research on liquids, also thanks to the use of model particles in computer simulations, has given birth to a fruitful branch: the *self-assembly*. Most of the works in the domain of self-assembly point to the use of building blocks (ranging from nano- to micrometers) with non-spherical shapes or directional, anisotropic potentials (and often mixtures of these features), that cannot be reduced to simple particles. An important feature of self-assembly is in that the aggregation relies on weak inter-particle interactions (hydrogen bonds, van der Waals force, etc.), as for instance the hydrogen bonds, the Van der Waals force, etc., and not on strong interactions (covalent, metallic, etc.). The main goal is to obtain structures that show prefixed local arrangements of the constitutive particles from which a macroscopic structure arises that is functional to outperform in certain tasks, depending on the specific purpose. Generally, in the self-assembly process the components are initially put in a disordered configuration and then organize into specific structures, according to a desired pattern, without the influence of any external forces. Among the abundance of possible solutions, the specific binding capacity of DNA results particularly promising, in view

---

<sup>9</sup>Though different microscopic mechanisms can contribute to the formation of such macroscopically disordered structures, the models and techniques used in studying glasses and gels are often similar, if not the same.

of the realization of structures with peculiar geometries. In this context, DNA-coated colloids have also assumed great importance [Alivisatos et al. (1996); Mirkin et al. (1996); Seeman (2003); Valignat et al. (2005); Biancaniello et al. (2005); Dreyfus et al. (2010); Geerts and Eiser (2010); Rogers and Crocker (2011)]. Understanding and, ultimately, controlling the properties of amorphous materials is one of the key goals of material science. The properties of a material depend on the interactions among its building blocks and by the conditions in which they are prepared. It is by tuning these two properties that different structures can be obtained. As more than one components are implied, their relative population - the composition  $c$  - offers a suitable macroscopic tuning parameter. According to the Gibbs phase rule, in a binary mixture a two-phase region has two degrees of freedom. For colloidal systems, a good choice is the composition  $c = N_X/N$  of a reference species  $X$  with respect to the total population and the total packing fraction  $\phi$ . It would be highly beneficial to devise new ways of tuning the properties of the gels exploring novel interactions scheme between the constituent particles, where the processes that bring to the gel formation can hopefully be controlled operating on macroscopic observables as well as on simple fluid constituents. In the last years, a number of efforts in depicting more complex particles emerged [Yethiraj and van Blaaderen (2003); De Michele et al. (2006); Bianchi et al. (2006)] and new experimental processes are used in order to obtain more complex gels formed by different species of colloidal particles.

### 1.1 Thesis aim and layout.

**AIM.** In this thesis we explore the possibility of having a macroscopic parameter that grants the tuning of some specific properties of the final, aggregated structure, but without intrinsically complex particles. Instead of particular shapes or anisotropic inter-particle potentials, we use colloids of the same size with isotropic SW potential, the building blocks typical of simple liquids. For such a simple model colloid, inter-species and intra-species interactions can be distinguished. The selectivity between species is introduced to obtain a tuning parameter. For single-species monodisperse systems, the density is a main control parameter in the aggregation process. Varying inter-species interactions, then, multicomponent mixtures of colloids offer a way to form a completely new class of materials. Once the demixing effect is enhanced due to the interaction selectivity, we aim to qualitatively and quantitatively prove that different final gels can be obtained whose demixed structure depends on  $c$  (the composition of the two species). We choose this route because this represents the simplest system where composition fluctuations may be enhanced, with consequent demixing. When the inter-species attraction is reduced, the system has a strong tendency to demix.

The arrested phase separation scenario for one-component mixtures (1CM) can be envisaged for mixtures made of two or more components. Already in the case of a two-component mixture (2CM) there is a fundamental increase in complexity. The thermodynamic instabilities are expected to be driven by both density ( $\phi$ ) and composition ( $c$ ) fluctuations, that bring to condensation and demixing, respectively. We aim to show that the theoretical framework of

arrested phase separation holds: we use its extension from the 1CM classical gelation case, to a 2CM gelation and **we address the question of whether it is possible to arrest composition fluctuations (demixing) in a manner similar to the arrest of density fluctuations in 1CM (condensation).**

**REALIZATION.** The variation from simple to complex fluids embeds new physics, as well as the possibility of phenomenological comprehension and design of new materials. The acquisition of expertise in the modeling of such systems and in their analysis are - at the same time - the target and the tools that are developed here. Clearly the number of parameters involved grows with the tunability that one desires to achieve, so computer simulations are ideal for such an exploration. We use the Thermodynamic Perturbation Theory to explore the phase diagram of the 2CM systems. Molecular dynamics simulations with model colloids are used to actually obtain the 2-component gels. In the symmetric case of two components of equal composition, we name the resulting structure a *BiGel*. What we propose is completely different from stabilizing the phase separation in binary liquids (what has been called a *bijel*) through freezing of the positions of colloids at the liquids' interface [Herzig (2008)]. In fact, we propose instead that the colloids themselves would form a *bicontinuous structure* and, more importantly, we do not limit ourselves to the stabilization of the phase separation process but we show that the arrest of phase separation can be generalized and experimentally used by means of tunable interactions among the constituents.

Because of the challenge offered by the study of structural properties for amorphous systems, some new analysis tools (conductivity, porosity, topology) as well as the experimental realization have been developed within the research group and together with external collaborators. The 2CM gelation is studied theoretically, but also experimentally. DNA-coated colloids (DNACCs) nowadays offer the essential features for implementing the interaction selectivity: we use DNACCs for testing experimentally the realization of gelation through demixing. As DNACCs, we used polystyrene hard spherical colloids coated with DNA single strands<sup>10</sup>, which are specifically functionalized to attain the interaction selectivity we ask for. The size of the colloidal particles, which is of the same order of magnitude as the wavelength of visible light, opens up the possibility of performing direct observation of the particles in real space: in particular we use confocal microscopy<sup>11</sup>. BiGels have been actually observed, for the first time ever, thanks to state-of-art experiments (in collaboration with the research group of Erika Eiser, Cavendish Laboratories, Cambridge, U.K.) and we will provide their description, as they represent the proof of concept of BiGel formation driven by demixing.

**SUMMARY.** We present a novel gelation mechanism through arrested demixing in colloidal

---

<sup>10</sup>This kind of system embeds combined mechanisms of charge plus steric tuning [Seeman (2003); Valignat et al. (2005); Dreyfus et al. (2010); Rogers and Crocker (2011)].

<sup>11</sup>Colloids of distinct species are labeled with distinct photosensitive dye. Light scattering is commonly used to probe static and dynamical behavior of colloidal suspensions. Instead, the complementary approach of direct imaging is used, which works instead in wavevector space [Dhont (1996a)], is used instead.

mixtures, implemented by tuning of inter-species attractions. This leads to the formation of a yet unexplored class of materials. Employing a computer model, and through demanding numerical simulations, we investigate the gelation dynamics and the structural properties. We point out similarities and differences between the binary system and its well-known monodisperse counterpart (gel). We also show how the interplay of fluctuations in different variables can bring to different arrested structures. Thanks to a new analysis tool we developed, we can report analysis about the geometrical and the topological properties of BiGels. The computational tools and new analysis techniques open the doors to the characterization of amorphous systems also in the experimental realm (as post-processes) in addition to the computational one. We support our findings with experiments, in the case where 2-components are present in the same concentration. The BiGel formation constitutes the proof for the generalization of arrested phase separation mechanism.

### 1.1.1 Layout.

In the following Chapter 2, we portrait an introduction to the gelation phenomenon and its observation. Specifically, we will treat the phenomenology of the aggregation for one-component colloidal systems and will explain the passage to the coarse-grained model particles, inserting it into the context of numerical simulation (Par. 2.1). In the same chapter, some observables for investigating the gelation are described in more detail (Par. 2.3). After a focus on the informations carried by means of the static structure factor, we will briefly introduce the characterization method of the percolation. This will be put in connection, respectively, with the concepts of percolation and porosity.

In Chapt. 3 the model used for theoretical calculations, simulations and experiments is discussed. In particular, we will start with the adoption of the square-well model and will explain its main features. The consequent modification to a multi-component colloidal system is then elucidated (Par. 3.1.1). This model and its 2-component counterpart will be employed in the theoretical calculations used for drawing the demixing behavior under arrested phase separation (Par. 3.2.1). At the end of the chapter, we introduce a method of study for topology that we extensively adopt for the characterization of arrested amorphous structures.

These techniques and ideas are at the basis of the results, presented in the next Chapt. 4. Here the numerical and the experimental outputs are explored and analyzed. The chapter includes the analysis from numerical simulations, with a comparison between this new gel family with the known one-component counterpart. From the dynamical properties (Par. 4.1) the focus will be moved to the structural properties of the final arrested structures (Par. 4.1.3). This analysis is conducted, among other tools, by means of both the structure factor and the topology. After that, we will show how the BiGel is actually obtained in the experimental colloidal system (Par. 4.2), hence demonstrating the validity of the used protocol for enhancing the demixing. The passage to the experiments, where enhanced demixing is expected, is depicted.

In the conclusive Chapt. 5, we will discuss the impact of the physics embedded in the Bigels in the frame of new materials and their possible uses. We trace the first distinctive features of multi-component gels from the experimental point of view. The introduced analysis tools are

## Chapter 1. Introduction.

---

also discussed, together with their applicability to systems other than colloidal gels. Finally, conclusions are thus traced about the concepts of structure tunability and the generalized mechanism of arrested fluctuations.

**RELATED WORKS.** As a complement to the principal subject, in appendix we discuss two further projects developed during the thesis:

- in Appendix A, we describe how the gelation can be used to obtain structures that, even for low content of colloidal particles, can feature high electrical conductivity;
- in Appendix D, an analytical treatment is reported and proved to account for the finite-size effects in fractal (Apollonian) packings of  $d$ -dimensional spheres.

## 2 Colloidal aggregation and gelation.

**OUTLOOK.** In this chapter we provide an overview on the phenomenon of gelation, together with the introduction of some methods used for its characterization. The focus is on monodisperse systems, but all the concepts here introduced will be used for multi-component systems in the next chapters.

Two main sections compose the chapter. In first place, the phenomenology of gelation will be treated in its general aspects (Par. 2.1): the notion of *non-equilibrium* and the description of the phase diagram are followed by the presentation of the short-ranged attractive colloids. We will then explain the passage to the *square-well* (SW) model (Par. 2.2) along with its introduction into the field of *numerical simulations* (Par. 2.2.1).

The investigation conducted within this thesis is mainly carried out through simulations, but we present some observation measurements that are usually performed on gels also experimentally (Par. 2.3). In particular, we will introduce the concept of *percolation* and its meaning for gelation (Par. 2.3.1). The percolation concept is also the basic ingredient of a study we made on monodisperse gels of SW particles, that is put in Appendix A. For the study of the multi-component gelation, however, we focus on other two measurements (among others). The first quantity we studied is the *static structure factor* (Par. 2.3.2). The scattering of light is a common investigation probe and the structure factor constitutes a prototypical measurement in soft matter. This quantity can be studied also for particle systems generated by means of numerical simulations, so making its use fully valuable<sup>1</sup>. The second quantity provides a characterization regarding both the overall structure, as the *porosity*, and local features, like the thickness of the gel's arms. As it is a new method that we implemented, this will be introduced in the next chapter 3.

---

<sup>1</sup>On the other hand, nowadays the reverse is also true: analysis methods applied on numerically generated configurations of particles can be adopted to explore real world data.

## 2.1 Phenomenology.

According to the IUPAC definition of colloidal particles [Everett (1972)], a colloidal dispersion is a system in which particles of nanometer to micron size, of any nature, are dispersed in a continuous phase (a solvent) of different composition. Soft matter systems can contain other unities in solution, such as short polymeric chains, salt dissociated into ions, etc., smaller than the colloidal particles (the solute). Both the solute and the solvent can be in any of the three states of matter, thus giving rise to a large variety of colloidal dispersions. See Tab.1.1. The solute can be either of solid particles as, for example, polystyrene, polymethylmethacrylate (PMMA) or silica spheres, or complex objects such as polymer chains. Also anisotropic (non spherical) particles, as clays or globular protein solutions, can be treated as colloidal systems<sup>2</sup>. In the following, we do not explicitly treat the solvent, whose effect is only implicitly assumed: this brings to a complete lack of hydrodynamical effects, assuming to be in conditions where they do not play an important role in the gelation process [Furukawa and Tanaka (2010); Whitmer and Luijten (2011); Cao et al. (2012)]. In suspensions of colloidal attractive particles (because of depletion or some other effect discussed in the previous chapter), a structural arrest is observed under quench: the *colloidal gelation* [Segré et al. (2001); Dinsmore and Weitz (2002)]. Before describing the gelation process, we show in Fig. 2.1 a sequence of configurations depicting the aggregation of spherical colloids with short-ranged attraction (that we obtained from MD simulation), in order to familiarize with the morphology of such materials.

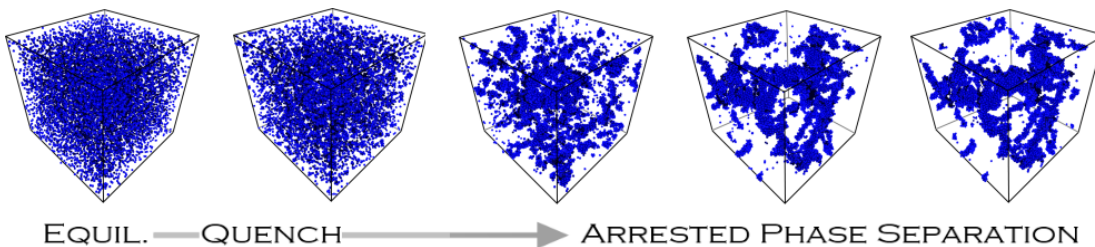


Figure 2.1: An example of aggregation for the short-ranged SW model (introduced in in Par. 2.2), at occupied volume fraction (density)  $\phi = 0.03125$ . These pictures are 3D renderings capturing the system before the aggregation (equil.), during the quench and, finally, at its arrested state.

The slowing down of dynamics, that is triggered by the quench (and starting from the equilibrium phase, like in Fig. 2.1), is associated to the formation of long-living structures bringing a change in viscoelastic properties. Colloidal systems present a complex phase diagram [Mallamace et al. (2000); Segré et al. (2001); Trappe et al. (2001)] that may be described using, as parameters, the occupied volume fraction  $\phi$  and the inverse of attraction energy  $(U/k_B T)^{-1}$ , where  $U$  is the total potential energy of the system. In Fig. 1.3 the attraction vs. density behavior (phase diagram) is divided in regions correspondent to the parameters pertaining to

<sup>2</sup>This diversity gives access to a lot of important properties related, for example, to the phase diagram [Dorsaz et al. (2008)] and to the nucleation of crystals [Ruzicka et al. (2011); Cardinaux et al. (2007)].



different kind of materials.

At high occupied volume fraction (concentration), the colloids become crowded leaving pores with sizes typically smaller than a colloidal diameter, and a glassy dynamics establishes: the system behaves as an attractive glass [Donth (2001); Sciortino (2002)]. At higher temperature, instead, it is  $(U/k_B T)^{-1} \gg 1$  and the inter-particle attraction does not affect significantly the dynamics: the system behaves as a repulsive glass. In glasses, particles are trapped into cages made of neighboring particles and the dynamics is characterized by two times: the first one is the typical time of diffusion inside the cage, whereas the second one is the typical time for the cage to break and for particles to diffuse outside it.

At low volume fraction and high strength of attraction, instead, the system behaves as a gel. The nature of bonds generally determines a subdivision of gels in two categories: *strong* (chemical) gels and *weak* (physical) gels. Chemical gels, that can be produced by a rapid quench or by light irradiation, are obtained when covalent bonds form. These bonds cannot break anymore and gel phase remains stable against a raise in temperature. In physical gels, weak bonds form (like for example hydrogen bonds, or due to effective interactions, as the depletion attraction) which are reversible: the sol phase can be recovered by increasing the temperature. The physical gels behave like liquids on sufficiently long time-scales. The fluctuations due to thermal energy can act, in this case, by continuously forming and breaking such bonds, so that - as opposed to chemical gels - no real transitions are observed from the viscous regime to the elastic one. See Par. 2.3 for more details. According to this terminology, the gels we are mostly going to deal with are weak gels, as we will consider reversible bonding. Nonetheless, for quenches inducing strong inter-particle attraction, the bonds may be considered as permanent compared to observation time-scales.

For colloidal suspensions at low volume fractions and strong attraction between particles, the kinetics of the gelation process may be characterized by diffusion and aggregation: particles in solution diffuse until they touch and react getting bonded [Witten and Sander (1981); Jullien and Kolb (1984); Brown and Ball (1985)]. As particles stick together to become clusters, the clusters themselves continue to diffuse, collide and aggregate. This diffusion and aggregation kinetics may be different passing from a system to another. Nevertheless two limiting regimes of kinetics have been identified: rapid, diffusion-limited cluster aggregation (DLCA) and slow, reaction-limited aggregation (RLCA). Each regime exhibits distinct behaviors, characterized by a different morphology of the clusters, different cluster mass distribution, and different kinetics of aggregation. Some basic features of the DLCA model are illustrated in Par. 2.2.1. It is worth to notice that this behavior does not depend on the detailed nature of the colloid, provided that the essential physical interactions are the same (as, for instance, inter-particle attraction within a finite range).

### 2.1.1 Gelation as non-equilibrium process

The phase transition that brings to crystallization has been a long studied problem. The nucleation and growth mechanism is predicted from the classic theory to occur when for a large enough radius the (favorable) volume term starts to dominate on the (unfavorable)

## Chapter 2. Colloidal aggregation and gelation.

---

surface term in the free energy expression

$$\Delta G = \rho V \Delta \mu + \gamma S . \quad (2.1)$$

Here  $V$  and  $S$  are the volume and the surface, respectively, of a nucleus forming in bulk liquid with density  $\rho$ , with surface free energy  $\gamma$  and with a chemical potential difference  $\Delta\mu$  between the solid and the liquid. But differently from a purely hard-sphere system, where only crystal and fluid phases are present (Fig. 2.2a, top), the introduction of attractions determines a three-phase equilibria picture (Fig. 2.2b, top). When the attractions are short-ranged, the gas-liquid (or fluid-fluid) equilibrium becomes metastable (Fig. 2.2c, top), as in protein systems.

Transitions involving three-phase equilibria, or metastable states, can be produced in colloidal systems with the addition of polymers in solution (see later for the “depletion interaction”), in order to widen the region where phase separation is expected. Such systems may show a frustrating behavior: depending on the initial conditions (as, for example, polymers concentration and colloid volume fraction), colloidal systems can form gel-like phases instead of crystals. Under aggregation, in fact, spherical colloidal particles develop mesoscopic structures on length-scales ranging from few to tens of diameters, and the aggregation proceeds to the formation of a space-spanning network (a gel). This state of ramified space-filling gel, whether experimental or simulated, is not that of equilibrium: gelation is a form of *non-equilibrium* behavior. An example of the metastable phase diagram’s region for a colloidal suspension is shown in Fig. 2.2 (bottom). Here a gas-liquid binodal (or coexistence) curve and spinodal lines are indicated, which define the aggregation in such a region.

Under quench, the mechanism of arrested phase separation can have place. The binodal denotes the condition at which two distinct phases may coexist, i.e. state points of minimum-energy equilibrium states of the system. Entering the spinodal curve (unstable region), fluctuations in density lead to instability of the solution, which phase separates and decomposes into multiple phases<sup>3</sup>. If the system is taken into the metastable region between the binodal and spinodal lines<sup>4</sup>, the free energy change upon formation of a small concentration fluctuation is only negative once the concentration fluctuations have formed a nucleus with a critical size. Below this size, incipient droplets will re-dissolve. Above this size they will grow and a phase-separated morphology will emerge with formation of compact clusters, via the mechanism of nucleation and growth. The formation of separate regions is favored by the negative change in free energy (due to concentration fluctuations) into the spinodal region: this phenomenon is called spinodal decomposition, that brings to open, stringy structures [Butler and Heppenstall-Butler (2003)]. The different mechanisms result then in different morphologies, as shown in Fig. 2.2 (bottom).

---

<sup>3</sup>The occurrence or lack of the spinodal decomposition could depend, in principle, on the particular way the spinodal curve is crossed entering the metastability region (as, for instance, different quenching rapidity). However, it has been confirmed both by simulations and experiments that, apart for a change in the period of latency before the settling of fluctuations becomes noticeable, the mechanism of spinodal decomposition always takes place once the spinodal line is trespassed.

<sup>4</sup>If an extreme in temperature is present, known as the *critical point*, then it coincides for the binodal and the spinodal curves.

## 2.2. From colloid-polymer mixtures to the square-well model.

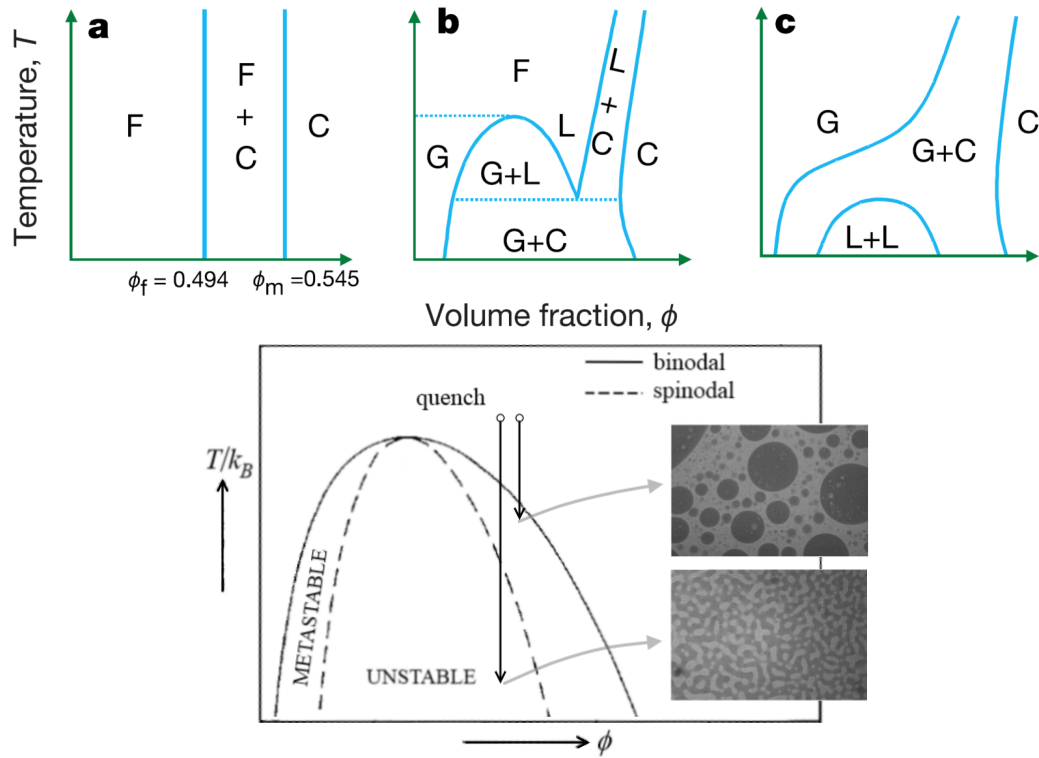


Figure 2.2: **(Top)** Different schematic phase diagrams (from [Anderson and Lekkerkerker (2002)]) for pure hard-spheres system **(a)**, with only fluid (F) and crystal (C) phases; hard-spheres with long-range attractions **(b)**, where also a gas (G) phase is present, and the case with short-range attractions **(c)**, where L-L transition becomes metastable. **(Bottom)** Schematic of the L-L region for colloidal dispersion (adapted from [Rouw et al. (1989)]). The line that separates the coexistence region from the phase-separated region is the *binodal*. This is further sub-divided by the *spinodal* line (unstable region): the system spontaneously favors spinodal decomposition. Indicated are possible quenches. Two images, obtained from confocal laser scanning microscopy on gelatin mixtures show the different phase-separated morphologies [Butler and Heppenstall-Butler (2003)]: random, polydisperse droplets (nucleation and growth mechanism) and a bicontinuous morphology (spinodal decomposition).

## 2.2 From colloid-polymer mixtures to the square-well model.

**DEPLETION INTERACTION.** In the instability scenario of spinodal decomposition, local density fluctuations set in, and this compromises the heterogeneity of the system. By arresting the fluctuations, an amorphous structure emerges as a result of a coarsening process<sup>5</sup>. By now, we are dealing only with local differences (fluctuations) in density which arrest because of the slowing down of the dynamics. This mechanism, responsible for the aggregation towards a gel structure, will be explained and expanded in Par. 3.2.1. In the next chapter we will use and

<sup>5</sup>It is discussed if such a mechanism could also provide a gelation-like description for materials typically formed at higher density. In particular, it is debated whether dynamical heterogeneities, occurring in glass and jamming transitions, may play the same role as the critical fluctuations in ordinary spinodal decomposition [Coniglio et al. (2008)].

generalize the idea of arresting such fluctuations.

Different phenomena can make the system enter the spinodal region, with consequent decomposition and structuration: examples are the cooling (temperature driven), the sedimentation (density change), the screening of Coulomb repulsion (van der Waals attraction produces G-L separation [Schroeder (1999)]), or the addition of non-adsorbing depletants (change of colloidal attraction) [Allain et al. (1995); Wu et al. (2003); Carpineti and Giglio (1992); Bibette et al. (1992)]. We briefly review here this latter example, whose major interest depends on the controllable attraction that can be induced among the colloidal particles by the addition of a non-adsorbing polymer [Asakura and Oosawa (1954); Vrij (1976); Poon (1998); Verhaegh et al. (1999)]. Adding non-adsorbing polymers to a hard-sphere colloidal suspension results in an attractive force which produces a similar gas/liquid phase transition<sup>6</sup>: colloid-polymer mixtures can in fact phase separate into coexisting colloid-rich and colloid-poor phases [Ilett et al. (1995)]. The colloid-rich phase is either crystalline or fluid in nature [de Hoog et al. (2001)], depending on the depth and range of the attractive potential, while the colloid-poor domain is always fluid<sup>7</sup>. Lubricating oils and paint are common examples of colloid-polymer mixtures in which phase stability is desired.

The non-adsorbing polymer molecules are expelled from the region between two colloidal particles when their surface separation becomes smaller than the size of the polymer chains [Asakura and Oosawa (1954); Vrij (1976)]. In Fig. 1.2 (right) the colloid-polymer mixture is represented. The exclusion of polymers from the space between the colloidal particles, leads to an unbalanced osmotic pressure difference, which pushes the colloidal particles together. This results in an effective attraction between the two colloidal particles: the *depletion attraction*. In a mixture of colloids and non-adsorbing polymers, then, the depletion effect between the colloidal particles can be expressed in terms of an effective potential  $U(r)$  [Likos (2001)], that is essential for modeling real materials. It corresponds to the work required to bring two colloidal particles from infinity to a distance  $r$  in a given polymer solution [Asakura and Oosawa (1954); Vrij (1976)]. If the attraction is large enough, phase separation can occur in the colloid-polymer mixture [Gast et al. (1983); Lekkerkerker et al. (1992)]. In the absence of polymers ( $U = 0$ ), instead a dilute suspension of hard-sphere particles does not aggregate (colloidal fluid). When the  $U$  is increased (for example, to approximately  $5 k_B T$  in the case of PMMA colloidal suspensions) by the addition of polymer, the particles aggregate and form the weak solid, random structure of a gel.

The depletion potential can be controlled by means of both the size and concentration of

---

<sup>6</sup>A clear distinction exists between polymers adsorbed on the colloidal surfaces and those free in solution. The two situations lead to qualitatively different effects. In the adsorption case, the polymer chains, in a good solvent, resist the approach of other surfaces through a loss of conformational entropy. Colloidal surfaces are then maintained at separations large enough to damp any attractive (London-van der Waals) force and the colloidal suspension results stabilized [Napper (1983); Carvalho et al. (1993)].

<sup>7</sup>Structural studies of transient colloid-polymer gels reveal gravitational settling for moderate colloid volume fractions  $\phi$ . By increasing polymer concentration, these gels exhibit periods of latency before settling becomes noticeable [Pusey et al. (1993); Grant and Russel (1993); Verhaegh et al. (1999)]. At the cessation of this rapid settling, the sediment retains a slightly ramified structure. Then sediment slowly compactifies approaching random close packing (or partially crystallizing) to  $\phi \gtrsim 0.6$ : the transient gel results to be a long-lived metastable state *en route* to thermal equilibrium. The latency period sharply increases with both polymer concentration and  $\phi$ .

## 2.2. From colloid-polymer mixtures to the square-well model.

polymers. The spatial range of attraction in fact is approximately twice the polymer's typical size, i.e. the radius of gyration  $r_g$ . This interaction develops an attractive well  $U_{\text{dep}}$  which acts between colloids in a range  $\Delta = 2r_g$ . For the simple case of colloidal hard spheres with diameter  $D = 2R$ , the potential between two particles is given by:

$$\frac{U}{k_B T} = \begin{cases} +\infty & \text{if } r < D \\ U_{\text{dep}} = -\Pi_p V_{\text{overlap}} & \text{if } D < r < D + \Delta \\ 0 & \text{if } r > D + \Delta \end{cases} \quad (2.2)$$

$\Pi_p$  is the osmotic pressure of the polymers and  $V_{\text{overlap}}$  is the volume of the overlapping depletion zones<sup>8</sup> between two particles at center-to-center separation  $r$ . A schematic of the depletion potential and of the resulting phase diagram are shown in Fig. 2.3. As approaching makes the “excluded volumes” overlap, the total volume available to the polymers increases, thus increasing their entropy (at the expense of some colloidal entropy). Partition is predicted by statistical mechanics into colloid-rich and polymer rich phases. The topology of the phase diagram strongly reflects the dependence on the relative range  $\xi = \Delta/2R$  of the inter-particle attraction range  $\Delta$  over the inter-particle hard-core repulsion  $\leq 2R$  (panels (b) and (c) of Fig. 2.3). For small polymer to colloid ratios,  $\xi \lesssim 0.1$ , the addition of enough polymers (i.e. high enough chemical potential  $\mu_p$ ) causes the phase separation into coexisting colloidal fluid and crystal [Poon et al. (1993); Ilett et al. (1995)]. At higher polymer concentrations, crystallization can be avoided and, instead, a variety of non-equilibrium behavior is observed. Clear experimental evidences for the effect of the range on the equilibrium phase behavior have been provided by works on colloid-polymer mixtures [Bibette et al. (1992); Poon et al. (1994); Ilett et al. (1995)]. Nonetheless, a reduction in the depletion attraction at even higher polymer concentrations was also observed, as arisen from the increased polymer-polymer interactions [Ye et al. (1996)].

**SHORT-RANGE ATTRACTION.** In Asakura-Oosawa-Vrij model, geometrical arguments show that for sizes ratios  $\xi = \Delta/D \leq 0.07735$  there are no higher-order many-body interactions beyond the effective pair potential, while multiple overlaps of the depletion zones can occur for larger  $\xi$ . Theoretical studies on depletion-driven aggregation have mainly focused on the limit where polymers are small as compared to the colloidal size, as a feature shared by most of the systems is the presence of a *short-range attraction* between the aggregating particles<sup>9</sup>.

<sup>8</sup>Explicitly, it is  $V_{\text{overlap}} = \left\{ 1 - \frac{3r}{2D(1+\xi)} + \frac{1}{2} \left[ \frac{r}{D(1+\xi)} \right]^3 \right\} \times \frac{\pi}{6} D^3 (1+\xi)^3$ , where  $\xi = \frac{\Delta}{D}$  is the relative range of the attractive part of the potential in Fig. 2.3(a).

<sup>9</sup>Recently, however, theories are being developed that cover a wider colloid-polymer size ratio range [Moncho-Jordá et al. (2003)]. In practical systems, also size polydispersity, surface charges or different depletant schemes play a role in polymer-colloid mixtures [Tuinier et al. (2003); Fiocco et al. (2010)]. Particles with a longer-range attraction typically have many ( $\sim 10$ ) neighbors, while those with a shorter-range attraction typically have only three to five neighbors. The internal structure of transitional clusters reveals a further difference: clusters of particles with long-range interactions have a volume fraction of  $\phi \sim 0.46$  (the hard-sphere freezing point being higher, at  $\phi \sim 0.49$ ), while those of particles with short-range interactions do not have a well defined volume fraction, due to their fractal nature [Prasad et al. (2007)].

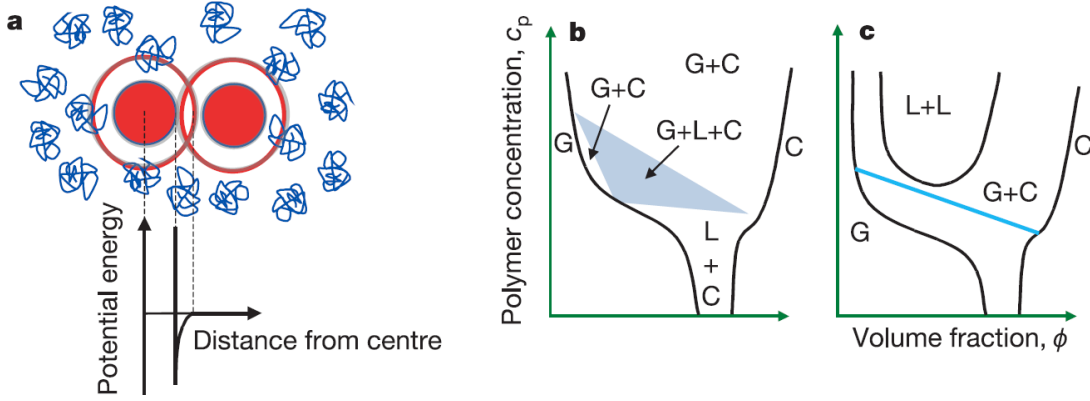


Figure 2.3: Generic depletion potential for colloid-polymer mixture (a) and the schematic phase diagrams (b) and (c), adapted from [Anderson and Lekkerkerker (2002)]. The hard-core repulsion has range equal to the colloidal diameter, the excluded volume of size  $D$ , while the inter-particle attraction has range  $\Delta$ . Phase diagrams are similar to those in Fig. 2.2, but polymer concentration has a role of inverse temperature. The polymers can partition into different coexisting phases, whose indicative lines are not necessarily horizontal. The ratio  $\xi = \Delta/D$  controls, together with the potential's depth, the topology of the resultant equilibrium phase diagram: the different phase diagrams are shown for large polymer chains (i.e.  $\xi$ ) in (b) and for small  $\xi$  in (c).

In this thesis we focus on the case of sufficiently small  $\xi$ , for which theory predicts [Gast et al. (1983); Lekkerkerker et al. (1992)] that inter-particle attraction has the effect of expanding the fluid-crystal coexistence region and to make the gas-liquid (liquid-liquid) equilibrium become metastable.

How “small” is sufficient for  $\xi$  generally depends on the precise form of the attractive part of the inter-particle potential<sup>10</sup>. In the limit of an infinitely-short range attraction of depth  $\gg k_B T$ , the simplest available model is that of diffusion-limited cluster aggregation (DLCA). This computational model, early variants of which were studied as far back as the late ‘60s [Sutherland (1967); Finegold (1976)], was first considered in the context of fractal growth in independent works by [Meakin (1983)] and [Kolb et al. (1983)]. See next Par. 2.2.1 for further details. What is essential in the DLCA model are the “infinitely short range” plus the “infinitely deep well” of the attractive potential among particles. This particular class of potential naturally represents the limiting case of particles that, under aggregation, form a strong gel. Note that a well-defined infinitely short range limit exists, the Baxter sticky hard sphere (SHS) system [Baxter (1968)], where the inter-particle potential takes the form:

$$\frac{U_{\text{SHS}}}{k_B T} = \lim_{\delta \rightarrow 0} \begin{cases} +\infty & \text{if } r < D \\ \ln \left[ \frac{12\tau\delta}{D+\delta} \right] & \text{if } D < r < D+\delta \\ 0 & \text{if } r > D+\delta \end{cases}, \quad (2.3)$$

<sup>10</sup>For depletion attraction, it is needed  $\xi \sim 0.25$  if in good, near-theta solvents [Ilett et al. (1995)].

## 2.2. From colloid-polymer mixtures to the square-well model.

where  $\tau$  represents the “stickiness” parameter. Thus, an infinitely deep well would correspond to an infinite stickiness. The SHS potential is defined such that while  $U_{\text{SHS}} \rightarrow -\infty$  in the limit  $\delta \rightarrow 0$ , the second virial coefficient remains finite, and is given by

$$\frac{B_2^{\text{SHS}}}{k_B T} = 2\pi \int_0^\infty \left(1 - e^{-U_{\text{SHS}}/k_B T}\right) r^2 dr = \frac{2}{3}\pi D^3 \left(1 - \frac{1}{4\tau}\right) \left[\text{HS limit: } \frac{2}{3}\pi D^3\right]. \quad (2.4)$$

Phase separation and dynamical arrest for particles interacting with “mixed” potentials have been shown to have spinodal decomposition, governed by the integral features of the interaction potential described by the normalized second virial coefficient [Gibaud et al. (2011)]. In particular, the arrest line is mainly determined by the attractive well depth or bond strength. The Baxter limit of SHS model, fundamental in the analytical solution of the (Ornstein-Zernike equation) for hard sphere fluids [Baxter (1968); Barbooy and Tenne (1979); Gazzillo and Giacometti (2004)], can be and has been frequently used to interpret the behavior of experimental systems with short-range inter-particle attractions, especially in scattering experiments, by matching second virial coefficients. The second virial coefficient  $B_2$  is experimentally measurable, e.g. by light scattering [Brunetti et al. (1983); Rosenbaum et al. (1996)].

The equilibrium behavior of the SHS system has been a matter of debate [Stell (1991); Marr and Gast (1993)], also for what matters the generic form of the SHS phase diagram shown in Fig. 2.2(c, top) and the fluid-crystal coexistence at low enough values of  $\tau$ . The theoretical  $B_2$  correspondence was in fact expected to be valid only for systems with stickiness  $\tau \gtrsim 1$  [Stell (1991)]. Noro and Frenkel have entered the debate on how to link experiments and theory for systems with short-ranged inter-particle attraction [Noro and Frenkel (2000); Foffi and Sciortino (2006)]. They have shown that the different short-ranged systems at equal density, effectively share the same thermodynamic properties if they are characterized by the same reduced virial coefficient

$$B_2^* = (3/D^3) \int \left(1 - e^{-U/k_B T}\right) r^2 dr. \quad (2.5)$$

They also provided a mapping of such a behavior by using the square well (SW) form for the attractive part of the potential. The Noro-Frenkel scaling holds when the range of the potential is less than about 5% of the particle hard core diameter [Foffi and Sciortino (2006); Malijevsky et al. (2006)]. In particular, short-range attractive colloidal spheres are in equilibrium fluid phase for  $B_2^* \gtrsim B_2^{*c}$ , where  $B_2^{*c}$  is the (scaled) second virial coefficient that signals the presence of a critical point of gas-liquid phase separation. The value of  $B_2^{*c}$  has been computed by computer simulations and is approximately equal to  $-1.2$  [Miller and Frenkel (2003); Largo et al. (2008)]. If the attractive range is short enough, then the NF-scaling states that all the potentials give the same thermodynamics and a short-range SW can model the interaction, in the form

$$U_{\text{SW}} = \begin{cases} \infty & r \leq D \\ -c & D < r \leq \lambda D \\ 0 & r > \lambda D \end{cases} \quad (2.6)$$

## Chapter 2. Colloidal aggregation and gelation.

---

Here  $\lambda = 1 + \Delta$  and  $\epsilon > 0$  are respectively the potential range and its attractive depth. In the case of Eq. (2.6) with  $\Delta \ll 1$ , it results  $B_2^* = 1 - 1/4\tau$ , where  $\tau^{-1} = 4(\lambda^3 - 1)[\exp(\epsilon/k_B T) - 1]$  is the explicit expression for the Baxter stickiness parameter. The condition for the existence of a homogeneous SW fluid is given in terms of  $\tau$  as  $\tau \gtrsim \tau_c$ . The value of the critical stickiness parameter has been eventually found to be  $\tau_c \sim 0.11$  [Miller and Frenkel (2003); Largo et al. (2008)].

The above description is able to capture the correlation of  $B_2$  with the equilibrium solubility of a wide variety of globular protein and colloidal suspensions [Rosenbaum and Zukoski (1996); Rosenbaum et al. (1996)] so indicating quite accurately the ability of the SW model to describe, for instance, protein solution thermodynamics [Ramakrishnan and Zukoski (2000)]. By accounting for a finite probability for clustered colloids to dissociate back into the suspension, the same model has proved essential for studies aimed to capture the correct location of the metastable spinodal and, also, to understand the competition between crystallization and gelation [Dixit and Zukoski (2003); Kulkarni et al. (2003)].

### 2.2.1 Computer models.

**A SUCCESSFUL STORY.** The effectiveness of using non-adsorbing polymers, in the control of magnitude and range of inter-particle interaction, has been confirmed mainly by experimental<sup>11</sup> studies [Ye et al. (1996); Verhaegh et al. (1999); Eckert and Bartsch (2002)] and especially focusing on phase behavior [Vincent et al. (1980); De Hek and Vrij (1981); Russel et al. (1992)]. What is more, the simplicity of the depletion attraction well describing the effective interaction potential  $U(r)$  between the colloids has given the possibility not only of mapping it with even simpler potentials, but also allowed fundamental contributions from numerical simulations. In fact, the simulation of system constituted by ensembles of model particles has enabled the numerical study of liquids by means of computing machines. For example, the interactions among PMMA spheres in suspension are well approximated by a hard-sphere potential [Pusey and van Megen (1986); Poon et al. (1993)] that was, along with its two-dimensional counterpart (hard disks), one of the first systems ever studied using numerical simulation techniques. The target was of understanding the thermodynamics of the liquid and solid phases, and their corresponding phase transition [Rosenbluth and Rosenbluth (1954); Wood and Jacobson (1957); Alder and Wainwright (1957)]. In particular, in 1957 Alder and Wainwright studied<sup>12</sup> the dynamics of a system of hard, two-dimensional discs [Alder and Wainwright (1957)]. With the nowadays computing power, numerical simulation techniques are common tools in

---

<sup>11</sup>Neutron-scattering measurements, performed by means of the partial structure factor, were conducted after matching between the scattering length density of the solvent with that of the polymer. Confocal Scanning Laser Microscopy, or other direct imaging techniques, also started to be used in conjunction with the introduction of colloidal silica particles containing a fluorescent coating.

<sup>12</sup>Much of this work was firstly undertaken at the Los Alamos Scientific Laboratory on the world's first Electronic Numerical Integrator And Computer (ENIAC) [Lesczynski (2012)]. Later, Rahman and Stillinger used a more realistic Lennard-Jones interaction potential to study motion in water [Rahman and Stillinger (1971)]. In the 70s and 80s there was a flourishing literature mostly focused on polymers and proteins, were the paper on BPTI (bovine pancreatic trypsin inhibitor) dynamics may be regarded as the first MD modeling of a protein [Rahman and Stillinger (1971)].



## 2.2. From colloid-polymer mixtures to the square-well model.

the investigations of the transport phenomena and structural properties of colloidal gelation<sup>13</sup>. Also, a better understanding of the experimental observations of gelation is offered by using colloidal models. By careful tuning of particle concentrations, dense or tenuous gels or glasses phases can be formed<sup>14</sup>. Moderate concentrations of polymer cause the suspensions to separate into coexisting colloidal fluid and colloidal crystalline phases, whereas more polymer leads to “gel” states in which crystallization is suppressed. Studies of the intensity of scattered light at low angles and dynamic light scattering at larger angles suggest the following picture of the gels (techniques of light scattering are introduced in Par. 2.3.2). Initial rapid diffusion-limited aggregation (DLA) of the particles via the depletion attraction produces a close-packed assembly of clusters. Subsequent slower consolidation of the clusters weakens them to the point where they no longer support their weight and gravitational settling occurs [Pusey et al. (1993)]. Indeed, the DLA is one of the first models used in numerical simulations to give fruitful results in the context of gelation.

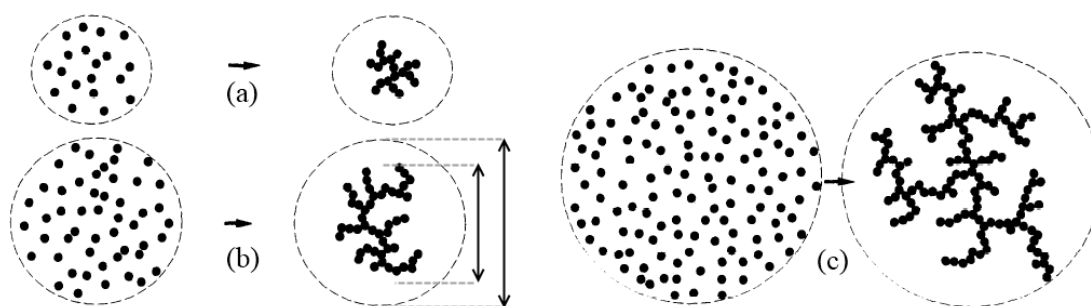


Figure 2.4: Schematic of gelation due to fractal growth, adapted from [Poon and Haw (1997)]. Because of the DLA mechanism, the clusters begin to contact each other across the macroscopic system: a system-spanning cluster, or gel, is formed. If regions of different sizes are considered where the unaggregated particles are originally contained, the same mechanism bring to cluster substantially smaller than the region (a), when this is little, while a larger aggregate forms in larger regions (b). The radius of the aggregate grows quicker than the radius of the original region, up to a value where they have same size (c).

**SIMPLE MODELS.** One of the key ideas that launched the modern study of particle aggregation is that of fractals [Mandelbrot (1983)]. Stimulated by the observations of aggregating iron nanometric particles [Forrest and Witten (1979)], an initial breakthrough was made by proposing the diffusion-limited aggregation model [Witten and Sander (1981)], later used to interpret the structure of real particle aggregates, in their case aggregated colloidal gold [Weitz and Oliveria

<sup>13</sup>Despite the short history of the field, at the beginning of 2012 the query “colloid simulation” results in nearly 1,800 papers from the PubMed biographical database. Importantly, this area is growing fast: its rise is bound to increase, in view of the deep implications into the strong field of colloidal gels (about 16,500 results for “colloid gel”) and because of the continuous boost provided by computational techniques and industrial interests.

<sup>14</sup>The glass transition is typically achieved by increasing the packing fraction of colloids. Addition of polymer causes the system to re-enter the glassy state, although the arrest in dynamics is caused by particle bonding (attractive glass), rather than a cage effect of neighbors (repulsive glass). There are no significant differences in either structure or local density fluctuations between any repulsive or attractive glass.

(1984)]. This extreme case, where the evolution on the aggregation is limited by the time taken for the particles (or clusters) to diffuse and encounter one another, is called diffusion-limited cluster aggregation (DLCA), which generalizes the DLA mechanism by allowing the clusters of particles to diffuse and encounter. In this model, two colliding particles immediately bind permanently. An example is shown in Fig. 2.4. Alternatively, when particles are considered that may not stick immediately because of an energy barrier, then the aggregation is said to be reaction-limited (RLCA). In this case, the binding probability is less than unity; models with unit binding probability, but a finite probability for subsequent unbinding have also been studied [Shih et al. (1991)].

In RLCA the sticking probability can be low enough that two approaching clusters can, on statistical basis, sample all possible mutual configurations before they finally stick together [Sorensen and Roberts (1997)]. Thus the smallest clusters in the distribution have a high probability of interpenetrating the large ones. This effect leads to less tenuous clusters respect to DLCA. As a consequence the fractal dimension in RLCA results higher than the one of DLCA [Lin et al. (1990)].

Irreversible aggregation is strongly related, in the case of compact clusters, to the phase separation problem. Indeed, irreversible aggregation can be seen as a phase separation process in the deep-quench limit (from infinite to zero temperature), when separation proceeds only by decreasing total energy, making the breaking of clusters very rare<sup>15</sup>.

The structural aspects of DLCA were first considered almost solely from the point of view of the structure of individual clusters. DLCA clusters are fractals, i.e. the mass of a cluster ( $m$ , proportional to the number of particles in a cluster,  $n$ ) scales with its radius of gyration  $r_g$  as

$$n \sim m \sim r_g^{d_f} \quad (2.7)$$

where  $d_f$ , the *fractal dimension*, is less than the corresponding spatial dimension  $D$ . Unlike cluster structure (fractal dimension), the kinetics of DLCA (e.g. the evolution of the mass distribution) is found to depend quite strongly on the diffusive dynamics of the growing clusters. The average mass is a good candidate for the description of the aggregation process only when the cluster size distribution is quasi-monodisperse<sup>16</sup>. This condition is not fulfilled in the reaction-limited regime, in the DLCA regime at very high initial monomer concentration, nor in the initial stage of DLCA aggregation when the memory of the initial monodisperse distribution is not yet lost.

Still, successfully explored by means of computer simulations, DLCA has been one the first successful non-trivial colloidal gelation models. An example is in Fig. 2.5. Clusters are clearly surrounded by empty spaces, appearing during the aggregation: the sequence of full and empty spaces introduces a *characteristic length*<sup>17</sup>. The clusters have roughly the same size

---

<sup>15</sup>In such conditions, mechanisms like the evaporation condensation are less effective than diffusion and coalescence of the entire clusters.

<sup>16</sup>This is also connected to the experimental issue of the percolation framework. See Par. 2.3.1.

<sup>17</sup>Colloid-polymer gels reveal large differences in the local structure within a single system [Verhaegh et al.

## 2.2. From colloid-polymer mixtures to the square-well model.

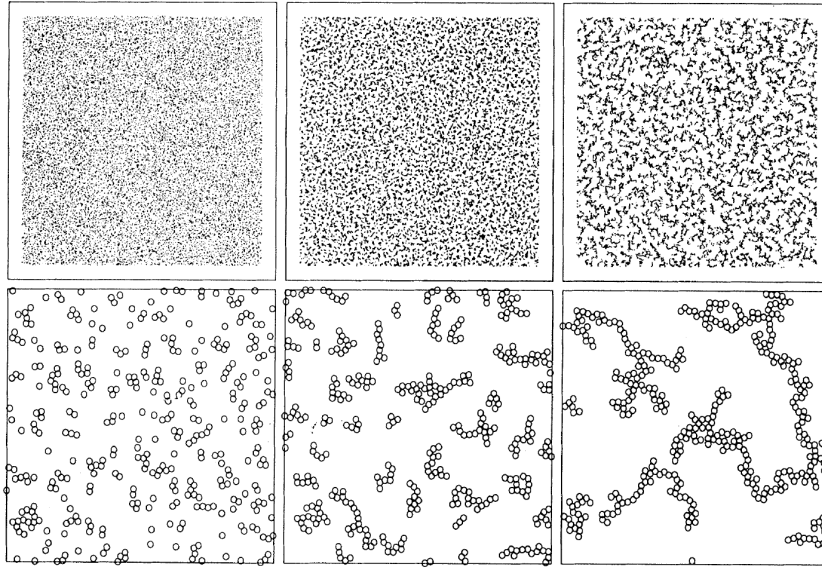


Figure 2.5: **(Top row)** Three different snapshots of a two-dimensional system of 32000 particles undergoing diffusion-limited cluster aggregation. Adapted from [Sciortino et al. (1995)]. The occupied volume fraction is  $\phi = 0.013$ . **(Bottom row)** The same data on a ten times bigger scale.

(in agreement with the bell-shaped form of the cluster size distribution); on increasing the time, the size of the cluster increases but the structure of the alternating regions with different density is preserved.

Gelation in this context is considered a direct consequence of the growth of fractal structures: growing fractal clusters must eventually fill space [Kolb et al. (1983); Herrmann and Kolb (1986)]. Since  $d_f < d$ , the size  $r_g$  of the growing aggregate increases faster than the size  $R$  of the region originally containing its constituent particles, as  $n$  grows, a point will be reached when  $r_g \sim R$ . At the gel point  $r_g = R \equiv R_{gel}$ , the fractal clusters contact each other across the macroscopic system: the system is filled by the gel. In this simple picture, the gel is then an assembly of fractal clusters whose size  $R_{gel}$  strongly depend on the total volume fraction  $\phi_0$  as

$$R_{gel} \propto \phi_0^{1/(d_f-d)}. \quad (2.8)$$

Equation 2.8 clearly implies that the fractal clusters forming the gel become *smaller* with increasing initial concentration. This behavior has been shown to work reasonably well for systems at initial particle volume fraction up to  $\phi_0 \approx 0.1$  [Bibette et al. (1992); González and Ramírez-Santiago (1995)]. This argument stays also at the base of the possibility to quantify the fractality through scattering techniques (Par 2.3.2).

---

(1999): at a given time there are regions where the gel structure consists of alternating patterns of colloid-rich and colloid-poor regions with a characteristic length scale. See also Par. 2.3.2 for their characterization.

**FURTHER MODELING AND OBSERVATIONS.** Nevertheless, this simple picture is not completely satisfactory. It says nothing about how the particles and clusters aggregate, it neither includes nor provides any information as to the particle and cluster dynamics or structure; the fractal dimension  $d_f$  is simply assumed.

In general, the next step for the implementation of less crude computer models implies the introduction of more parameters. Indeed, the model of square-well (SW) particles presented in Eq. 2.6 is closely related to the DLCA, which in fact represents the SW limiting case with infinitely short range and infinitely deep well. One of the first differences with DLCA, even for very short ranges of attraction, is that more compact arms are observed to form the gels obtained with the SW model, thus better mimicking the experimental findings. If particles are considered to be bonded when their center-to-center separation falls below a cutoff value  $r_c = 2(R + r_g)$ , the colloidal radius plus the depletion range<sup>18</sup>, then an average particle's bond number  $n_b$  can be defined. This is the number of bonds that the particle form with its neighbors. By determining the distributions of  $n_b$  and by looking at all particles within the clusters of a given mass, it is possible to account for the observation that the mean bond number increases slightly with the cluster mass because a smaller fraction of particles resides at the cluster's surface. Approximately 40% of the particles in the gel have four bonds or more, suggesting that there might be nodes, or blobs, distributed throughout the structure. Moreover, we will see in Par. 3.1.1 that in the case of short-range attractions,  $n_b \propto U_{\text{tot}}/N$ , i.e. it is proportional to the total potential energy averaged over the particles, an important indicator of the local structure.

The Molecular Dynamics of the SW model is at the core of this thesis, and in the next Chapt. 3 both the simulation technique and the model with its parameters will be specified. The SW is the main colloid model we use to simulate gel aggregation under *quench*, i.e. suddenly driven towards a non-equilibrium state where the gel structures emerge with their typical space-spanning branches (Par. 3.1.1). The different ways a colloidal suspension can be brought out of equilibrium depend in general on the specific system, but the power of the SW model for short-ranged inter-particle attractions relies on both its mapping capability and its simplicity<sup>19</sup>. In fact, at a given volume fraction  $\phi = V_{\text{occ}}/V$  occupied by the colloids ( $V_{\text{occ}}$  is the volume occupied by the colloids,  $V$  the total volume), as soon as the stickiness becomes  $\tau \gtrsim \tau_c$  the system enters the non-equilibrium region and then only the four parameters  $\xi$  (attraction range),  $\epsilon$  (attraction strength),  $T$  (temperature) and  $\phi$  are sufficient for a complete description of the state-point. We use a temperature-quench and we will show how the dynamical arrest acts. A particular focus will be put on the parameters involved in the control of the dynamics: in particular, the introduction of a new (selectivity) parameter in the definition of the SW potential will enable the definition of different colloidal species. This will be shown to allow a tuning in both the dynamics of the aggregation process and of the final (arrested) gel structures.

---

<sup>18</sup>This cutoff can be effectively defined also as the location of the first minimum of the pair distribution function.

<sup>19</sup>For example, recall that in the coarse-grained numerical approach we use, there is complete lack of hydrodynamical effects.

## 2.3 Observing aggregation.

### 2.3.1 Percolation.

The way the aggregation proceeds after the quench, unfortunately, cannot be stated looking at the state point on the phase diagram. To this aim, different observables are usually studied, by devising techniques that have been adopted both in experiments and numerical simulations. As the gel phase sets in, the emergence of an amorphous ramified macromolecule that spans all the system is observed. This allows to tackle the issue of gelation under the light of theories of emerging critical phenomenon, and in particular under the point of view of percolation. In fact, when a sol to gel transition happens, a connectivity transformation have taken place, whose similarity with other connectivity processes, i.e. in communication networks, epidemiology, electrical power grids, microfluidics, forest fires, etc., grants a fruitful theoretical background. At first used for describing the slow passage of a liquid through a filtering medium, the concept of percolation has in fact attracted great interest in the last decade and is now a consolidated mathematical branch used for studying critical phenomena.

A burst of research activity on gels in the 80s, with particular emphasis on polymeric materials, aimed to describe the gelation in terms of percolation models [Whitney and Burchard (1980); Schmidt and Burchard (1981); Martin et al. (1987)]. For example it was observed that collagen proteins, the *gelatin*, may form a reversible (physical) gel when temperature is sufficiently low. Exceeding the denaturation temperature, instead, gelatin chains behave as linear polymers in solution and, in turn, can form a permanent (chemical) gel when agents able to cross-link the molecules are added to the solution. This results in gelatin proteins connected to form an elastic network that extends macroscopically<sup>20</sup>.

The gelation regarded as a transition, due to the formation of a macroscopic network which makes the system able to bear stress, would transform a viscous liquid into an elastic disordered solid. Such a description is often employed on simplified lattice models where each site (node) of the lattice represents a monomer (or a colloid) and where only bonds among first-neighbors are allowed. The concept of percolation involves the possibility of connecting together extrema by providing a viable path between them. In the case of interacting particles, this concept translates into the presence of a non-interrupted chain of bonds that connect macroscopically distant portions of the system. Despite such a simplification, they can account for important macroscopic quantities regarding the gel formation. This is principally due to the universality classes of the critical phenomenon, the *percolation transition*.

Percolation transition is a purely geometrical transition and as a consequence the percolation theory focuses on geometrical properties of formed structures, defined from the positions of the monomers/colloids considered in certain (fixed) spatial configurations. The gelation transition is then a connectivity transition. The so-called polymerization degree (or extent),  $p$ ,

---

<sup>20</sup>A reverse gelation transition, called “gel-sol” transition, may also occur when enzymes able to degrade the (chemical) bonds are introduced. Such a transition is particularly important in biology, as the process of dissemination of tumors in human body involves the degradation of the extracellular matrix (ECM), a gel made of various proteins, including gelatin. In this case the degradation process can solubilize the gel and bring the ECM to a liquid state, where cells are no longer confined and can freely diffuse.

## Chapter 2. Colloidal aggregation and gelation.

which corresponds to the ratio between the actual number of formed bonds to the maximum number of formable bonds, is used as a control parameter, with the implicit assumption that other parameters, like temperature  $T$ , density  $\phi$ , or time parameters, are proportional to it. See Fig. 2.6 as an example of composite where metallic particles are segregated, at different densities, displaying a gel-like structure at density higher than a threshold: the critical value at the transition,  $p_c$ .

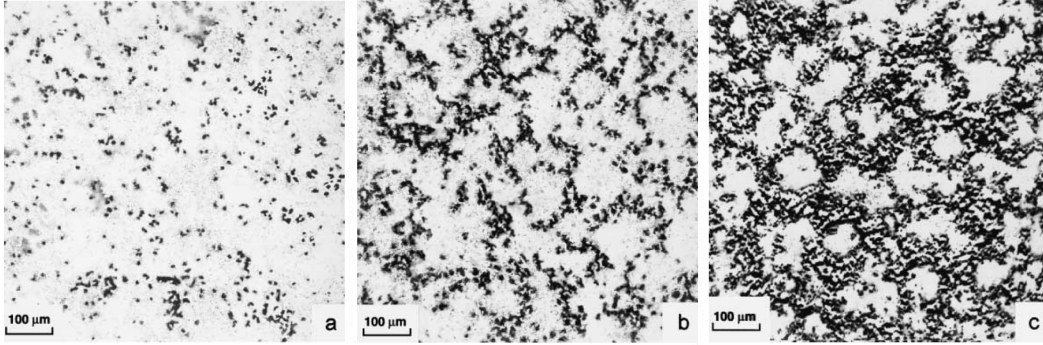


Figure 2.6: Structure of a segregated composite PVC-Ni (nickel immersed in polyvinylchloride matrix) by optical microscopy, adapted from [Mamunya et al. (2002)]. The filler content have packing fractions (a)  $\phi < \phi_c$ , (b)  $\phi \approx \phi_c$ , (c)  $\phi > \phi_c$ , where  $\phi_c = 0.041$  is the calculated percolation threshold in terms of occupied space, for such composite.

**FEATURES AND MODELING.** In the thermodynamic limit where an infinite system is considered, for a particular critical value  $p_c$  of  $p$  an infinite cluster appears. The sol phase corresponds to a solution of disconnected (finite) clusters with  $p < p_c$ , while at  $p \geq p_c$  the gel phase is characterized by the presence of a percolating (infinite) cluster that spans the whole system [Kirkpatrick (1973); Stauffer (1981); Stauffer et al. (1982); Herrmann et al. (1983)]. In the theoretical framework of critical phenomena, the quantity  $(p - p_c)$  represents the distance from the transition. Near the transition, the macroscopic quantities describing the system behave as power laws  $(p - p_c)^a$ .

From an experimental point of view, the sol phase can be characterized by finite viscosity, whereas the gel phase exhibits elastic behavior, due to the presence of a macroscopic interconnected stress-bearing molecule<sup>21</sup>. The gelation threshold can be measured by rheology experiments as the point that marks the passage from a dominant viscous regime to an elastic one<sup>22</sup>. In this context, the viscosity would diverge as  $(p - p_c)^{-k}$  below the transition, and stays infinite above it, while the elastic modulus is zero below the transition and grows above it as  $(p - p_c)^f$ . Near the transition, various classes of percolation exist, for example the *random* or

<sup>21</sup>The intersection point of the loss modulus  $G''(\omega)$ , related to the viscosity coefficient  $\eta$ , and the storage modulus  $G'(\omega)$ , related to the elastic response, with  $\omega$  is frequency of the applied stress, is customary associated to the gelation threshold [Bland (1960)].

<sup>22</sup>The presence of the percolating cluster does not necessarily produce a sharp change in the viscoelastic properties of the system, and weak gels may result similar to highly viscous liquid: the presence of the percolating cluster strongly influences the properties of the system if bonds can be regarded as permanent.

the “pacman” percolation classes [Stauffer and Aharony (1994); Abete (2006)], with different critical exponents<sup>23</sup>.

The experimental determination of both the density of the percolating cluster and the weight average mass can be performed by weighting the macromolecule: in order to perform such a measurement, the gel phase must be separated from the sol phase (for example by centrifugation, but computational analysis techniques also exist, which rely on data retrieved by microscopy imaging). Such separation of the sol and gel phases is very difficult to achieve experimentally<sup>24</sup>, and the clusters in this process tend to break [Stauffer et al. (1982)].

De Gennes proposed [De Gennes (1976)] an analogy between the macroscopic elastic constant of a spring network and the macroscopic conductivity of a resistor network, as both are due to the percolating cluster. Since the earliest works of [Gurland (1966)], it has been customary to associate the insulator-to-conductor transition with the formation of a cluster of electrically connected filler particles which extends through the whole sample. See Fig. 2.7. The transport properties of such cluster is defined by the conductances of the contacts (bonds) between the particles, a natural step to map this system onto an equivalent resistor network.

Such models usually involve 2D square (or 3D cubic) lattices whose sites, representing the conductive particles, are randomly occupied and nearest neighbors considered interconnected (site percolation model) or, similarly, where nearest neighbors are randomly interconnected by bonds of given conductance (bond percolation model). The resulting system is called a *random resistor network*<sup>25</sup>. Pushing further the analogies proposed by de Gennes, the exponents  $f$  of the elastic modulus and  $k$  of the viscosity have been put in direct relation to, respectively, the critical exponents  $t$  and  $s$  of the conductivity in random resistor and random super-conducting networks [De Gennes (1976, 1978)]. He considered a network in which bonds are substituted with a super-conducting junction (couples of stably bonded particles), whereas absent bonds are substituted with resistors of finite conductance. The percolating cluster of energetically bonded particles would produce a macroscopic infinite viscosity.

However, such connectivity-based description of the insulator transition manifests some fundamental incompatibilities for those cases without any sharp cutoff of the connectivity. Indeed, the percolation formulation requires the connections between the filler particles to be of the “on-off” binary sort: this is in contrast, on one hand, with inter-particle potentials where the bonded (on) state cannot be unambiguously distinct from the unbound (off) state, and, on the other hand, with a more refined conductivity description which accounts for

---

<sup>23</sup>These exponents are universal, i.e. they do not depend on the microscopic details of the system, but only on global characteristics like the dimensionality of the system, or whether or not there are long range correlations between particles and bonds. Systems with the same values of such exponents are said to belong to the same universality class [Stanley (1987)].

<sup>24</sup>The gel extraction may be achieved only incompletely, as finite clusters may be trapped into the gel phase. Moreover, the cluster radius may increase by dissolution of the sample.

<sup>25</sup>The conductivity of an (infinite) random resistor network at  $p \gtrsim p_c$  will behave as a power law of the form  $\sigma = \sigma_0(p - p_c)^t$ , where  $\sigma_0$  is a pre-factor and  $t$  is the direct current transport critical exponent. Note that the so-called transport non-universality is also found experimentally and several works have been devoted to it [Johner (2009)].

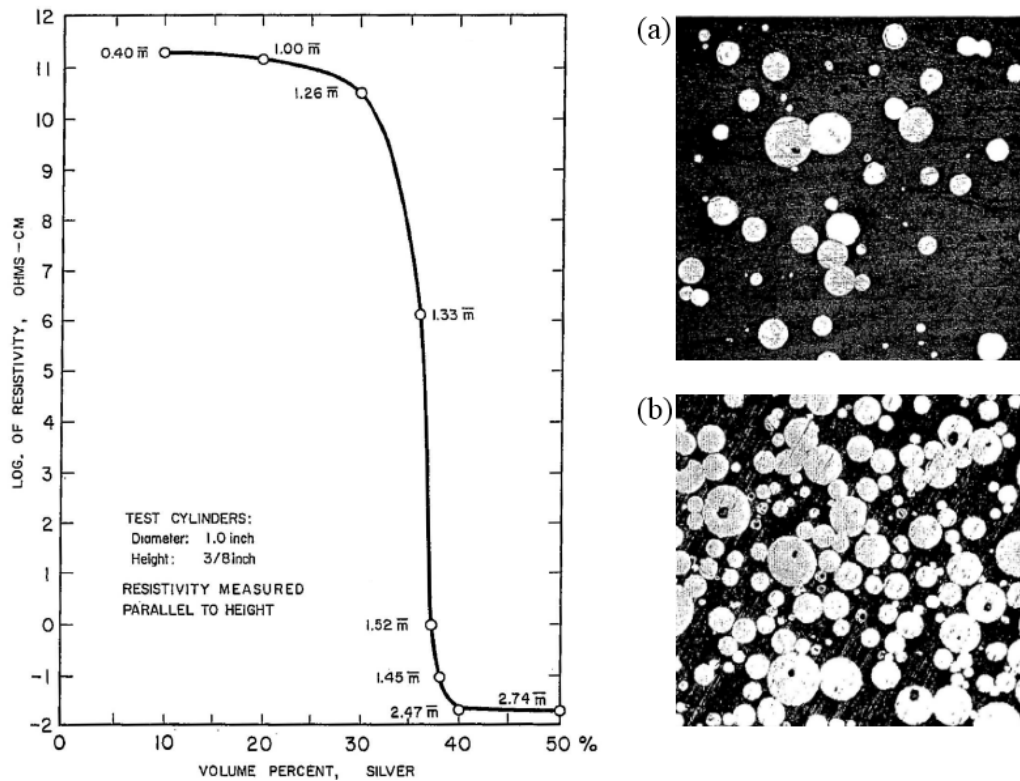


Figure 2.7: Silver-bakelite conductive composites, adapted from [Gurland (1966)]. **(Left)** Resistivity (inverse of conductivity) as a function of the filler volume fraction  $\phi$  (expressed in percent). **(Right)** Micrographs of the composites. (a)  $\phi = 0.1$ , (b)  $\phi = 0.4$ . For the scale, the real length of the micrograph side is  $\sim 1.45$  mm.

non-finite cutoffs<sup>26</sup>. Moreover, dangling ends that contribute to the mass do not contribute to the conductivity, so that above the transition threshold the macroscopic conductivity does not necessarily follow the same growth as, for instance, the mass of the percolating cluster.

**OPERATIONAL DEFINITION IN PBC SIMULATIONS.** In the resistor-network approach, the system is often defined as percolating once two extrema (conducting plates or poles) are connected together by a pattern of bonds formed among the nodes. This percolation definition is not unique. In fact, especially when treating the configurations of particles (nodes) extracted from a numerical simulation, the periodic boundary conditions (PBC) have to be taken into account. The PBC are used to minimize the finite size effects which often affect simulations: the bulk condition is fairly well approximated by using simulation boxes, let's say of size  $L$ , where no walls are present and where continuity of the system is attained in every direction

<sup>26</sup>The tunneling is the microscopically justified electron inter-particle conduction mechanism, whose conductance decays exponentially over the distance with a characteristic decay length in the order of a few nanometers and only for macroscopic fillers an abrupt cutoff description of inter-particle connectivity may still be suitable. This ceases to be valid for nanometric fillers, which have one or more characteristic dimensions that are comparable with the distances of tunneling.



( $x$ ,  $y$  and  $z$  in the 3D case) by implementing crossing rules [Hansen and McDonald (2006)]. As a result, the assessment whether percolation is achieved or not, has to rely on a different evaluation by respect to the 2-plates case.

Provided that the bonding rule is well established for the particles (or nodes) in a fix position in the box volume  $V$ , where for instance  $V = L^3$  if a cube is considered, bonds can exist at the crossing of the the volume border, at least in one of the euclidean directions. The most simple way of treating this case, is to proceed as follows: in a first step, all the clusters must be individuated, using the PBC rules for the possible crossing bonds; next, the system is replicated around the original one, and once again all the clusters must be individuated, where now the PBC is also present but on an increased, 3-fold scale. See Fig. 2.8 as an example for a 2D model structure. In this peculiar example, it is clear that a cluster in the vertical direction is percolating in the plates direction, but without any space spanning cluster: in fact, the only cluster which crosses the borders and bounds to itself creates, once replicated, 3 clusters. The percolation in the thesis work is defined as having at least one cluster that, in periodic boundary conditions, touches itself in such a way that it creates one unique cluster, crossing along all the directions. This is sometimes called a *wrapping percolation*.

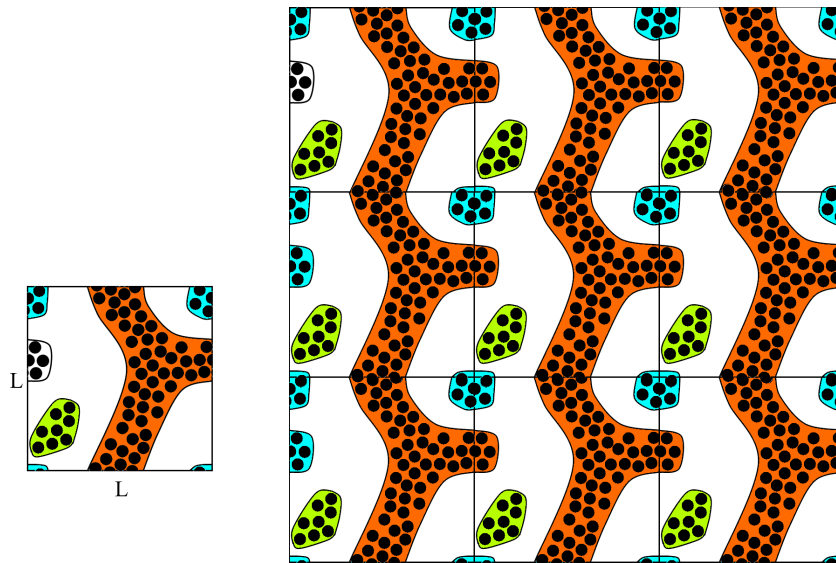


Figure 2.8: **(Left)** A schematic 2D gel structure with periodic boundary conditions. Clusters are identified and differently colored, with a line embedding the different clusters drawn to simplify the visualization. **(Right)** The same system, replicated in the two Euclidean directions. This example highlights also the aliasing feature due to the introduction of a length-scale  $L$  for the replicated system.

Off-lattice or continuum models have also been introduced [Feng et al. (1987)] and, in random resistor networks, a certain correspondence exists between the bond occupation probability  $p$  and the occupied volume fraction  $\phi$ . When dealing with such systems, a problem associated with the concept of contact becomes more evident. For example, for a system of equally-sized

## Chapter 2. Colloidal aggregation and gelation.

---

hard spheres randomly dispersed in the continuum, if no potential is defined for the bonding, would originate contacts and global connectivity only at the close packing limit, at a volume fraction of  $\phi \approx 0.64$  [Donev (2006)], way higher than the filling fractions at which the insulator-to-conductor transition is experimentally observed.

If a cutoff on the minimal distance between two spheres is introduced (below which these are considered connected and beyond which these are considered disconnected) the resulting formulation is called cherry-pit model [Zweifel et al. (1998-04-01); Johner et al. (2008)]. Also for these continuum systems, if we associate to every connected particle couple a bond of a certain conductance, near the critical concentration, the bulk conductivity will again follow a power law of the same form, but in terms of the volume fraction:

$$\sigma = \sigma_0(\phi - \phi_c)^t .$$

Moreover, if  $t$  is (under isotropic conditions) universal, the percolation critical concentration  $\phi_c$  is system-dependent and will vary for different morphologies.

The concept of studying the conductivity rests however untouched: it uniquely relies on the fact that a structure formed by conductive particles results globally conductive when the minimum inter-particle distances is short enough. The conductivity of a system under gelation, can be thus studied for extracting information on the global structure of the aggregating particles.

This constitutes a side-project of the thesis: we studied monodisperse colloidal gelation under the tunneling conductivity paradigm. With the correct approach where one takes into account the non-finite electron transport distance, one can in principle detect changes in the fluid structure under gelation, even far from the critical point. We have worked in such a direction for monodisperse systems of SW colloidal particle, and results can be found in the Appendix A. We show how the natural branching structuration due to gelation brings to enhance the conductivity of systems otherwise bound (in the fluid, isotropic regime) to poor conductivity. As this is not the topic proposed for the thesis, indeed such a description is relegated in Appendix A.

### 2.3.2 Characteristic length.

Usual approaches to determine percolating quantities (as the weight average mass - i.e. the mean cluster size, - or the average cluster diameter - i.e. the connectedness length) light scattering measurements may be performed. In such measurements, the sample needs to be dissolved in a known quantity of solvent in such a way that each cluster is separated from the others. Therefore, light scattering experiments must be performed in dilute solutions, but since the size of the clusters may increase during the dissolution due to swelling, it is possible that the measurement of the mean size (or gyration radius) may be corrupted. What is more, even if providing a certain characterization, the theory of critical phenomena cannot be used to describe the dynamical evolution of gels and the changes in mechanical response due to the formation of the spanning macromolecule. In fact it describes a purely static transition

corresponding to topological changes of the system. Other measurements are thus more often used to this end, and in what follows, after a closer view on the percolation description, we will introduce the most used method: the study of the structure factor.

In general, there are two ways of probing structures with radiation: by direct imaging, e.g. with a microscope, or by interpreting the scattered, or diffracted, radiation (usually in the far field). The two methods are complementary. Imaging in real space, effectively “seeing”, provides direct information on the basic structure of the “scattering units”, usually in a small region of the sample. In Appendix B the confocal microscopy is presented: this experimental technique, that gives access to direct imaging of colloids and their gel structures, is used for the study concerned by the thesis. Here, however, we shortly review the important concepts connected with imaging, whose validity goes beyond the used technique.

**STRUCTURE FACTOR.** A fundamental object that is used in the study of the dynamical behavior of liquids is the time-dependent generalization of the equilibrium pair distribution function, the so called van Hove function [Van Hove (1954)]. For a system composed by  $N$  particles (considered as  $\delta$ -scatterers) in a volume  $V$ , in which the position of the  $\alpha$ -th particle at time  $t$  is  $\vec{r}_\alpha(t)$ , the local density in space and in time  $\rho(\vec{r}, t)$  can be defined, and the van Hove function corresponds to its autocorrelation:

$$G(\vec{r}, t) = \frac{1}{\rho} \langle \rho(\vec{r}, t) \rho(0, 0) \rangle = \frac{V}{N} \langle \delta^3(\vec{r}_\alpha(0)) \delta^3(\vec{r} - \vec{r}_\beta(t)) \rangle . \quad (2.9)$$

This describes the probability of finding a particle around  $\vec{r}$  at time  $t$ , given that there is a particle in the origin at time  $t = 0$ . It separates into two terms, usually called the self part  $G_s(\vec{r}, t)$  and the distinct part  $G_d(\vec{r}, t)$ , given respectively by the sum over the diagonal terms  $\alpha = \beta$ , and by the sum over the off-diagonal terms  $\alpha \neq \beta$ . They describe respectively the probability that the particle in  $(\vec{r}, t)$  is the same that was in  $(0, 0)$ , or a different one. For  $t = 0$  one has  $G_s(\vec{r}, 0) = \delta^3(\vec{r})$  and  $G_d(\vec{r}, 0) = \rho g(\vec{r})$ , where  $g(\vec{r})$  is the static pair correlation function. The space Fourier transform of  $\rho(\vec{r}, t)$  is the density fluctuation of wavenumber  $\vec{k}$ ,

$$\rho_{\vec{k}}(t) = \int d\vec{r} e^{-i\vec{k}\vec{r}} \rho(\vec{r}, t) ,$$

whose mean square value is called *static structure factor*,

$$S(\vec{k}) = \frac{1}{N} \langle |\rho_{\vec{k}}|^2 \rangle = \int d\vec{r} e^{-i\vec{k}\vec{r}} G(\vec{r}, 0) = 1 + \rho \int d\vec{r} e^{-i\vec{k}\vec{r}} g(\vec{r}) . \quad (2.10)$$

In a more convenient way, when isotropy is considered for the scatterers (particles), it can be rewritten as

$$S(q) = 1 + \frac{N}{V} \int_0^\infty 4\pi r^2 (g(r) - 1) \frac{\sin(qr)}{qr} dr , \quad (2.11)$$

where the  $q$  notation is often found for the wavenumber. The corresponding transform of  $G(\vec{r}, t)$  gives the autocorrelation function of density fluctuations, also called intermediate

## Chapter 2. Colloidal aggregation and gelation.

---

scattering function or coherent scattering function,

$$F(\vec{k}, t) = \frac{\langle \rho_{\vec{k}}(t) \rho_{-\vec{k}}(0) \rangle}{\langle |\rho_{\vec{k}}|^2 \rangle} = \frac{1}{S(\vec{k})} \int d\vec{r} e^{-i\vec{k}\vec{r}} G(\vec{r}, t) .$$

By considering only the self part of the van Hove function, we obtain the self intermediate scattering function or incoherent scattering function. Finally, Fourier transforming over time, we obtain the coherent dynamical structure factor

$$S(\vec{k}, \omega) = \frac{S(\vec{k})}{\pi} F(\vec{k}, \omega) = \frac{S(\vec{k})}{2\pi} \int_{-\infty}^{\infty} e^{i\omega t} F(\vec{k}, t) \int d\vec{r} e^{-i\vec{k}\vec{r}} G(\vec{r}, t)$$

that, for classical systems, is an even function of both  $\vec{k}$  and  $\omega$ . In investigating the properties of liquids, there are some differences in the case of scattering of light by respect to the case of slow neutrons. First, the light scattering is completely coherent, so that no information can be gained on self part of  $S(\vec{k}, \omega)$ . Second, the wavelength of light (of the order of 4000 – 8000 Å) has to be used within the “hydrodynamic region” ( $k \approx 10^{-3} \text{Å}^{-1}$ ), that is often bigger than the inter-particle distances.

It is worth to notice that over sufficiently large length-scales the behavior of the  $S(\vec{k})$  is due to the contribution of different relaxation processes characterized by different relaxation times. Close to the sol-gel transition, the relaxation process is controlled by the growth of the connectivity inside the system, as the mean molecule size critically grows. In the cases when the static structure factor  $S(\vec{k})$  is experimentally measured using energies much greater than  $k_B T$  for the wavelengths of interest (like, for instance, by means of X-rays, electrons of fast neutrons), the scattering can be treated, to a very good approximation, as being elastic. If it is case, then the so-called *elastic sum rule* holds, stating that the cross-section is proportional to

$$\int_{-\infty}^{\infty} d\omega S(\vec{k}, \omega) = S(\vec{k}) .$$

The position of the small-angle peak in the structure factor,  $k_m$ , indicates a characteristic length scale,  $\xi_m \sim 2\pi/k_m$ . This length have to some extent describe an evolving “characteristic” length scale as aggregation proceeds. Each growing cluster can be seen as surrounded by a “depletion zone”, where the density of particles is lower than the system average [Dubois and Cabane (1989)]. The small-angle peak is the signature of this developing density modulation. Thus *the characteristic length scale represented by the small-angle peak is given by the radius of the typical cluster plus its depletion zone*. Care must always be taken when interpreting  $g(r)$ , however: in fact it is usually averaged by taking every particle at the “origin” in turn; then the pair correlation function measures an average “environment” seen by all particles, not just those near the centers of the clusters.

The low- $k$  behavior can be masked by the presence of trivial thermal fluctuations, that are also found in the non-aggregated system (i.e., at  $t = 0$ ). The signal from the thermal fluctuations becomes negligible only when the aggregation process has gone so far to produce a large ( $\gg 1$ ) average mass.

**OBSERVING GELATION.** Some of the first important results on the ongoing gelation phenomenon, as explored by the study of structure factor, concern the salt-induced aggregation of monodisperse, charged polystyrene spheres dispersed in water [Carpinetti and Giglio (1992)], and the temperature-induced aggregation of monodisperse surfactant-stabilized oil-in-water emulsion droplets [Bibette et al. (1992)]. The technique of small-angle light scattering (SALS) was used in both cases<sup>27</sup>. It was showed that, as aggregation proceeds, spontaneous ordering occurs on a mesoscopic length scale  $\gtrsim 10$  particle diameters. They observed that the mesoscopic structure persists as aggregation proceeds towards the point where a single, internally non-compact cluster spans space. This is the occurrence of gelation, whose key signature is the presence of a brightening and collapsing “ring” in the SALS pattern. Consensus emerged that the peak in the small-angle scattering is associated with some kind of “depletion region” [Gunton J.D. and Sahni (1983); Langer (1992); Bailey et al. (2007)] surrounding each growing cluster, where the peak’s collapse and brightening are strongly reminiscent of the spinodal decomposition. When the system arrives at the gel point, the peak observed via scattering techniques “freezes”, indicating the arisen structural arrest<sup>28</sup>. This can be seen in Fig. 2.9 (left).

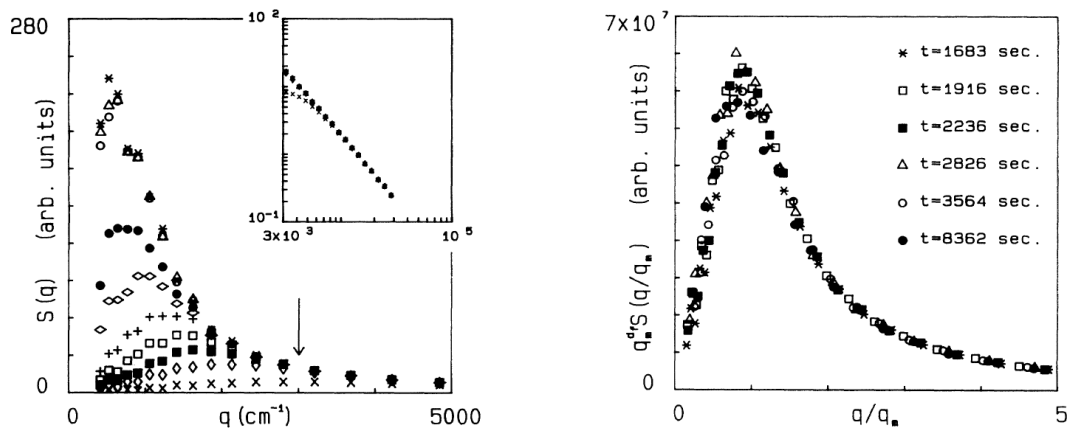


Figure 2.9: **(Left)** Plots of scattered intensity distributions of various times during the aggregation, from [Carpinetti and Giglio (1992)]. A solution of polystyrene spheres ( $0.0190\mu\text{m}$  in diameter, volume fraction  $\phi = 2.96 \times 10^{-4}$ ) in a water-heavy-water mixture aggregates by  $\text{MgCl}_2$  salt addition. The curves grow and shift up to saturation, and cover a time range from  $t = 722$  to  $60753$  s (from bottom to top). Starting from the wavelength indicated by an arrow, the large- $q$  asymptotic behavior is considered and shown on a log-log plot in inset. **(Right)** The scaled structure factor, Eq. 2.12, at later stages of the aggregation process (times are indicated in seconds).

<sup>27</sup>Depending on the particle size, the incident radiation wavelength has to be decided. Colloidal particles can be studied by means of both light or neutrons scattering.

<sup>28</sup>Note that the depletion zone in  $g(r)$  persists in the final system-spanning gel, just as the “frozen peak” persists in the structure factor  $S(k)$  at the gel point.

## Chapter 2. Colloidal aggregation and gelation.

---

The fractal dimension of the macromolecule formed by diffusion aggregation processes may be measured by light scattering experiments, investigating the behavior of the static structure factor  $S(q)$  as a function of the wavenumber  $q$  [Carpinetti et al. (1990); Carpinetti and Giglio (1992)]. Carpinetti and Giglio experimentally showed that scattered intensity in diffusion-limited cluster aggregation does display a peak<sup>29</sup>, which grows and shifts in  $k$ -space during the aggregation kinetics [Carpinetti and Giglio (1992)]. They found that after an initial regime, the scattered intensity seems to scale as predicted for late-stage decomposition theories, if one substitutes the fractal dimension of the clusters  $d_f$  to the space dimension  $d$  in the scaling plot. The growth of the scattered intensity stops when the less and less dense fractal clusters completely span the available space, leaving in the frozen scattered intensity state a memory of the growth process. Such observations have been confirmed by computer simulations [Pusey et al. (1993); Haw et al. (1994); Sciortino et al. (1994-08-01); González and Ramírez-Santiago (1995)]. Even in the two-dimensional case, a growing and moving peak in the scattered intensity is observed. It was conjectured that the peak was a manifestation in Fourier space of the depletion region, which develops around the growing clusters.

At higher concentrations the dynamics is very fast, the mass growth is not a simple power law, and the size distribution is not characterized by just one single size, as it happens instead for the DLCA case. There is a peak in the scattered intensity at all concentrations. At high concentration, the amplitude of the peak is rather small, consistent with the fact that just before gelation, the average cluster size is small. At  $\phi > 0.25$  the kinetics of aggregation never enters the regime of self-similarity. The aggregation process is so fast that there is no time to forget the initial monodisperse distribution state and crossover to the universal law for the cluster size distribution. At lower densities, instead, the kinetics is much slower. In the late-stage decomposition and in the deep-quench limit, when a sample is quickly transferred from the high temperature one-phase region deep into the coexistence region, the cluster structure is compact and the leading aggregation mechanism is diffusion and coalescence of clusters [Sciortino et al. (1995)].

After an initial period during which droplets of the minority phase are formed, the separation process proceeds via diffusion and clustering of droplets. Under deep quench, separation proceeds only along a path of decreasing total energy and cluster breaking is very rare. The growing cluster acts as a trap for the near clusters, decreasing the probability of finding clusters nearby its sticky boundaries<sup>30</sup>.

**SCALING FUNCTIONS.** It emerges from observations in scattering studies of aggregating colloids, as well as in simulated systems, that over a range of scattering vectors around the small-angle peak, the time-dependent structure factor  $S(k, t)$  shows a *dynamic scaling* prop-

---

<sup>29</sup>When gel formation is due to DLCA or RLCA processes, the gelation process corresponds to the formation of an interconnected network which evolves dynamically, but the same approach as the chemical gelation holds within the appropriate observation time scale.

<sup>30</sup>The gel structures have scatter profiles very close to those of dense liquids. It was found, especially for gels with occupied volume fractions ( $\phi \gtrsim 0.1$ ), that the overall shape of pair correlation function is typical of those seen in dense liquid structures [Varadan and Solomon (2002)].

erty. Carpineti and Giglio [Carpineti and Giglio (1992)] found that at intermediate times the scaled structure factor

$$\tilde{S}(k/k_m) = k_m^\gamma S(k, t) \quad (2.12)$$

takes an invariant form, with  $\gamma \sim 1.90 \pm 0.02$ , i.e.  $\gamma \approx d_f$  the (single cluster) fractal dimension (Fig. 2.9). For the scaled scattering curves to collapse to a single function in the fractal regime, i.e. at large  $k$  where  $S(k) \sim k^{-d_f}$ , Eq. 2.12 requires  $\gamma = d_f$ . This does not explain though why a scaling exponent  $\gamma = d_f$  also seems to lead to data collapse at and below the peak in  $S(k)$ , where  $S(k) \sim k^{-d_f}$  clearly does not hold. The scattered intensity shows a well defined peak that moves in time. The kinetic process is separated in three regions: an initial region where no scaling in  $k^{d_f} S(k/k_m)$  is observed, an intermediate region where scaling is observed, and a saturation region where no further change in the dynamical structure factor is observed.

For dynamic scaling to hold, there must be a single length scale which characterizes the aggregating system, all other lengths in the problem being proportional to this length and thus having the same time-dependence. Instead, two length scales can be identified in principle (also from the form of the pair correlation function  $g(r)$ ): the “cluster size”,  $r_c$ , (i.e. the point at which  $g(r)$  first decreases below unity), and the outer radius of the depletion zone,  $r_k \approx \xi_m$  (where  $g(r)$  recovers to unity). Over the intermediate time regime when dynamic scaling holds, therefore, we must have  $r_k/r_c = \text{constant}$ .

One advantage of simulations is that the various length scales may be directly calculated. On the other hand, experimentally the average separation  $\langle x \rangle$  and the average (median) radius of gyration of clusters  $\langle r_g \rangle$  are measured. It is not clear, however, how  $\langle x \rangle$  and  $r_c$  or  $r_k$  should be related, and experimental results do show inconsistencies [Earnshaw and Robinson (1995)] with the simulated constant  $r_k/r_c$  [Haw et al. (1995)].

Moreover, the scaling exponent  $\gamma$  in Eq. 2.12 seems to depend on the volume fraction. At high volume fraction an unexpectedly low estimate of  $\gamma$  is obtained. If we identify  $\gamma$  with the fractal dimension of clusters  $d_f$ , this seems the reverse of the often-stated expected increase in the fractal dimension of clusters with increasing system concentration [Kolb and Herrmann (1985)]. Thus it is not clear that  $\gamma$  may always be simply associated with  $d_f$ .

It has been argued by [Sciortino et al. (1995); Sciortino and Tartaglia (1995)] that the observed scaling in *fractal* aggregation is only “apparent” rather than theoretically meaningful; their argument is related to the simple picture of gelation where the size of the fractal clusters must grow faster than the size of the “depletion regions” surrounding the clusters. This means there are at least two length scales in the fractal aggregation system which evolve differently in time: scaling by a single characteristic length is violated. Moreover, it has been noted that a scaling function for the structure factor cannot be universal, strongly depending on the initial conditions (principally the occupied volume fraction) and coarsening process [Sciortino et al. (1995)].

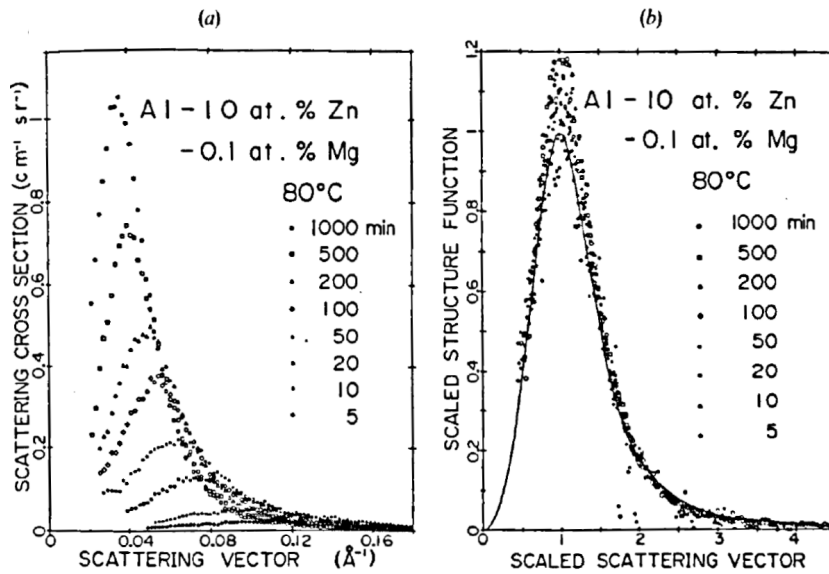


Figure 2.10: Scattering intensity for Al-Zn system with Mg for the stabilization of the quenched vacancy, adapted from [Furukawa (1985)]. **(a)** Bare scattering functions for various times. **(b)** The scaled scattering function constructed by the same data as (a). The solid curve indicates Eq. 2.23 with  $\gamma = 4 = d + 1$ .

**ANALYTICAL APPROXIMATION.** Small-angle scattering (SAS) is measured in order to study the droplets growth near the critical point for fluid mixtures. The detection of correlations between different interfaces, and in particular, between remote surface segments of one and the same particle, has opened the way to theoretical approaches, most of which have tried to view under a unifying picture the decomposition process. In particular, it was observed (by X-ray or neutron SAS) that the appearance of a  $k^{-4}$  behavior of the structure factor reflects the appearance of a well-developed droplet interface. Such a decay, named after Porod and Debye, is known as *Porod's law* [Porod (1951, 1952); Debye et al. (1957); Sinha et al. (1988); Glatter (1991)]. In a system composed of distinct mesoscopic particles, all small-angle scattering can be understood as arising from surfaces or interfaces. In the range of validity of the Porod's law, however, is relatively small on the usual scale of SAS: in this regime, correlations between remote surface segments and inter-particle correlations are so random that they average out. Therefore one can distinguish the local interface roughness.

We now introduce a semi-empirical formulation for the structure factor that brings to an analytical formulation. Importantly, such a treatment has been primarily suggested and used for the description of late stages of the phase separation process where a bicontinuous structure emerges. In the case of gelation, where the spinodal decomposition is arrested, such a treatment is also expected to hold in aggregation stages distant from the early thermal fluctuations due to the quench. But in the gelation process of colloidal particles, the definition of bicontinuous structures is not obvious: we will come back later to this in Chap. 4, where results will be shown regarding double, inter-penetrating gel structures.



The scaling form of the Structure Factor 2.12 is often found written as

$$\tilde{S}(kR(t)) = [R(t)]^{-d} S_k(t) , \quad (2.13)$$

where  $R$  is the length-scale of the sub-systems where phase separation occurs independently until percolation arises. The transformed density  $\rho_{\tilde{k}}(t)$  assumes the role of order parameter, which is assumed to be a conserved quantity as the material cannot move over the distance much larger than  $R$ . Used at the small wavenumber limit, this means that

$$\lim_{k \rightarrow 0} \langle |\rho_k(t)|^2 \rangle = \lim_{k \rightarrow 0} \langle |\rho_k(0)|^2 \rangle = \lim_{k \rightarrow 0} S_k(0) , \quad (2.14)$$

i.e., the large length-scale structure factor  $S_0$  does not change in time<sup>31</sup>. By assuming the initial value may be neglected [Furukawa (1984, 1985, 1989)], the scaling function 2.13 does not contain constants. This argument holds its validity for liquids where no important structuration emerges before quenching.

While the thermal fluctuations drive the early stages of the phase separation process, they are not dominant in the late stages, where instead surface tension becomes important. It has been shown [Furukawa (1989)] that for the order parameter it can be used a kinetic equation like

$$\frac{d}{dt} \rho_k(t) = M_k(t) k^\beta \mu_k(t) , \quad (2.15)$$

where  $M_k(t)$  is the mobility and  $\mu_k(t)$  is the (transformed) chemical potential<sup>32</sup>. Thus, for small- $k$ , a behavior

$$S_k(t) \propto k^{2\beta} \quad (2.16)$$

is expected. With the usual the kinetic equation for which  $\beta = 2$ , the  $k^4$  behavior (and related scaling) is recovered [Katano and Iizumi (1984); Hoffer and Sinha (1986); Wiltzius et al. (1988)]. During phase separation, the chemical potential  $\mu$  is not a conserved quantity and it gives

$$\lim_{r \rightarrow \infty} \langle \mu(\vec{r}) \mu(0) \rangle - \langle \mu(0) \rangle^2 \propto r^\nu , \quad \nu > 0 . \quad (2.17)$$

Passing to the Fourier transform, this implies that  $\langle |\mu_k|^2 \rangle \propto k^{\nu-d}$ , where  $d$  is the Euclidean dimensionality. A minimum for  $\nu$  exists that is independent on  $\beta$ . In fact from Eq. 2.15, for the structure factor  $S_k(t) = \langle |\rho_k(t)|^2 \rangle$  results the equation of motion

$$\frac{d}{dt} S_k(t) = 2M_k(t) k^\beta \langle \mu_k(t) \rho_{-k}(t) \rangle \quad (2.18)$$

<sup>31</sup>The long range (small wavelength) limit of the structure factor gives the (isothermal) compressibility of a fluid  $\kappa_T = -\frac{1}{V} \frac{\partial V}{\partial p} \Big|_T = \frac{1}{\rho} \frac{\partial \rho}{\partial p} \Big|_T$ , where  $\rho = N/V$  is the number density. The relation with the structure factor reads  $S(0) = k_B T \frac{\partial \rho}{\partial p} \Big|_T = k_B T \rho \kappa_T$  and captures the fluid's resistance to uniform compression. It provides also the thermodynamic link for analytical approaches relying on the Ornstein-Zernike equation.

<sup>32</sup>This is in the same spirit as for the Cahn-Hilliard-Cook equation  $\frac{d}{dt} \rho_k(t) = M_k(t) k^2 \mu_k(t) + f_k(t)$ , where the fluctuating force has the dissipative property  $\langle f_k(t) f_{-k}(t') \rangle = 2M_k(t) k^2 \delta(t-t')$ .

## Chapter 2. Colloidal aggregation and gelation.

---

and this in turn gives

$$\langle \mu_k(t) \rho_{-k}(t) \rangle \leq \langle |\mu_k(t)| |\rho_k(t)| \rangle \propto k^{(v-d)/2} \langle |\rho_k(t)| \rangle \leq k^{(v-d)/2} \left[ \langle |\rho_k(t)|^2 \rangle \right]^{1/2} \propto k^{(v-d)/2} S_k^{1/2}. \quad (2.19)$$

Then, using the results 2.16 and 2.18, we have

$$\frac{d}{dt} S_k(t) \sim \frac{1}{t} S_k(t) \propto k^{2\beta} \leq k^\beta k^{(v-d)/2} k^\beta \Rightarrow v \geq d. \quad (2.20)$$

For the other extreme of the scaling function at large length-scales, the fractal argument holds. However, in its early formulations the  $k$  relation simple relied on the Euclidean dimensionality. For sake of simplicity, Furukawa argued [Furukawa (1989)] that the tail of the scaling structure factor  $\tilde{S}(x)$  shall be approximated to a simple power-law  $x^{-\gamma}$ . Here  $\gamma$  may be equal to  $d+1$ , but generalizations to fractal behaviors can give different values (e.g.  $\gamma = d_f + 1$ ). The tail should depend on the surface condition of the droplets.

The scaling structure factor should than have the following asymptotic forms:

$$\tilde{S}(x) \propto \begin{cases} x^\delta & \text{for small } x \\ x^{-\gamma} & \text{for large } x \end{cases}. \quad (2.21)$$

where  $\delta = 2\beta$  and where  $k/k_m$  is the ratio over the peak position  $k_m$ . As explained before, no constants are expected and, thus, we can assume that the asymptotic behavior gives a sufficient description. This means that we can assume

$$1/\tilde{S}(x) = ax^{-\delta} + bx^{-\gamma}, \quad (2.22)$$

where the constants  $a$  and  $b$  can be fixed imposing the function to have a maximum in  $x = 1$  and that the value in the maximum is  $\tilde{S}(1) = 1$ . A function which satisfies these properties is given by

$$\tilde{S}(x) = \left(1 + \frac{\gamma}{\delta}\right) \frac{x^\delta}{\frac{\gamma}{\delta} + x^{\delta+\gamma}}. \quad (2.23)$$

Although this is only one of many possible equations satisfying all the above conditions, its good agreement was found for numerical simulations [Furukawa (1984); Thakre et al. (2008)] as well as for experimental results [Poon et al. (1995); Dhont (1996b); Gibaud and Schurtenberger (2009)]. The scaling property is sometimes used by collapsing the functions in accordance with the obtained parameters, in the form

$$\bar{S}(x) = \frac{S(x, t)}{S_m(t)}, \quad x = k/k_m(t). \quad (2.24)$$

Example of scaling are shown Fig.s 2.10 (right) and 2.11, used to account for experimental and simulation data, respectively. Thanks to the possibility offered by this phenomenological,

analytical approximation, the characteristic lengths of the domains can be extracted from the peak positions of the fitted functions by  $R(t) = 2\pi/k_m(t)$ . It is believed that this route to the average domain size provides a worthwhile alternative to the more common approaches based on the first or second moment of  $S(k)$ , especially when the structure factors are compounded with noise.

Recently there have been some discussion on the kinetics of demixing in colloid-polymer and Lenard-Jones mixtures [Aarts and Lekkerkerker (2004); Thakre et al. (2008)]. By keeping track of the evolution of the low- $q$  region of the structure factor, it is possible to keep track of the typical demixing domain size and its evolution. This approach fits perfectly in the context of the thesis, where a mixture of different species has to be treated. The structure factor, defined as  $S(\mathbf{k}, t) = \langle \rho_{\mathbf{k}} \rho_{-\mathbf{k}} \rangle$ , where  $\rho_{\mathbf{k}}$  are the Fourier transform of the density variable (see also Eq. 2.10), can be computationally achieved in this case of 2-component mixture by using [Thakre et al. (2008)]

$$\rho_{\mathbf{k}} = \sum_{i=0}^N b_i \exp(i\mathbf{k} \cdot \mathbf{r}_i(t)) \quad (2.25)$$

where  $b_i$  takes the values  $\pm 1$  depending of which species (or component) is considered, and  $N$  is the number of particles. In this case only 2 species are considered to form the mixture, as it is the main case the thesis aim to study. As pointed out by [Thakre et al. (2008)], Furukawa's function is consistent with the dynamical scaling hypothesis, which is expected to hold for the evolving phase separated domains. An offset in the wave number, introduced as a third fit parameter to improve the quality of fit, would spoil this scaling invariance and is therefore not recommendable. As a particular case of Eq. 2.23, Furukawa proposed a form for the demixing fluid where  $\delta = 2$  and  $\gamma = 4$  [Furukawa (1984)]:

$$\tilde{S}_k(t) = S_m(t) \frac{3(k/k_m(t))^2}{2 + (k/k_m(t))^6}, \quad (2.26)$$

that we will use, together with its generalized version, for characterizing some of the results of the thesis in Par. 5.1.

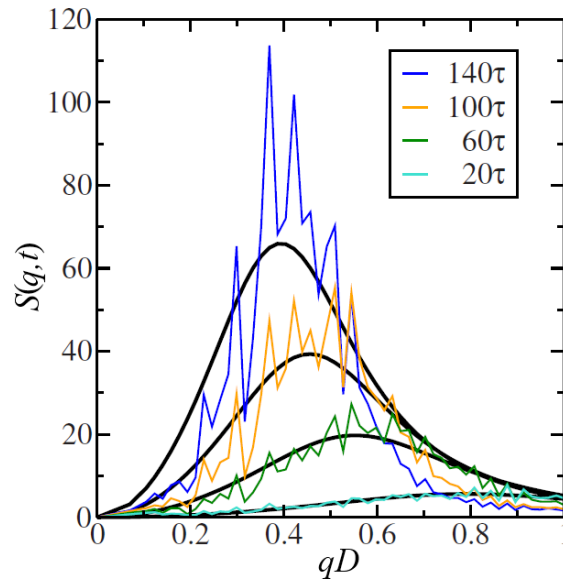


Figure 2.11: Spherically averaged structure factors  $S(q, t)$ , adapted from [Thakre et al. (2008)], for four times (time  $t$  is in unities of  $\tau = \sqrt{mD^2/\epsilon}$ ,  $D$  is the diameter), after quenching a homogeneous Lennard-Jones fluid. In this case, the spinodal decomposition takes place. In order to improve the signal-to-noise ratio, the data shown are averages over four independent MD simulations. Thick smooth lines represent fits with the Furukawa function, see Eq. 2.26. As time advances, the position  $q_m$  of the peak shifts to lower wave numbers, and the height of the peak increases, indicating that the domains are growing.

## 3 Demixing: simulations, theory and experiments.

**OUTLOOK.** The square well (SW) model for colloidal particles, introduced in the previous chapter, is here adopted in the context of numerical simulations. This model plays a fundamental role in the colloidal gelation. Not only it can well represent both the DLCA and the RLCA kinds of aggregations, but is also prototypical for the study of more dense amorphous systems, like glasses [Dawson et al. (2001); Foffi et al. (2002); Zaccarelli et al. (2005); Krekelberg et al. (2007)], and outlines the dynamics underlying processes like crystallization or gelation. In Par. 3.1 we describe how molecular dynamics (MD) is used for SW particles.

In particular, the typical dynamics of colloidal gels is shown to be followed by the SW particles. Its simple implementation for MD simulations also makes the SW apt to fundamental and yet simple modifications, able to account for different phenomena. The possibilities offered by having different species of colloids are discussed in Par. 3.1.2: we introduce mixtures of more than one species, where the distinction and tuning of inter- and intra-species interactions may have a major role in modeling new complex composites as well as in studying their physics.

In Par. 3.2, the spinodal decomposition mechanism (see Chap. 2) is used in the present chapter for a SW model adapted for multi-component mixtures. In particular, for 2-components mixtures (2CM) the two main phase separation mechanisms, condensation and demixing, are explained in Par. 3.2.1 as unified under the common framework of spinodal decomposition. To this end, the Thermodynamic Perturbation Theory (TPT) is shortly introduced. The spinodal decomposition region of the 2CM will be shown, providing a basic proof for a possible tuning of this competition.

In conclusion of this chapter, in Par. 3.2.2 we will introduce a measure for the topology and porosity. This is a novel method that we implemented, which relies on the construction of surfaces embedding the gel branches and, consequently, on their analysis. Such a method will be used, in the next chapter, in order to characterize the arrested structures.

### 3.1 Model and Simulation Protocol

Routes that exploit spontaneous self-assembly in thermal equilibrium are important, but non-equilibrium processes offer more control - because assembly is then governed not just by

thermodynamic conditions but by the process history. Among the most promising precursors for assembling, new classes of non-equilibrium materials are colloidal particles with specific interactions. For both the experimental realizability and the theoretical approach they allow, particular importance have materials with tunable properties made up of constituents with simple geometry<sup>1</sup>. Thus, we focus on the square well (SW) potential: it is a potential of mean force, since the solvent is modeled implicitly, that well approximates the short-ranged interactions responsible for the formation of amorphous structures typical of a vast number of materials. We make use of large-scale computer simulations to explore the gelation of a mixture of SW particles.

In particular, binary mixtures of SW colloidal particles will be introduced, whose potential is the simplest implementation apt to retain the underlying physics we try to capture. The selectivity among species, as defined by means of the interaction potential itself, will play a major role. We will present the particular case of two species - hence the *binary* - but the definitions and methods we use are general and easily scalable to systems made of more components. For the 2-component mixtures (2CM), we explore the kinetic arrest that leads to the creation of amorphous soft-solid materials with a specific focus on the resulting binary, inter-penetrating gels. In what follows, we describe the simulation methods and its passage from the monodisperse system (one-component mixture, 1CM) to the system of interest made of two (or possibly more) components.

### 3.1.1 Molecular Dynamics

**FEATURES OF SW MODEL.** The molecular dynamics (MD) is a deterministic simulation technique, where initial particle positions and momenta determine their trajectories<sup>2</sup>. MD simulations can be applied to study systems following probability distributions of microcanonical ensemble (constant NVE) and the canonical ensemble (constant NVT), among others [Frenkel and Smit (2002); Hansen and McDonald (2006); Rapaport (2009)].

The numerical implementation of a model enters the description of the physics, as it is supposed to possibly retain the behavior, in our case, of a complex fluid under quench, within a coarse-grained approach. As already discussed in Par. 2.2, the SW model offers the possibility of a satisfying description, in dynamical and structural terms, of a wide range of systems with short-range attraction. The SW model in Eq. 2.6, is here re-written:

$$U_{SW} = \begin{cases} \infty & r \leq D \\ -\epsilon & D < r \leq \lambda D \\ 0 & r > \lambda D \end{cases} \quad (3.1)$$

---

<sup>1</sup>The demand for structures of increasing complexity with novel properties has triggered exploration of the self-assembly of anisotropically interacting particles [Glotzer (2004); Jackson et al. (2004); Glotzer and Solomon (2007); Blaak et al. (2007); Walther and Muller (2008); Goyal et al. (2010)].

<sup>2</sup>Unlike MD, the Monte Carlo (MC) simulation technique differs in that relies on probabilities. One of the advantages of MD over the MC is that the complete trajectories are available for analysis, and then dynamic properties of a system can be computed.

While the square well potential have an unphysical shape, it has been widely used to successfully model colloids with short range attractions [Foffi et al. (2005b); Lu et al. (2008); Gibaud et al. (2012)], since the relevant physical properties depend only weakly on the shape of the potential [Noro and Frenkel (2000)].

We fixed the diameter to  $D = 1$  and the attractive range to  $\lambda = 1.03$ , a value often used in MD simulations of square-well fluids, gels and glasses [Zaccarelli et al. (2001, 2005); Krekelberg et al. (2007)]. We recall that the chosen short-range  $\lambda$  allows to work in the theoretical framework where the Baxter stickiness parameter<sup>3</sup>  $\tau$ , defined as  $\tau^{-1} = 4(\lambda^3 - 1)[\exp(\epsilon/k_B T) - 1]$ , is related to the second virial coefficient by  $B_2^* = 1 - 1/4\tau$  (see Par. 2.2). We set  $k_B = 1$ , so that the temperature is measured in the unity of the well depth  $\epsilon$ . With the present choice,  $T = 1$  corresponds to a thermal energy  $k_B T$  equal to the attractive well depth. Time is measured in units of  $D\sqrt{m/|\epsilon|}$ . In our reduced units, we fix the Boltzmann constant  $k_B = 1$  and the mass of the particles to unity,  $m_n = m = 1$ .

**SIMULATION TECHNIQUE.** The intermolecular force is the gradient of the potential with respect to particle displacements. Along with the simplicity of implementation, the numerical simulations of SW particles have to be performed with techniques that can differ from the ones used for systems of atomic-like particles<sup>4</sup> with continuous potentials. In fact, in the extremely coarse-grained approaches of potentials with infinite derivatives, as for the SW or the even simpler hard-sphere (HS) potentials, some of the molecular dynamics schemes cannot work. Event-driven (ED) algorithms constitute a powerful and efficient MD simulation method that can be used to numerically simulate particle systems with discontinuous potentials [Rapaport (1997, 2009)]. They are often used in the study of particulate systems, such as granular materials or powders. The ED protocol only considers analytically calculable points in time, where physically relevant events occur. During a simulation, collisions are tracked in the form of events. A collision at a certain time triggers an event after a certain delay  $\Delta t$ . Events form a calendar sorted by the time when they will occur, and when all events for a particular time have been handled, the simulated time is advanced to that of the next scheduled event. After a collision, only few events will change priority, or are erased, with possible new events entering the calendar. With this scheme it is possible to circumvent the lack of finite derivatives for the SW potentials [Leegwater et al. (1989); Rapaport (2009); De Michele (2011)] and, thus, we use the ED protocol for running our simulations<sup>5</sup>.

Some labor-saving techniques exist in MD simulation for atomic like particles, which are fully applicable to the SW model. For a system of  $N$  particles, the most time-consuming part of the

<sup>3</sup>Baxter [Baxter (1968)] solved the Percus-Yevick approximation for hard spheres with a zero-range attraction,  $\lambda \rightarrow 0$ , and an infinite reduced well depth  $\epsilon/k_B T \rightarrow \infty$ . The SW model enters such an approximation if  $\lambda \lesssim 5\%$  of the diameter. A universal phase diagram for colloids with short-range attraction had been constructed that suggested that the gelation line coincides with the phase separation boundary in the Baxter model [Lu et al. (2008)].

<sup>4</sup>Atomic-like particles are simply defined by a vector indicating their center, plus a radial potential.

<sup>5</sup>Note that the event-driven technique allows “Newtonian” molecular dynamics simulations, whereas other techniques need to be used if other effects have to be accounted, like for example the Brownian simulations. However, within our coarse-grained approach, we don’t need to explicitly treat the solvent or its effects [Foffi et al. (2005b)].

### Chapter 3. Demixing: simulations, theory and experiments.

---

simulation is represented by the calculation required to evaluate which of the  $N(N-1)/2$  pair distances interact. The Verlet (or neighbour) list and the cell (or linked) list techniques are applied to speed up the force calculation [Frenkel and Smit (2002); Hansen and McDonald (2006)]. The Verlet list method works by keeping a periodically updated list of the neighbors of each particle, while the cell list works reducing the calculus of distances to portions of space considered as independent. In the particular case of ED MD, some optimizations for these algorithmic strategies have been recently introduced [De Michele (2011)].

**SIMULATING THE QUENCH.** In the context of numerical simulations, thermostats are used to provide the correct ensemble behavior, as in the NTV ensemble case of our simulations. The thermostats can be used to tune the temperature, as well as for keeping it fixed. Mimicking the effect of a *quench* is thus feasible, in simulations, by using a thermostat protocol to lower the temperature. In simulating an annealing dynamics, the simplest form of reducing the kinetic energy is by periodically multiplying the particles velocities by a scaling factor  $\lambda_T$ , defined as

$$\lambda_T = \sqrt{(T/T_i)}. \quad (3.2)$$

Particle velocities are rescaled from an instantaneous temperature  $T_i$  (measured immediately after a velocity update of the MD) to the desired temperature  $T$ , so that the resulting total kinetic energy is

$$K = \frac{3}{2} N k_B T = \frac{1}{2} \sum_n^N m v_n^2, \quad (3.3)$$

where the sum is over all the  $N$  particles of mass  $m_n = m$ . The scheme of velocity scaling used to maintain constant  $K$  is called an *isokinetic thermostat*. Of course, the same scheme can be used for modifying  $K$  at will. The velocity scaling scheme can be performed at every step, or only every a few steps, and is relatively easy to implement. It does not strictly follow the canonical ensemble, though in practice the amount it deviates from the correct NVT ensemble is quite small<sup>6</sup> (by comparison of the velocity distribution with a Gaussian).

For our simulations, we use a different, popular velocity scaling thermostat. It is that of Berendsen [Berendsen et al. (1984)]: here the scale factor is modified as

$$\lambda_T = \left[ 1 + \frac{\Delta t}{\tau_T} \left( \frac{T}{T_i} - 1 \right) \right]^{\frac{1}{2}}, \quad (3.4)$$

where  $\Delta t$  is the MD time-step and  $\tau_T$  is a constant called the “rise time” of the thermostat. The latter describes the strength of the coupling of the system to a hypothetical heat bath. Larger  $\tau_T$  correspond to weaker couplings, i.e., the larger  $\tau_T$  the longer it takes to achieve a given  $T_i'$  after an instantaneous change from some previous  $T_i$ . The time at which  $T$  is reached decreases by the same decrease factor of  $\tau_T$ .

---

<sup>6</sup>Moreover, the velocity scaling suffers the drawback of not being time-reversible, but this property becomes important only in some advanced MD techniques and behind our necessities.



**PROTOCOL FOR GELATION.** The gelation process is induced by quenching SW model colloids. Once a configuration of particles is provided, it is relaxed for a fixed amount of time to a high, equilibrium temperature  $T = 100$  (in unities of the well depth), in order to ensure both the randomness of initial configuration and its thermodynamical correct behavior. At such a temperature, the system behaves as a hard-spheres fluid. At this point, we set the desired final temperature to  $T = 0.05$  and start the quench simulation. Note that  $T = 0.05$  is well below  $T_c \simeq 0.3$ , the temperature associated to the critical point of the phase diagram for such 1CM systems of SW. See Par. 2.1.1. As it will be discussed in Par. 4.2.1, a similar protocol is applied in experiments, where the temperature of a colloidal suspension, firstly heated to an equilibrium temperature where colloids bonding is irrelevant, is lowered in such a way to ensure the rapid formation of bonds. As it happens for the experimental quenches, then, it is important to start from an equilibrium configuration, because the ageing of the aggregation process under quench would otherwise keep trace of the initial structure. The simulations are performed at very fast rate of cooling, provided by the inverse of the parameter  $\tau_T$  of Eq. 3.4, so that crystallization is avoided [Yip and Rubia (2009); Royall and Malins (2012)] and, instead, gelation can take place.

The ageing physics related to the aggregation process imposes a demanding computational effort in order to obtain a significant description of the observables. By working with out-of-equilibrium systems, in fact, it becomes incorrect to perform temporal averages during a run, as the measurements now strictly depend on the history of the specific sample. This brings to two main consequences:

1. averages must be performed on independent runs for the same state-point of the system (density, quench temperature, etc.);
2. dealing with a deterministic protocol, each run must start from an independent configuration of particles centers and momenta;
3. the simulations must stop only once the arrest of the dynamics has been attained.

Thus, various simulations must be performed for each choice of the parameters and all the NTV simulations have been performed for a total of  $N = 10^4$  particles in a fixed volume with periodic boundary conditions, and for every set of parameters we simulated 10 independent realizations.

We solved the 1<sup>st</sup> issue by providing random, independent initial configurations of particles. This required a suitable method for obtaining many starting configurations, different and independent among each other (2<sup>nd</sup> issue). The efficiency must not affect the wanted independence among the starting configurations, and some techniques exist which provide the desired amount of uncorrelated configurations. One of these consists in running one (or few) MD simulation of an initial given starting configuration at high temperature and, at time intervals where the system decorrelates completely, the relative configurations are extracted.

In turn, these will serve as starting points for the quenches. But a drawback exists for this method, especially for dense colloidal systems, where the decorrelation time increases and, as a consequence, the original single run would result too time consuming.

Instead of dealing with this sequential method, other important approaches exist in order to obtain independent starting configurations, usable in parallel. Their use results more convenient than the sequential approach, in that one can obtain independent configurations in parallel and without the analysis required to ensure the decorrelation. A popular way of generating random configurations consists in a random sequential adsorption (RSA) method of the particles into the voids [Swendsen (1981); Aste and Weaire (2008)]. Many RSA algorithms have been developed but, in particular for HS particles, they still encounter slowness problems due to high density. An alternative method consists in “growing” the system of particles of the desired diameters, randomly distributed inside a box. During the thesis, a new, fast algorithm has been developed that generates initial configurations with the “growing” approach. It generates random configurations of hard spheres by growing them starting from randomly placed points in the box<sup>7</sup>. Details of the algorithm are in Appendix C. This procedure ensures both a rapid growth of a HS system with the desired density and, starting from randomly placed points, it also ensures a complete independence between the resulting configurations. As explained in Appendix C, it does not provide exactly equilibrated configurations, so that (short) simulations at high temperatures still need to be performed, as previously described. The 3<sup>rd</sup> issue listed before, regarding the way of assuring the reached arrested phase, requires a large simulative effort, because long times for each simulated quench must be provided. This is also connected to a fundamental point in the definition of colloidal gel. Apart from the presence of a percolating cluster, the experimental feature of gels is that an arrest can be observed in its dynamics, by structure factor or other analysis<sup>8</sup>.

**ARREST OF ICM GELS.** In Fig. 3.1(left) the total potential energy  $U$ , divided by the number  $N$  of particles, is shown for runs of simulated SW ICM systems at various densities. Each curve is the average made over the 10 independent runs. In particular, as we consider short-range attractions, this ratio has the property of being proportional to the the average number of bonds that each particles shares with its neighbors, i.e.  $n_b = 2|U/N|$ . For some representative densities,  $n_b$  is shown in Fig. 3.1(right). In the specific case of Eq. 3.1, a pair of particles is considered as bound when entering the attractive range, i.e. where their relative distance is  $r < \lambda D$ . Under the simulative point of view, two colloids modeled with SW potential will rest bound, and cannot escape the attractive range, only when their kinetic energy is insufficient. Using Eq. 3.1, we can thus see that statistically a dependence is introduced on temperature  $T$ , with the term  $\exp(\epsilon/k_B T) - 1$  representing the escape (unbounding) probability.

---

<sup>7</sup>The growth method (in every Euclidean dimension) is different by respect to the usual “cherry-pit” method [Lubachevsky and Stillinger (1990); Lubachevsky et al. (1991); Kansal et al. (2002)]. It assigns to each particle a temporary interaction potential, whose range has a cutoff shorter than the desired radius,  $< D/2$ . At each step of the growing procedure, all the particles with overlapping potentials dynamically move, depending only on the overlapping neighbor particles, and are inflated accordingly.

<sup>8</sup>In Par 4.1.1, we will also use the Mean Square Displacement (MSD), another measurement commonly used - especially in simulation context - to check the occurrence of the arrest of dynamics.

Dealing with numerical simulations, we obtain from the measure of the total energy, or from the evaluation of  $n_b$ , a precious indicator of the dynamics. The fact that these two measurements reach a plateau represents a fingerprint of the occurred arrest of the dynamics. This is a first, important signature of gelation mechanism for a system of colloidal particles under quench. Another feature of gelation that we have already discussed, and that is experimentally found, is the growth and arrest of the peak value of the structure factor. This feature can be observed for the SW particles under quench, as shown in Fig. 3.2, confirming the dynamical arrest taking place for the model we use. The static structure factor is calculated using the definition (see Eq. 2.10)

$$S(q) = \frac{1}{N} \langle \rho_q \rho_{-q} \rangle,$$

where the density  $\rho_q = \sum_n^N \exp(i\vec{r}_n \cdot \vec{q})$  is defined on all particles. Averages of  $S(q)$  are calculated on up to 300 independent directions of the scattering vector  $\vec{q}$ . In the inset of Fig. 3.1 (right), the final  $S(q)$  curves for some densities are also reported. Here we note the typical dependence on density: while at local length-scales ( $qD \gtrsim 4$ ) is similar for all the densities, the peak relative to the long length-scales shifts towards higher  $q$  values. Similarly to what happens in experiments, and as discussed in Par. 2.3.2, this displacement leaves a shorter  $q$ -window where the fractal interpretation takes place.

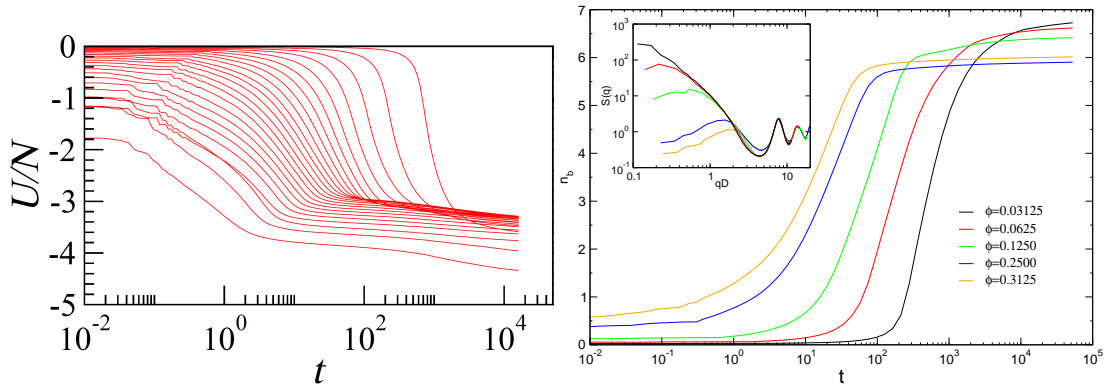


Figure 3.1: **(Left)** Curves of average energy per particle  $U/N$ , for SW systems at various packing fractions. Each curve is the average over 10 independent runs. For some of these, we shown **(right)** the average bonding value  $n_b$ : for short-ranged attraction, this is directly proportional to the total potential energy of the system,  $n_b = 2|U|/N$ . For the final, arrested configurations, we show in *inset* the corresponding structure factors  $S(q)$  (again, each curve comes from an average on configurations from independent runs). While the local length-scales ( $qD \gtrsim 4$ ) is similar for all the densities, the peak relative to the long length-scales shifts towards higher  $q$  values and leaves a shorter  $q$ -window where the fractal interpretation takes place.

Gelation here is defined to occur when the dynamics of the colloidal fluid arrests. This definition of gelation is more strict than the one that takes into account only the percolation property,

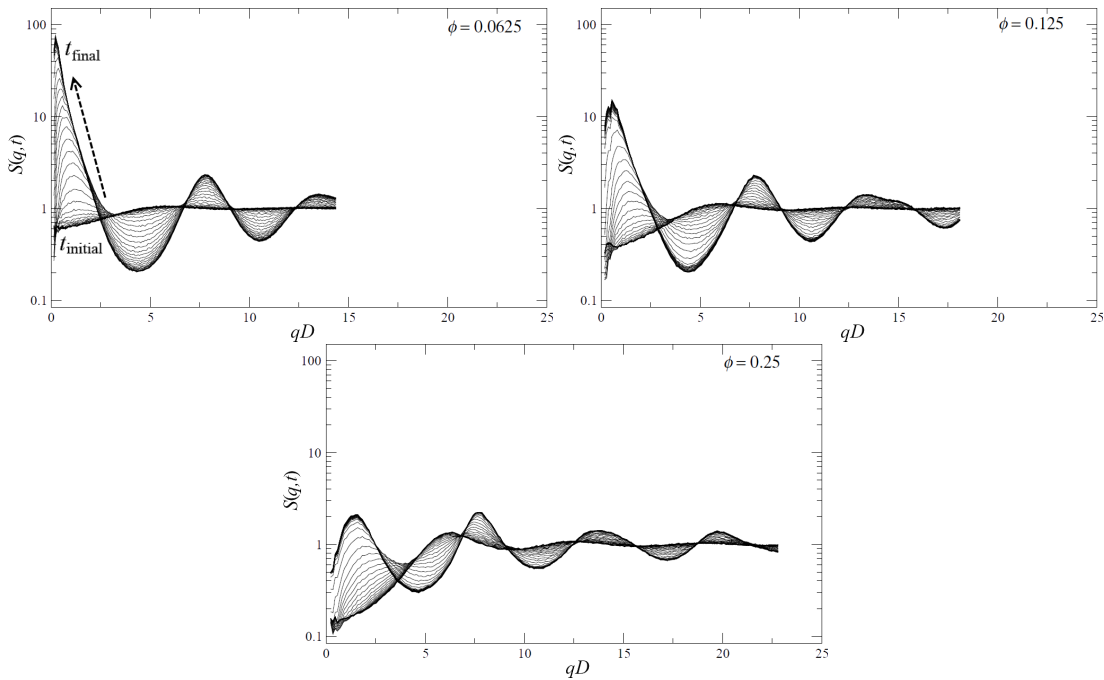


Figure 3.2: Evolution of the structure factor for the 1CM system, at densities  $\phi = 0.0625$  (**top left**),  $0.125$  (**top right**) and  $0.25$  (**bottom**). The shift (towards smaller  $q$ ) and rise (up to a stable height) of the peak relative to long length-scales (low  $q$ ) is present at each density and agrees with the experimental observations for the gelation process. This is represented, as an example, with a dashed arrow for the  $\phi = 0.0625$  case.

i.e. the stage where a network of bound particles forms a percolating cluster that spans the simulation box [Goyal et al. (2010)]. In fact, percolation may occur even at equilibrium as a transient configuration and represents, then, a necessary but not sufficient argument. On the contrary, the gelation qualified by means of arrested dynamics indicates whether the final out-of-equilibrium structure has been attained in order to match the chemical (strong) gel analogy. By definition, it is a sufficient condition that has to be guaranteed in addition to the percolation property. Operatively, a structure is considered to percolate when at least one cluster spans the whole simulation box and, replicating the box, such cluster bounds to all its replicated images<sup>9</sup>. In the framework of numerical simulations, the box has finite volume and contains a finite number of particles, thus percolation can be reached only at sufficient colloidal volume fractions. Apart when very low densities are expressly considered, this finite-size effect is typically unimportant in experiments, where the aggregation behaves more closely to the thermodynamic limit.

<sup>9</sup>See Par. 2.3.1 for details on percolation features and definition.

### 3.1.2 One to more components.

We pointed out already that distinguishing among the different species, a possibility offered by the simple and yet particular nature of a selective potential interaction, brings as a consequence to deal with “complex fluids”. The addition of a new parameter, namely the *composition parameter*  $c = N_R/N_{\text{tot}}$ , i.e. the fraction of component of a reference species R, makes the 2-component mixture (2CM) become a prototype of complex fluid, even if the model at its basis is as simple as the SW. Labeling the 2 species as R and G, and their respective numbers  $N_R$  and  $N_G$ , we have  $N_{\text{tot}} = N_R + N_G$ . The total packing fraction is

$$\phi_{\text{tot}} = \frac{\pi}{6} D^3 \frac{N_{\text{tot}}}{V}. \quad (3.5)$$

We are assuming a colloidal mixture made up of 2 components (or species), but this representation and its relative discussion can be easily enlarged considering more species into the mixture. As explained in Par. 1.1, we aim to answer the question whether it is possible to arrest fluctuations of composition, e.g. to obtain *demixing*, in the same manner or similarly to the arrest of density fluctuations for the 1-component case (1CM), e.g. *condensation*. If the arrest mechanism is the same, but with a competition between the local differences (fluctuations)  $\delta c$  or  $\delta\phi$  driving the aggregation, then for 2 (or more) components the consequent aggregation could form separate gels, made up of distinct species of colloids, sharing the same space and thus forming a double, interpenetrating gel.

**THE 2CM MODEL.** In the following we introduce a square-well (SW) model with selectivity interaction, where we can tune the inter-species interaction trying to enhance the demixing. A similar approach has been adopted in the study of eye-lens cold cataract, where the competition between condensation and demixing has been found to arise from the tuning of the interaction of the  $\alpha$ -crystalline and the  $\gamma$ -crystalline proteins (giving different transparency regimes). See Fig. 3.3.

The model we adopt uses isotropic pair-interactions, where the particles of different species interact via a hard-sphere potential coated with a short-range attractive part<sup>10</sup>. The full potential is given by:

$$U_{ij}(r_{ij}) = \begin{cases} +\infty & \text{if } r_{ij} < D \\ -\epsilon_{ij} & \text{if } D < r_{ij} < \lambda D \\ 0 & \text{if } r_{ij} > \lambda D \end{cases}. \quad (3.6)$$

<sup>10</sup>Another model has been recently proposed [de las Heras et al. (2012)], which forms bicontinuous structures. This system adopts HS particles coated with specific patchy sites instead of a shell-shaped well. Despite its great tunability, unfortunately the used patchy model do not specify interaction selectivity solely based on the species, but rather different patches with different selectivities have been proposed. Thus, our SW model can better suite the purpose of explaining, with a minimum increase in number of parameters, how to form gel structures where demix is enhanced.

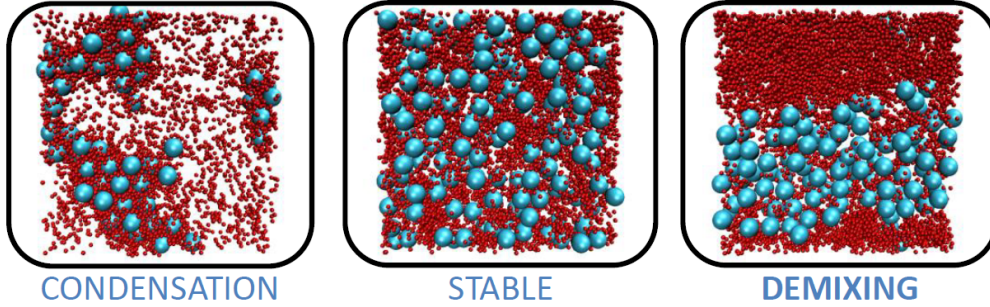


Figure 3.3: Examples of condensed (left), stable (center) and demixed (right) phases, adapted from [Dorsaz et al. (2008)]. Binary mixture of  $\alpha$  (blue, big spheres) and  $\gamma$ -crystalline proteins (red, little spheres) are simulated for different inter-species attraction strenghts. The aggregation under quench bring to different aggregation behaviors: for similar intra- and inter-species attraction (**left**), the condensation mechanism prevails, while at the opposite, demixing becomes dominant when intra-species attractions are stronger than the inter-species attraction (**right**). For a certain region of parameters, a stability among the two can be reached (**center**), in the sense explained in Par. 3.2.1. For details on this particular example, refer to [Dorsaz et al. (2008)].

From now on, we use as notation for the two species the labels  $R$  and  $G$ , i.e.  $i, j = R, G$ . As in Eq. 3.1, describing the 1-component mixture (1CM) inter-particle potential, here the diameters of the species are chosen to be the same and equal to unity, as well as the masses  $m_R = m_G = m$ , and the attractive range has been fixed to the same value  $\lambda = 1.03$ . The key parameters are now the interaction depths  $\epsilon_{ij}$ . The intra-species attraction (i.e. between like-particles) is chosen of unit depth,  $\epsilon_{RR} = \epsilon_{GG} = 1$ , while the inter-species attraction  $\epsilon_{RG}$  acts as a tuning parameter: we have chosen to make it range from the unit depth, where it recovers the 1CM system, down to the pure HS repulsion, i.e.  $\epsilon_{RG} = 0$ . With this choice of parameters, the tendency to demix due to composition fluctuations is strongly enhanced. Apart from the density  $\phi_{\text{tot}}$ , the 2CM are further characterized by the composition parameter  $c = N_R/N_{\text{tot}}$ , that corresponds to a composition  $1 - c = N_G/N_{\text{tot}}$  for the second species. For several 2-components and 1-component mixtures (2CM and 1CM), at different compositions  $c$  and densities  $\phi_{\text{tot}}$ , we have performed MD simulations with the event driven protocol. As for the 1CM case, all simulations were performed for  $N_{\text{tot}} = 10^4$  particles contained within a volume  $V$  and under periodic boundary conditions. The initial configurations for both the 1CM and the 2CM systems are prepared with the same protocol as for the 1CM case, by equilibrating independent starting configurations at high temperature  $T = 100$ . In this regime the attractive part of the interaction is negligible and the system reduces to a simple monodisperse hard-spheres fluid. Again, for every set of the chosen parameters  $c$  and  $\phi_{\text{tot}}$  we simulated 10 independent realizations.

In Fig. 3.4 the evolution of energy is shown, upon quench, for 2CM with symmetric composition  $c = 0.5$ . We note similar features to the 1CM case in Fig. 3.1 (left), but also a noticeable

difference emerges: here the arrest occurs with a final energy value that depends monotonically on the total density. Instead, in the 1CM a peak value is found around the critical value  $\phi = 0.25$ . This is one of the first differences that we point out with the classical, simple gelation case for the one-component system.

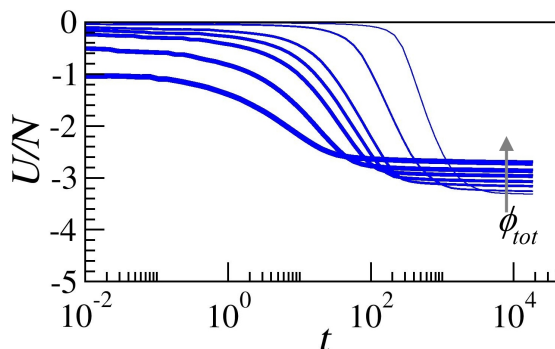


Figure 3.4: The average energy per particle is shown, as a function of time, for symmetric ( $c = 0.5$ ) 2CM at various packing fractions. In these cases, the two species equally contribute to the total density  $\phi_{\text{tot}}$ . Here  $\phi_{\text{tot}}$  ranges from 0.025 to 0.3. As for the 1CM case in Fig. 3.1 (left), three phases can be distinguished. After the temperature is lowered to the quench value, a certain delay exists before the aggregation sets in: this delay is bigger for lower  $\phi_{\text{tot}}$ . During the aggregation phase, the energy drops until it reaches a plateau. Unlike the 1CM, here we note that the plateau value increases monotonically with  $\phi_{\text{tot}}$  (where instead it has a peak around the critical density for the 1CM case). For specific comparison, see further in Fig. 4.3 and relative discussion.

**INTERPENETRATING DOUBLE GELS.** Under this protocol, the 1CM system is known to be unable to reach equilibrium, undergoing a gas-liquid transition<sup>11</sup> that eventually brings to gelation [Foffi et al. (2004)]. In the next paragraph, we will use this model within the Thermodynamic Perturbation Theory and show that the pure inter-species repulsion enhances the demixing. Before passing to the thermodynamic perturbation theory (TPT) and later to the experiments, we show here by means of simulations how the demixing actually occurs for the model we used.

Our simulations clearly show that the gelation is equally reached by the 2CM system under study. In Fig. 3.5 some configurations of a simulated 2CM system under quench are shown, at different times during the gelation process. In this example  $(\phi_{\text{tot}}, c) = (0.125, 0.5)$ . We note that the demixing takes place for these binary systems at all the simulated state points  $(\phi_{\text{tot}}, c)$ . Each one of the two species (but the same discussion applies for more components) forms a sub-gel, whose structure is arrested in a similar fashion to the 1CM case (where gelation is driven only by density fluctuations).

<sup>11</sup>Several routes to the gel state have been examined in literature, with a special emphasis on the differences and analogies with glass formations. Under this point of view, the gel state would reflect an arrested phase separation occurring when the phase-separation dynamics generate regions of local density sufficiently large to undergo an attractive glass transition [Foffi et al. (2005b); Manley et al. (2005)].

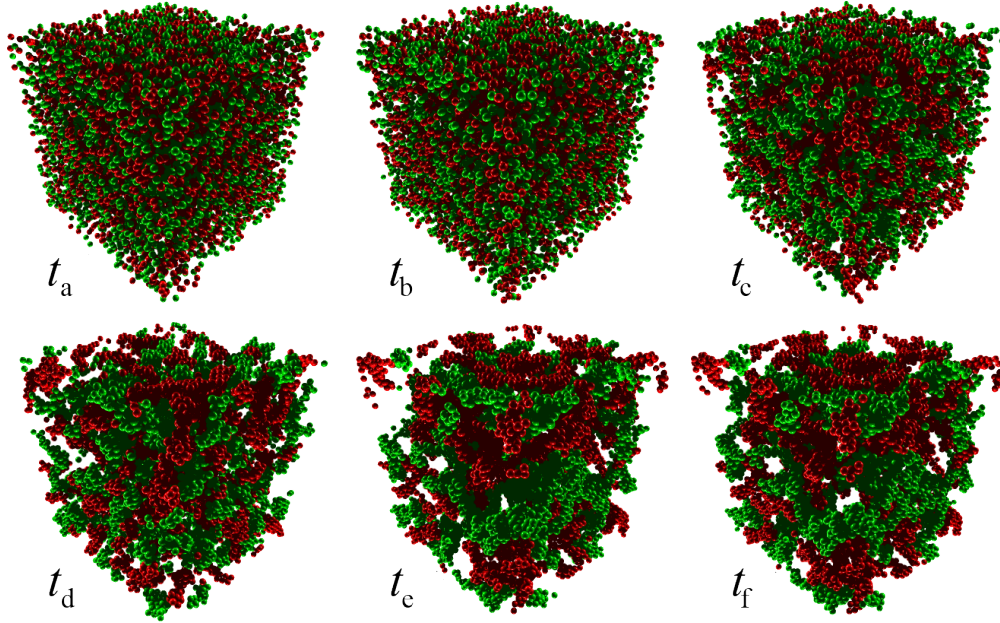


Figure 3.5: 3D renderings of configurations during the quench for a symmetric (i.e. composition  $c = 0.5$ ) 2CM of SW model colloids. The total packing fraction (density) is  $\phi_{\text{tot}} = 0.125$ . The average bonding evolution for this state point is shown - as green curve - in Fig. 3.4. During a run, the configurations  $t_i$  are sampled in logarithmic times as  $t = 0.01 \times 1.3^{t_i}$ . Here we show  $t_a = 20$ ,  $t_b = 30$ ,  $t_c = 35$ ,  $t_d = 40$ ,  $t_e = 50$  and  $t_f = 60$ . For  $t < t_a$  the time-sampling is too fine to notice structural changes, as can be noted also from the corresponding behavior in energy at the early stage. Afterwards, the aggregation takes place and the local differences (fluctuations) in composition and density compete ( $t_a \lesssim t \lesssim t_d$ ). Only undulations of the arms take place on long time-scales, for  $t > t_d$ , without disrupting the structure. The configuration stabilizes in a gel-like configuration with interpenetrating arms belonging to the two sub-gels, each one made up solely by one species.

## 3.2 TPT and topology

### 3.2.1 Condensation vs. Demixing.

**MODIFYING THE PHASE DIAGRAM.** Moving from one component fluid to binary mixtures considerably enhances the complexity of the phase behavior. In addition to the gas-liquid phase separation observed in one component systems, such binary mixtures can also undergo a demixing transition<sup>12</sup>.

Thus, even in the case of a 2 component mixtures (2CM), a fundamental increase in complexity is expected. Despite the practical and conceptual differences, however, a mechanism of dynamics arrest similar to that of the 1CM scenario can be envisaged for 2CMs, and in general

<sup>12</sup>In recent years, the study of demixing and its properties have revealed their importance in physical systems belonging to domains distant from soft matter, as disparate as for example in giant magnetoresistivity, Bose-Einstein condensates, microfluidics and cold trapped atoms [Menyhard et al. (2000); Trofimov et al. (2002); Hellweg et al. (2003); Akdeniz et al. (2006-06-01)].



for mixtures made by components of different species. The composition  $c = N_R/N_{\text{tot}}$  must in fact be specified in addition to the overall packing fraction  $\phi$ . As stated by the Gibbs' phase rule, the phase diagram of binary mixtures can present several coexisting phases, critical lines and higher order critical points. The system's free energy being also a function of  $c$ , the thermodynamic instabilities are consequently driven by both density and composition fluctuations. In the 2CM, two coexisting phases can have different compositions and densities. We recall that the phase separation is called condensation or *demixing*, depending on whether the two phases differ more in density or composition, respectively. We will show that it is possible to arrest composition fluctuations, within the same theoretical framework, similarly to density fluctuations to obtain gelation.

The phase diagram is determined by the competition between gas-liquid and mixing-demixing phase separation [Pini et al. (2003)]. The presence of an additional degree of freedom, the relative composition of the two species, considerably widens the spectrum of critical behaviors. The phase diagram topology is very sensitive to the precise combination of the parameters that characterize the interactions between the components. For mixtures of particles with short-ranged attractions belonging to different species ( $R$  and  $G$  in the 2CM case) a quantitative investigation of the phase diagram is still lacking. We used thermodynamic perturbation theory (TPT) to conduct the stability study for the 2CM of Eq. 3.6.

Note that the set of parameters would be enriched even further by considering mixtures with more than two components. For the binary mixture with equal attraction range  $\lambda$  but tunable strengths, in fact, it is possible to tune intra-species interactions ( $\epsilon_{RR}$  and  $\epsilon_{GG}$ ) and the inter-species interaction ( $\epsilon_{RG}$ ) for a total of three possible interaction parameters. However, increasing the number of components  $n$ , the number of tunable parameters would rapidly grow as  $n \cdot (n + 1)/2$ , offering a large palette of interaction patterns to explore. However, our 2CM system with  $\epsilon_{RR} = \epsilon_{GG}$  and  $\epsilon_{RG}/\epsilon_{RR} = 0$  is already expected to produce the desired shift in aggregation mechanism, introducing the competition of demixing and condensation. In this sense, this colloidal fluid represents the essential particle model, although defining a complex fluid, able to show such a behavior<sup>13</sup>.

Our attempt relies on reducing drastically the parameter space, considering equal sizes, equal intra-species interaction ranges, equal interaction strengths between like particles ( $\epsilon_{RR} = \epsilon_{GG}$ ), and a ratio of the interaction strengths between unlike species set to  $\epsilon_{RG}/\epsilon_{RR} = 0$  is introduced.

**THERMODYNAMIC PERTURBATION THEORY.** The TPT for monodisperse short-range fluids was proved able to describe the phase diagram of colloidal particles interacting by depletion interactions [Gast et al. (1983)] and this theory was used to understand the interplay between phase coexistence and the glass line [Foffi et al. (2002)]. More recently, TPT has been used in the study of protein aggregation linked to the cold cataract formation in eye-lenses [Dorsaz

<sup>13</sup>It has been suggested that purely entropic effects can have a major role in driving demixing [Dijkstra and Frenkel (1994)] (for a system of coarse-grained hard-core repulsing particles that differ in size). For sake of completeness, then, we used the same simulation protocol also for 2CMs made up of a SW component and a HS component, i.e.  $\epsilon_{GG} = 1$ ,  $\epsilon_{RR} = 0$ ,  $\epsilon_{RG} = 0$ . We will name this further system as SW+HS and present this system as a term of paragon, for reasons that will be clear in the next chapter.

(2009)]. Even if the perturbative approach is known to give quantitatively imprecise results near phase boundaries and near criticality<sup>14</sup>, in principle the method is applicable to general mixtures for which the convergence of integral equation based methods is still out of reach. The TPT allows the determination of the instability surface (the spinodal) and also gives important insights into the coexistence boundaries (the binodal). This preliminary theoretical study will open the way to study the gelation process based on the connection between the fluctuation driving the aggregation and the final, arrested structures for which they are responsible (this connection will be more explicitly treated in Par. 4.1.2). The spinodals of the 2CMs are computed using a thermodynamic perturbative approach [Hansen and McDonald (1986); Barker and Henderson (1967)] in the TPT framework.

The traditional descriptions of liquids or colloidal systems uses the fact that the intermolecular pair potential can be split into two parts: a steep, short range repulsion and a smoothly varying longer range attraction. It is now well accepted that the way in which the molecular hard cores pack determines the structure of most simple liquids, at least at high density, while the attractive interactions give rise to a uniform background potential which provides the cohesive energy of the liquid, but has little effect on its structure [Hansen and McDonald (1986)]. A further simplification consists in modeling the steep repulsion present when the distance between the particles is small by effective HS interactions and the attractive part of the interaction is treated as a perturbation of the reference system.

We assume that the interactions between particles are pair-wise additive and that the system is homogeneous. The TPT consists in computing the effect of the perturbation on the thermodynamics and the pair distribution function of the reference system via an expansion in power of the inverse temperature [Hansen and McDonald (1986)]. The general stability picture of the 2CM case is expected to be independent of the approximations used (approximations for the second and higher order terms have also been proposed) and a first order approximation is certainly sufficient for the purpose of the present study.

The idea of TPT consists in deriving the equation of state of the interacting system by treating the attractive potential  $u_{ij}(r)$  (where the indexes  $i$  and  $j$  may refer to the two species  $R$  or  $G$ ) as a perturbation of the hard-sphere (HS) potential  $u_{ij}^0(r)$ . This leads to an expression for the Helmholtz free energy, which can then be analyzed to find the instability boundary and the phase diagram.

The equation of state of the interacting system is derived by treating the attractive potential  $\epsilon_{ij}(r)$  as a perturbation of the hard-sphere potential. For the first order case, the Helmholtz free energy  $F$  reads

$$\frac{F - F_0}{Nk_b T} = \frac{1}{2} \rho \beta \sum_{i,j=1}^2 c_i c_j \int \epsilon_{ij}(\mathbf{r}) g_{ij}^0(\mathbf{r}) d\mathbf{r} + O(\beta^2) \quad (3.7)$$

---

<sup>14</sup>Within perturbation theory it is possible to reproduce the main phase diagram topologies obtained from Hierarchical Reference Theory (HRT), Mean Spherical Approximation (MSA) or Grand Canonical Monte Carlo (GCMC) approaches [Pini et al. (2003); Kofinger et al. (2006); Wilding et al. (1998)].

where  $F_0$  and  $g_{ij}^0(R)$  are the free energy and the partial radial distribution function of the unperturbed system. The overall number density is defined by  $\rho = (N_R + N_G)/V = 6\phi_{\text{tot}}/(\pi D^3)$  and the relative composition of the two species by  $c_i = N_i/N_{\text{tot}}$ . Details of the TPT calculation of the 2CM can be found in [Dorsaz et al. (2008); Dorsaz (2009)].

The Helmholtz free energy per particle,  $f$ , is used to express two alternative conditions of thermodynamic stability for a binary mixture in terms of its partial derivatives [Tisza (1977)]:

$$\left\{ \begin{array}{l} f_{cc} > 0 \\ \text{and} \\ f_{vv} - \frac{f_{vc}^2}{f_{cc}} > 0 \end{array} \right. \quad \text{or} \quad \left\{ \begin{array}{l} f_{vv} > 0 \\ \text{and} \\ f_{cc} - \frac{f_{vc}^2}{f_{vv}} > 0 \end{array} \right. \quad (3.8)$$

where  $f_{\mu\nu} \equiv \frac{1}{2} \left( \frac{\partial^2 f}{\partial \mu \partial \nu} \right)_T$ ,  $f_{\mu\mu} \equiv \frac{1}{2} \left( \frac{\partial^2 f}{\partial \mu^2} \right)_{T,\nu}$  ( $\mu, \nu = v, c$ ), and  $v = \rho^{-1}$  is the volume per particle.

We used the Boublik-Mansoori-Carnahan-Starling-Leland (BMCSL) equation of state for the free energy of the binary hard-sphere reference mixture  $F_0$  [Carnahan and Starling (1969); Boublik (1970); Mansoori et al. (1971)] and the partial radial distribution  $g_{ij}^0(r)$  functions were computed solving the Ornstein-Zernike equations with the partial direct correlation functions  $c_{ij}(r)$  of the binary mixture obtained by Lebowitz within the Percus-Yevick (PY) approximation [Lebowitz (1964)]. In order to correct the shortcomings of the PY hard sphere distribution functions (the values at contact  $g_{ij}^0(d_{ij})$  and the slopes  $g_{ij}^0{}'(d_{ij})$  are both too small in magnitude) we used a generalization procedure for mixtures [Verlet and Weis (1972); Henderson and Grundke (1975)]. (Refer to Smith et al. (2008) for the computational approach to the radial pair distribution function, using the Verlet-Weiss procedure, for hard spheres.) In order to determine if the instability is mainly driven by mechanical or material fluctuations (i.e. density  $\rho$  or composition  $c$  fluctuations) one can diagonalize the stiffness or *stability matrix* [ $f$ ] (i.e. the matrix of the partial derivatives of  $f$ ) through an orthogonal change of basis [Tisza (1977); Chen and Forstmann (1992)].

In one-component systems, the inverse of the isothermal compressibility  $\chi_T^{-1} \equiv (\partial^2 f / \partial v^2)_T$  is a primary stability indicator and vanishes as the instability - called *mechanical instability* - is reached. It occurs when density fluctuations become infinite and, for 1CM, it is responsible for the usual gas-liquid phase transition. In binary mixtures, the system might become mechanically unstable without the inverse of the corresponding compressibility  $\chi_{T,c}^{-1} \equiv (\partial^2 f / \partial v^2)_{T,c}$  vanishing, i.e., this stability indicator is no longer a unique quantity in binary mixtures. Besides mechanical instability, strong composition fluctuations can lead to demixing, i.e. a separation of the system into phases of different composition. In this case  $(\partial^2 f / \partial c^2)_{T,v}$  is a material stability indicator that diverges as the instability boundary is reached (and the corresponding primary stability indicator is provided by  $(\partial^2 f' / \partial c^2)_{T,p}$ ). Except in special cases, both mechanical and material instabilities will in general appear simultaneously.

We consider a non-orthogonal transformation which allows to relate the eigenvalues of the quadratic form to physically meaningful quantities [Tisza (1977); Ursenbach and Patey (1994)].

The normalized eigenvectors can be written as

$$\vec{z}_{\pm} = \begin{pmatrix} x_{\pm} \\ y_{\pm} \end{pmatrix}$$

and have correspondent eigenvalues  $\lambda_{\pm}$ . See Fig. 3.6.

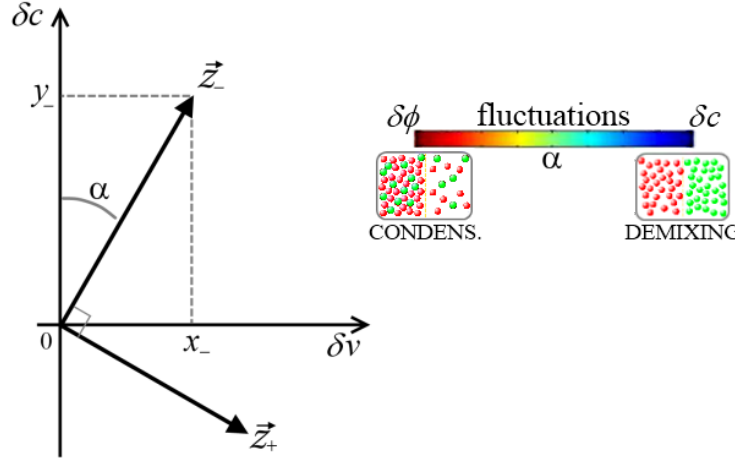


Figure 3.6: Schematic view of the orthonormal vectors  $\vec{z}_{\pm}$  and the stability indicator  $\alpha$ . The instability will be predominantly of demixing type when  $\alpha$  is close to 0 and of condensation type when  $\alpha$  is close to  $\pm\pi/2$ . The abscissas represent fluctuations of the volume per particle,  $v = \rho^{-1}$  (thus related to fluctuations in density  $\phi$ ), while the ordinates represent fluctuations in composition  $c = N_R/N$  of the reference species  $R$ .

The nature of the instability is then characterized by the angle

$$\alpha = \arctan\left(-\frac{f_{vc}}{f_{vv} - \lambda_-}\right) \quad (3.9)$$

where  $\lambda_-$  is the smallest eigenvalue of the stability matrix ( $\lambda_+$  being the largest). At an instability boundary, the determinant  $\det[f] \equiv \lambda_- \lambda_+$  vanishes, i.e. the stability matrix becomes singular. The border of a stability region is thus indicated by the smallest eigenvalue  $\lambda_-$  going to zero. The above relation holds for  $[f]$  non diagonal ( $f_{vc} \neq 0$ ). The angle  $\alpha$  between the eigenvector corresponding to  $\lambda_-$  and the axis representing fluctuations of composition, acts as a stability parameter: it indicates whether composition or density fluctuations dominate (from  $\alpha = 0$  to  $\alpha = \pm\pi/2$  respectively). This formalism was first introduced by Chen and Forstmann [Chen and Forstmann (1992)] to characterize the instability of binary mixtures as an alternative to the Bhatia-Thornton partial structure factors [Bhatia and Thornton (1970)], the latter being less suited when fluctuations in both density and composition are taking place at the same time. This can be visually rendered with a color gradient, whose palette

goes from the extreme of dominating demixing,  $\alpha = 0$ , to the opposite extreme of dominating condensation,  $|\alpha| = \pi/2$  (see Fig. 3.7).

**DRIVING THE SPINODAL DECOMPOSITION.** The results for a binary mixture of SW colloidal particles with different inter-species attraction strengths are shown in Fig. 3.7. The spinodal surfaces, evaluated as a function of temperature  $T$ , density  $\phi$  and composition  $c$ , indicate boundaries between the stability and instability regions of the phase diagram. Moreover, the calculation indicates whether the system is more prone to condensation (density fluctuations) or demixing (composition fluctuations). This information is encoded by means of a color gradient in Fig. 3.7. For identical inter-species and intra-species attractions the result is trivial (Fig. 3.7, top) and corresponds to 1CM. In this case, the diagram is invariant with respect to a change of  $c$  and only  $\phi$  fluctuations are predicted to drive the spinodal separation. As soon as the inter-species attraction is reduced, however, a demixing region emerges around the symmetry line  $c = 0.5$  (Fig. 3.7, center). When the mutual attraction is completely eliminated, (Fig. 3.7, bottom), a pronounced demixing region takes over most of the spinodal surface. The 1<sup>st</sup> order TPT calculation is shown in Fig. 3.7 for the spinodal separation for the SW binary model introduced in Par. 3.1.2. The stability parameter  $\alpha$ , indicating which kind of fluctuations are driving the phase separation, is encoded with colors: it is blue when  $c$ -fluctuations dominate (demixing), while it is red when the instability is driven by the density fluctuations (L-V transition).

The behavior in Fig. 3.7 is general as it takes place whenever a selective interaction between species exists: if the particles of one specie aggregate prevalently with them of the same specie, we could then build up a system when the demixing is enhanced. Later we will present an experimental setup for obtaining colloids with such a selectivity and we will subsequently use a model which retains the main physics. The structures obtained with molecular dynamics simulations will be analyzed, focusing on the characterization of the 2CM structures in comparison with the 1CM fluid.

#### 3.2.2 Porosity.

**ARREST OF PHASE BOUNDARIES.** Large colloids, such as emulsion droplets, can also be used to mimic granular systems, and eventually some of the techniques applied in this field can be fruitfully used in the study of the arrested phase separation underlying the gel formation. Fluid-fluid phase separation occurs in emulsions, rapidly followed by slow coarsening of the two phases. While the initial phase separation is too rapid to be observed by confocal microscopy, the subsequent coarsening process follows a three-stage process: interfacial-tension driven coarsening, gravity driven flow and finally interface formation [Aarts et al. (2005)]. The shape of the meniscus formed by the interface gives an estimate of the interfacial tension  $\gamma$  between the two fluid phases [Aarts (2005)] that is extremely low ( $\gamma \sim 0.2 \mu\text{N m}^{-1}$ ), especially when compared to fluid-fluid interfaces of molecular liquids (the air-water interfacial tension

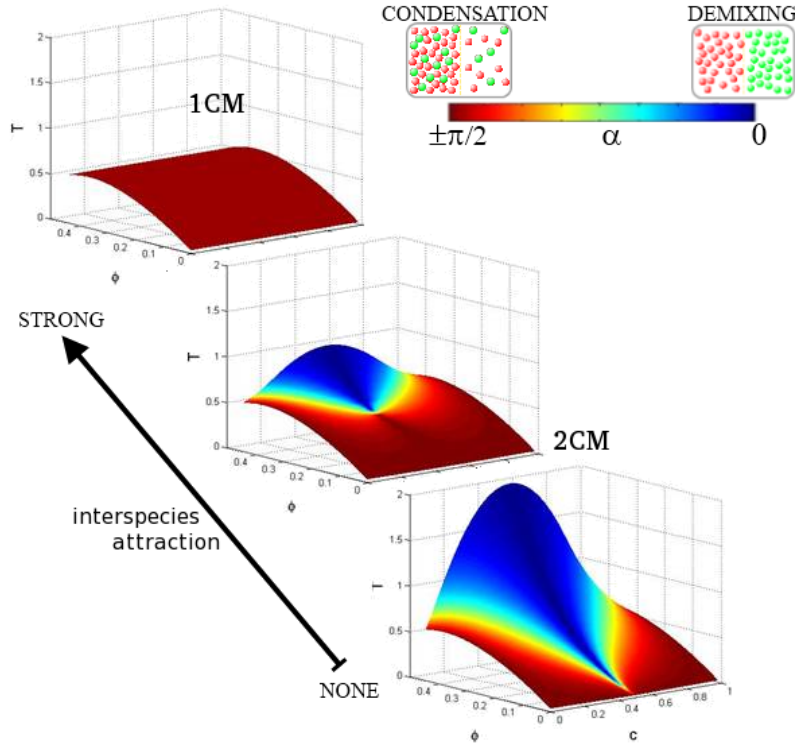


Figure 3.7: Thermodynamic perturbation theory (TPT) calculation of the instability region boundary (spinodal surface) for 3 cases: a single-component mixture ( $\epsilon_{i \neq j} = \epsilon_{ii}$ , 1CM) and two binary mixtures, 2CM, with residual inter-species attraction ( $\epsilon_{i \neq j} = 0.5$ ) and without inter-species attraction ( $\epsilon_{i \neq j} = 0$ ). The colors represent the fluctuation angle  $\alpha$  (see text) and express whether the gas-liquid phase separation is driven more by the density (red) or composition (blue) fluctuations.

is of order  $\gamma \sim 50 \text{mN m}^{-1}$ ). The consequence of such low interfacial tension is that thermal fluctuations can create undulations, or roughness, at an interface<sup>15</sup> of order  $\sim \sqrt{k_B T / \gamma}$ . Studies on bicontinuous mixtures have triggered new methods and techniques, especially related to the problem of characterizing the medium under the point of view of the porosity. In Fig. 3.8 a schematic representation is depicted of a microscopic structure of the system during the gel life time, whose arms are embedded in a surface, so to mimic bicontinuous fluids. First of all the bicontinuous network resulting from spinodal decomposition exhibits quasi-ordered concentration fluctuations, characterized by a wavelength  $\xi_m$  which accounts for the maximum at  $q_m$  in  $I(q)$  (or  $S(q)$ ). It is not straightforward to relate the geometry of the surface to its topology and, at last, to a quantification of the porosity.

The bicontinuous network also explains the regular distribution of bright and dark regions

<sup>15</sup>A density mismatch between the solvent and colloid can also create thermal capillary waves at the interface. The characteristic capillary length  $\xi \sim \sqrt{\gamma / g \Delta \rho}$ , which is in the  $\mu\text{m}$  regime, and the time scale associated with the decay of interfacial fluctuations  $\tau \sim \xi / \gamma$  is of the order of seconds for colloidal systems. Hence, these thermal capillary waves can be observed by confocal microscopy, as was done by [Aarts et al. (2004); Aarts (2007)].

visible in optical micrography [Verhaegh et al. (1997)]. The Porod tail  $q^{-4}$  of  $I(q)$ , typically observed from scatterers with smooth surfaces [Glatter (1991)], also typical of spinodal decomposition, is due to the interfaces between colloid-rich domains and the colloid-poor domains. Note that the Porod law is observed at  $q$ -vectors smaller than those expected for the scattering from the particle surfaces. Indeed, non-fractal colloidal aggregates exhibiting Porod behavior have already been reported in reversible aggregation condition [Broide et al. (1993)]. The model of spinodal decomposition driven gelation also accounts for the turbidity behavior since this depends on the optical contrast between the two phases<sup>16</sup>.

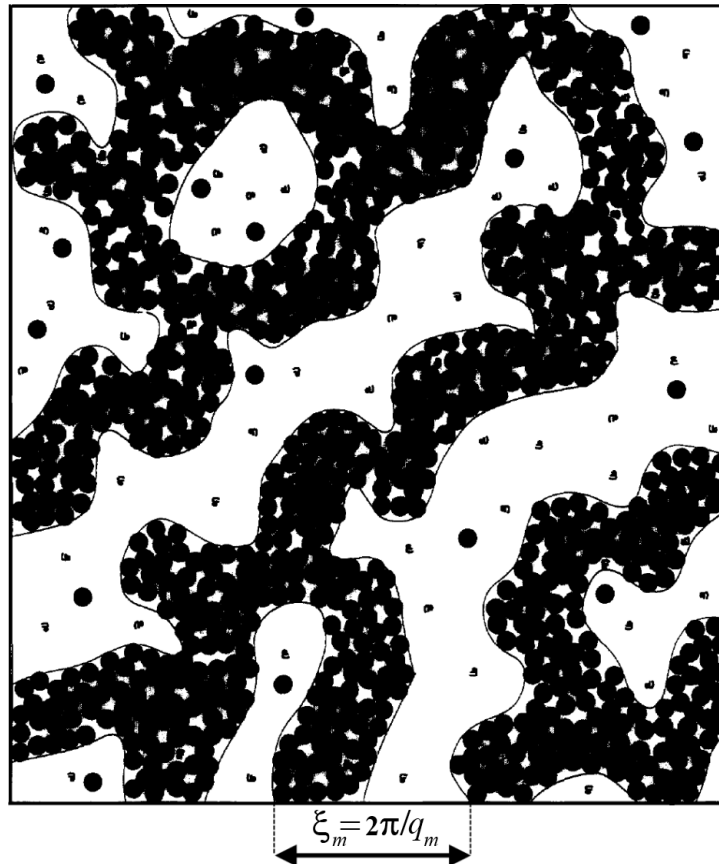


Figure 3.8: Schematic representation of a bicontinuous network, endowed with a characteristic length scale  $\xi_m$  (wavelength of concentration fluctuations, which is inversely proportional to  $q_m$ ). Colloid-rich and colloid-poor domains are separated by sharp interfaces, explaining the Porod decay in the scattering intensity at high wave vector. The colloid-rich domains consist of a percolated colloidal structure. Adapted from [Verhaegh et al. (1997)].

**SURFACE RECONSTRUCTION AND ANALYSIS.** Different methods have been devised for the study

<sup>16</sup>The turbidity increases during the gel formation because the amplitude of the concentration fluctuation, and thus the optical contrast grows (Fig. 6 of [Verhaegh et al. (1997)]). Accordingly, when the gel is formed, it attains a plateau value. Furthermore, when the system is macroscopically phase separated the turbidity in both phases is lower than in the initial stages of the process.

first, and the analysis later, of interfaces. In the case of colloidal particles under aggregation, however, and particularly for simulations where no explicit solvent is accounted for, there is not an obvious, identifiable surface. Thus a new method has been enhanced and implemented during the thesis, that relies on the construction of a fictitious surface that is built so to tightly embed the arms of the gel structure. From the analysis of this surface, non-trivial information on both the overall structure (for example porosity) and the local features (for example arm's thickness) can be extracted.

The basic technique has been used in the investigation of boundaries in surfactant phases. The calculations are based on a single scalar  $\Phi(\vec{r})$  which describes the local oil-water concentration difference [Belushkin and Gompper (2009)]. The geometrical properties of the boundaries are evaluated on the isosurface  $\Phi(\vec{r}) \equiv 0$ , which thus defines the position of the surfactant amphiphilic (mono)layer. The elastic properties of such layer can be described by the Canham-Helfrich Hamiltonian [Canham (1970); Helfrich (1973)]

$$\mathcal{H} = \int dA [\tau + 2\kappa(H - c_0)^2 + \bar{\kappa}K] ,$$

where  $\tau$  is the surface tension,  $\kappa$  is the bending rigidity,  $\bar{\kappa}$  is the saddle-splay modulus,  $c_0$  is the spontaneous curvature, and  $H$  and  $K$  are the mean and the Gaussian curvatures, respectively. The integration extends over all the layer surface. For each point  $\vec{r}$  on a surface  $A$ , the main curvatures are defined as  $C_1(\vec{r}) = 1/R_1$  and  $C_2(\vec{r}) = 1/R_2$ , where  $R_1$  and  $R_2$  are the minimum and maximum radial measures, respectively, of how the surface bends in different directions at the  $\vec{r}$  point. See Fig.3.9. The mean and the Gaussian curvatures are defined as

$$H(\vec{r}) = \frac{C_1 + C_2}{2} , \quad K(\vec{r}) = C_1 C_2 . \quad (3.10)$$

Because of the unmatched unities, a direct comparison with the Gaussian curvature can be carried out by considering the mean squared curvature:

$$H^2(\vec{r}) = \left( \frac{C_1 + C_2}{2} \right)^2 . \quad (3.11)$$

Due to the oil-water symmetry in balanced microemulsions, the spontaneous curvature  $c_0$  vanishes. The surfactant monolayer corresponding to the isosurface  $\Phi \equiv 0$  is extracted as a triangulated surface using the GNU Triangulated Surface Library [Popinet (2000–2010)]. The distributions of the mean square curvature,  $H^2$ , and of the Gaussian curvature,  $K$ , are calculated for the isosurface.

The surfactant monolayer is very well described by a minimal surface. Therefore the  $H^2 dA$  term vanishes and the Canham-Helfrich Hamiltonian is extended by including higher-order terms in  $K$  [Bruinsma (1992)], so that

$$\mathcal{H}_1 = \int dA [\bar{\kappa}K + \bar{\bar{\kappa}}K^2] ,$$



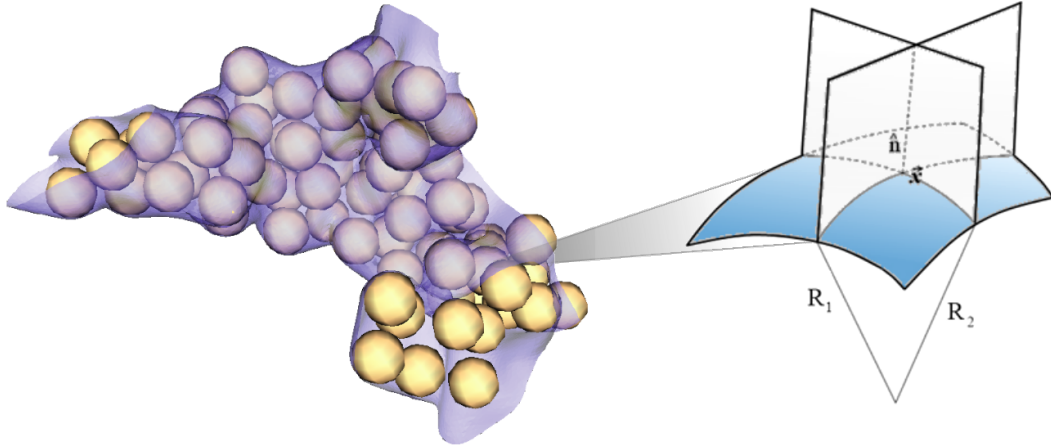


Figure 3.9: **(Left)** Surface enveloping the underneath arm portion of a model gel. **(Right)** The surface reconstruction enables the study of its local features through the principal curvatures  $C_1(\vec{r}) = 1/R_1$  and  $C_2(\vec{r}) = 1/R_2$ , generally defined for every point on the surface. In our case of a discretized surface, the curvatures can be defined for every discrete face  $\delta A$  by differentiating the neighbor normal directions  $\delta \hat{n}$  (see text).

where the surface tension term  $\tau dA$  has been neglected by considering the isosurface  $\Phi \equiv 0$  as a liquid membrane. For minimal surfaces the Gaussian curvature  $K \leq 0$  on the whole surface. The requirement that minimal surfaces of non-planar configuration be stable leads to  $\bar{\kappa} > 0$  such that the second term is negative. In order for the Hamiltonian to be stable with respect to the creation of infinitely narrow necks ( $K \rightarrow -\infty$ ) the last term has to be positive, thus  $\bar{\bar{\kappa}} > 0$ . For a fixed value of  $\bar{\kappa}$ , the value of  $\bar{\bar{\kappa}}$  is determined by the length scale of the unit cell such that the cubic phases are local minima of  $\mathcal{H}$ .

Approaches based on the Canham-Helfrich Hamiltonian have been shown to be related to the Ginzburg-Landau free-energy functional approach, and the elastic constants  $\kappa$  and  $\bar{\kappa}$  of the curvature energy have been calculated in terms of the parameters of the Ginzburg-Landau theory [Gompper and Zschocke (1991, 1992)]. In this case, the negative value for the surface tension value,  $\tau < 0$ , sets the normalization of the Hamiltonian  $\mathcal{H}$ . Moreover, the elastic constant  $\bar{\kappa}$  can be set in such a way that it takes into account the minimization of the Hamiltonian for  $\bar{\bar{\kappa}} = 0$ , and finally this results in

$$\mathcal{H}_2 = \int dA [\tau + \bar{\kappa}K + \bar{\bar{\kappa}}K^2],$$

where now  $\tau < 0$ ,  $\bar{\kappa} < 0$  and  $\bar{\bar{\kappa}} > 0$ .

**THE EULER CHARACTERISTIC.** In the specific case in which spherical particles are considered to bond together if within a certain range  $d \leq (1 + \Delta)D$ , the construction of the surfaces embedding the aggregate particles has to be devised in such a way that a unique surface links bonded colloids. Only after this construction process, every analysis is possible.

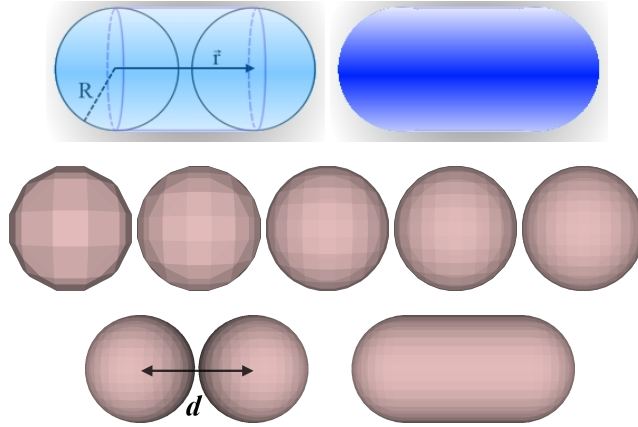


Figure 3.10: **(Top row)** The construction of the enveloping surface (of the gel arms) is made by 1) putting a cylinder among every couple of colloids at distance lower than a specified bonding value, 2) defining a scalar field  $\Phi(\vec{r})$  that is positive inside the cylinders and spheres and negative outside, 3) calculating the isosurface  $S|_{\Phi(\vec{r})=0}$  of the field. Finally, 4) a space gridding is used to discretize the surface. **(Central row)** Surface reconstruction of a single sphere at various gridding refinements. **(Bottom)** Surface reconstruction of a cylinder starting from two close enough (bonded) spheres.

For the surface reconstruction, we adopt the following space-filling procedure: each unbound colloid is represented by a sphere, and each pair of bound colloids is assumed to be connected by a cylinder. Next, we define a distance function  $\Phi(\vec{d})$  which is a scalar field representing the shortest distance from any point in space  $\vec{d}$  to the structure, namely the center of a colloid for unbound colloids or the axis of a cylinder for bound colloids. The scalar field  $\Phi(\vec{d})$  linearly decreases, from a positive value, equating 0 at distance  $R$ , i.e. the colloidal radius. The distance function results positive inside and negative outside the constitutive elements (spheres or cylinders). Then, the enveloping surface is computed at the isosurface  $\Phi(\vec{d}) \equiv 0$  of the scalar field. Once it has been calculated for all the cylinders and all the remaining spherical caps, plus the complete spheres associated to non-aggregated particles, then the surface triangulation is performed starting from a 3D grid of the space. On the top of the triangulation, faces rest defined, whose average area strictly depends on how refined is the space gridding. Some examples are shown in Fig. 3.10.

Once the triangulated surface is defined, it is possible to calculate the principal curvatures  $C_1$  and  $C_2$  at any point on the surface by finite differences (implemented in the Gnu Triangulated Surface library, GTS). In turn, this allows the calculation of mean squared and the Gaussian curvatures,  $H^2$  and  $K$  respectively.

A peculiar way of characterizing porosity can be introduced that uses such quantities. In fact, an important *topological invariant* is known to be evaluable based on them. It is the *Euler Characteristic* (EC),  $\chi$ , a quantity which provides a connection between the geometry and the topology of surfaces:

$$2\pi\chi = \int K dA + \int k_g dl, \quad (3.12)$$

where the left integral is made on the overall surface  $A$ , and the right one is made on its contour  $l = \partial A$ , i.e., on the possible line that defines the boundary of  $A$  if it is not closed. The  $k_g$  factor is called the geodesic curvature. In particular, the EC measure is sensible to the presence of voids and saddles of the surfaces, that are strictly related to pores and branching points, respectively, belonging to the gel structure. This measure can be directly related to the porosity in the case of amorphous structures, like gels, as already pointed out for dipolar colloidal gels [Miller et al. (2010)]. Moreover, the fact that EC is a topological invariant means that its value remains the same for a configuration under shear or other topological transformations, provided that no breaks are caused to the structure.

As we do not apply periodic boundary conditions to the surface reconstruction procedure, but instead, we assume that the colloidal structure is embedded in empty space, the opened surfaces that introduce boundary lines are suppressed. As a result, the contribution to the Euler characteristic from the boundary can be omitted. Only closed surfaces remain and thus  $\chi$  is evaluated using the Gauss-Bonnet theorem as the integral of only the Gaussian curvature over the closed surface:

$$\chi = \frac{1}{2\pi} \int K dS . \quad (3.13)$$

Note that this method is not limited to the gel structures. On the contrary, it is a general approach particularly suitable for every system where surfaces can be explicitly defined. Restraining ourself to the field of colloidal aggregation, the unique limit to the use of such technique is the request for the positions and sizes (and possibly a bonding distance) of the colloids, so that imaging procedures like the confocal microscopy result particularly important (see Appendix B). This allows to univocally estimate the porosity of the structure and, as a side-product, the distribution of  $K$  can also be used to evaluate what are the main features of the embedding surface. More examples, from the calculations on the gels obtained by MD, will be discussed and showed in the Par. 4.1.3.



## 4 Results: BiGels from arrested demixing.

**OUTLOOK.** In this chapter the main results of the thesis are presented, for both the simulations and the experiments, and with particular emphasis on the former. We will show that it is actually possible to arrest fluctuations of composition (demixing) in the same fashion to the arrest of density fluctuations for the 1CMs (condensation). Refer to Par. 3.1.2 for the relative discussion. Also, we will quantify the differences arising when arrested demixing prevails on condensation. Most of the analysis methods used here have been previously introduced in Chapt. 2.

In Par 4.1.1 the Mean Squared Displacement will be used for the description of the arrest as well as the average bonding. The 1CM-2CM comparison is reported both for the dynamics and for the final, arrested structures. The analysis are focused on the differences with the 1CM gelation. The comparisons will highlight aspects of the physics of the gelation process. A particular focus is reserved to the symmetric 2CM, i.e. with composition parameter  $c = 0.5$ . In fact, the equimolar binary mixture with both (selectively) attractive species represents the system where demixing is maximized for all the volume fractions (see for example Fig. 3.7 and relative discussion). The arrested structure formed by the symmetric 2-component mixture is what we call a *BiGel*.

We will use the Structure Factor (introduced in Par. 2.3.2) and another, nodal observable, concerning the arrested gel structures, will be used too: the Euler Characteristic is quantified in order to characterize the porosity of the 1CM gels and 2CM BiGels. In order to unveil the role of steric effects on aggregation, we will also compare a SW+HS system, that enriches the picture concerning the aggregation in presence of a second component.

Finally, the experimental setup of colloidal spheres coated with specific DNA strands will be revised, in Par. 4.2. By enabling the desired selective interactions, they constitute the first, reliable system for testing the aggregation of the multi-component SW model. The binary mixtures of DNA-coated colloids, experimentally investigated, will be shown to actually form BiGels, the proof of concept for the arrested demixing.

## 4.1 BiGel: numerical simulations.

We study the kinetic and structural characteristics of 2CM aggregates and discern the main differences or similarities with gels made of only 1 component (1CM). We address this study by means of extensive computer simulations. Quenches of 2-component mixtures (2CM) of SW particles with selective attraction are performed at temperature  $T = 0.05$ . Details on the model and relative parameters are in Par. 3.1.1. Various state-points after the quench, performed for different densities  $\phi_{\text{tot}}$  and relative compositions  $c$ , are analyzed in what follows.

Although demixing is observed at all densities, we clearly distinguish two regimes. In the vicinity of the single-component regime,  $c \approx 0$  or  $c \approx 1$ , the majority species percolates and forms a gel structure, while the other one forms isolated clusters. Several spatial configurations of the arrested 2CM structures obtained from simulations are shown in Fig. 4.1 for different compositions and Fig. 4.7 also for different densities. In particular, in the left panel of Fig. 4.1 the passage from the monodisperse 1CM arrested system to a symmetric ( $c = 0.5$ ) 2CM system is also schematized (for a total packing fraction  $\phi_{\text{tot}} = 0.15$ ).

Close to the symmetric composition,  $c \approx 0.5$ , interpenetrating branching is observed, and each species forms an independent gel. Composition fluctuations act on relatively short time scales compared to the arrest, thus each of these sub-gels contains only one species. We name this novel material composed of two arrested interpenetrating gels a *BiGel*. In the the right panel of Fig. 4.7, a BiGel realization (with  $\phi_{\text{tot}} = 0.125$ ) is shown. We will show that the arrested demixing, understood as a result of arrested phase separation, is responsible for the BiGel formation, and we will describe the sub-gels structuration in comparison with the monodisperse case.

As for a simple gel, the structure is more open at lower densities and becomes compact at higher densities. At the highest density investigated here,  $\phi_{\text{tot}} = 0.5$ , there are no more density inhomogeneities, in agreement with the behavior observed in gels [Foffi et al. (2005a)]. Bigels, however, significantly differ from gels because the two species are always completely demixed.

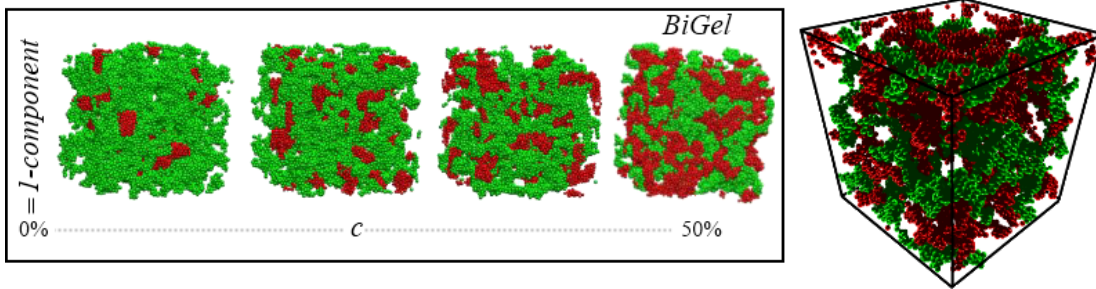


Figure 4.1: **(Left)** Some sketches of final structures, after quench, of 2-component mixtures ranging from the 1CM ( $c = 0$ ) to the symmetric 2CM ( $c = 0.5$ ). The total packing fraction is  $\phi_{\text{tot}} = 0.15$ . In all the cases,  $\epsilon_{RR} = \epsilon_{GG} = 1$  and  $\epsilon_{RG} = \epsilon_{GR} = 0$ . **(Right)** We call a BiGel the final, arrested structure obtained with the symmetric 2CM. In this case  $\phi_{\text{tot}} = 0.125$ .

### 4.1.1 Dynamics and arrest.

For the purpose of sorting out similarities and differences between aggregates of 1CM and 2CM, we simulated 1CM systems at packing fraction  $\phi$  and 2CM systems at the double packing fraction,  $\phi_{\text{tot}} = 2\phi$ . We focus on the symmetric 2CM, with relative composition  $c = 0.5$  of the two species. In this paragraph we will also focus on the description of three representative densities:  $\phi_{\text{tot}} = 0.125, 0.25$  and  $0.5$  (corresponding to  $\phi = 0.0625, 0.125$  and  $0.25$ , respectively), i.e. the same already used for Fig. 4.5.

**MSD AND AVERAGE BONDING.** The slowing down of the kinetics, due to quench, is often investigated by means of a dynamic quantity that allows the actual description of the arrest: the *mean squared displacement (MSD)*. This is calculated<sup>1</sup> as

$$MSD = \langle |\vec{r}(t) - \vec{r}(0)|^2 \rangle_N, \quad (4.1)$$

where the brackets indicate the average over the  $N$  particles and  $\vec{r}(t)$  is the position of a particle at time  $t$  after the quench (supposed to occur at  $t = 0$ ), i.e. for times after which the energy has stopped to decay. For a 1CM system it is  $N = N_{\text{tot}}$ , while it is  $N = N_{\text{tot}}/2$  when the single species of a  $c = 0.5$  2CM are considered. Thus, the kinetic of the process that - after the quench - makes the system undergo a phase separation and subsequent arrest, is briefly presented in Fig. 4.2. Here, the comparison of the arrest for single components of the symmetric 2CM is shown, together with the *MSD* for the relative 1CM systems at half packing fraction  $\phi = \phi_{\text{tot}}/2$ .

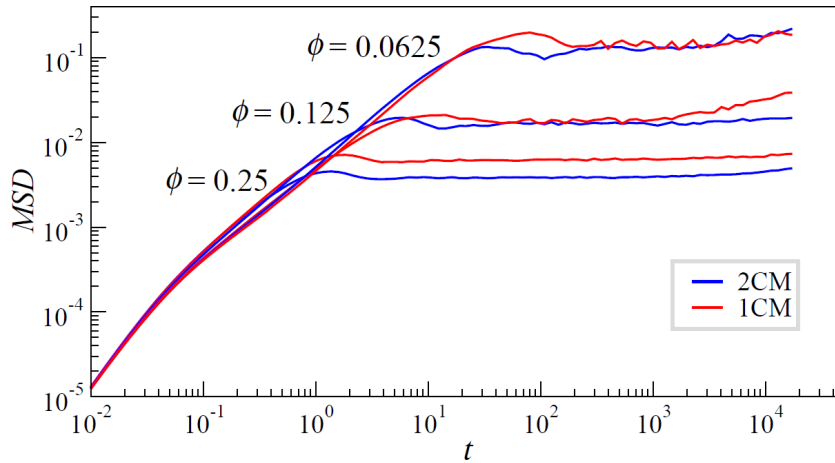


Figure 4.2: The Mean Squared Displacement (*MSD*), during the quench, for the reference total densities  $\phi_{\text{tot}} = 0.125, 0.25$  and  $0.5$ . The *MSDs* of monodisperse 1CM at densities  $\phi = \phi_{\text{tot}}/2$  are compared with the *MSD* of the single species of the relative symmetric 2CMs.

<sup>1</sup>This quantity is one of the most important observables of dynamics. For fluids, it is related to the self-diffusion coefficient  $D_0$  through the Einstein equation  $D_0 = \lim_{t \rightarrow \infty} \langle |\vec{r}(t) - \vec{r}(0)|^2 \rangle / 6t$ . Moreover, its derivative is linked to the velocity auto-correlation function  $\langle \vec{v}(t) \cdot \vec{v}(0) \rangle$  by the Green-Kubo relation  $MSD = 2 \int_0^t d\tau (t-\tau) \langle \vec{v}(t) \cdot \vec{v}(0) \rangle$ .

## Chapter 4. Results: BiGels from arrested demixing.

---

Each curve results from averaging over independent runs. Moreover, for the symmetric model (with interaction wells  $\epsilon_{RR} = \epsilon_{GG} = 1$  and  $\epsilon_{RG} = \epsilon_{GR} = 0$ ) we can distinguish among the two species  $R$  and  $G$ , and the average is performed in this case also over the two components. We can clearly see from the *MSD* that the single components (blue curves) of the binary system arrest in the same fashion as the monodisperse system (red curves). This comparison also highlights some slight differences. For example, a clean separation exists, in the case of high density  $\phi = 0.25$ , and such a separation shrinks for lower densities; a small drift can be also observed for the lowest densities, affecting the 1CM more than the 2CM also at  $\phi = 0.125$ . In general, the 2CM systems present a quench dynamics that arrests faster than the correspondent 1CM: this is also observed in Fig 4.5 and is due - as increasing densities are considered - to the presence of a second species. The aggregation of a sub-gel from 2CM at density  $\phi_{\text{tot}}$  is similar to that of the gel obtained from the 1CM at half density  $\phi$ , but similarities decrease as a result of the reduced available space and to the HS interaction with the other sub-gel.

The slowing down of the dynamics, testified by means of the *MSD*, shows that the particles move only at very short times, exploring the space of bonds. For longer times, the plateau indicates that the formed structure is arrested and can only explore a limited space. The height of the plateau similarly decreases with  $\phi$ . In a similar fashion, the energy starts to level out after a first drop, and the system is extremely slowed down. Differences in aggregation can be then observed also by means of the average bonding per particle  $n_b$ , linked to the energy of the system, previously introduced in Par. 3.1.1 (in Fig. 3.1 for the 1CM). For the three representing densities, this is shown in Fig. 4.3. Here, apart from the plateau emerging and its bigger separation for higher density, the difference in aggregation characteristic time is also evident by comparing the sub-gels (of symmetric 2CM) and the relative 1CM gel.

A BiGel corresponds to the structure obtained from the arrest of the symmetric ( $c = 0.5$ ) 2-component mixture. As a consequence of the different aggregation mechanism, demixing in competition with condensation respectively, the arrest into gel-like structures shows then peculiar features affecting not only the local length-scales (which affect  $n_b$ ) but also the percolation.



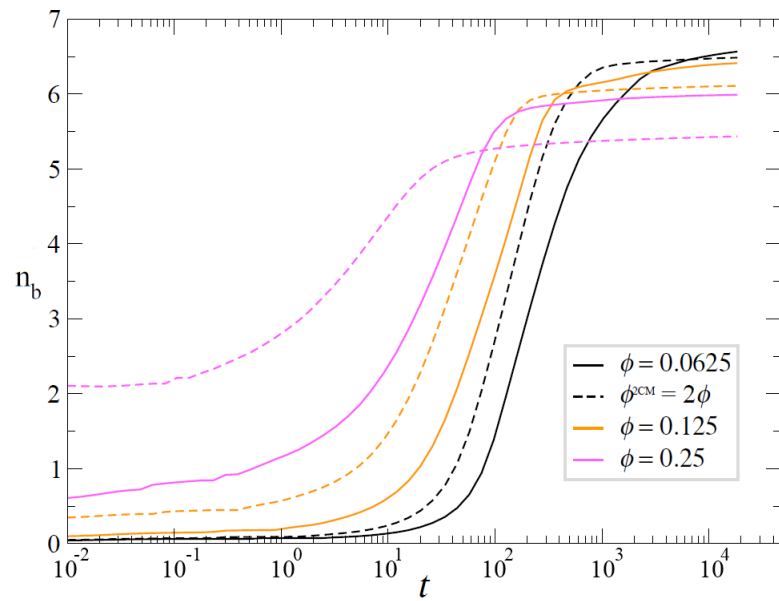


Figure 4.3: The evolution of the aggregation is easily readable from the average number of bonds,  $n_b = 2|U|/N$ , for 1CM (continuous line) and 2CM (broken line) at the same densities as in Fig. 4.2. This quantity is directly proportional to the potential energy per particle. The curves for the 2CMs, for total packing fraction  $\phi_{\text{tot}}$ , are clearly different from both the related 1CMs at  $\phi = \phi_{\text{tot}}/2$  and the 1CM with overall density equal to the 2CM's,  $\phi = \phi_{\text{tot}}$ . This result, together with the monotonicity of the final energy value for the 2CMs (see Par. 3.1.1 and Fig. 3.1), represents a difference with 1CM systems and with its aggregation process.

### 4.1.2 Percolation as fingerprint.

In Par. 2.3.1 we described the way (wrapping) percolation is analyzed in the context of numerical simulations. Here the results are shown for its application to the 2CM configurations. An average over 10 independent runs for various compositions  $c$ , but fixed total packing fraction  $\phi_{\text{tot}} = 0.15$ , highlights in Fig. 4.4 how the aggregation differs for different compositions. In this figure the values of the size of maximum cluster, normalized by the population  $N_i$  associated to the species<sup>2</sup> (dependent on  $c$ , where  $i = R$  or  $G$ ), are reported as a function of time during the quench. The maximum of cluster sizes is a possible indicator of gelation [Wessel and Ball (1992); Manley et al. (2004); Laurati et al. (2009)]. The value  $N_{\text{cluster},i}^{\text{max}}/N_i$  quantifies the number of particles of the species  $i$  forming the maximum cluster, divided by the number of particles belonging to that species. In this cases, the green lines correspond to the most relatively populated species (increasing in thickness as  $c$  goes from 0.5 to 0.85), while the red lines represent the second species of the mixture (correspondingly, decreasing in thickness as  $1 - c$  goes from 0.5 to 0.15).

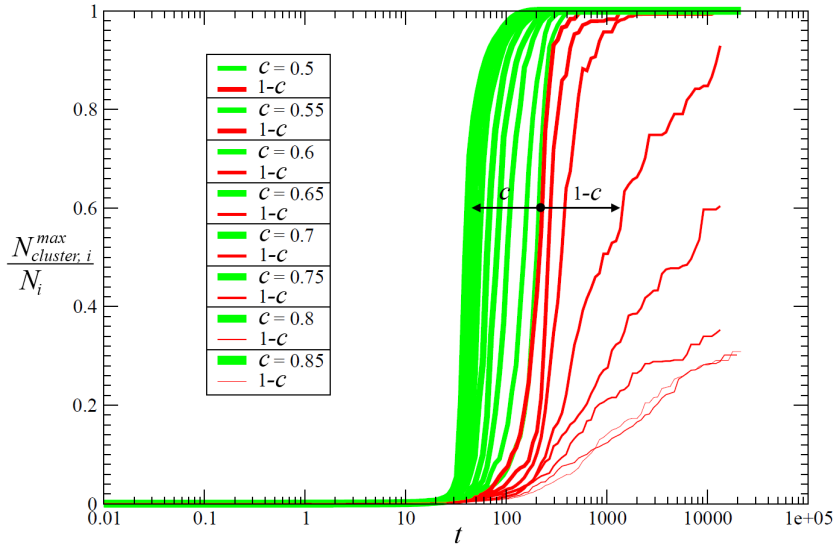


Figure 4.4: Evolution of the biggest cluster present in the system during the quench. The 2 distinct species of 2CM systems are presented, all at total density  $\phi_{\text{tot}} = 0.15$  but with different compositions. The green curves refer to the dominant species,  $c$ , while the red to the other species,  $1 - c$ . They reveal a distinct time-scale for aggregation: the dominant species aggregate faster at increasing  $c$  (thicker lines); instead the  $1 - c$  species pass from a regime where it ends up forming a percolating structure ( $1 - c \lesssim 0.4$ ) to a regime where isolated agglomerates are formed into the matrix formed by the dominant species ( $1 - c \gtrsim 0.45$ ). The change in regime strongly depends on the overall density, as later depicted in Figs. 4.6 and 4.7.

Note that some of the red curves interrupt at a value  $N_{\text{cluster},R}^{\text{max}}/N_R < 1$ , indicating that the

<sup>2</sup>The total population, sum of the two species, is  $N_{\text{tot}} = 10^4$ .

particles of the corresponding species do not form a unique cluster: as illustrated by Fig. 4.1 (left), the red species can end up in isolated clusters, trapped in the matrix formed by the most populated species. This depends also on differences in the aggregation time for the two species: the most populated species ( $G$  in this examples) reach a steady, unique cluster made up by all the  $G$  particles in times shorter by 1 – 2 orders of magnitude compared to the  $R$ , less populated species. Thus, the fast structuration of the  $G$  aggregate results in a slowing down in the aggregation of the  $R$  particles<sup>3</sup>.

A differentiation in aggregation time is obtained also for fixed composition  $c$  and varying packing fractions  $\phi_{tot}$ . In particular, we show in Fig. 4.5 the comparison between the 1-component mixture ( $c = 0$  or  $c = 1$ ) and the symmetric 2CM case ( $c = 0.5$ ), for three representative total packing fractions. We consider  $\phi_{tot} = 0.125, 0.25$  and  $0.5$  for the 2CM symmetric systems (blue curves), and  $\phi = \phi_{tot}/2$  for the corresponding 1CM systems (red curves). The thickness of the curves in Fig. 4.5 is increased at increasing density.

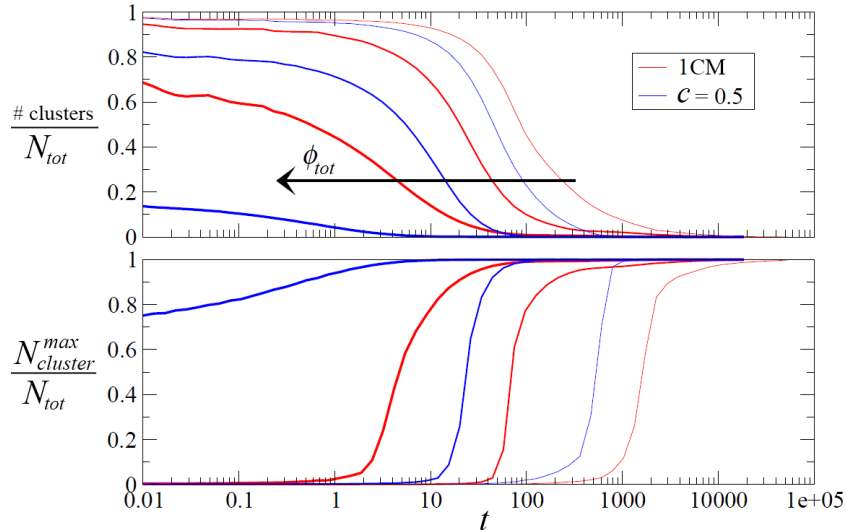


Figure 4.5: **(Top)** Evolution of the number of clusters present during the aggregation, for the same systems and representative densities  $\phi_{tot} = 0.125, 0.25$  and  $0.5$  (corresponding to  $\phi = \phi_{tot}/2$  for the 1CM). Thicker lines represent denser systems. The 1CM and symmetric 2CM systems reveals a different time-scale of aggregation: the single species of the 2CM aggregate faster than the corresponding monodisperse counterparts. This can be easily addressed to the presence of the second species, that constraints through steric effect (HS repulsion) the other species. **(Bottom)** The same kind of evolution is revealed by following the size of the biggest cluster present in the system.

As expected, shorter aggregation times correspond to higher packing fractions. In particular,

<sup>3</sup>From the interrupted red lines, however, it is not clear whether the less populated species would eventually be able to form a unique cluster for longer times, but the morphology indicates that it is unlikely that the isolated clusters could touch, at least for the total density considered here (in any case, the low quenching temperature prevents these clusters from spontaneously disrupt).

## Chapter 4. Results: BiGels from arrested demixing.

---

we show in the bottom of the figure the evolution of  $N_{cluster}^{max} / N_{tot}$  during the quench, where now  $N_{cluster}^{max}$  is the maximum size of clusters of the system and  $N_{tot}$  the total population. In the top of the figure, instead, we measure the ratio of number of clusters over  $N_{tot}$ : when close to 1, this ratio indicates that mostly monomers (unbound particles) are found, while the value  $1/N_{tot}$  (that would have 0 value in the thermodynamic limit) represents the existence of a unique cluster.

Note that the binding is defined by means of the attraction potential: for the 2-component case this means that a cluster can belong to one species or the other, but no clusters can contain both. From the curves resulting from the representative packing fractions, the different structural evolution clearly arises for the binary case and its monodisperse counterpart, manifesting a much shorter aggregation time for the 2CM system. This is essentially due to the presence of a second species, meaning a higher occupation of space and, given the selective attraction, in turn this brings to a more rapid encounter of particles of the same species<sup>4</sup>. Orders of magnitude in time difference, finally, can be obtained in the aggregation as packing fraction is increased, for both the 1CM and the symmetric 2CM cases.

We previously defined a BiGel the arrested structure formed by a symmetric ( $c = 0.5$ ) 2-component mixture. To further characterize and distinguish the BiGels, we investigate the percolation properties of the arrested structure as a function of  $c$  and  $\phi$ . The possibility of identifying the two species gives access to further information. In particular, here we study the occurrence of percolation in the final, arrested state after the quench. If just one of the clusters spans the simulation box, we consider the system as percolating, but we can make a distinction: if only one out of the two species percolates (red *or* green), then we have *single percolation*; instead, when both species form percolating clusters (red *and* green), then we speak of *double percolation*. As discussed before, in the former case of single percolation, the non-percolating species forms isolated clusters that are trapped within the cavities of the gel formed by the other component.

This analysis reveals three different types of arrested structures. Below roughly 5% in density, most of the final configurations are made of disconnected clusters and no gel is observed, in agreement with previous observations from simulations in 1CM systems [Foffi et al. (2005a)]. Experimentally this finite size effect is absent. At higher densities, single percolation is always observed. Symmetrically respect to the  $c = 0.5$  composition (BiGel), double percolation emerges in the high density region. This behavior is depicted in Fig. 4.6. Here the bars give the information of the statistical occurrence of percolation: for each state-point ( $c, \phi$ ), 10 runs are performed and thus the height of the bars reflect whether all the samples at a given state-point give percolation (max height) or just a fraction of them (smaller height). We also used the symmetry around  $c = 0.5$  to have better statistics, as the systems are symmetric in nature by exchange of the labels  $R$  and  $G$ .

---

<sup>4</sup>This mechanism differs for the asymmetric 2CM, where  $c \neq 0.5$ , as explained before (the dominant species aggregate faster and the other is fragmented and trapped in its cavities).

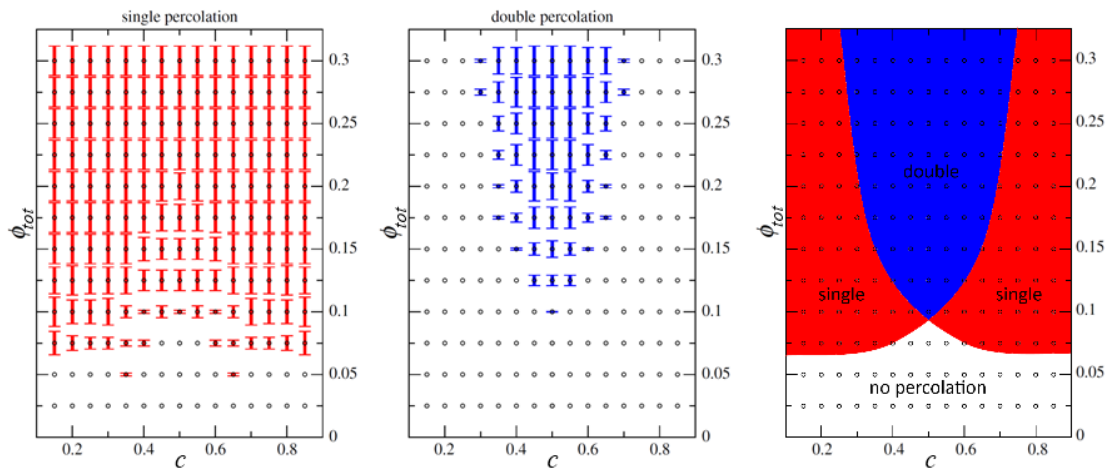


Figure 4.6: The percolation probability of 2-component mixtures (2CM) after quenching. Each circle represents the simulated parameters ( $c, \phi_{tot}$ ). **(Left)** The probability is calculated for one of the two species to percolate. The maximum height of the bar, for example at high density, corresponds to having 100% of percolation probability of at least one species: *single species percolation*. **(Center)** Bars are also used to visualize the percolation probability of both the species at the same time: *double percolation*. **(Right)** The first two diagrams for single and double percolation is schematically resumed in three principal regions. We note that while at low densities,  $\phi \lesssim 0.05$ , there is no percolation (probably due to finite effects), at intermediate densities the single species percolation is favored in systems with unbalanced populations of the two species (see also Fig. 4.4). At high densities at least one of the two species has formed a percolative structure. The double percolation results favored when the two populations are numerically in balance, close to the symmetric composition  $c = 0.5$ .

From these results it is clear that the BiGels correspond to 2CM arrested cases where it is more likely to find double percolation. These different, emerging regimes of percolation can be related to the spinodal surface of Fig. 3.7 (bottom), whose top view is redrawn in Fig. 4.7. In fact, the nature of the percolation at the simulated state-points closely reflects the TPT calculations. The interplay between the fluctuations in composition and in density gives rise to the different regimes: when the  $c$ -fluctuations prevail (demixing), both the components tend to percolate, whereas only one component percolates when density fluctuations dominate (condensation). This indicates how the underlying thermodynamic instabilities influence the final arrested structure. From Fig. 4.7 it is evident that the role of composition fluctuations is predominant at  $c = 0.5$  (BiGel). Several snapshots of such simulated systems are also shown in Fig. 4.7 (left) for different densities. We also indicate with a white star the state-point correspondent to the experimental realization studied before (Par. 4.2): compatibly with the experimental constraints due to the imaging techniques, it is chosen to stay in the region of maximal demixing (symmetric composition) that is also accessed by means of simulation without the drawback of strong finite size effects (which affects the evaluation of percolation for smaller packing fractions).

Since we are interested in the scenario where demixing can be enhanced and maximized, that

corresponds to the double percolation region around  $c = 0.5$ , in the remainder of the chapter we will focus on this symmetric case.

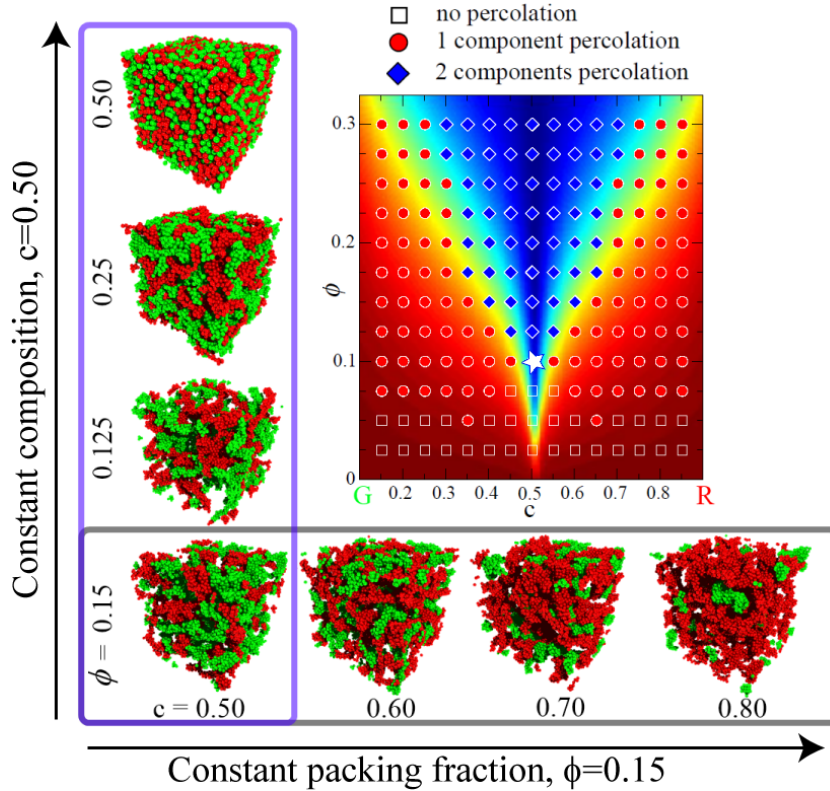


Figure 4.7: Percolation properties of the 2-component mixtures with potential wells  $\epsilon_{RR} = \epsilon_{GG} = 1$  and  $\epsilon_{RG} = \epsilon_{GR} = 0$  after quenching: each point represents the simulated parameters  $(c, \phi_{\text{tot}})$ . Blue diamonds indicate percolation of both species, red circles indicate percolation of only one species, squares indicate no percolation. The white star indicates the experimental value. The  $(c, \phi_{\text{tot}})$  phase diagram obtained with thermodynamic perturbation theory (same as in Fig. 3.7) is shown for comparison: a top view of it is used in the  $(c, \phi_{\text{tot}})$  plane obtained from simulations. Their correspondence indicates that both the species percolate when composition fluctuations drive the arrested phase separation. Snapshots of BiGels are shown for various compositions ( $\phi_{\text{tot}} = 0.15$ , **bottom**) and densities ( $c = 0.5$ , **left**).

### 4.1.3 Arrested Structure of the BiGel.

We now turn to the study of the geometry and the topology for the arrested structures of the 1CM (gel) and the symmetric 2CM (BiGel). For sake of simplicity, we use the three reference densities as in the previous paragraph. To understand the structural analogies between a BiGel and a 1-component gel, we will focus on BiGels at a total density  $\phi_{\text{tot}}$  and compare their two components separately (sub-gels) with gels at density  $\phi = \phi_{\text{tot}}/2$ . For the BiGels, we take advantage of the  $c = 0.5$  symmetry and evaluate the partial structure factors of the two species separately.

We employ two methods to investigate the structural properties, which provide complementary information. First, we consider the static structure factor  $S(q)$ , which gives an insight into the mass distribution at different length scales. Then we will use our method of surface reconstruction and we will evaluate the Euler Characteristic (see Par. 3.2.2) of the gel and single sub-gels of the BiGels. This latter method gives information about the topology and, hence, on the porosity of the structures. The analysis are carried out also for the attractive species (SW) of the symmetric mixtures of SW+HS particles, in order to provide further information on the steric effects due to the presence of a second species.

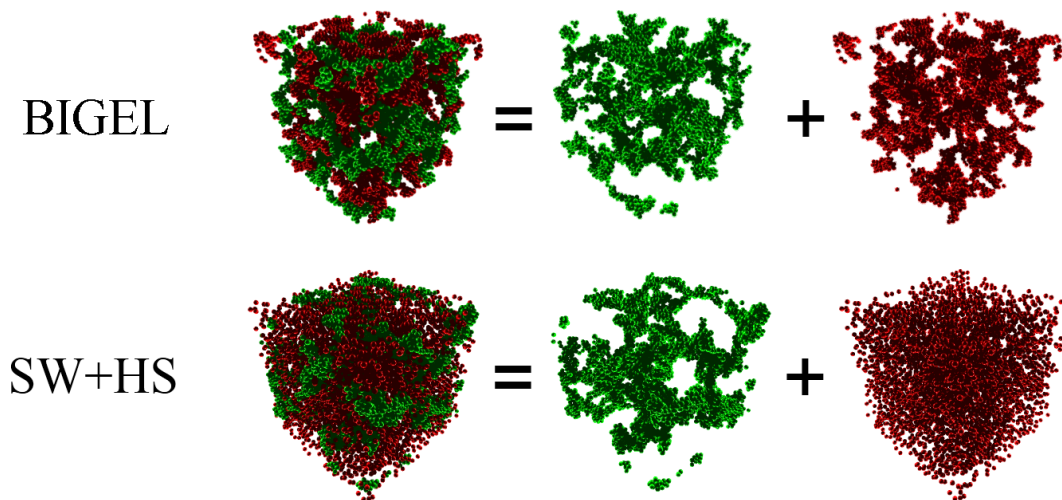


Figure 4.8: **(Top row)** An example of SW+HS variant of the 2CM system. The 3D rendering shows the decomposition of the two species, where the attractive SW part forms a gel-like structure, while the HS part remains dispersed. **(Bottom row)** The same decomposition for the BiGel (symmetric 2CM), where the two species both form a connected branched space-spanning structure. The two single components parts result from the demixing induced by the selective potential among species.

**BIGEL AND STERIC EFFECTS.** The presence of a second species influences the aggregation because of the excluded volume. It is not clear whether such a steric effect is directly due to the aggregation of the second species, or if it can be established even in absence of a second sub-gel. In order to test the possible effect of a second species which do not aggregate, but

that only causes an excluded volume, we use a variation of the symmetric 2CM. Along with the usual symmetric 2CM (whose arrested structure is called a BiGel), we have simulated another symmetric ( $c = 0.5$ ) 2CM where only one of the two components has intra-species attraction (SW), while the other component interacts solely with hard-sphere (HS) potential. This system has model parameters  $\epsilon_{GG} = 1$ ,  $\epsilon_{RR} = 0$  and  $\epsilon_{GR} = \epsilon_{RG} = 0$  (see Par. 3.2.1) and we call it SW+HS. An example of the arrested SW+HS system is shown in Fig. 4.8 together with an example of arrested BiGel. The same quench protocol is used for this model, as the one adopted for the BiGels and the 1CMs.

**STRUCTURE FACTOR.** This quantity can be measured in scattering experiments and it is directly related to the Fourier transform of the radial distribution function [Hansen and McDonald (2006)]. Structure factors have been discussed in the context of gels both for experiments [Carpinetti and Giglio (1992); Poulin et al. (1999); Cipelletti et al. (2000); Segré et al. (2001); Lu et al. (2008)] and simulations [Foffi et al. (2005b); Zaccarelli et al. (2008); Del Gado and Kob (2010); De Michele et al. (2011)]. The results for three representative densities are shown in Fig. 4.9. In all these cases, the structure factor of the gels agrees in a semi-quantitative fashion with the structure factor of the BiGels.

A difference in the local peak between the gels and BiGels emerges at  $\phi = 0.25$ , which corresponds to the critical density of the 1CM case [Miller and Frenkel (2003)]. At small inter-particle distances (large  $q$ ), the differences are minimal, while at large length-scales (small  $q$ ), the differences are more significant. This is a consequence of steric effects, as the inter-penetrating nature of the two sub-gels reduces density fluctuations. In other words, the two sub-gels are restraining each other and this effect is stronger at higher packing fractions.

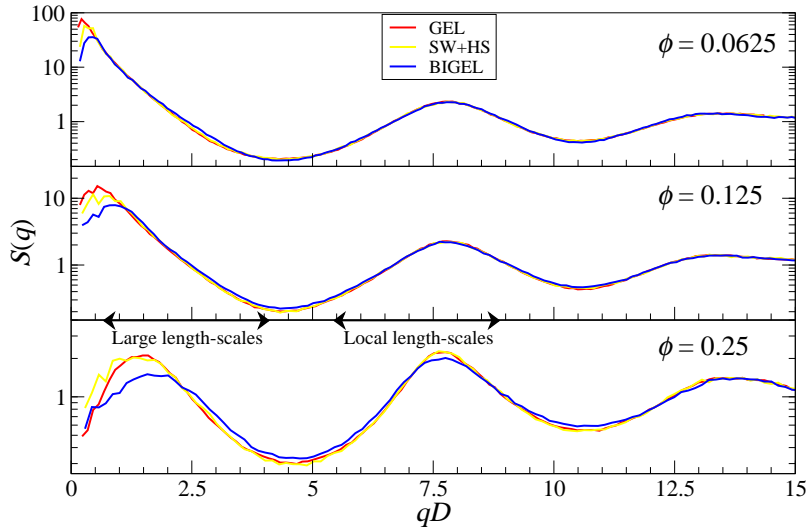


Figure 4.9: The structure factors  $S(q)$ , after the quench, for the reference total densities  $\phi_{\text{tot}} = 0.125, 0.25$  and  $0.5$ , whose corresponding 1CM densities are  $\phi = \phi_{\text{tot}}/2$ . The monodisperse gel is compared with the single species of the relative symmetric 2CM (BiGel) and the attractive SW species of the SW+HS systems.



It is natural to ask if this behavior being similar at each density, can be simply attributed to steric effects due to the presence of a second species and if its gel structure plays an important role. To clarify this point, we have performed simulations of a binary mixture in which one of the two species is purely repulsive and behaves as a simple crowding agent. We quench the SW+HS mixture ( $u_{RR} = 1$ ,  $u_{GG} = 0$ ,  $u_{RG} = 0$ ) adopting the same protocol used for the BiGels. In order to quantify the small  $q$  differences in the structure factors, we calculate the relative variation by respect to the 1CM gels

$$\frac{|S(q) - S_{\text{gel}}(q)|}{S_{\text{gel}}(q)}. \quad (4.2)$$

The results for the three representative densities are shown in Fig. 4.10. The resulting structure factors, in Fig. 4.9, show small- $q$  deviations in good agreement with the BiGels. We can conclude that such differences are due to general steric effects and not to the inter-penetrating nature of the two sub-gels. Instead, we note that the behavior of the SW+HS system is very similar to that of 1CM gels for large- $q$ .

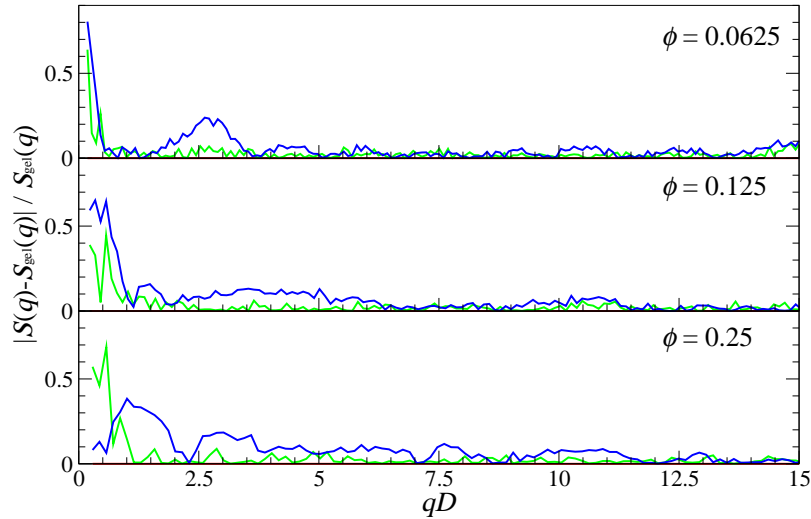


Figure 4.10: Relative variation, respect to the monodisperse  $S_{\text{gel}}(q)$ , of the  $S(q)$  for both the SW+HS and the BiGel. Same colors as in Fig. 4.9. The BiGel at critic density  $\phi = 0.25$  seems to show a more pronounced peak at the local length-scale. Its relative variation respect to the monodisperse  $S_{\text{gel}}(q)$  shows in fact that, the higher the density, the higher is the local-scale variation. We also see that the variation respect to the monodisperse case is always under the  $< 10\%$  at local length-scale and at low packing fraction. For the three reference packings the structure factor variation for sub-gels of the BiGel is compatible with the that of the SW(+HS) case. This means that steric effects due to the mere presence of a second species is the main factor for distinguish the arrested structures of 2CM from the 1CM ones. This also quantifies the large length-scale difference with the 1CMs, that is visibly dominating.

As expected, we note that the differences are more pronounced for small- $q$ , where they are of

## Chapter 4. Results: BiGels from arrested demixing.

the order of  $\approx 90\%$  for both the SW+HS and the BiGels. We can also detect the higher difference at local length-scales for the BiGel at  $\phi_{\text{tot}} = 0.5$ , corresponding to the critical density  $\phi = 0.25$  of 1-component gels. This follows the trend where an increasing difference emerges (up to an order of  $\approx 10\%$ ) at high- $q$  for higher densities. But a better statistics is needed to give conclusive answers. Instead, we can state that - apart from a systematic discrepancy at small- $q$  - the sub-gels obtained by demixing present structures remarkably similar to the ones attained by gelation of single-component, monodisperse systems.

**TOPOLOGY.** Our second analysis is based on surface reconstruction, which gives access to information about the topology and the geometry of the structures. As described in Par. 3.2.2, we developed and used a novel technique based on surface reconstruction, which closely follows the one successfully applied to study amphiphilic systems [Belushkin and Gompper (2009)]. More specifically, we construct a surface enveloping the arms of the gel. As an illustration, in Fig. 4.11 (top) we show two gel-like sub-structures that compose a BiGel at  $\phi_{\text{tot}} = 0.125$  compared to gels at half the density,  $\phi = 0.0625$ : their resulting surfaces for gels and BiGels are shown in Fig. 4.11 (bottom).

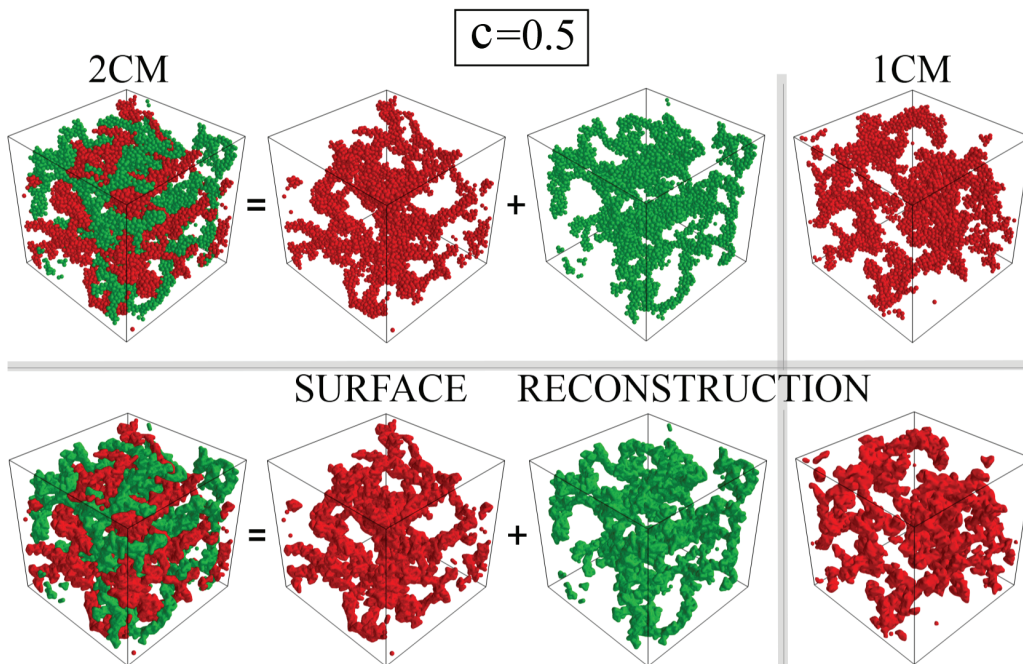


Figure 4.11: **(Top)** An example of a BiGel at total density  $\phi_{\text{tot}} = 0.125$  is shown together with its two sub-gels and a monodisperse gel at density  $\phi_{\text{tot}}/2 = 0.0625$ . **(Bottom)** Surfaces reconstruction corresponding to these structures.

Each point on the surface is characterized by a pair of principal curvatures  $C_{1,2}$  that determine the *Gaussian curvature*  $K = C_1 \cdot C_2$ , which describes the local geometry [Safran (2003)]. We

consider an overall property of the surface - its topology - in the sense of the *Euler characteristic*

$$\chi = \frac{1}{2\pi} \int K dS . \quad (4.3)$$

The value of  $\chi$  is a topological invariant that quantifies the number of objects, handles, and holes in a surface. In our case, it is directly related to the porosity of the gel, as already pointed out for dipolar colloidal gels [Miller et al. (2010)]. For a single convex, closed object, it is  $\chi_0 = 2$ , while negative values can be associated to non-convex surfaces. For the reconstructed surfaces of the three representative packing fractions, we show the distributions of the Mean Squared ( $H^2$ ) and Gaussian ( $K$ ) curvatures - see Eqs. 3.10 - in Figs 4.13 and 4.14, respectively. The values for the corresponding normalized Euler characteristic  $\bar{\chi} = \chi/N\chi_0$ , obtained with Eq. 4.3 divided by the maximum achievable  $\chi$  for  $N$  convex objects, are shown in the right panel of Fig. 4.14.

The  $H^2$  and  $K$  distributions are in unities of  $1/R^2$ , where  $R$  is the radius of a colloid, and exhibit several local features. For example, a spherical cap is characterized by identical principal curvatures  $C_1 = C_2 = 1/R$ , that give identical  $H^2 = K = 1/R^2$  from the definition of Eqs. 3.10 and 3.11. See example in Fig. 4.12 (left). Then, we expect that a peak is observed for such a value in both the distributions if spherical caps contribute to the enveloping surface. On the other hand, cylindrical surfaces would contribute with  $H^2 = 1/4R^2$  and  $K = 0$ , since the principal curvatures in this case are  $C_1 = 0$  and  $C_2 = 1/R$ . Besides, the  $K < 0$  domain corresponds to saddle-like geometries due to branching areas, as  $C_1 < 0$  and  $C_2 > 0$  (or the inverse); see for example Fig. 4.12 (right).

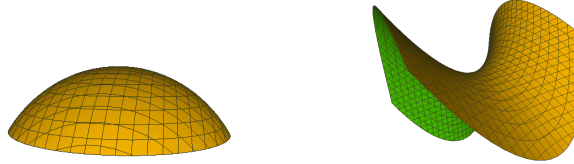


Figure 4.12: **(Left)** Example of gridded spherical cup surface: a prevalence of this shape would bring a Gaussian Curvature distribution's peak at  $K \sim 1/R^2$ . **(Right)** Example of gridded saddle surface: such a shape is defined by a positive  $C_1 > 0$  and negative  $C_2 < 0$  principal curvatures, so that it contributes to the negative region of the Gaussian Curvature distribution,  $K = 1/(C_1 C_2) < 0$ . Eventually a prevalence of similar saddles would then bring to a  $K < 0$  peak. These saddle and a convex truncated surfaces are representative of the peaks found in the  $K$  distribution. A peak in  $H^2$  distribution corresponding to the spherical cap also is present, but the saddle  $K < 0$  region is not reflected by any specific feature in the Mean Squared curvature distribution.

The distributions of the mean squared curvature are shown in Fig. 4.13 for the reference densities. We note that the arrested, attractive species of the SW+HS system presents the same surface features of the 1CM gels, while the BiGels present higher peaks referred to the

dominant structures (spherical caps and cylinders). This behavior denotes how the demixing affects the arms of the branches composing the sub-gels. As these local length-scale features are enhanced, the enveloping surface of the sub-gels present more bumps as a result of thinner arms: less colloids participate, in average, to the thickness of sub-gels branches and thus more spherical caps contribute to the surface. Moreover, the difference of BiGels with 1CM (or the SW+HS) gels are observed to increase for increasing packing fractions, as expected.

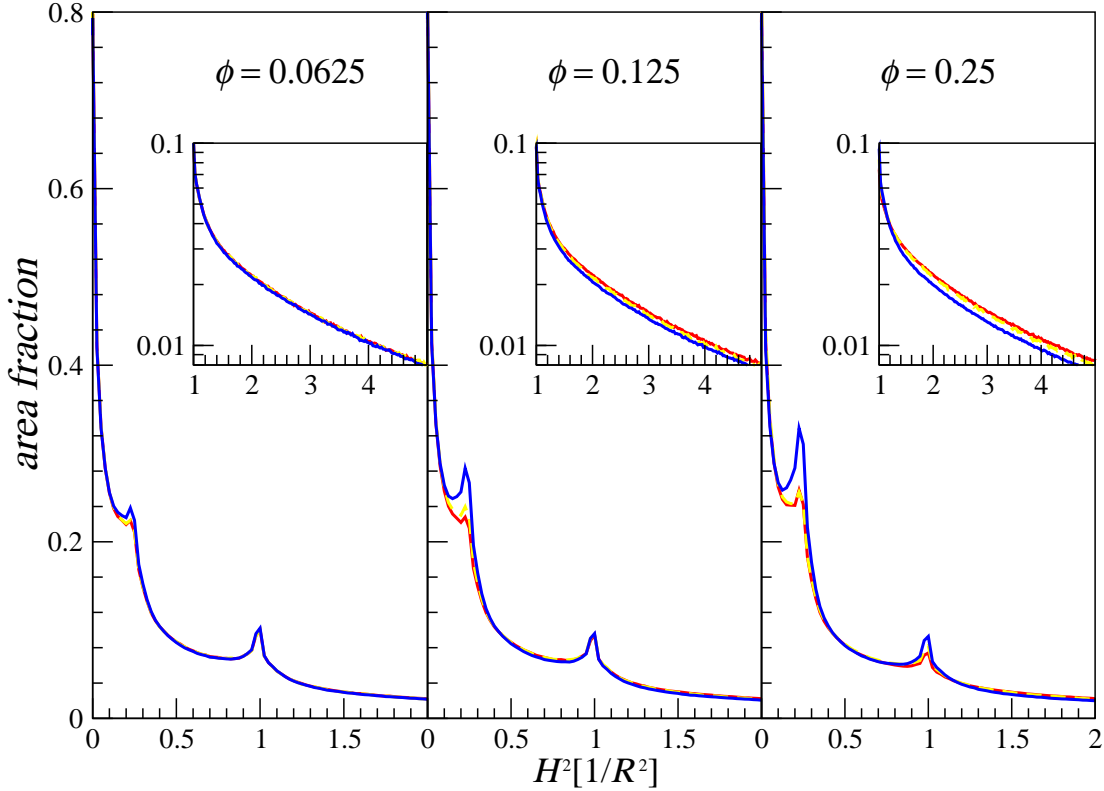


Figure 4.13: Distributions of the Mean Squared curvatures  $H^2$  for the gels (red lines), the attractive component of the SW+HS (dashed yellow lines), and the BiGels (blue lines). The results for three representative packing fractions  $\phi = 0.0625, 0.125$  and  $0.25$ : here  $\phi = \phi_{\text{tot}}$  is the density of one of the two species in the 2CM cases, as well as the density of the monodisperse gel. The  $H^2$  distribution captures the local surface geometry: the peaks relative to a cylindrical shape and to a spherical cap are clearly visible. Here  $R$  is the radius of the colloids and  $H^2$  is in unities of  $1/R^2$ . Each curve results from an average of measurements (as explained in the text) over 10 independent configurations. The curves referred to the SW+HS systems are in perfect agreement with those of the respective 1CM systems. Instead, differences emerge for the BiGel: the two main peaks are more pronounced and the tail of the distribution (insets) decreases faster. This behavior is due to the a lower thickness of the branches, that is reflected by a major presence of bumps in the surface.

Similar information can be extracted from the distribution of the Gaussian curvature. In Fig. 4.14 we show, together with these distributions (left panel), the respective Euler Character-

istics (right panel) as calculated by means of Eq. 4.3. The value  $K = 0$  reflects the cylindrical geometry typically found along the arms of the gel, and the  $K \approx 1/R^2$  peak serves as a measure of local undulations. At higher densities, both an increase of the  $K \leq 0$  part of the distributions and a decrease of  $\bar{\chi}$  are observed. This shows that both the gels and the sub-gels become more porous. It is also evident from the distributions of Gaussian curvature that the geometrical difference between the gels and BiGels grows, while essentially equal Euler characteristics show that the structures remain topologically very similar. The growing deviations in the  $K \approx 0$  and  $K \approx 1/R^2$  regions point towards the compaction and straightening of the individual arms of the sub-gels. As for the  $H^2$  distributions, we note the almost perfect superposition of the  $K$  distributions for the SW+HS with those of the relative 1CM gels. This implies that steric effects do not affect the features of the surfaces enveloping the structures, as they rely on the local geometry, in agreement with the results for the structure factor (Fig. 4.9).

The increased count of saddle shapes is reflected by more negative  $\bar{\chi}$ . This indicates also the smaller size of pores, as they grow in number but void space decreases for higher densities. Finally, regardless of the presence of a second species, these observations allow us to conclude that the porosity of gels and single components of BiGels are quantitatively similar.

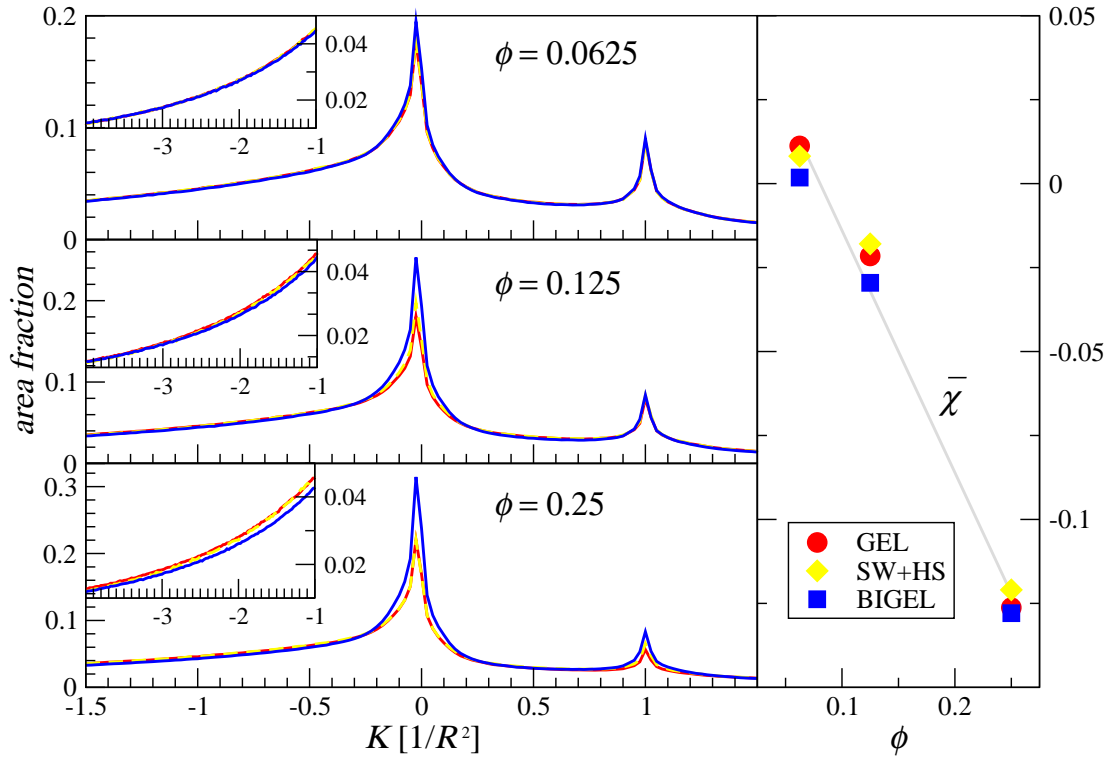


Figure 4.14: **(Left)** Distributions of the Gaussian curvatures  $K$  for the gels, the SW+HS, and the BiGels (compared as before). The monodisperse gels at  $\phi$  (red) are compared with the sub-gels of a BiGel (blue) and the SW component of the SW+HS system (yellow), at  $\phi_{\text{tot}} = 2\phi$ . The curves referred to the SW+HS systems agree with those of the 1CM systems. The insets show the tails of the distributions in the  $k < 0$  region, where saddles are the only kind of structures that give a contribution. At increasing density, a difference in the peaks clearly emerge for the BiGels: bumps on the surface give a bigger contribution. **(Right)** The Euler characteristic, normalized by the number of particles and the value for an isolated colloid:  $\bar{\chi} = \chi/N\chi_0$  ( $\chi_0 = 2$ ). Despite the possible differences in the  $K$  distributions, the normalized Euler Characteristic  $\bar{\chi}$  shows that the single components of the BiGels and the relative gels, together with the attractive species of the SW+HS systems, share the same topology.

## 4.2 Bigel: experiments.

### 4.2.1 From model to lab.

Here we focus on the actual realization of the non-equilibrium processes that bring to the gelation process resulting from fluctuations arrest of chosen, tunable quantities. This mechanism, as suggested by TPT and previous studies (see Par. 3.1.2 and 3.2.1) unveils a universal physical mechanism. In order to prove such universality, we make use of the DNA-mediated interactions for creating colloidal systems whose components show species selectivity. Arrested phase separation should then take place, as expected from theoretical framework previously illustrated. This part of the thesis has been conducted in collaboration with the group of Erika Eiser (Cavendish Laboratories, Cambridge, U.K.). The results of the experiments will be resumed in Chapt. 4.

In the promising field of self-assembly, alternatives exist that may offer controlled and/or inexpensive synthesis of nano- to micro-sized structures under mild conditions, and inter-species interactions play a fundamental role in mixtures of proteins, macromolecules and colloidal systems<sup>5</sup>. Although the selectivity of the interactions is often a result of the complex structure of the proteins, research on functionalized colloids unveils unprecedented possibilities of synthesizing simple particles with tunable interactions.

To this aim, the ability of DNA to carry information - its main role in biology - can be exploited for self-assembly processes [Whitesides et al. (1991); Rothmund (2006); Feldkamp and Niemeyer (2006); Simmel (2008)]. While most of the works focus on the direct assembly of DNA chains in supramolecular DNA structures [Aldaye et al. (2008); Pinheiro et al. (2011)], early observations already have reported reversible as well as highly specific binding acting between colloidal nanoparticles, when coated with complementary strands of DNA [Mirkin et al. (1996); Alivisatos et al. (1996)]. Research activity on colloidal suspensions has followed: DNA's ability to direct the patterning gives to such techniques the potential for facing many important scientific challenges.

**WHY THE DNACCs.** We propose the first experiments apt to the realization, as the proof of concept, of the enhanced demixing scenario we introduced. Binary mixtures of DNA-coated colloids (DNACCs), functionalized with selective intra-species attraction, represent the ideal candidate to best reproduce the theoretical and simulative results of the thesis<sup>6</sup>. In particular, here we describe equimolar ( $c = 0.5$ ) 2CMs, but the used methods can be applied to others molarities (or compositions) or to higher number of components (but this generalization goes beyond the scope of the thesis). In fact, DNACCs present highly tunable interactions and a vast parameter space (e.g., particle size, ligand structure and flexibility, coating density,

<sup>5</sup>Eye-lens protein systems, for example, can pass from condensation to demixing by a single point mutation, which is believed to alter the inter-species attraction [Dorsaz et al. (2011); Banerjee et al. (2011)].

<sup>6</sup>Research on DNACCs has until now mostly focused on the creation of three-dimensional crystalline assemblies [Nykypanchuk et al. (2008); Park et al. (2008)] or on the formation of particular designs of scaffolds or patterns [Wilner et al. (2009); Lin and Yan (2009); Gu et al. (2009)].

nucleotide sequence length and hybridization strength), that make them a promising tool to build colloids with programmable interactions [Mirkin et al. (1996); Alivisatos et al. (1996); Biancaniello et al. (2005); Geerts and Eiser (2010)].

We address the question of what happens out-of-equilibrium<sup>7</sup>, for binary mixtures of DNACCs covered with two different types of strands, the free ends of which are complementary and capable of forming bridges. The different species are defined through the different coating of the spherical colloids, in order to mimic the 2-component mixtures (2CM) with specific interactions modeled so far.

Under experimentally relevant conditions, DNA-coated colloids interact through entropic repulsion and hybridization-mediated attraction [Biancaniello et al. (2005); Dreyfus et al. (2009); Leunissen and Frenkel (2011)]. The attraction is mediated by hybridization of two complementary DNA single strands (ssDNA), which are held together by hydrogen bonds between the complementary bases<sup>8</sup>: adenine to thymine (A-T) and cytosine to guanine (C-G). By exploiting these pairing rules among bases, structures can aggregate depending on the programmable sequences of DNA grafted on the particles' surface<sup>9</sup>. The typical hybridization, in structural DNA technology, provides the interaction through a rigid core with *sticky ends*: the ssDN acts by forming, at contact, a linked double-helical region.

When temperature is lowered below a well defined (system-dependent) value, large aggregates form [Valignat et al. (2005); Aldaye et al. (2008); Park et al. (2008); Geerts and Eiser (2010); Sacanna et al. (2010); Rogers and Crocker (2011)]. This behavior is now understood in terms of the statistical mechanics of duplex formation between complementary single-stranded DNA filaments (ssDNA) coated onto different particles. Formation of these bonds results in an attractive interaction between colloids that is a monotonic, sharply decreasing function of temperature [Angioletti-Uberti et al. (2012); Mognetti et al. (2012); Varilly et al. (2012)]. For low packing fractions, 1CM of DNACCs are known to form an arrested, gel-like space-spanning structures [Geerts et al. (2008); Geerts and Eiser (2010)].

**EXPERIMENTAL SETUP.** Here we briefly introduce the main experimental features: for details, see Appendix E. We used two species of polystyrene colloids with diameters of 0.5  $\mu\text{m}$ . Polystyrene hard-sphere colloids, shown as a section in Fig. 4.15, are coated with fluorescent PEG and with DNA strands. The strands consist of a section of double-stranded DNA (dsDNA)

---

<sup>7</sup>The formation of a crystal implies, instead, an equilibrium process. Recently, a thermodynamic theory has been provided for the DNACC, as viable approaches to design crystal structures *a priori* [Angioletti-Uberti et al. (2012); Mognetti et al. (2012); Varilly et al. (2012)]. It uses a generalized, mean-field approach, which neglects fluctuations of the grafting density. Discrepancies arise only when these fluctuations become relevant. The theory results in quantitative to semi-quantitative agreement with the MC data.

<sup>8</sup>Each surface-grafted DNA strand can bind at most one partner DNA strand at a time. For this reason, the hybridization is considered as *valence-limited* [Zaccarelli et al. (2006)]. But the inter-particle interaction between DNACCs is not valence-limited, as the surface is densely coated, and in principle local fcc configurations of bonded DNACCs can take place. Designs are also possible for strands that bind to more than one partner simultaneously, but an entropic cost exists for bringing three or more strands together if grafted onto colloids (as opposed to the case when they are dispersed in solution), and such designs are not often applied for DNACCs.

<sup>9</sup>This process, combined with the current ability to synthesize almost any sequence in an automated fashion, also allows the manufacturing of new structures that are not found in nature [Seeman (2003)].



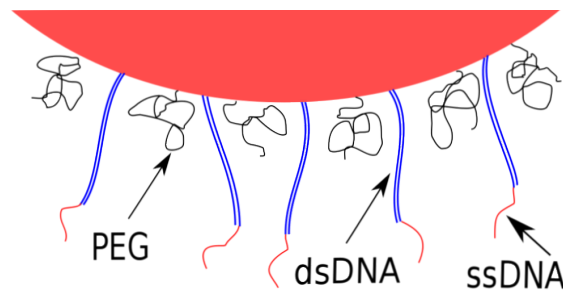


Figure 4.15: The HS polystyrene colloids (a section is here shown in red) are coated with PEG and dsDNA with ssDNA strands. The coating functionalization of the ssDNA enables the specificity in the attraction effective potential among colloids coated with complementary ssDNAs. In fact, given a coating C whose ssDNA can stick to the complementary C' ssDNA strands, only the resulting C-C' bonding can take place for this species. Beyond the DNA-functionalization, colloids are fluorescently coated, so that it can be also used to color-label the different species. For our experiments, we used red (R) and green (G) fluorescences. (Details in Appendix E.)

with length of 20 nm, which is grafted to the surface of the colloids<sup>10</sup> and terminates with a “sticky end”, i.e. a short sequence of single-stranded DNA (ssDNA). Note that the ratio between dsDNA length, which determines the range of the interactions, and colloidal diameter has a value 4%, which is close to the value used in the SW model ( $\lambda = 1.03$  corresponds to a value 3%) illustrated in Par. 3.1.1.

The ssDNAs enable the specificity in the inter-particle selective interactions. This is achieved by using the four different strands, labeled A, A', B and B'. The sticky ends of the strands A and B are complementary to those of A' and B' respectively. The binding free energies of the non-specific interactions A-B, A-B', A'-B and A'-B' are negligible compared to the hybridization free energies of A-A' and B-B'. We adopted a coating such to induce attraction effective potential among only colloids with equal coating. Two different implementations are used experimentally:

1. the species carry a different ssDNA coated encoding, A and B, whose relative complementary strands A' and B' are mixed in the solution, so forming bridges like A-A'-A and B-B'-B;
2. each species is coated with the two complementary ssDNAs, with no strands in solution, so defining the species A'A and B'B, and a competition among loops (on the same colloid) and bridges (among distinct colloids of the same species) takes place.

We used the first method for a preliminary structural study. The pair distribution function  $g(r)$ , calculated on positions data obtained by confocal microscopy<sup>11</sup>, is shown in Fig. 4.16.

<sup>10</sup>The dsDNA acts as an inert spacer and allows the sticky end to explore a larger volume around the grafting point.

<sup>11</sup>The size of the colloidal particles allows their study by means of a wide range of optical techniques, such as dynamic light scattering and confocal microscopy (see Par. 2.3 and Appendix B).

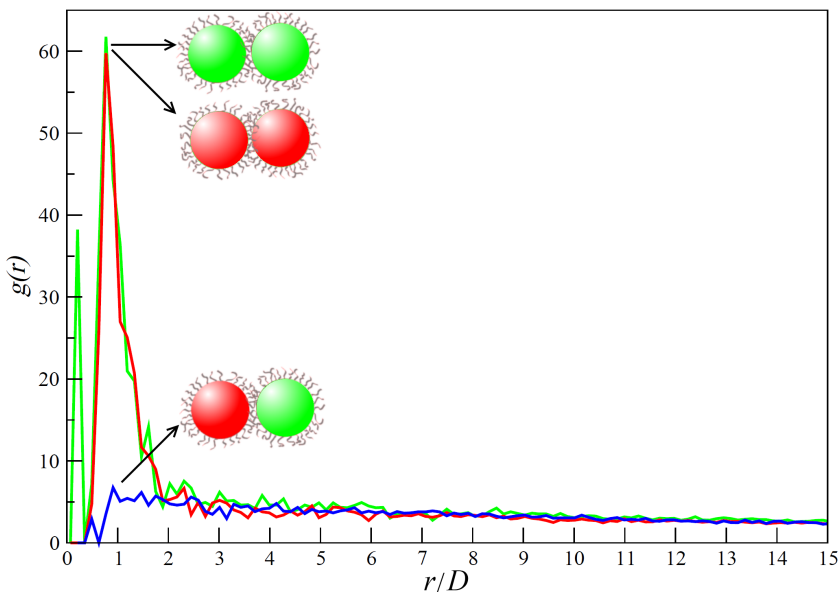


Figure 4.16: Experimental pair correlation function  $g(r)$  on BiGels on DNACCs of  $1\mu\text{m}$  in size. In this case we used a first series of experiments, with strands in solution have been used in order to provide the bindings A-A'-A and B-B'-B, between colloids coated with only A or B DNA sequences. Such a system is different from the AA' and BB' coated colloids used for the other experiments: in this second case, the colloidal size is not sufficient for obtaining data with small-errors on single particle positions. Clearly the  $RR$  and  $GG$  attractions are strongly dominant respect to the  $RG$  residual attraction. There are two commonly used types of procedures for making DNA coated colloids bind together.

**GELATION PROTOCOL OF DNACC 2CM.** Using the second method, instead, a second series of experiments has been conducted: a representation of the binding scheme is illustrated in Fig. 4.17. The species are labeled with different fluorescent dyes, red (R) and green (G), that make them distinguishable in confocal microscopy experiments. The DNA coatings are designed such that attraction is possible only between R and R or G and G, whereas G-R interaction is repulsive. Given a coating A whose ssDNA can stick to the complementary A' ssDNA strands, only the resulting A-A' bonding can take place for this species<sup>12</sup>. The same happens for B-B'. A schematic of two interacting R colloids is shown in Fig. 4.17.

Slow dynamic properties are expected to arise by using DNACCs which show short-ranged inter-particle attraction. The DNA-mediated colloidal aggregation is thermo-reversible and melting occurs sharply at the temperature  $\tilde{T}_m \approx 54^\circ\text{C}$ . The value of  $\tilde{T}_m$  is larger than the melting temperature  $T_m$  of free sticky ends in solution, and it is easily tuned by changing the DNA grafting density using inert polymers. Once sealed into the chambers, the samples are

<sup>12</sup>Binding is also possible between complementary strands grafted within a certain distance on the surface of the same colloid, producing “loops” [Leunissen et al. (2009)]. The overall intra-species attraction results from the competition between bridges and loops.

heated up from room temperature ( $RT \approx 22^\circ\text{C}$ ) to  $T = 60^\circ\text{C} > \tilde{T}_m$  and left until a homogeneous gas phase is formed. The samples are then quenched to RT. This quenching procedure is parallel to that used for the simulations, where the quench follows an equilibrium phase where the inter-particle attraction is negligible. At about  $45^\circ\text{C}$  large-scale aggregation initiates and within 5 minutes a demixed BiGel is formed (see next paragraph).

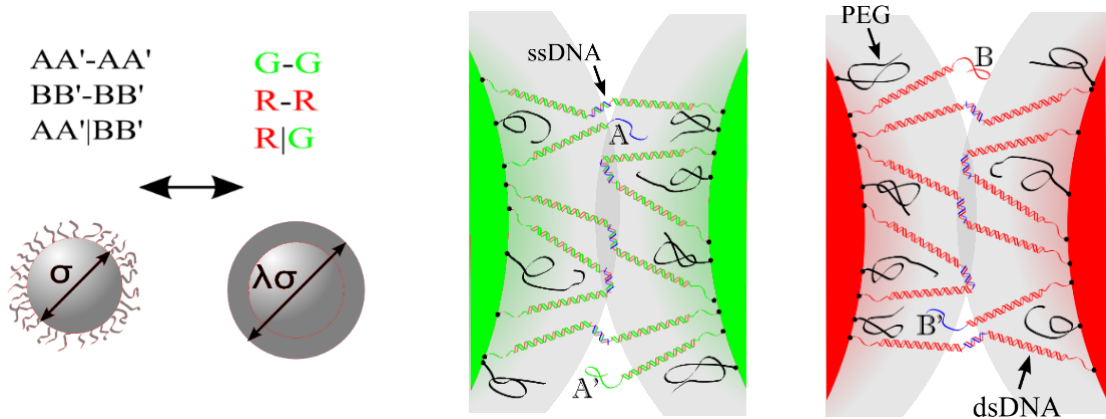


Figure 4.17: **(Left)** The HS polystyrene colloids are used to realize the selective inter-particle interaction among colloids, following the model. The specific (sections is here shown in red) are coated with PEG and dsDNA with ssDNA strands. The coating functionalization of the ssDNA enables the specificity in the attraction effective potential among colloids with equal coating. In fact, given a coating A whose ssDNA can stick to the complementary A' ssDNA strands, only the resulting A-A' bonding can take place for this species. In our experiments, each species is coated with the two complementary ssDNAs, with no strands in solution, so defining the species A'A and B'B, and a competition among loops (on the same colloid) and bridges (among distinct colloids of the same species) takes place. The PEG is fluorescent, so that is can be also used to label the different species: we used red (R) and green (G) fluorescences. Given the arbitrary of the system, the four combinations R-A'A and G-B'B, or G-A'A and R-B'B can be used. (In Appendix E further details are explained.)

The parallel between computer model<sup>13</sup> and experimental setup relies on the main physical characteristics of both the particles (HS core, short-ranged attraction, selective potential) and the quenching procedure (starting from a gas phase where the inter-particle attractions can be neglected down to a temperature that makes the particles aggregate).

#### 4.2.2 The actual BiGel.

Our prediction of the formation of a demixed phase, as supported by theory, can then be tested with the introduced experimental system. This route is used to test the demixing

<sup>13</sup>We consider the repulsive HS repulsion among colloids of different species. With such an approximation, we can usefully model the present coated colloidal interactions with the simple SW model, but with selective interactions  $\epsilon_{RR}$ ,  $\epsilon_{RG} = \epsilon_{GR}$  and  $\epsilon_{GG}$ .

## Chapter 4. Results: BiGels from arrested demixing.

mechanism and its enhancement. The attractive potential, enabled by the DNA coating, acts on like-particles (same species), while colloids of different species present only mutual hard-sphere-like repulsion. We present in this paragraph some confocal microscopy experiments performed on quenched<sup>14</sup> two-component mixtures of DNACCs with such selectivity, and for a symmetric composition  $c = 0.5$  of the two species.

A schematic of these particles is shown in Fig. 4.17. The colloids are labeled with different fluorescent dyes, red (R) or green (G), and the DNA coatings are designed such that only RR and GG attractions are possible, leaving the G-R interaction repulsive. In the experiment presented in Fig. 4.18, the surfaces with strands A and A' are coated with G dye, while the species with B and B' strands are not fluorescently coated. The imaging of the resulting aggregation show, in Fig. 4.18(left) and 4.18(center) (using bright field (BF) and fluorescence (FL) lighting techniques, respectively), the arrested gel structure for a sample of such a system. In Fig. 4.18(right), contour plots are made for the FL image combined with the subtracted BF image: they show a first signature of demixing, as it is possible to separately distinguish large, ramified structures. These structures are drawn in R and G colors. In this case the sample has total colloidal volume fraction  $\phi_{\text{tot}} \approx 0.05$ .

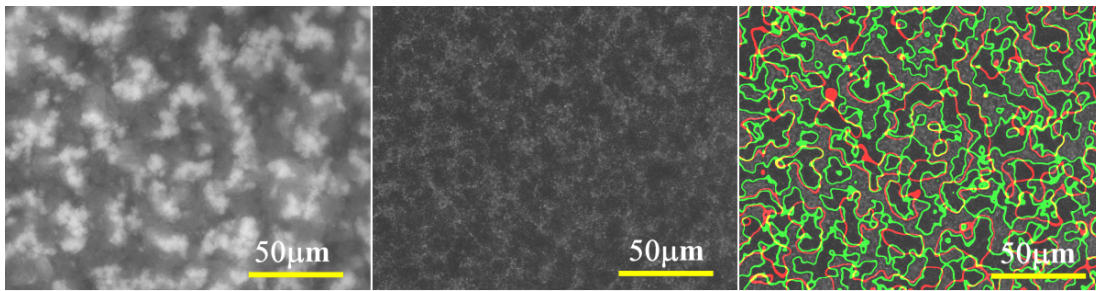


Figure 4.18: **(Left)** After annealing. A bright field (BF) image of a DNACC aggregate ( $\phi_{\text{tot}} \approx 0.05$ ,  $c = 0.5$ ) where only the G species is fluorescently coated, while the other is non-fluorescent. **(Center)** A fluorescent (FL) optical microscopy image of the same region, where the G fluorescent components result better resolved. **(Right)** Green and red lines are contour plots that highlight fluorescent and non-fluorescent (obtained per subtraction) aggregates, respectively.

When also the R dye is present, the difference in fluorescence of the colored coatings allows more detailed imaging by means of the confocal microscopy: the sample is irradiated with laser at R and G wavelength, in order to have a significant split in the respective light channels<sup>15</sup>. This sample is shown in Fig. 4.19(a): a BiGel is clearly observed, with its inter-penetrating,

<sup>14</sup>The samples are heated up until a homogeneous gas phase is formed and then quenched: large-scale aggregation initiates and a demixed BiGel forms. Details on the experiments are in Appendix E.

<sup>15</sup>The surfaces of G colloids is coated with strands A and A' in equal concentrations; analogously the surface of R colloids is coated with B and B'. Given the arbitrariness of the system, the two color-combinations R-A'A and G-B'B, or instead G-A'A and R-B'B can be used. To guarantee that our binary system is completely symmetric, all the experiments have been repeated after exchanging the DNA coatings between the fluorescent species. Details on the materials and the experimental methods are in Appendix E.

double-percolating nature. In this case a confinement of the colloidal samples in quasi-2D chambers, with thickness of a few microns, has enabled the systems to have volume fractions closer to those for which we have found double percolation in simulations<sup>16</sup>. It is in fact  $\phi_{\text{tot}} \approx 0.1$  ( $c = 0.5$ ). In Fig. 4.19(b) a detail is shown where the G and R components are separately visualized. The confocal technique also allows to reconstruct the 3-dimensional structure and, for this BiGel, an example of 3D reconstruction is shown in Fig. 4.20.

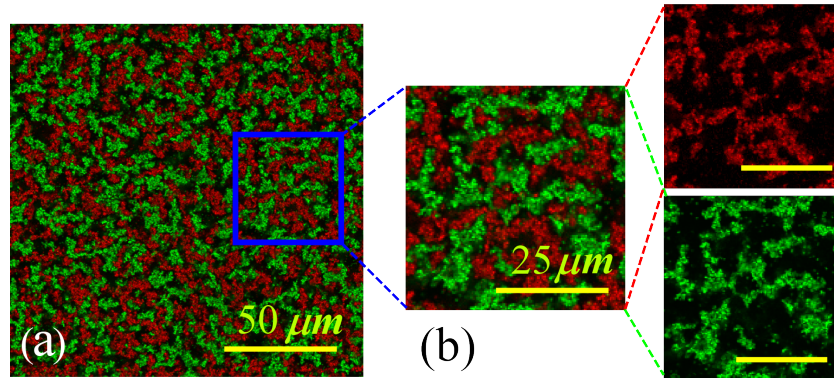


Figure 4.19: (a) Confocal image of the demixed BiGel showing R and G fluorescently labeled colloids (star symbol in Fig. 4.7). The section is taken in the middle of a sample with an overall thickness of  $20 \mu\text{m}$ . The scale bar is equal to  $50 \mu\text{m}$ . (b) Detail of image (a) for which we separate R from G aggregates. Here the scale bars are equal to  $25 \mu\text{m}$ .

In Fig. 4.7, the experimental state-point  $(c, \phi_{\text{tot}}) = (0.5, 0.1)$  is indicated within the phase diagram obtained with thermodynamic perturbation theory (TPT) and together with expected theoretical results for the percolation properties of 2CM systems. These results evidence the first, actual realization of a demixed BiGel, and reveal the correctness of the generalized theoretical framework. In fact, the AA' and BB' equimolar DNACCs mixture has been used in order to maximize the demixing mechanism over the condensation. The outcome of this maximization can be placed among the theoretical results: as described in Par. 4.1.3, the experiments have been performed in line with the prediction for the achievement of a double-percolating structure. Thus, the chosen experimental setup reflects the choice of working at conditions where the theory predicts an arrested phase separation with two inter-penetrating sub-gels, both percolating. As shown, in fact, the competition of demixing with condensation influences the final structuration in a way that can be understood upon analyzing the properties of percolation (refer to Par.s 2.3.1, 3.1.1 and 4.1.2).

<sup>16</sup>For the packing fractions of interest, multiple scattering highly reduces the quality of confocal image in bulk. For this reason, we have chosen to confine the colloidal samples in quasi-2D chambers of few microns thickness. In this way we can image systems with volume fractions close to those we simulate. Ssee Appendix E for details on the used imaging techniques.

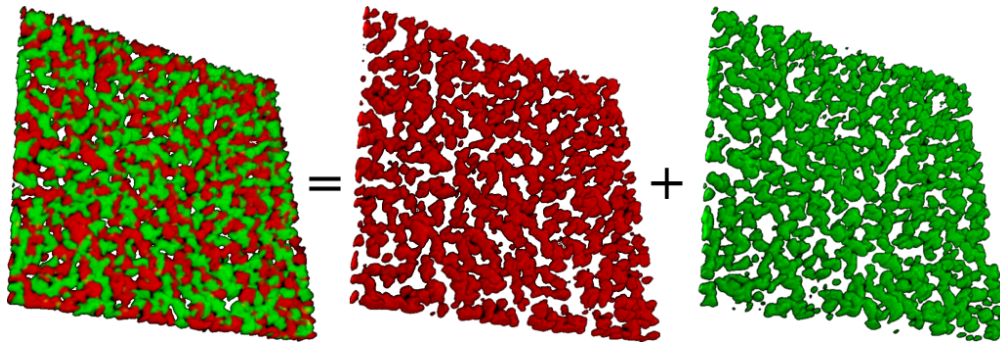


Figure 4.20: The same BiGel sample of Fig. 4.19, whose the 3D composition is reconstructed from the coplanar images from confocal microscopy experiments. This rendering (similarly to the simulated colloidal model) highlights the existence of double-percolating structures. Here the presence of small, not yet aggregated clusters, can be due to various effect: on one hand, the arms of a sub-gel can act as a matrix that traps (in the quasi-2D experiment) tiny aggregates of the other species; on the other hand, the imperfections of the coatings and possible hydrodynamic effects could have a role in the ageing process of gelation, causing local detachments.

## 5 Ongoing developments and perspectives.

**OUTLOOK.** In this final chapter, a series of analysis are shown, that are being performed. Such work in progress is important as it highlights the dynamical properties of the 2-component mixtures in the final stages of the aggregation. In particular, we use the Structure Factor and, as long as dynamics is concerned, its analytical (Furukawa) approximation: this unambiguously places the gelation through arrested demixing in the context of the arrested spinodal decomposition. The analysis are reported for both simulated and experimental samples. Conclusions are finally drawn regarding the generalization of the spinodal decomposition, enlarged to account for the competition of different mechanisms: we distinguished the condensation and the demixing. The aspect of the augmented span of parameters is also touched, with particular emphasis to the role played by the simple models, in a scenario where they can be (and have been) used to realize complex structures. We finish the chapter with some considerations where we suggest possible directions - as well as applications - for the present research.

### 5.1 Dynamics close to the arrest.

The aggregation of both BiGels and SW+HS can be probed by observing the evolution (upon quench) of the static structure factor. Refer to Par. 2.3.2 for its definition and to Par. 3.1.1 for the 1CM case. The results for these symmetric 2CM systems are shown<sup>1</sup> in Fig. 5.1 for the three reference total densities  $\phi_{\text{tot}} = 0.125, 0.25$  and  $0.5$  (see Fig. 3.2 for the 1CM system with densities  $\phi = \phi_{\text{tot}}/2$ ).

A peak clearly emerges for the  $S(q)$  in correspondence to the large length-scales (small wave-lengths  $q$ ) for the single components that form the demixed sub-gels. As in the 1CM case, this peak indicates the ongoing gelation phenomenon, strongly dependent on the spinodal decomposition<sup>2</sup>. The peak shifts towards lower  $q$  and, after a certain time, its position and height do not change: this arrest reflects the arrest described also with  $n_b$  or  $MSD$  (see Par. 2.2.1 and

---

<sup>1</sup>Each curve of Fig. 5.1 is an average over 10 independent runs. The symmetry has also been used for averaging also over the curves of the two single species, but this has not been possible for the SW+HS mixtures.

<sup>2</sup>We will see how the final curves of the partial and total  $S(q)$  recall those obtained for the experiments (Fig. 5.6).

Par. 3.1.1).

The  $S(q)$  at short, local length-scales (wavelength  $q \gtrsim 4$ ) of the single species is almost exactly coincident with the total structure factor: this reflects the demixed nature of the BiGels, in that the single species form similar, local structures. The overlap with the total  $S(q)$  breaks down for higher densities, because the sub-gel branches result closer and the decreased available space makes the local correlations increase.

A small- $q$  peak, extremely similar to the one for single species of BiGels, is observed for the SW component of the SW+HS systems (right panel of Fig. 5.2). Also in this case, the attractive component gives the fingerprint of the total structure factor, while the repulsive HS component plays a background role characterized by no spontaneous local structuration. The structuration of the HS species is observable only for higher  $\phi_{\text{tot}}$  (as the HS occupy the void space), driven by the matrix formed by the SW component arrested to form a gel.

The strong similarity of the  $S(q)$  for the BiGel and the SW+HS systems, regarding their attractive components and the total structure, are a clear indication that the presence of a second species (both attractive or repulsive) bring to the same arrested gel-like structures. This steric effect has been treated in the Par. 4.1.3 with a major focus on the final, arrested structures.

**LATE STAGES OF DEMIXING.** Recently, the spinodal decomposition occurrence has been discussed in relation to demixing in colloid-polymer and Lenard-Jones mixtures [Aarts and Lekkerkerker (2004); Thakre et al. (2008)]. By keeping track of the evolution of the small- $q$  region of the structure factor, it is possible to delineate the typical demixing domain size and its evolution. In Par. 2.3.2 an analytical approximation for the structure factor has been introduced [Furukawa (1989)], the Furukawa's scaling

$$\tilde{S}(q, t) = S_m(t) \frac{3(q/q_m(t))^2}{2 + (q/q_m(t))^6}. \quad (5.1)$$

This scaling, relying on a  $S(q)$  definition that accounts for the two components, has been proved to be particularly suitable for the description of the stages of aggregation where bicontinuous structures begin to emerge [Thakre et al. (2008)].

Thus, we test the scaling hypothesis on the 2CMs that bring to BiGels, where demixing drives the gelation process. The fits together with the structure factors are shown in Figs. 5.2, 5.3 and 5.4 for the BiGel at three reference densities. In particular, fits for the total density  $\phi_{\text{tot}} = 0.125$  are presented in Fig. 5.2 (top), and we propose a collapse of the data and the relative fits (as described in Par. 2.3.2) in Fig. 5.2 (bottom): the good agreement with the approximation highlights the consistency with the dynamical scaling hypothesis, which is expected to hold for the evolving phase when mesoscopic domains are separated.

On the other hand, the scaling is known to be a good approximation only up to packing fraction



## 5.1. Dynamics close to the arrest.

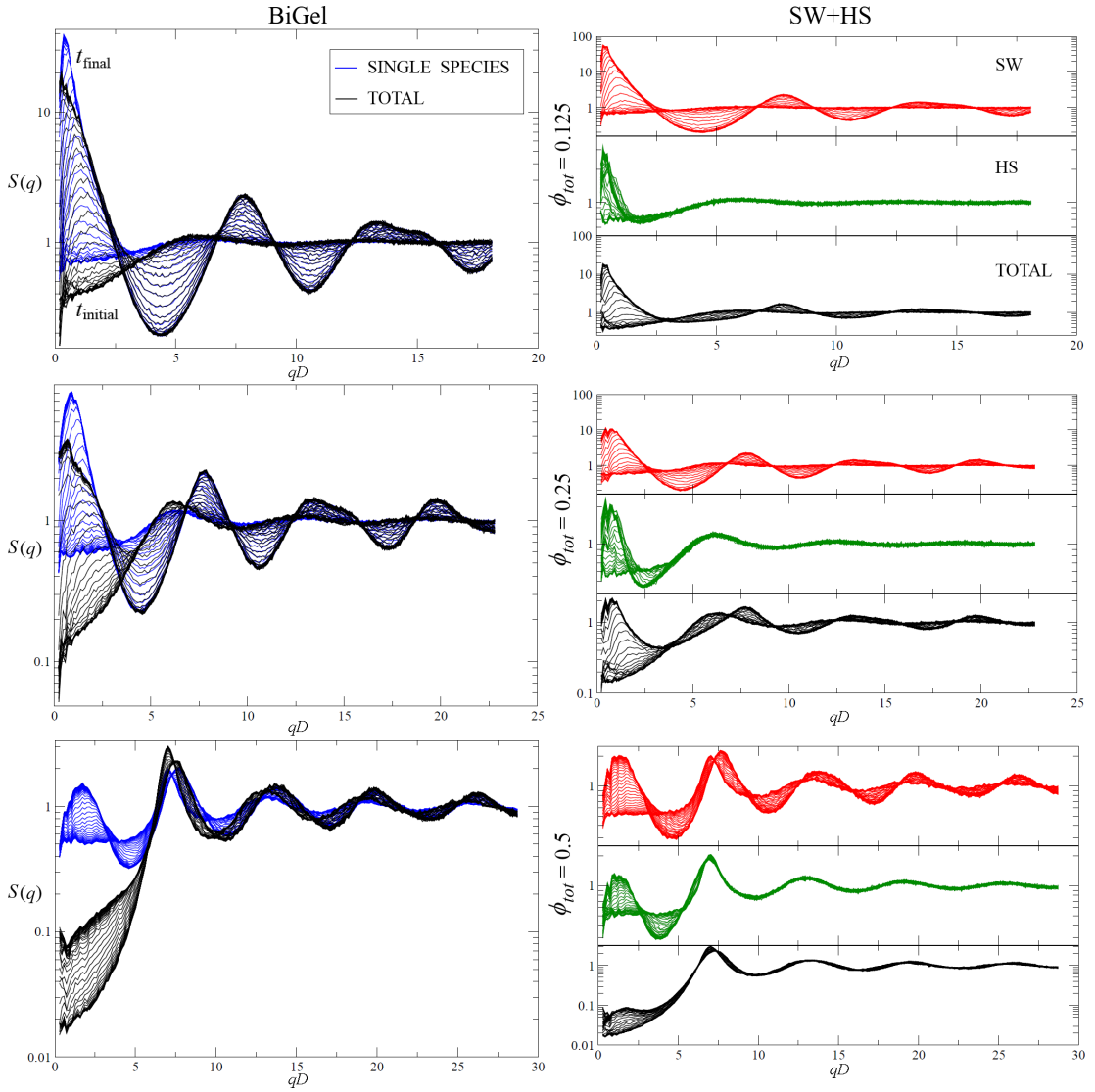


Figure 5.1: Structure factor evolution for the *symmetric 2CM* system (each species accounts  $\phi_{\text{tot}}/2$ ), at densities  $\phi_{\text{tot}} = 0.125$  (top),  $0.25$  (center) and  $0.5$  (bottom). **(Left)** The total  $S(q)$  (black lines) is compared with the partial  $S(q)$  (blue lines) of the 2 distinct species. For all the densities, and for both the total and single-species, the low- $q$  peak shifts towards smaller  $q$  and rises up to a stable height. For local length-scales ( $qD \lesssim 4$ ) the behavior of single-species is almost identical to the total structure, but differences emerge at high  $\phi_{\text{tot}}$ . Note: the agreement of total  $S(q)$  with the 1CM observations diminishes at high  $\phi_{\text{tot}}$ . **(Right)** Same as on the left panel, but for the SW+HS variant of the 2CM system. The total  $S(q)$  (black) are compared with the partial  $S(q)$  of the attractive (SW, red) species and the repulsive (HS, green) species. As for the BiGel formation, the shift and rise of the low- $q$  peak is observed. Note: the SW (attractive) component behaves as the BiGel's single species, while the HS (repulsive) component shows a structuration as consequence of the SW aggregation. The total  $S(q)$  results in an increasing disagreement with the monodisperse 1CM at higher densities (see Fig. 3.2).

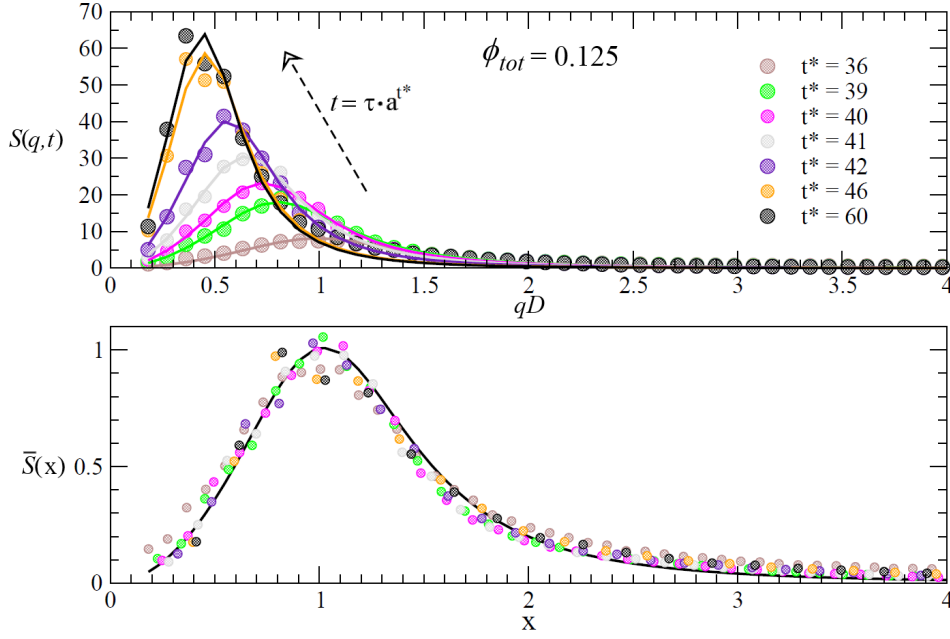


Figure 5.2: **(Top)** The analytical approximation Eq. 5.1 is used to fit the total  $S(q)$  during the final stages BiGel aggregation ( $\phi_{tot} = 0.125$ ). The configurations have a power-law sampling  $t = \tau \cdot a^{t^*}$ , where  $\tau = 10^{-2}$  is the minimum time, the constant ( $> 1$ )  $a = 1.3$  gives the separation increase for consecutive configurations, and  $t^* = 1, 2, \dots, t_{final}$  label the configurations. **(Bottom)** The scaling  $\bar{S}(x)$  of Eq. 2.24 is obtained, where  $x = q/q_m$  and where the height is rescaled by  $S_m$ .

$\sim 0.1$ , and this is confirmed also in the case of BiGels. As expected, the analytical approximation holds for the lower densities, and becomes less precise for the highest. For BiGels at higher densities, in fact, the differences with the analytical form result more pronounced, as shown in Fig. 5.3 and 5.4.

Note that using the Furukawa's function as a fit, the fitting parameters  $S_m(t)$  and  $q_m(t)$  have an immediate meaning: they refer to the height and wavelength values of the small- $q$  peak (explained in Par. 2.3.2), as it grows and shifts during the gelation process. They also quantify the emergent structuration and the mesoscopic domain sizes with characteristic length

$$L_m(t) = \frac{2\pi}{q_m} . \quad (5.2)$$

The time series of parameters can be used. In Fig. 5.2, for example, the collapse of the data on a master curve has been obtained by rescaling using the series of parameters. In Fig. 5.5, instead, the evolution of the parameters is explicitly shown for the aggregation during the quench for the three representative packing fractions.

The record of the fitting parameters for all the times gives a clear signature of the arrested

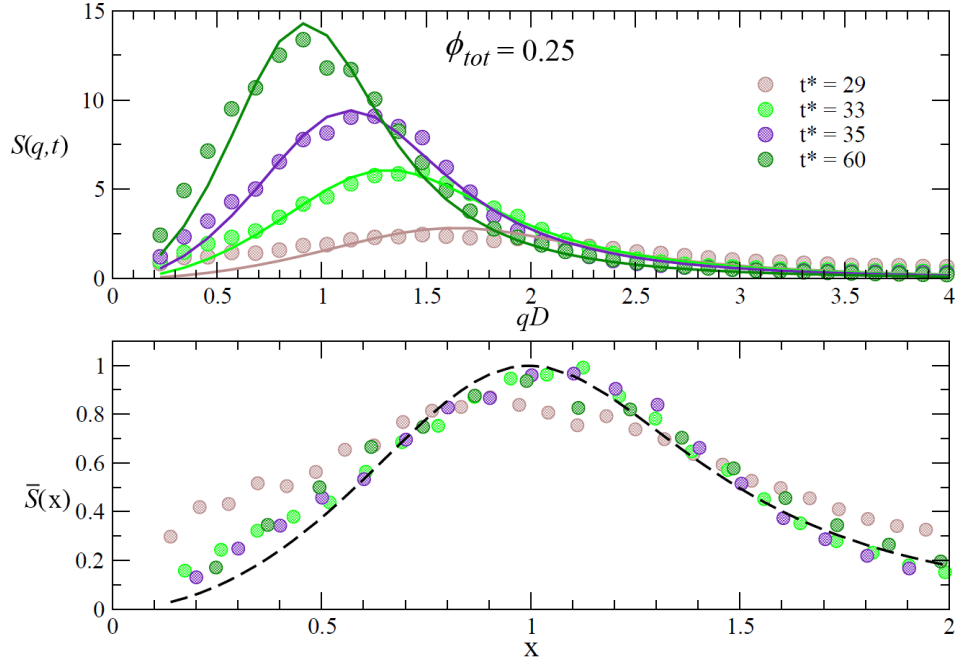


Figure 5.3: The fits with Furukawa's approximation is reported for  $\phi_{tot} = 0.25$ , together with the scaling, as in Fig. 5.2. By comparison with the previous, less dense system, here a less precise scaling follows.

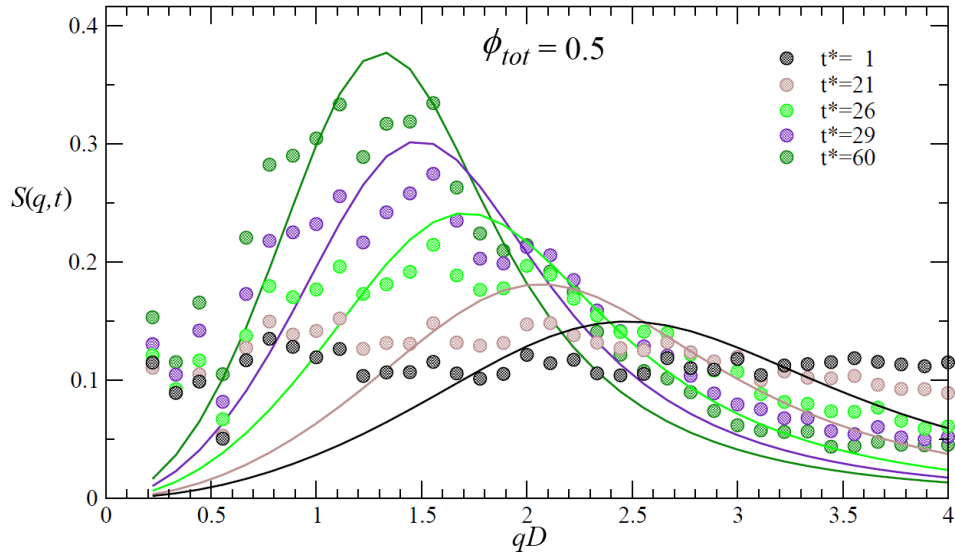


Figure 5.4: The fits with Furukawa's scaling function for the denser reference system,  $\phi_{tot} = 0.5$ . As expected, at this density the approximation clearly loses its validity.

dynamics that brings to gelation. In particular, we find that both the  $S_m(t)$  and  $q_m(t)$  reflect the slowing down and successive arrest: in particular, the growth in size of the corresponding domains (Eq. 5.2) is plotted. The values of  $L_m(t)$  identify, once the arrest is occurred, the main distance between the ramified structures that characterize the BiGel. Such a distance is

sensibly shorter for higher densities, as a result of the decreased free volume. This behavior is directly reflected by the porosity, of which we propose a measure in the next paragraph.

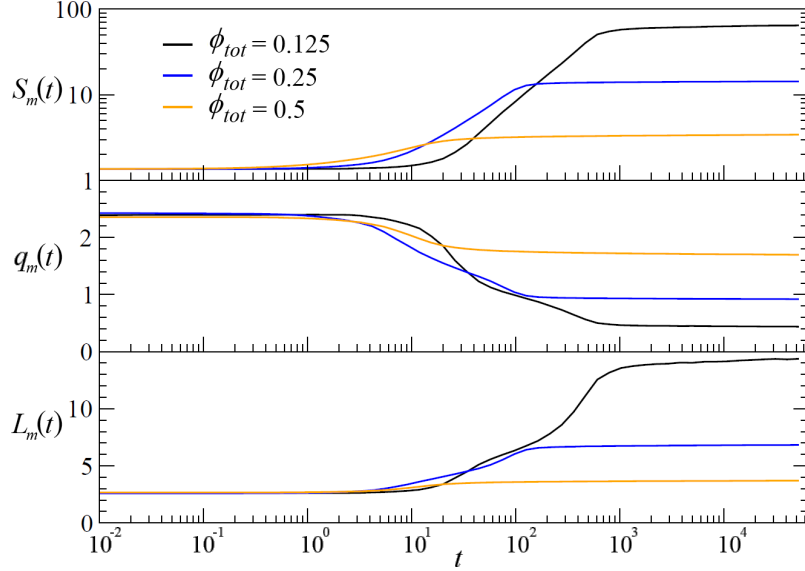


Figure 5.5: The fitting parameters of the low- $q$  peak are shown, as a function of time, for the  $S(q)$  of BiGels. Here  $S_m$  gives the peak's intensity,  $q_m$  is its position (wavelength) and  $L_m = 2\pi/q_m$  gives the characteristic size (Eq. 5.2).

### 5.1.1 Microscopy intensity measurements for BiGel.

The symmetry among the two species, in the equimolar case  $c = 0.5$ , can be investigated by means of the scattered intensity and, in turn, the Structure Factor. Similarly to what was done by Aarts and Lekkerkerker (2004), by Fourier transforming the direct images of the BiGel (and by integrating the result over the scattering angle, as by definition, Par .2.3.2) we obtain the relative structure factor. The different color channels R and G give access to the sub-gels structures, hence we can also measure their scattering intensity separately.

In Fig. 5.6 the intensity of the scattered light  $I \propto S(q)$ , integrated on the scattering angle, is shown for the two components - red and green points - and for the complete BiGel (blue points). The superposition of the R and G points reflects the structural similarity of the relative sub-gels: the symmetric composition  $c = 0.5$  makes the resulting structures be interchangeable, a fact that we will use in the analysis of the simulated BiGels, as it is possible in this case to average observable quantities over both the components.

As it happens for the simulated BiGels (see later in the present chapter), the single components present a more pronounced small-wavelength peak compared to that of the total structure. This simply reflects the larger voids one has once considering only one species and disregarding the other.

On the top of the measurements, fits are shown in Fig. 5.6 with lines. These are performed

using the Furukawa approximation [Furukawa (1989)] introduced in Par. 2.3.2, whose shape characterizes the final stages of gelation. As expected, a very good agreement exists, for both the single sub-gels and for the BiGel, thus providing further evidence of the correct spinodal-decomposition framework, driving the structuration in presence of strong demixing.

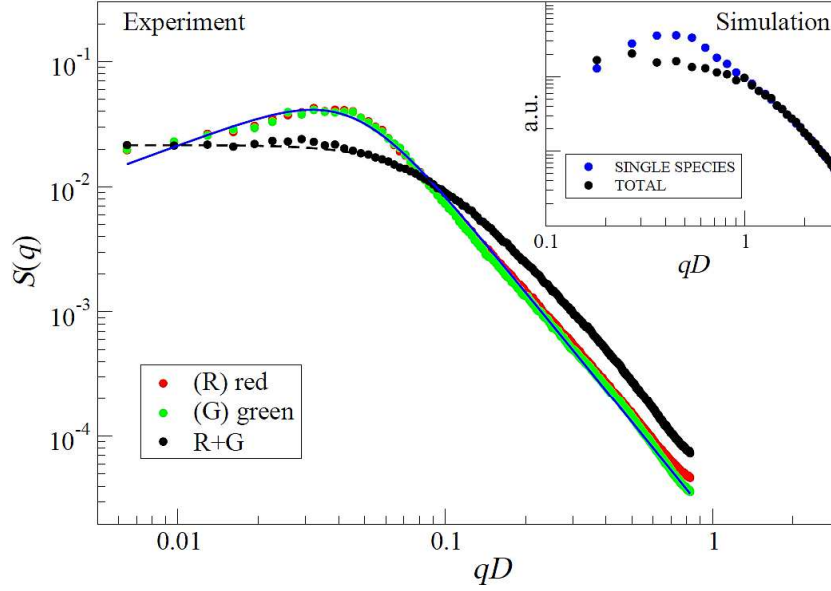


Figure 5.6: Scattering intensity for the BiGel obtained by quenching a symmetric 2CM of DNACCs (diameter  $D = 0.5\mu\text{m}$ ), the same as in Fig. 4.19. Red and green points are relative to the R (BB') and G (AA') components, respectively. The black points result from the whole BiGel structure. Both the continuous blue and the dashed black lines are fits made using the Furukawa approximation of Eq. 2.23. These provide the fitting parameters:  $d_f = \gamma - 1 = 1.622$  and  $\delta = 0.794$ , for the single sub-gels, and  $d_f = \gamma - 1 = 1.577$  and  $\delta = 0.006$ , for the BiGel. The fractal dimension  $d_f < 2$  is compatible with the quasi-2D experiments. In the inset, the final  $S(q)$  results are shown for the simulated BiGel at  $\phi_{\text{tot}} = 0.125$  (close to the density used in experiments). As for the experiments, we note an enhanced small- $q$  peak for the single components by comparison with the whole BiGel structure factor (see Figs 5.1 and 4.9).

### 5.2 Perspectives.

**ARREST OF FLUCTUATIONS: TUNABILITY FROM GENERALIZATION.** The spinodal decomposition mechanism, at the basis of the gelation, has been proven to occur for the case of demixing. Under quench, colloidal particles with mutual inter-particle attraction undergo an arrested phase separation: this is driven by local fluctuations in density  $\phi$  when the particles are indistinguishable. In this case condensation occurs. But when a distinction can be provided such that colloids are identified as belonging to different species, and when the attraction acts with selectivity rules between those species, there is competition with local fluctuations in their relative composition. In this case, the demixing phenomenon may take place, where particles of each species aggregate separately from them of distinct species. We enhanced this process, in the case of two species of square-well (SW) model colloids, by providing two conditions: the intra-species attraction overcomes the inter-species attraction, and the relative population of the two species is symmetric, i.e. has composition  $c = 50\%$ . The theoretical approach, supported by first order perturbation calculations, has explicitly shown how the passage from condensation (usual gelation) to demixing (due to selectivity) is affected by both density and composition fluctuations. Extensive numerical simulations have been performed, with the aim of testing the occurrence of gelation in the framework of selective interactions among two species. Simulations of quenches have been performed on the SW model colloids with selectivity encoded in the attractive wells. The variety of computed state-points  $(\phi, c)$  has provided data on dynamics and on the final arrested structures, then analyzed by means of different techniques. We obtained the evidence of actual demixing acting on these 2-component mixtures (2CM), and of the arrest in gel-like formations characterized by demixed structures. The study of percolation features of the mixtures has highlighted two main aspects: first, that far from the symmetric  $c = 50\%$  composition, isolated clusters of the minority species end up trapped in the percolating structure made of the other, dominant species, and second, that also a separation in the aggregation time-scales emerges when the population is not symmetric. What's more, the percolation analysis allowed to understand how the competition between condensation and demixing is reflected by the final, arrested gel phase. In fact, a strong agreement have been found regarding the regions of the  $(\phi, c)$  diagram: if demixing dominates, then both the two species form percolating structures, while only one of the two species aggregate in a percolating structure when condensation dominates. This means that not only the composition parameter  $c$  influences the kinetics of the aggregation of the two types of components, but it is also reflected in the conformation of the final arrested structures. This also proved the maximum enhancing of demixing for the symmetric 2CM.

**BiGELS: STRUCTURAL AND DYNAMICAL CHARACTERIZATIONS.** We named a BiGel the arrested, space spanning, interpenetrating structure composed by the demixed sub-gels that result from the quench of a  $c = 50\%$  mixture of colloids with selective attractions. We then focused on the symmetric mixtures and compared the formation of their single sub-gels to the classical 1-component (1CM) gels. The Structure Factor analysis during the quench has shown how

the gelation brings to structures that are locally very similar, but differ at large length-scales. In particular, we have pointed out the possible effects that a second species have on the aggregation. Such effects emerge more at high densities than at low densities, and we tested the steric effect due to the presence of a hard-sphere (HS) second species.

We simulated and analyzed quenches of SW+HS symmetric mixtures applying the same protocols used for the 2CM and the 1CM. Indeed, we have found that the steric effects are responsible for the differences in the aggregation of the two (selectively) attractive species of the 2CM by respect to the 1CM case. The study of the Structure Factor has shown something more, regarding the late stages of BiGel formation: we have recovered the (Furukawa) scaling that characterizes the spinodal decomposition for systems that phase separate in bicontinuous structures. This is another evidence of the common, generalized framework of spinodal decomposition that we proposed for the description of gelation. Nonetheless, the comparison with the simple one-component gel has thus revealed substantial differences due to the demixing. But the structures also present striking similarities on the large length-scales. We quantified such similarities, as we have found that the 1CM gel and the sub-gels of a BiGel share the same porosity (this result also applies in the SW+HS case). This evaluation has been conducted by means of a novel analysis technique, where the reconstruction of the surface embedding the gel structures allows the calculation of their topological properties. The results point out that elongated and thinner branches form the sub-gels of a BiGel, if compared with those of a gel, but that porosity does not changes in the two cases, thus justifying their global similarity. A proof of concept for the gelation driven by demixing has also been provided experimentally. Polystyrene colloids has been coated with specific DNA strands to acquire the desired selective attraction and also to mimic the main SW model features. The test on a 2CM of such DNA-coated colloids has provided the tangible evidence of the BiGel formation.

**FINAL REMARKS AND PERSPECTIVES.** The augmented number of parameters, due to the introduction of distinguishable species, increases the possibility of tuning the gelation process, as well as the resulting structures. We discussed in particular the properties of 2-component mixtures. But mixtures with  $n > 2$  components can be made, that in general give  $n \times (n - 1)/2$  mutual interactions and as many parameters, in addition to the temperature  $T$  and the density  $\phi$ . In Eq. 3.6 we defined the inter-particle interactions  $U_{ij}$  with relative well depths  $\epsilon_{ij}$  dependent on the species, and we treated the particular case of  $i, j \leq n = 2$  species:

$$I_2 = \begin{pmatrix} \epsilon_{11} & \epsilon_{12} \\ \epsilon_{21} & \epsilon_{22} \end{pmatrix} = \begin{pmatrix} 1 & 0 \\ 0 & 1 \end{pmatrix}. \quad (5.3)$$

This is a  $2 \times 2$ , diagonal interaction matrix. Its  $n \times n$  version can be envisaged,

$$I_n = \begin{pmatrix} \epsilon_{11} & \dots & \epsilon_{1n} \\ \dots & & \dots \\ \epsilon_{n1} & \dots & \epsilon_{nn} \end{pmatrix}, \quad (5.4)$$

## Chapter 5. Ongoing developments and perspectives.

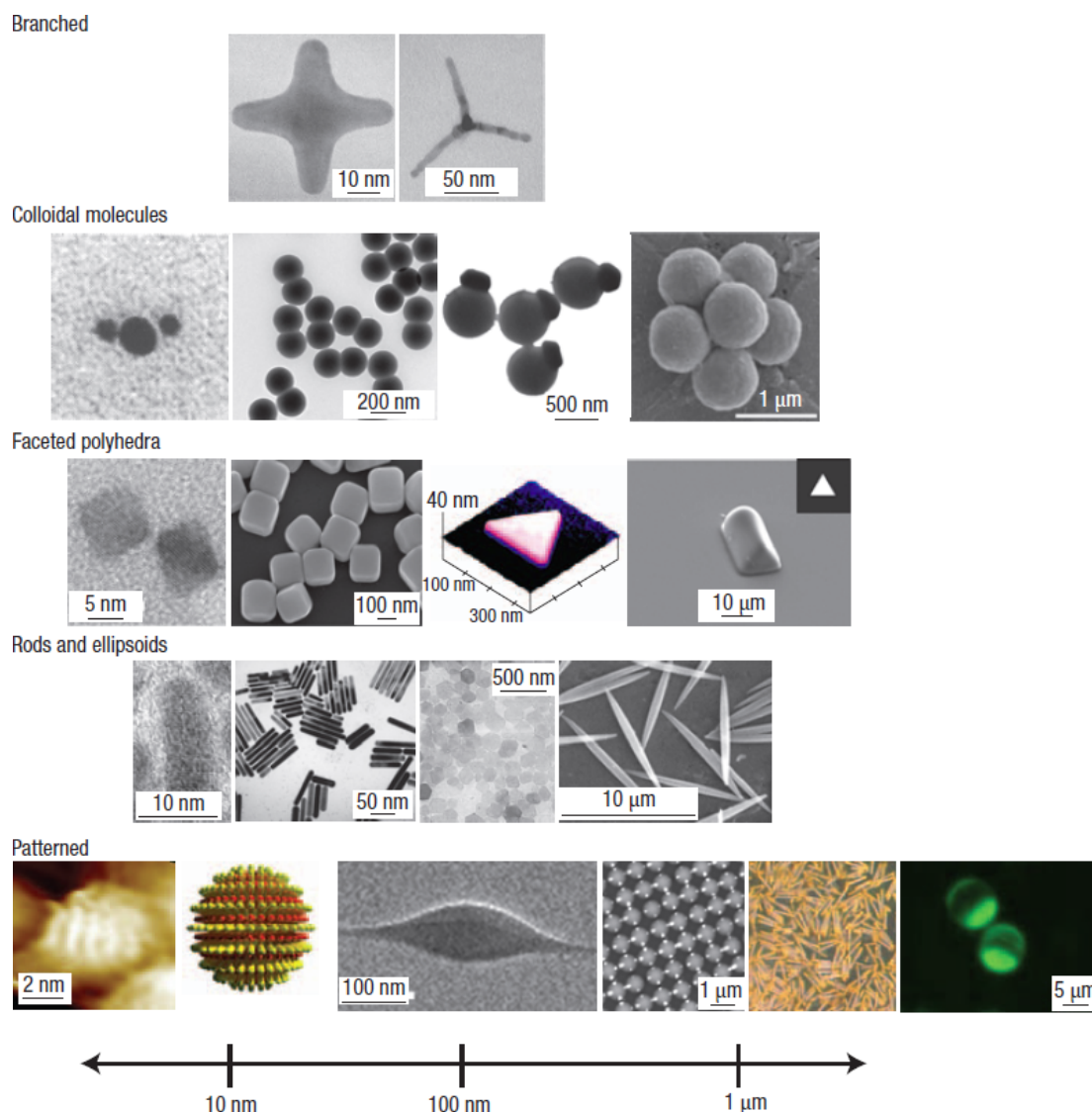


Figure 5.7: Adapted from [Glotzer and Solomon (2007)]. The nowadays available techniques offer the possibility of synthesizing a reach collection of anisotropic particles. Here we reproduce some representative examples of such building blocks (for the complete list of references to these pictures see [Glotzer and Solomon (2007)]). They are classified in rows by anisotropy type and increase in size from left to right according to the approximate scale at the bottom. From top to bottom, we show branched particles, colloids, faceted particles, rods and ellipsoids, and patterned particles. Note how in this classification, even if the single colloids have simple spherical shapes, small aggregates of them may exhibit anisotropic features (from left to right: polydisperse DNA-linked gold nanocrystals, silica dumbbells, asymmetric dimers, and fused clusters).

that would provide a generalized approach to the choice of parameters, in general, and to the competition between condensation and demixing, in particular.

A whole new family of materials may be created, where selectively interacting particles form



structures with controlled topology, solely relying on the relative presence of the simple constituent particles. Other than this, supplementary parameters could still be introduced (see example of anisotropic particles in Fig. 5.7).

In this thesis we focused on spherical particles of equal sizes and with isotropic potentials, but other shapes, as well as size polydispersity or directional potentials are viable routes for obtaining more sophisticated ways of controlling the aggregation. One of the main points is that complexity emerges, even if the constituents particles are the same simple particles that define simple liquids (recalling Chapter 1). This is due to the selective interactions, that also define the species. The amorphous structures, formed under the demixing mechanism, may also give rise to new properties. Just to mention a few, as the sub-gel topology of a BiGel results the same of a normal colloidal gel, one can think of using a 2CM where one of the two species has electrical conductive properties, so to have a material with a low content in metal depending on the single gel topology, but the mechanical properties of a denser inter-percolating BiGel. Other applications can use the different aggregation time-scales of the two species in the case of an asymmetric mixture: the slowly formed, isolated clusters are likely to present a compact crystalline structure and, thus, an gel structure with trapped colloidal crystals could be obtained. Apart from the practical use one can think of, the essence of gelation mechanism has been touched by this thesis, aiming to enlarge its comprehension. The universal mechanism of arrested phase separation have been explored when driven by fluctuations in different macroscopic parameters. This study can establish the basis for further specific studies and, together with the availability of new analysis tools, for new applications and technologies in soft matter.



# A Appendix: Conductivity enhancement from colloidal gelation.

**ENHANCING CONDUCTIVITY.** One important class of materials is that of nanocomposites, which consist in a large number of nanometric particles, like nanotubes or graphene sheets (the filler), dispersed in a more or less ordered fashion in some sort of matrix, most commonly constituted by a polymer. The reasons behind these materials (like concrete, ceramic-ceramic composites for planes, or car parts made up of carbon fiber-epoxy) may be the achievement of improved mechanical properties or the achievement of improved electrical properties with respect to the insulating matrix.

We present a model of conductivity where the filler particles form a network of globally connected objects via tunneling. Such a model does not need any abrupt cutoff of the tunneling to induce the insulator-conductor transition and, importantly, we show how the conductivity is enhanced when the particles form gel-like structures. We introduce an approximation route and explicit formulas based on the critical path method, which allow a quick and precise estimation of the overall system conductivity.

Percolation formulations generally require a sharp cutoff of the connectivity between the particles of the system in order to be applicable<sup>1</sup>. Yet, there is general agreement that, at least near the transition region, the main conduction mechanism between the conductive particles of the composite is quantum mechanical electron tunneling, and tunneling implies no abrupt interruption of the connectivity.

This conflicts with a percolation description. Such a formulation may cease to be valid especially for macroscopic filler composites<sup>2</sup>. Good conductivity at very low concentrations is the rationale behind basically all the works dealing with carbon nanotubes and carbon (or metal) nanofibers.

---

<sup>1</sup>The mainstream theory used to account for conductivity in function of the density  $\phi$  of the fillers is percolation theory [Kirkpatrick (1973); Stauffer and Aharony (1994)] and identifies the insulator-to-conductor transition with the formation of a network of electrically connected conductive particles, which extends through the material.

<sup>2</sup>For conductive plastics, the most extensively used additives are carbonaceous fillers, especially carbon black (CB). The degree of structure of the CB has profound consequences on the electrical properties of the composite. High-structured carbon blacks (HSCB) offer good conductivities at low  $\phi$  compared to less structured ones [Donnet (1993)]. The low-structured CBs (LSCB) are basically loose (generally spherical) CB particles. LSCBs have also larger sizes, in the order of hundreds of nanometers.

## Appendix A. Appendix: Conductivity enhancement from colloidal gelation.

---

**TUNNELING AND COLLOIDAL MODEL.** The present work has been done in collaboration with Biagio Nigro and Claudio Grimaldi (LPM, EPFL). Here we use the gelation of model colloidal particles to show that, in spite of a potentially little presence of metal (carried by the colloids), and even considering a simple spherical shape for the fillers, once in gel structures they can provide an optimal strategy for reducing the average distance among particles and obtaining good conductivities. Moreover, gels offer a rheological behavior that may introduce high electrical conductivity in the soft-matter domain.

We use MD computer simulations to study how the tunneling conductivity  $\sigma$  in the arrested gel phase depends on  $\phi$ . We will show that it remains relatively high even for packing fractions<sup>3</sup> as low as 3%.

Our simulations involve conducting colloids modeled as in Par. 3.1.1: the system mimics  $N$  spherical particles dispersed in an continuous insulating medium. The occupied volume fraction is  $\phi = \pi \rho D^3 / 6$  (where  $D$  is the sphere diameter,  $\rho = N/L^3$  is the number density and  $L$  is the box size). We assume that the conductance between any two particles  $i$  and  $j$  is dominated by electron tunneling processes, with conductance  $g(\delta_{ij})$ , defined by:

$$g(\delta_{ij}) = g_0 \exp\left(-\frac{2\delta_{ij}}{\xi}\right) \quad (\text{A.1})$$

where  $\delta_{ij} \equiv r_{ij} - D$  is the closest distance between particle surfaces,  $r_{ij}$  is the center-to-center distance between particles,  $\xi$  is the tunneling decay length, and  $g_0$  is a prefactor that we define as our unit of conductance; the conductance between two touching colloids is therefore defined to be  $g(0) \equiv 1$ .  $\xi$  depends on the potential barrier separating conducting and insulating phases, and typically ranges from a fraction of a nanometer to a few nanometers [Nabok et al. (2004)]. Consequently,  $\xi/D \lesssim 0.1$  for particles larger than a few nanometers, for which, consistently with Eq. A.1, charging and Coulomb interactions effects on electron transfer can be safely neglected at room temperature.

As explained in Par. 3.1.1, for colloidal systems with short-ranged attractions,  $\lambda/D \lesssim 0.05$ , thermodynamic properties at a given  $\phi$  depend not on the specific shape of the potential  $u(r)$ , but only on its integral, expressed as a reduced second virial coefficient  $B_2^* = (3/D^3) \int dr r^2 [1 - e^{-u(r)/k_B T}]$ , where  $T$  is the temperature [Noro and Frenkel (2000); Foffi and Sciortino (2006); Malijevsky et al. (2006); Lu et al. (2008)]. In particular, short-ranged attractive colloidal spheres are in an equilibrium fluid phase for  $B_2^* \gtrsim B_2^{*c}$ , where  $B_2^{*c} \simeq -1.2$  [Miller and Frenkel (2003); Largo et al. (2008)] is the critical scaled second virial coefficient. We use the short-range square-well (SW) model in Eq. 2.6 for the colloidal interaction,

$$u(\delta_{ij}) = \begin{cases} \infty & \delta_{ij} \leq 0 \\ -u_0 & 0 < \delta_{ij} \leq \lambda D \\ 0 & \delta_{ij} > \lambda D \end{cases} \quad (\text{A.2})$$

---

<sup>3</sup>In the low- $\phi$  regime, we also find that  $\sigma$  is only moderately affected by varying  $\xi/D$  by as much as one order of magnitude, where  $\xi$  is the characteristic tunneling decay length.

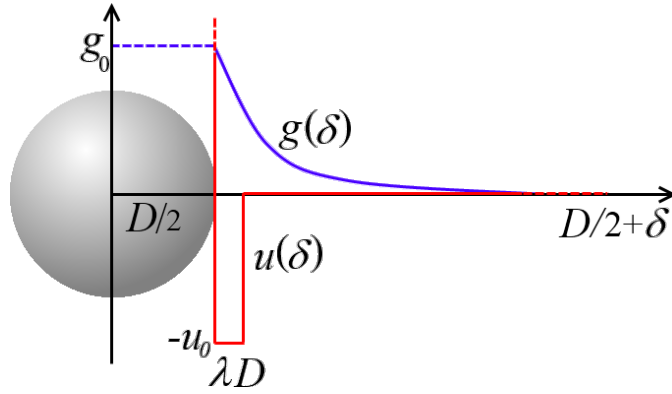


Figure A.1: Schematic representation of the SW model potential (red line) and of the tunneling conductance (blue line). The variable  $\delta$  measures the closest distance between surfaces of colloids. Indicated are the well depth  $u_0$  and the range  $\lambda D$  of the potential, as well as the contact value  $g_0$  of the conductance.

where  $\lambda \ll 1$  and  $u_0 > 0$  are, respectively, the dimensionless potential range and depth. As in Eq. A.1,  $\delta_{ij}$  denotes the closest distance between surfaces of particle pairs. The scaled virial coefficient of the potential in Eq. A.2 can be expressed as  $B_2^* = 1 - 1/4\tau$ , where  $\tau^{-1} = 4[(1 + \lambda)^3 - 1][\exp(u_0/T) - 1]$  is the Baxter stickiness parameter [Baxter (1968)]. Consequently, a homogeneous SW fluid exists when  $\tau \gtrsim \tau_c$ , where  $\tau_c \sim 0.11$  is the critical value of the stickiness parameter [Miller and Frenkel (2003); Largo et al. (2008)].

The inter-particle attraction enhances conductivity by drawing the particles closer together; in particular, the population of particles with separations lower than  $\lambda D$  increases, thereby promoting short-length tunneling processes, which result in larger  $g(\delta_{ij})$ . Thus, SW fluids of conducting particles can display enhanced conductivity  $\sigma$  relative to the hard-sphere case as  $\tau$  is decreased [Nigro et al. (2012)]. Specifically, in attractive colloidal fluids where  $\lambda \rightarrow 0$ ,  $\tau = 0.2$ , and  $\xi/D = 0.01$ ,  $\sigma$  is relatively large and depends only weakly on  $\phi$  for  $\phi \gtrsim 0.2$  [Nigro et al. (2012)]. Short-ranged attractive colloids constitute homogeneous fluids for  $B_2^*$  above the value  $B_2^{*c}$  (i.e.,  $\tau > \tau_c$ ); below that, a phase separation region exists where they can arrest and form spanning, arrested structures that may sustain shear stresses even at low  $\phi$  [Lu et al. (2008); Foffi et al. (2005b,a); Del Gado (2010)]. In these configurations larger tunneling conductivities might be expected, compared to the fluid phase at a given  $\phi$ , because the mean particle separation falls below  $\lambda D$ .

**FAVORABLE STRUCTURES FROM GELATION.** To explore this possibility, we generate colloidal gel structures from molecular dynamics (MD) simulations of  $N = 10^4$  identical colloids of mass  $m$ , square well depth  $u_0 = 1$ , and  $\lambda = 0.03$ ; a critical temperature  $T_c \simeq 0.3$  corresponds to these parameters. We code Newtonian dynamics via a standard event-driven algorithm [Rapaport (1997); Foffi et al. (2005a)]. At  $t = 0$  we select five different packing fractions, ranging from  $\phi \simeq 0.03$  to  $\phi \simeq 0.3$ , and equilibrate initial configurations at  $T = 100 \gg T_c$ , where these systems

## Appendix A. Appendix: Conductivity enhancement from colloidal gelation.

behave as hard-sphere (HS) fluids:  $B_2^* \sim 1$ . We define two particles as bonded when  $\delta_{ij} \leq \lambda D$ , so that the average number of bonds per particle is  $n_b = -2U/(Nu_0)$ , where  $U/N$  is the potential energy per particle calculated from 30 independent realizations. For  $t > 0$ , we quench the system to  $T = 0.05 \ll T_c$  with the same protocol described in Par. 3.1.1.

To characterize the conductive properties of these structures, we analyze the time evolution of the percolation critical distance  $\delta_c$ , defined as the shortest  $\delta_{ij}$  such that the subnetwork defined by all bonds satisfying  $\delta_{ij} \leq \delta_c$  forms a percolating cluster [Nigro et al. (2012)]. We show below that  $\delta_c$ , which characterizes the global connectivity of the system, provides a useful approximation for the tunneling conductivity.

At short times, particles are dispersed nearly homogeneously and  $\delta_{ij}$  (and therefore  $\delta_c$ ) decreases as  $\phi$  increases. See Fig. A.2(a). However, when the system is arrested at long times, the vast majority particles forming the spanning gel structure have separations lower than  $\lambda D$ , and  $\delta_c$  becomes small (about  $0.01D$ ) and independent of  $\phi$ . Nevertheless, though the final value of  $\delta_c$  is the same, there are significant  $\phi$ -dependent differences in reaching this state. For the three largest concentrations,  $\delta_c$  monotonically approaches the arrested state value; instead, for  $\phi = 0.0613$  and  $0.03125$ ,  $\delta_c$  exhibits a pronounced maximum at intermediate times, followed by a sudden drop towards the arrested state, which may reflect the formation and subsequent disappearance of a fluid of particle clusters [Lu et al. (2006)]. In this intermediate regime, where the particles are largely aggregated into nearly close-packed clusters, the mean distance between clusters is larger at lower  $\phi$ . As shown in Fig. A.2(a), percolation occurs only for higher  $\delta_c$ .

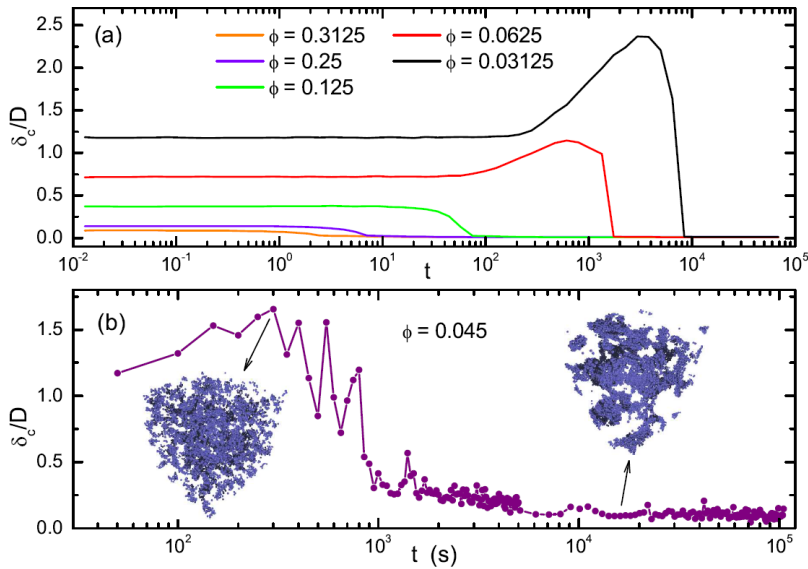


Figure A.2: (a) Evolution of the critical connectedness distance  $\delta_c$  for gels simulated at different packing fractions. (b) Time dependence (in seconds) of the critical distance extracted from the measured spatial positions of PMMA particles in a polymer-colloid system [Lu et al. (2008)]. For times larger than about  $10^4$  s the system is in an arrested gel state.

**FROM MODEL TO LAB.** To assess the applicability of these simulation predictions to physical systems, we perform the same analysis on gels formed in an experimental attractive colloid system [Lu et al. (2008)]. We use PHSA-coated PMMA spheres in CXB/DHN [Lu et al. (2006)], with  $D \simeq 1120$  nm and  $\phi = 0.045$ , and introduce a non-adsorbing linear polymer, polystyrene with molecular weight  $M_W = 695,000$ , that forms random coils in solution with radius  $R_p = 33$  nm, so that  $\lambda = 0.06$  [Lu et al. (2008)]. We select a sample with polymer concentration  $c_p = 3.31$  mg/ml, which phase separates and arrests to form a gel [Lu et al. (2008)]. Using confocal microscopy [Lu et al. (2007)], we locate each particle individually [Lu et al. (2006, 2007, 2008)], thereby allowing the same analysis as performed on the MD data. Strikingly, the evolution of experimental  $\delta_c$  is in qualitative agreement with the MD simulations at similar  $\phi$ , as shown in Fig 2(b). Although the initial low-time plateau cannot be sampled practically in these experiments, a maximum of  $\delta_c$  is discernible at  $t \simeq 300$  s, followed by a rapid drop of  $\delta_c$  at longer times. For  $t \gtrsim 10^4$  s, the system reaches the arrested gel state, and  $\delta_c/D \simeq 0.1$ , independent of time. This transition associated with the formation of an arrested gel, consistent with behavior observed in simulation, is illustrated by the renderings of the measured particle positions in Fig. A.2(b).

The qualitative agreement between simulation and experimental data demonstrates the validity of our theoretical approach, which we extend now to predictions of the tunneling conductivity. Starting with the critical path approximation (CPA), we estimate the conductivity by means of the CPA formula:

$$\sigma_{\text{cpa}} \simeq \sigma_0 \exp\left(-\frac{2\delta_c}{\xi}\right), \quad (\text{A.3})$$

where  $\sigma_0$  is a constant prefactor [Ambegaokar et al. (1971); Pollak (1972)]. When the  $\delta_{ij}$  distances are widely distributed on a length scale of the order of  $\xi$ ,  $\sigma_{\text{cpa}}$  provides a robust estimate of system conductivity for dispersions of tunneling connected particles [Nigro et al. (2012); Ambrosetti et al. (2010)]. We combine the time evolution predictions for  $\delta_c$ , as shown in Fig. A.2(a), with Eq. A.3, to yield an estimate for the time evolution of the system conductivity. We observe that a broad distribution of  $\phi$ -dependent  $\sigma_{\text{cpa}}$  conductivities, spanning about ten orders of magnitude, drastically narrows in the arrested gel state, where  $\sigma_{\text{cpa}}$  remains at a constant high value<sup>4</sup> for all  $\phi$ , as shown for  $\xi = 0.1D$  with solid lines in Fig. A.3. Interestingly, for the two lowest  $\phi$  values, the maximum of  $\delta_c$  due to the transitory fluid of clusters is reflected by a huge minimum of  $\sigma_{\text{CPA}}$ ; fluids of clusters of conducting particles appear to be substantially worse conductors than a homogeneous fluid of the same composition.

To test the accuracy of the results obtained using the CPA approximation, shown in Fig. A.3, we solve numerically the tunneling resistor network equations. For each simulation-generated configuration, we assign the inter-particle conductances of Eq. A.1 to each pair of particles. For all realizations, we calculate network conductance by combining numerical decimation with a

<sup>4</sup>In plotting the CPA conductivity results of Fig. A.3 we have fixed the prefactor appearing in Eq. A.3 to  $\sigma_0 = 0.1$ , which is the value found for hard-spheres fluids [Nigro et al. (2012)].

## Appendix A. Appendix: Conductivity enhancement from colloidal gelation.

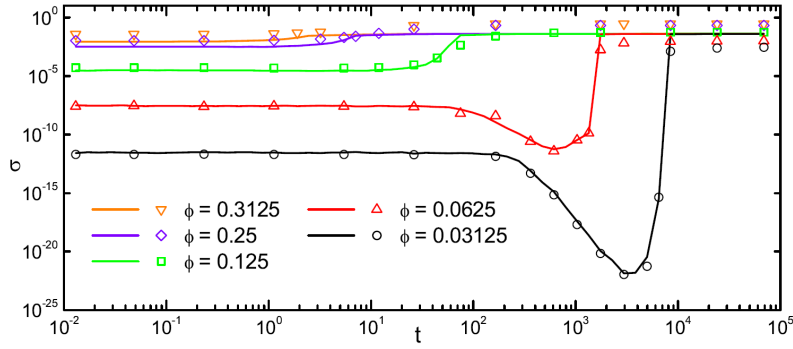


Figure A.3: Time evolution of the conductivity  $\sigma$  for  $\xi/D = 0.1$  during the formation of the colloidal gel. The symbols refer to numerical solution of the tunneling resistor equations. The solid lines represent the CPA conductivity  $\sigma_{\text{CPA}}$  obtained from Eq. A.3 with  $\sigma_0 = 0.1$ .

preconditioned conjugate gradient method and extract  $\sigma$  from the resulting distribution [Nigro et al. (2012)]. The  $\sigma$  values obtained through this network approach are in quantitative agreement with those calculated in the CPA approximation, as shown by the agreement between open symbols and solid lines in Fig. A.3. The slight discrepancy in  $\phi$ -dispersion of arrested states likely arises from the short- and moderately-dispersed distances between the neighboring particles of the spanning gel structure, which make Eq. A.1 less accurate.

**CONSTRAINTS AND POSSIBILITIES.** The significantly higher  $\sigma$  in the long-time arrested gel state relative to the initial fluid-like state, most pronounced for low  $\phi$  and highlighted in Fig. A.3, suggests the general possibility that arrested gel structures could have higher  $\sigma$  relative to other structures formed from tunneling particles in colloidal suspensions at the same  $\phi$ . To test this possibility, we generated equilibrium fluids at various  $\phi$  of both HS and SW particles, with  $\tau = 0.2 > \tau_c$ ; we determine  $\sigma$  for  $\xi/D = 0.01$ , as previously described, and compare with the long-time  $\sigma$  of the arrested gel state as a function of  $\phi$ . In all cases, at any given  $\phi$ , the gel state has a higher  $\sigma$  than that of the SW fluid, which in turn is always higher than that of the hard-sphere fluid, as shown with circles, diamonds and squares, respectively, in Fig. A.4. The  $\sigma$  values for gel and SW fluid converge for high  $\phi \gg 0.3$ ; by contrast, for  $\phi \lesssim 0.2$ ,  $\sigma$  of the arrested state is many orders of magnitude higher than that of either fluid. Interestingly, while  $\sigma$  depends heavily on  $\phi$  in both fluid cases, it is relatively constant in the gel case, even for  $\phi \approx 0.03$ , as shown in Fig. A.4.

Finally, to explore how the conductivity varies with tunneling decay length, we calculate  $\sigma$  of arrested gels with different  $\phi$  and  $\xi/D$ . We observe that  $\sigma$  only weakly depends on  $\xi/D$  in the gel state, due to short inter-particle distances within the gel. Indeed, the relevant length-scale is  $\delta_c/D$ ; in the arrested state,  $\delta_c \approx 0.01D$ , and tunneling is generally unaffected so long as  $2\delta_c/\xi \lesssim 1$ , i.e., as long as  $\xi/D \gtrsim 0.02$ . At much lower values,  $\xi/D$  suppresses inter-particle tunneling, so that  $\sigma$  is small even in the arrested gel state.

Our predictions from simulation may have significant effects in relevant, real-world colloidal



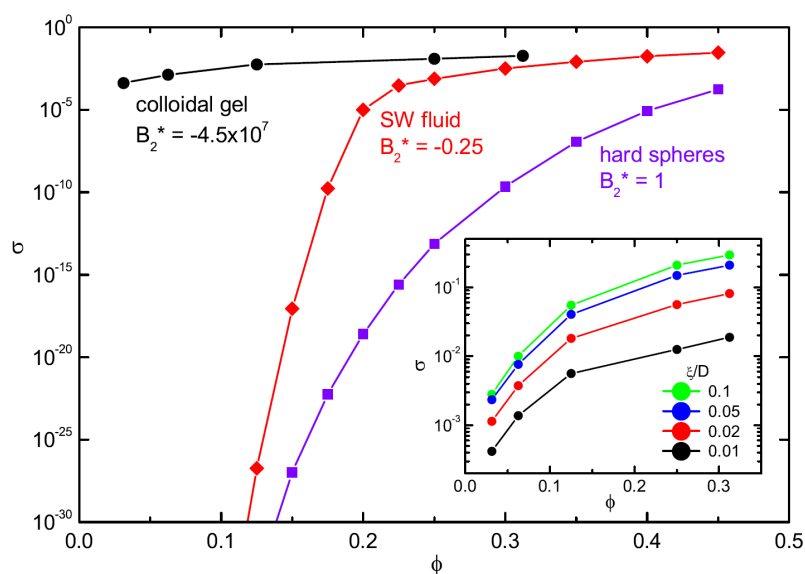


Figure A.4: Conductivity  $\sigma$  as a function of the packing fraction  $\phi$  for the arrested gel state (filled circles), equilibrium SW fluids (filled diamonds), and equilibrium HS fluids (squares). For all cases  $\xi/D = 0.01$ . The conductivities for SW and HS fluids have been obtained from Monte-Carlo simulations of systems with  $N = 2000$  particles. Inset:  $\phi$ -dependence of  $\sigma$  for the arrested gel state calculated for different values of  $\xi/D$ .

systems. In general, for attractive systems, polymers mediating the depletion interaction have radii larger than about 1-5 nm [Ramakrishnan et al. (2002)]. To have attraction range values on the order of a few percent of the particle diameter, the conducting particles should have sizes not smaller than about 50-100 nm. Therefore, for typical tunneling decay lengths of a few nm, conductivities like those in Fig. A.4 may yet be achievable in the lab, at least in principle. The conducting particles remain a major challenge, and suspensions of larger metallic particles show significant sedimentation, that may compromise the formation of gels. Potential solutions around this problem include using metal-coated PMMA particles, low-structured carbon black particles, conducting polymer particles, or synthesizing gels in a micro-gravity environment, such as that provided by the International Space Station. These systems contrast previous work where conducting particles were embedded in pre-existing gel networks [Fizazi et al. (1990)], by contrast, in the present system, the conducting particles establish simultaneously both the gel network and the conducting path.

Our results demonstrate that conduction via tunneling in gels of conducting colloidal particles can occur with realistic assumptions for the microscopic parameters, opening up the possibility of creating new, lightweight conductive materials with novel mechanical and electrical properties.



## B Appendix: Imaging with Confocal Microscopy.

Scattering techniques average over a large ensemble, so measurements can be fast and statistical uncertainties small. Light scattering provides then quantitative characterization of the average structure and dynamics of suspended particles. Structural and dynamic heterogeneities typically cannot be detected and spatially mapped with light scattering, like in the case of gels.

To this aim, *confocal microscopy* is instead used in the study of colloidal gels, glasses, and binary fluids [Dinsmore et al. (2001); Prasad et al. (2007)]. The measurements allow to track three-dimensional positions of colloidal particles with a precision  $\lesssim 10$  nm (which is in general a small fraction of each particle's size) and with a time resolution sufficient for recording the thermal motions of several thousand particles at once. The imaging principles are schematically depicted in Fig. B.1.

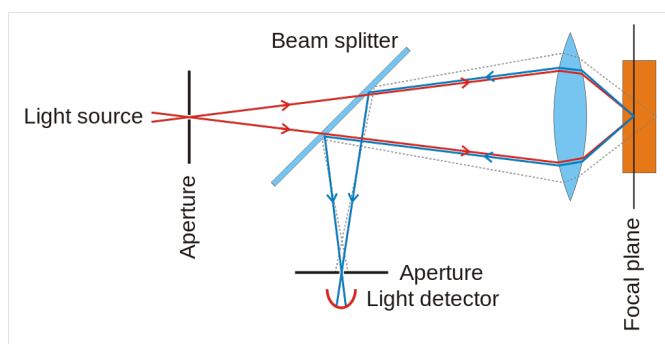


Figure B.1: Schematic diagram of a conventional confocal microscope. The key to the technique is the use of a pinhole aperture that is confocal with the image point. The screen with the pinhole lies in the back focal plane of the sample with respect to the objective, thus rejecting most out-of-focus light. The aperture blocks light from other points in the sample and permits the imaging of a unique, well-defined spot deep inside the sample. Rotating mirrors are often used to scan the sample, pixel by pixel, and such a rotation (together with the images recording rapidity) defines the rate-limiting step for obtaining an image.

## Appendix B. Appendix: Imaging with Confocal Microscopy.

---

A confocal microscope uses point illumination and a pinhole in an optically conjugate plane in front of the detector to eliminate out-of-focus signal - the name “confocal” stems from this configuration. Once the solvent matches the refractive index of the particles, it is possible to look several tens of colloidal radii into the sample, without noticeable loss of resolution. As only light produced by fluorescence very close to the focal plane can be detected, the image’s optical resolution is limited principally by movement of the particles. These types of microscopes are particularly good at 3D imaging and surface profiling of samples<sup>1</sup>. In Fig. B.2, as an example, a single confocal image and a complete 3D rendering are shown, representing the reconstruction of positions of PMMA spherical particles which form a gel under depletion attraction [Lu et al. (2008)].

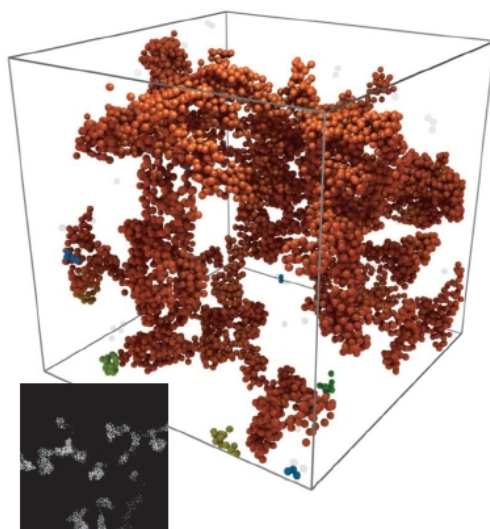


Figure B.2: 3D reconstruction and confocal image of a gel of spherical PMMA particles, from [Lu et al. (2008)].

The structural information captured with this technique allows to characterize both the structure and the dynamics of these materials in quantitatively new ways. For example, one can quantify the topology of chains and clusters of particles as well as by measuring the spatial correlations between particles with high mobilities. This experimental technique and related analysis are often used as the most valid complement of light scattering studies.

The use of a confocal microscope in colloid physics, however, requires specialized samples and, in particular, the development of powerful image-analysis algorithms. These measurements provide qualitatively new understanding of colloidal aggregation and phase transitions. For gels and dense binary fluids the confocal microscope permits unique insight into the structural heterogeneities of the material.

Gels formed by depletion or temperature driven destabilization have weaker attractive forces,

---

<sup>1</sup>This technique has been applied, for example, to the study of colloidal glasses structures [van Blaaderen and Wiltzius (1995); Weeks et al. (2000)].

---

and thus a stable gel phase forms at higher volume fractions. The topology of these gels at short length scales below a cluster size becomes important and confocal microscopy provides valuable information on these dense systems.



## C Appendix: Growth of random configurations of hard spheres.

We developed a novel algorithm with the aim of creating random configurations of hard spheres (HS) enclosed in a box of size  $L$ . The algorithm works in all the Euclidean dimensions  $d$ , so that  $V = L^d$  is the box's volume. It generates configurations of  $N$  HS with diameter  $D$  starting from  $N$  points randomly placed into the box. The way these points are inflated is described in what follows. The growth method uses an approach different by respect to the usual "cherry-pit" method [Lubachevsky and Stillinger (1990); Lubachevsky et al. (1991); Kansal et al. (2002)]. We do not use the random sequential addition (RSA) algorithm, often applied in the context of jamming hard spheres [Talbot et al. (1991)]

In the following we introduce the basics steps of the developed algorithm. As a first step, the relative distances between all the point are calculated. Given a distance  $r_{ij}$  among the centers of the particles  $i$  and  $j$ , the diameter  $D_i = 2 \times \min(r_{ij})$  will be assigned to the particle  $i$ . The diameters are given up to the desired value  $D$ : the packing fraction at each step  $n$  of the algorithm is then  $\phi_n < \phi$ , where

$$\phi = C_d D^d \quad (\text{C.1})$$

is the target density, and where

$$C_d = \frac{2\pi^{d/2}}{\Gamma(d/2)d} = \begin{cases} \frac{1}{2^d} \frac{\pi^{d/2}}{(d/2)!} & \text{for even } d \\ \frac{1}{2^{(d-1)/2}} \frac{\pi^{(d-1)/2}}{d!!} & \text{for odd } d \end{cases} .$$

is the curvature factor. For  $d = 3$ , Eq. C.1 gives the usual  $\phi = N\pi D^3/6$ . A neighbor list is implemented in order to keep a low computational cost of the entire algorithm. For each particle  $i$ , the distances  $\vec{r}_{ij}$  are computed with the other particles  $j$ . The molecular dynamics is such that, at each step  $n$ , a displacement  $\Delta\vec{r}_i$  is computed for all the  $i \leq N$  particles as

$$\Delta\vec{r}_i = \sum_j^{\text{neigh.}} \frac{A_n}{2} \left[ f_n P(r_{ij}) \frac{\vec{r}_{ij}}{r_{ij}} + (1 - f_n) \vec{r}_{ij} \right] \quad (\text{C.2})$$

## Appendix C. Appendix: Growth of random configurations of hard spheres.

---

where  $P(r_{ij}) = D \exp[-f_n(r_{ij}/D)^d]$  represents a pair-wise function calculated into a cutoff  $r_{ij} < D$ , where  $f_n = \phi_{n-1}/\phi$  is the fraction of density obtained at the precedent step, and where  $A_n = A_{n-1} \exp(-d\phi_n)[1 + f_n - f_{n-1}]$ , with  $A_0 = 1$ , is an adaptive term depending on the story<sup>1</sup>. The simulation depends also on different circumstances. In fact, it could happen that a local jamming among particles not yet arrived to size  $D$  may occur: in this case, a contraction of all the particles is performed such that the density will come back to the  $\phi_{n-1}$  values and, in order to unjam, little random displacements are made. After each step, when all the particles that had to move have been displaced, the new minimal distances are calculated, and the new density  $\phi_n$  as well. The growth procedure stops when all the particles reach the desired diameter  $D$ .

The proposed algorithm can tackle packings of high densities without any important increase of the computation time: in its PYTHON implementation, it takes  $\sim 3$  walltime minutes for packing  $N = 10^3$  spheres to  $\phi = 0.6$ , and it scales linearly with  $N$ . In order to analyze whether a jamming is going to occur, the (normalized) *polydispersity*  $p_n$  and the *compressibility*  $Z_n$  histories are tracked:

$$p_n = \frac{\langle \sqrt{\langle R_{i,n}^2 \rangle} - R_{i,n} \rangle}{R} \quad (\text{C.3})$$

where the average is made on all the  $i$  particles of radius  $R_{i,n} < R$ , while the Carnahan-Starling equation for compressibility in  $d = 3$ , with the Kolafa's correction [Carnahan and Starling (1969); Boublik (1970)], is

$$Z_n = \frac{1 + \phi_n + \phi_n^2 - \frac{2}{3}(\phi_n^3 + \phi_n^4)}{(1 - \phi_n)^3}. \quad (\text{C.4})$$

By simply checking whether these two quantities are lowering along the last 2 steps, is a sufficient indication for deciding to contraction plus shaking procedure. The polydispersity and compressibility evolutions are shown, for few examples, in Fig. C.1. Note that a little number of steps is needed to attain the final density, passing from a order of 10s to a order of 100s (the plots in figure refer to  $N = 3 \times 10^3$ ) for densities ranging from  $\phi = 0.15$  to  $\phi = 0.6$ .

The *ad-hoc* molecular dynamics used for our packings will be shown to reach configurations close to the equilibrium ones, i.e. configurations attained by HS free to move and to interact following the simple Newtonian laws [Kirkwood (1935); Hansen and Verlet (1969); Cheng et al. (2002)]. Even though, basic differences emerge due to the ad-hoc dynamics.

There are various theories which predict the low and medium volume fraction structure of HS

---

<sup>1</sup> $P(r_{ij})$  could be considered as repulsive, adaptive potential, but the lack of physical dynamics makes this parallel incorrect.



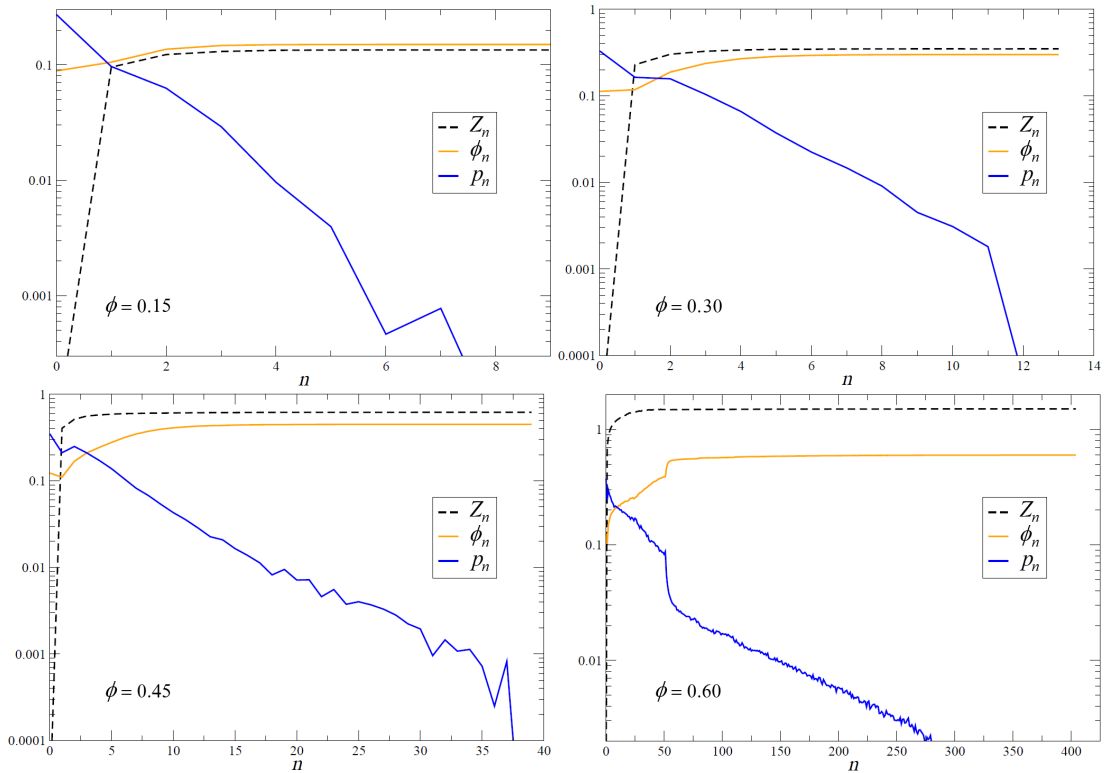


Figure C.1: The compressibility  $Z_n$  (Eq. C.4, dashed lines), the polydispersity  $p_n$  (Eq. C.3, blue lines) and the density  $\phi_n$  are shown as a function of algorithm steps. These curves are not averaged over many runs, but single runs are considered for various final packing fractions  $\phi$ .

fluids<sup>2</sup>. None of these, however, is expected to work reliably<sup>3</sup> at high  $\phi$ .

A comparison for the final packing is possible<sup>4</sup>, relying on statistical physics. In Fig. C.2 there we show the comparison of the pair distribution functions  $g(r)$  for final configurations (obtained from single runs of the algorithm) and the relative Verlet-Weis predictions at various densities [Smith et al. (2008)]. Note how the lack an equilibrium dynamics makes the resulting configurations strongly depend on the random positioning of the initial growing points: the peak relative to the initial random placements are mitigated for higher densities, where an increase in overlaps bring to an increased number of displacements and, as a result, a loss of

<sup>2</sup>The phenomenological Carnahan-Starling approach works remarkably well for low to medium volume fractions. The Ornstein-Zernike relation works for the liquid branch of the HS equation of state [Hansen and McDonald (1986)]. For liquid states, the Percus-Yevick closure is often used, especially Verlet-Weis correction [Hansen and McDonald (1986); Zaccone and Del Gado (2010)].

<sup>3</sup>One recent study in the spirit of these approaches has predicted the number of contacting neighbors as a function of volume fraction [Zaccone and Del Gado (2010)].

<sup>4</sup>The densest packing for  $d = 3$  has been proven to be attained by the FCC lattice with packing fraction  $\phi_{\max} = \pi/\sqrt{18} \approx 0.7404$  [Hales (1992)]. With the Verlet-Weiss correction to the Percus-Yevick structure factor for hard spheres, the simplest formulation predicts a glass transition at  $\phi_g = 0.525$  (which is low compared to the known jamming transition density  $\phi_j \approx 0.64$ ) [Hansen and McDonald (1986); Torquato et al. (2000); Zaccone and Del Gado (2010)].

**Appendix C. Appendix: Growth of random configurations of hard spheres.**

memory of the initial configuration.

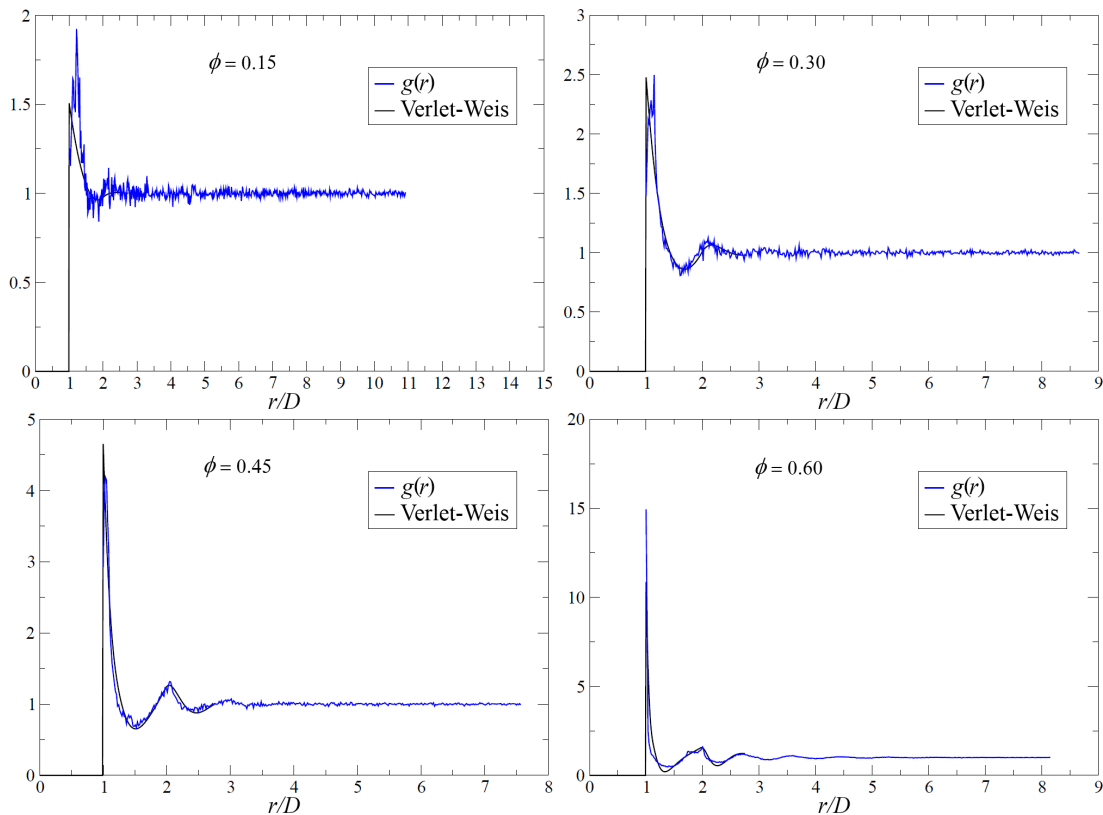


Figure C.2: Pair distribution functions  $g(r)$  relative to final configurations, at different densities, from the same, single runs of Fig. C.1. The blue lines indicate the actual data obtained from the proposed algorithm, while the black lines indicate the Verlet-Weis approximations for a hard-sphere liquid at equilibrium. For low packing fractions, the initial random placement of growing points strongly influences the final result. For higher densities, instead, more steps and consequently more movements for the spheres (as they are inflated) makes the first configuration be completely changed: the analytical equilibrium approximation works better. Close and above the ideal jamming density ( $\phi_g = 0.525$ ) the algorithm shows to form more locally compact (crystal-like) arrangements, reflected in the pronounced peaks of the  $g(r)$ .

## D Appendix: Physical fractals of spheres.

A modified version of the algorithm for the creation of packings (introduced in Appendix C) is here presented for spheres (or circles, depending on the dimension) with high polydispersity. The present work, conducted during the thesis, has started as a method aimed to account for inserting and filling the void space of amorphous structures, in order to characterize their porosity. It turned out that the pursuit of perfect space filling enters the broad span of theories connected with self-similarity and, hence, fractals. With the help of the developed algorithm, later introduced in its new version, we have been able to analytically introduce corrections, due to the finite size effect, to the usual power-law distribution for fractal objects. Such corrections result in a generalization of the scale-free distribution and allow a quantitative study for finite ranges of sizes  $s \in [s_{\min}, s_{\max}]$ , the *physical fractals*, and not only for the asymptotic limit  $s_{\min}/s_{\max} \rightarrow 0$  (in what follows,  $s$  is used instead of  $D$  for the diameters). Moreover, the new, efficient space-filling algorithm has been developed which generates osculatory random Apollonian packings (AP) of spheres with a finite range of diameters: not only the known AP's fractal dimensions are recovered but an excellent agreement with the generalized law is proved to be valid within the overall ranges of sizes.

**THE PURSUIT OF PERFECT PACKING.** The problem of finding the circle inscribed into the interstices between mutually tangential circles and tangent to them (a so-called *osculatory packing*), historically attributed to Apollonius of Perga, was solved by Descartes and independently rediscovered various times [Soddy (1936)]. Leibniz pointed out the possibility of obtaining a peculiar kind of packing by iterating the procedure of inserting such *kissing* circles, whose size decreases as the inserting procedure goes on [Hirano (2010)]. By starting from an initial configuration and by recursively filling the space with the osculatory packing down to arbitrarily small diameters, the *Apollonian packing* (AP) is constructed. In Fig. D.1 two examples of AP are presented for Euclidean dimension  $d = 2$ . The structure of an AP is *self-similar* because it is repeated on different scales of observation. In general, the self-similarity can be exact or statistical and leads to a fractal. The main quantity characterizing a fractal structure is the *fractal dimension*,  $d_f$ , which is a (Lipschitz) invariant of the set descending from the

## Appendix D. Appendix: Physical fractals of spheres.

---

Hausdorff-Besicovitch (HB) measure definition and possibly differs from the Euclidean dimension  $d$  [Mandelbrot (1983); Fröhlich and Ruelle (1983)].

The osculatory packing construction has been extended to  $d > 2$  and the study of systems of polydisperse spheres is made in the attempt of understanding how their fractality affects some macroscopic observables and, by reverse, how their formation mechanism influences their fractality. In particular, in  $d = 3$ , the AP has been proposed as a model for dense granular systems [Anishchik and Medvedev (1995)]. It has been also used in describing stress yielding properties of materials, for example in concretes [Aste and Weaire (2008)], as well as in the study of seismic gaps or geological faults [Baram et al. (2004)]. Moreover the scale-free properties of the AP are of particular interest in the context of complex networks [Andrade et al. (2005); Doye and Massen (2005)]. Recently AP of non-spherical objects have also been studied [Dodds and Weitz (2003); Delaney et al. (2008)].

While the application and the characterization of the AP has been widely studied, there is no exact theoretical prediction for the value of  $d_f$  in 2 and 3 dimensions and various techniques have been developed to build AP and numerically evaluate their  $d_f$ . For example, it has been calculated for the plane tiled with circles obtained by the circular inversion method [Manna and Herrmann (1991)]. In  $d = 3$ , a generalized inversion algorithm has been adopted [Borkovec et al. (1994)].

So far we have discussed the deterministic AP but it has been proved that its fractal nature emerges also when a random sequence of space-filling insertions is pursued. In this generalized model [Manna and Herrmann (1991); Manna (1992)], called random Apollonian packing (RAP), the circles are inserted one at time with center positions randomly chosen; after the insertion, the diameter is simply inflated until it touches a previously inserted circle. Extended models make use of simultaneously inflating circles. All these models, deterministic or not, are shown to have universal features belonging to a broader class of models called “packing-limited growth” [Dodds and Weitz (2002)]. The RAP relies on the fact that all the osculatory packings in a certain dimensionality must have the same fractal dimension [Boyd (1973)]. Several routes to RAP has been devised; we suggest Refs. [Amirjanov and Sobolev (2006); Dodds and Weitz (2002); Delaney et al. (2008)] as a short review.

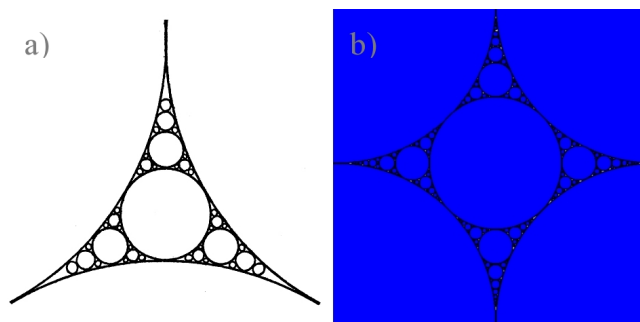


Figure D.1: Apollonian packings for  $d = 2$ : a) classical example from Ref. [Kasner and Supnick (1943)]; b) an example of random packing from the algorithm ( $s_{\max}/L = 1$ ) as explained later in the text.

---

**APOLLONIAN PACKINGS AND PHYSICAL FRACTALS.** Both deterministic and random procedures, when studied numerically, are affected by finite-size effects. In the context of AP (as in its random counterpart), starting from a given configuration of equal spheres of diameter  $s_{\max}$ , the impossibility of having packings with arbitrarily small sizes means that the asymptotic limit

$$s_{\min}/s_{\max} \rightarrow 0 \tag{D.1}$$

(where  $d_f$  is defined) will never be reached.

It would be interesting to systematically characterize the deviation from such a limit. We propose a simple solution to this problem and we find that, taking finite size effects into account, the fractal dimension remains well defined also for finite ranges  $s \in [s_{\min}, s_{\max}]$ . We introduce the basic ideas and observables and we provide an analytic solution for the problem of evaluating  $d_f$  for a finite size range. Afterwards, we will introduce a new algorithm to construct *osculatory random AP* in arbitrary dimension with the possibility of tuning the size ratio defined in eq. (D.1). After having verified its correct asymptotic behavior, we shall finally use this novel algorithm to test the proposed finite size correction.

In what follows, we refer to the hard spheres as the set of non-overlapping geometrical objects (also for dimensions different from  $d = 3$ ) and the size  $s$  then refers to the diameter. Given a packing of equal hard spheres which occupy a volume fraction  $\phi$ , the porosity  $\varepsilon \equiv 1 - \phi$  (in  $d = 2$  and in  $d = 3$  there is a maximum that corresponds to the hexagonal and to the fcc arrangement, respectively [Hales (1992)]), can be decreased by filling the free interstices with smaller spheres; by iterating the insertion procedure of smaller spheres, the final packing results to be a fractal as  $s_{\min}$  goes to 0, which corresponds to the limiting value  $\phi = 1$ . At equal number  $N$  of total inserted objects, the Apollonian packing (AP) is known to be the densest of these packings [Aste and Weaire (2008)]. Despite the universality of  $d_f$  for all osculatory packings [Boyd (1973)], i.e. for all configurations in which any interstice is filled with the largest possible hard sphere, there is not yet an analytical expression of the AP's fractal dimension. The fractal dimensions  $d_f = 1.305684$  and  $d_f = 2.473946$  have been numerically calculated for the AP in  $d = 2$  and  $d = 3$  respectively [Manna and Herrmann (1991); Borkovec et al. (1994)]. In general the relation  $d - 1 \leq d_f \leq d$  is valid, as confirmed by numerical simulations [Kinzel and Reents (1998)] and the AP scale-free nature is expressed by the size distribution

$$n(s) \propto s^{-(d_f+1)}, \tag{D.2}$$

a power-law defined for all the positive diameters  $s$  [Manna (1992)].

Fractals are implicitly understood to be scale-free structures and eq. (D.2) is a consequence of that. However, when a finite range of sizes exists, the fractal is called a *physical fractal* [Martínez-López et al. (2001a); Lakhtakia (1995)]. In this case, the distribution of  $s$  is limited to an interval  $[s_{\min}, s_{\max}]$ , where  $s_{\min}$  and  $s_{\max}$  are the smallest and the largest diameters of the packing, respectively. Various practical methods have been introduced to calculate the fractal dimension: *box-counting*, for example, is applied in the case of physical fractals [Martínez-López et al. (2002); Williams (1997)] and to direct measurements of physical

## Appendix D. Appendix: Physical fractals of spheres.

---

systems [Valle et al. (2005)].

We use two typical observables, the inverse cumulative distribution (number of spheres with size greater or equal to  $s_{\min}$ ) and the porosity, which under the asymptotic condition (D.1) are respectively given [Manna and Herrmann (1991)] by

$$N(s_{\min}) = \sum_{s_i > s_{\min}} 1 \propto s_{\min}^{-d_f}, \quad (\text{D.3a})$$

$$\varepsilon(s_{\min}) = 1 - \sum_{s_i > s_{\min}} s_i^d \propto s_{\min}^{d-d_f}. \quad (\text{D.3b})$$

These measures can be used to estimate the  $d_f$  for packings of polydisperse hard spheres: for different occurrences of  $s_{\min}$ , the fractal dimension can be evaluated as smaller  $s_{\min}$  are considered in the measure of the values (D.3a) and (D.3b) [Aste and Weaire (2008)]. All the different methods for evaluating the  $d_f$  of packings rely on the fact that the fractal dimension definition works only approaching the asymptotic condition (D.1). This means that, for finite ranges of diameters, relevant deviations exist starting from  $s_{\min}/s_{\max} \gtrsim 1/5$ , as explicitly highlighted in Ref. [Anishchik and Medvedev (1995)].

**FINITE SIZE DEVIATION.** The main idea is that the geometrical building rule itself, with its iterativity, defines the fractal-like behavior, while the finite interval of sizes influences only the quantity of objects used for the building. The self-similarity of a set then implies the existence of a set of similarities in the generation of the fractal, which is beyond the mere agreement of the value of the fractal dimension [Martínez-López et al. (2001b)].

This idea can be quantitatively rendered. For a random AP where the osculatory packing constrain is respected at each insertion (building iterative rule) we expect that the value for  $d_f$  will remain the same. Due to the fractal nature of AP and RAP the power-law (D.2) should hold and we make the ansatz that the finite size correction is completely accounted for the proportionality constant of the distribution. In the finite case, we rewrite  $n(s)$  as  $n_f(s)$ :

$$n_f(s) \equiv f(s_{\min}, s_{\max}) s^{-(d_f+1)}. \quad (\text{D.4})$$

The recursive fractal construction is accounted by the power-law and we calculate now the corrections to eqs. (D.3a) and (D.3b) through the use of  $f(s_{\min}, s_{\max})$ .

The fraction of space occupied by  $N_{s_{\max}}$  spheres of maximum size is by definition

$$\phi_{s_{\max}} = 1 - \varepsilon_{s_{\max}} = N_{s_{\max}} \frac{C_d s_{\max}^d}{V}, \quad (\text{D.5})$$

where  $V$  is the total volume and the curvature factor is

$$C_d = \frac{2\pi^{d/2}}{\Gamma(d/2)d} = \begin{cases} \frac{1}{2^d} \frac{\pi^{d/2}}{(d/2)!} & \text{for even } d \\ \frac{1}{2^{(d-1)/2}} \frac{\pi^{(d-1)/2}}{d!!} & \text{for odd } d \end{cases}.$$

The total number of spheres  $N$  and volume fraction  $\phi$  can be expressed using the 0-th and

---

$d$ -th moments of the distribution (D.4) as:

$$N \equiv N_{s_{\max}} + \int_{s_{\min}}^{s_{\max}} n_f(s') ds', \quad (\text{D.6a})$$

$$\phi \equiv \phi_{s_{\max}} + (C_d/V) \int_{s_{\min}}^{s_{\max}} n_f(s') s^d ds'. \quad (\text{D.6b})$$

A natural condition arises assuming that all the space shall be occupied as the filling procedure continues; this means that, for any positive value of  $s_{\max}$ , it is

$$\lim_{s_{\min} \rightarrow 0} \phi = 1. \quad (\text{D.7})$$

Using eq. (D.4) into eq. (D.6b) with the limit (D.7), we obtain the distribution's proportionality constant as

$$f(s_{\min}, s_{\max}) = N_{s_{\max}} \frac{\varepsilon_{s_{\max}}}{\phi_{s_{\max}}} (d - d_f) s_{\max}^{d_f}. \quad (\text{D.8})$$

It is important to notice that it does not depend on  $s_{\min}$ . Inserting this result into eqs. (D.6a) and (D.6b) finally gives:

$$\frac{N}{N_{s_{\max}}} = 1 + \frac{(d - d_f)}{d_f} \frac{\varepsilon_{s_{\max}}}{\phi_{s_{\max}}} \left[ \left( \frac{s_{\min}}{s_{\max}} \right)^{-d_f} - 1 \right], \quad (\text{D.9a})$$

$$\varepsilon = \varepsilon_{s_{\max}} \left( \frac{s_{\min}}{s_{\max}} \right)^{d - d_f}. \quad (\text{D.9b})$$

Note that eqs. (D.3a) and (D.3b) are the particular asymptotic cases of their more general expressions (D.9a) and (D.9b), as expected. These results remain valid in the limit  $V \rightarrow \infty$ . Despite the simple hypothesis made, now we have an explicit expression for the observables which allows to evaluate the deviation from the ideal case (D.1).

**THE FILLING ALGORITHM.** In order to test the previous results, AP have been generated with the help of a new numerical algorithm (which works in any Euclidean dimension  $d \geq 1$ ). The developed algorithm has the same basic behavior as the *random Apollonian packing* (RAP) mechanism, where the filling process starts with an initial population of hard-spheres of a specified diameter ( $s_{\max}$ ) and proceeds with new spheres added one at a time into the unoccupied space; randomly fixing the center of any new sphere, its size is determined by extending the diameter until it touches its closest sphere. But the RAP is not expected to build osculatory packings at each insertion, as we demand in order to check the theoretical previsions. In the algorithm we propose, random movements are additionally performed by the inserted spheres, in order to enhance the filled space accepting only the displacements that allow its diameter to grow (possibly up to  $s_{\max}$ ).

No distribution of sizes for the spheres to insert is *a priori* chosen, nor any initial population. Only the length-scales  $s_{\min}/s_{\max}$  and  $s_{\max}/L$  are the parameters to be decided, where  $L$  defines

## Appendix D. Appendix: Physical fractals of spheres.

---

the total volume  $V \equiv L^d$  of an initially empty box. Periodic boundary conditions are used so that possible interactions with walls can be ignored. In deterministic algorithms, the  $d + 1$  “appropriate” first neighbours must be identified so that the center’s coordinates of a new sphere could be calculated (Soddy’s rule); instead this random approach only has the non-overlapping constraint, meaning that the overall computational complexity is decreased.

A regular squared mesh with lattice constant  $a_{\text{lattice}}$  is defined into  $V$  and its nodes are used as starting centers for the spheres to be inserted. The only requirement on the lattice constant is to be sufficiently smaller than  $s_{\text{min}}$ . A fixed lattice constant could be preferred in some cases (the computational cost depends of course on the implementation); we tested  $a_{\text{lattice}} = s_{\text{min}}/3$  to be a good parameter, but a recursive remeshing has been preferred and used to assure the requirement to be fulfilled.

As the first sphere is inserted at random on a starting center, it doesn’t encounter any other spheres and its diameter can be expanded to  $s_{\text{max}}$ . The starting centers it will cover will then be erased. One sphere at a time is subsequently inserted, according to the following scheme:

- 1: it is placed at random on one of the remaining starting centers (nodes);
- 2: its diameter is increased up to  $s_{\text{max}}$  or until it touches a previously inserted sphere;
- 3: a random displacement within a maximum length  $\Delta r \ll s_{\text{min}}$  (average displacement  $\Delta r/2$ ) is accepted only if this lets the diameter to grow;
- 4: step 3 is iterated if the newly calculated diameter is  $s < s_{\text{max}}$ ;
- 5: if  $s_{\text{max}}$  is reached or if the maximum number of displacement attempts  $(s_{\text{max}}/\Delta r)^2$  is reached, then the procedure stops.
- 6: once a sphere has been inserted, the starting centers it covers can be erased.

The stopping conditions 5 rely on the possible random walk a sphere would need to explore a space of size  $s_{\text{max}}$ . A maximum displacement length  $\Delta r = |\Delta \vec{r}| \ll s_{\text{min}}$  gives an average attempted displacement  $\Delta r/2$  and the number  $n_a$  of attempted displacements has been chosen to be the constant

$$n_a = \left( \frac{s_{\text{max}}}{\Delta r} \right)^2$$

corresponding to the number of steps for a random walk to explore a region of diameter  $s_{\text{max}}$ . Of course a higher  $n_a$  could result in a higher final packing fraction, but our calculation show poor improvement coupled with higher computational cost. During the procedure, spheres with final  $s < s_{\text{min}}$  are erased. The overall filling procedure ends when no other starting centers are present. In Fig. D.2 snapshots are shown for different  $s_{\text{min}}/s_{\text{max}}$  in  $d = 2$  and  $d = 3$ . For our simulations we used the value  $L = 1$ , the others lengths being consequently defined with respect to it. Once a value is chosen for  $s_{\text{max}}/L$ , the ratio  $s_{\text{min}}/s_{\text{max}}$  is investigated.



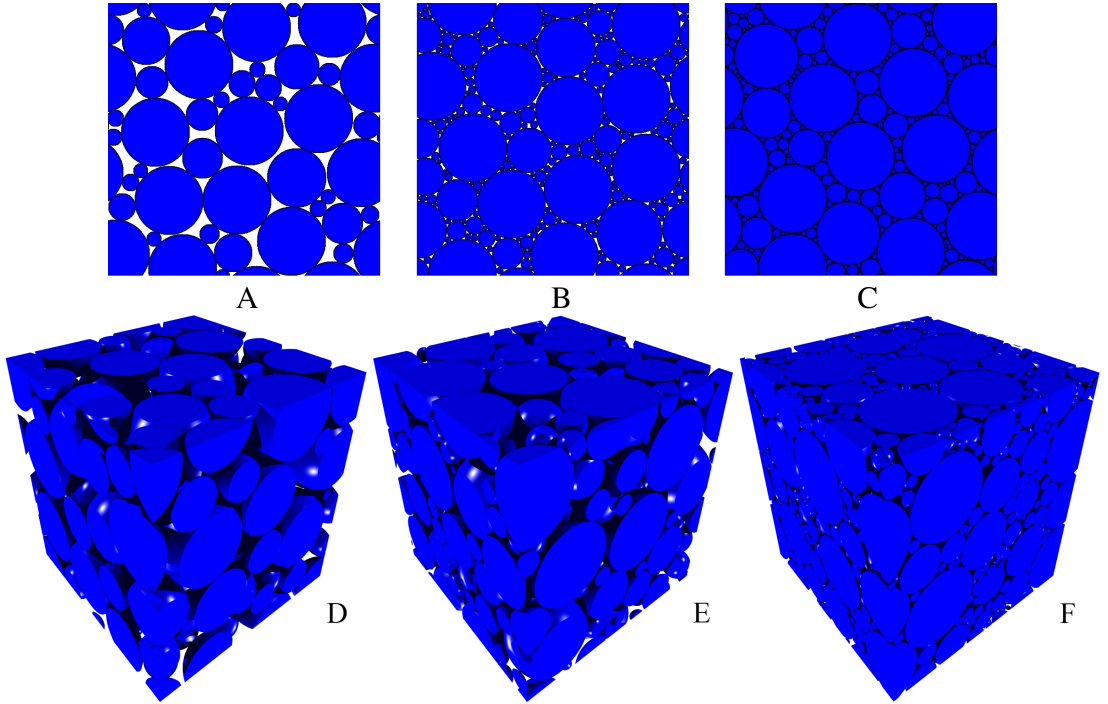


Figure D.2: Snapshots of packings from independent algorithm runs: for  $d = 2$  (**top**) with  $s_{\min}/s_{\max} = 1/5, 1/20, 1/50$  for A, B and C respectively (and the same  $s_{\max}/L = 1/4$ ); for  $d = 3$  (**bottom**) with  $s_{\min}/s_{\max} = 4/10, 2/10, 1/10$  for D, E and F respectively (and the same  $s_{\max}/L = 1/3$ ).

**EFFICIENT PACKING FOR RAPID FRACTAL CONVERGENCE.** For the different values of  $s_{\max}$  we have tested, we observed the same behaviour for decreasing  $s_{\min}$ ; in the next paragraph we report on the results for 370 runs performed with  $s_{\max} = 1/5$  in  $d = 2$  and for 170 runs with  $s_{\max} = 1/3$  in  $d = 3$ . These results are shown in Fig. D.3, where each symbol represents the value averaged over 10 independent runs.

For any configuration of  $N_{s_{\max}}$  non-overlapping spheres in the total volume  $V$ , there always exist some values  $d_f < d$  for which the condition (D.7) is satisfied. This does not imply the existence of a method capable of filling volume accordingly to (D.9a) and (D.9b), but simply implies that if such an “iterative method” exists, then it allows the space to be occupied with a certain  $d_f$ . If this method consists in recursively filling the voids, each time maximizing the occupied space, then it should always present the same fractality as an AP. We expect that with such a kind of filling, including the algorithm presented here, not only the correct asymptotic power-law behaviour has to be obtained, but also that the more stringent expressions (D.9a) and (D.9b) are fulfilled in the overall range of sizes. While power-laws (D.3a) and (D.3b) are known to work for  $s_{\min}/s_{\max}$  smaller than  $1/5$ , eqs. (D.9a) and (D.9b) are in fact expected to work in the whole interval  $s_{\min}/s_{\max} \in [0, 1]$ .

We begin by testing the asymptotic behaviour of our oscillatory RAP on the power law presented in eq. (D.2) with the values of  $d_f$  for  $d = 2$  and  $d = 3$  obtained from previous calculations on AP [Manna and Herrmann (1991); Borkovec et al. (1994)]. As can be argued from Fig. D.3,

## Appendix D. Appendix: Physical fractals of spheres.

in both cases good agreement exists for low enough values of  $s_{\min}/s_{\max}$ , proving the correct AP asymptotic behaviour for the data obtained by the algorithm.

The numerical results deviate from the fractal asymptotic regime above certain size ratios, where we expect instead that our equations should still hold. To this aim we fit the data points for  $d = 2$  and  $d = 3$  with eqs. (D.9a) and (D.9b) in the full range of sizes. It is important to stress that the value  $N_{s_{\max}}$ , which enters the definition of  $N/N_{s_{\max}}$  and  $\varepsilon_{s_{\max}} = 1 - \phi_{s_{\max}}$ , is not a fitting parameter. In fact it is known as the average number of spheres of diameter  $s_{\max}$  in the obtained packings.

Results are shown in Fig. D.3; a comparison with the values known in the literature is reported in Tab.D.1. The deviation from the asymptotic power-law is evident for  $N/N_{s_{\max}}$ , while no deviation is observed for the porosity, as the porosity holds its power law form in eq. (D.9b).

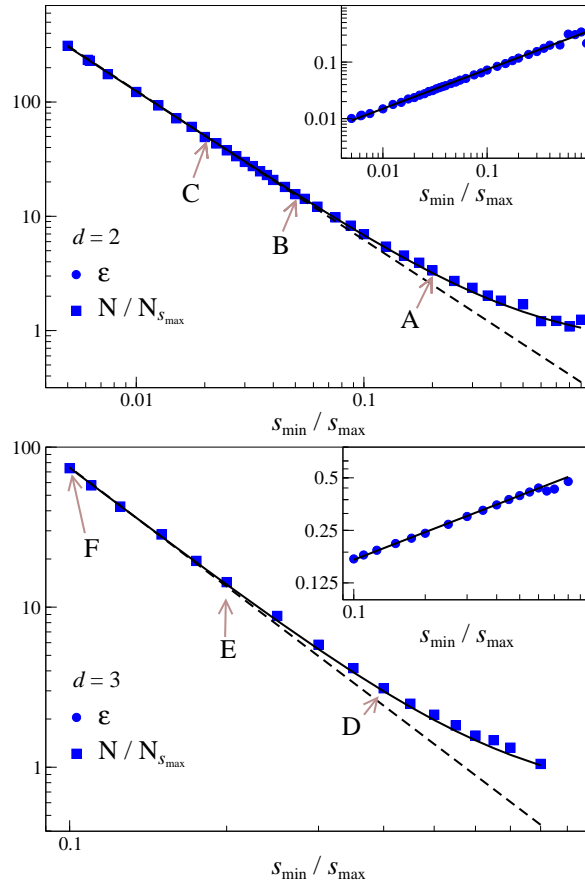


Figure D.3: Number of inserted spheres  $N$  (over  $N_{s_{\max}}$ ) as function of the scale parameter  $s_{\min}/s_{\max}$  for  $d = 2$  (top,  $s_{\max}/L = 1/5$ ) and  $d = 3$  (bottom,  $s_{\min}/L = 1/3$ ). Each symbol represents the average over 10 independent realisations of our random AP. The dashed lines represent eq. (D.3a), while the solid lines correspond to the fits made using (D.9a). Porosities  $\varepsilon$  for the same systems are shown in the respective insets: the curves from eqs. (D.3b) and (D.9b) coincide with a power law. The positions for samples A, B, C, D, E and F in Fig. D.2 are indicated on the curves.

dimension	$d_f$ [Manna and Herrmann (1991); Borkovec et al. (1994)]	$d_f$ (fit)
$d = 2$	1.305684	$1.3045 \pm 0.0006$
$d = 3$	2.473946	$2.4739 \pm 0.0014$

Table D.1: values for the evaluated fractal dimension (in 2 and 3 Euclidean dimensions) compared with the known ones.

The  $N/N_{s_{\max}}$  curve results to describe the data better than its asymptotic counterpart. The fits finally allow an independent estimation of the fractal dimension  $d_f$ : our fitted fractal dimensions are in a very good agreement with the known values. Note that the possibility of fitting in the whole  $s$ -range, plus the use of independent simulations, allows to evaluate  $d_f$  by simulating a relatively small number of spheres.

**SOME REMARKS.** We have studied the properties of space filling packings of spheres. In particular we have derived the finite size correction to the distribution laws that characterize the Apollonian packing fractals. In the case of sizes limited to a finite interval, the ratio between the smallest and the largest spheres does not go to zero and deviations are indeed expected from the typical power laws. Two main observables have been studied, the ratio of the total number of spheres over the number of largest spheres, i.e.  $N/N_{s_{\max}}$ , and the fraction of unoccupied space, i.e. the porosity  $\varepsilon$ . We provide simple analytical expressions for them, solely based on the hypothesis that the packed spheres totally occupy the space if the minimum diameter tends to zero.

In order to test our prediction, an efficient algorithm has been introduced to generate oscillatory random AP, not based on any *a priori* size distribution. This algorithm allows to fix, as input parameters, the largest and smallest sizes. In the limit of vanishingly small diameters, disordered Apollonian packings are recovered with the correct asymptotic behaviour, as proved by testing the data obtained from the new packing algorithm. The laws corrected for finite sizes have been tested by varying the interval of sizes for fractal objects (circles in  $d = 2$  and spheres and  $d = 3$ ) and the result of the fits allows to verify the values of the fractal dimension which came out in agreement with the values known from the literature.

It is interesting to note that the laws we derived apply to the whole range of size ratios. This suggests that even in the case of packings with a very narrow interval of sizes, the space filling construction preserves its fractal nature. These simple results could be applied to the broad class of “packing-limited growth” models and physical fractals for which the general conditions (D.4) and (D.7) are valid. We finally propose to use the rapid convergence to an oscillatory packing enhanced with the proposed algorithm, together with the possibility of using the whole range of sizes for the evaluation of the fractal dimension, as a possible feasible test on recent studies on Apollonian gaskets at higher dimensionality [Farr and Griffiths (2010)].



## **E Appendix: Materials and experimental setup.**

The DNA is attached to the surface of the streptavidin coated colloids via biotin-streptavidin linkage. The structure of the strands is: Biotin – 5'– TTTTT – dsDNA spacer – TTTTT– ssDNA sticky end – 3'. The dsDNA rigid spacer is made of 60 base-pairs ( 20 nm in length) and the sequences of 5 thymine bases are added to confer more flexibility to the construct. The four sticky ends are A=5'–AT CCC GGC C–3', A'=5'–GG CCG GGA T–3', B=5'–CG CAG CAC C–3' and B'=5'–GG TGC TGC G–3'. The  $T_m$  of the complementary strands A-A' and B-B' are respectively 33.3°C and 33.5°C at 26 mM ionic strength whereas the nonspecific bonding probability between strands is negligible. The colloids, from Microparticles GmbH, are fluorescently coated in red (R) and green (G). All the combinations (R-A'A, G-A'A, R-B'B, G-B'B) have been tested to ensure the elimination of spectra overlaps (see SI for details).

The experiments are carried out in TE buffer (10 mM TRIS-HCl pH 8 + 1 mM EDTA) with the addition of 20 mM NaCl. The density of the solution is matched to that of polystyrene (1.05 g/cm<sup>3</sup>) by adding sucrose.

Though the biotin-streptavidin bond is unlikely to break at RT a small percentage of the DNA strands might detach upon exposure to high temperatures. Such strands might graft onto free binding sites on colloids of the wrong species resulting in a non-specific attraction. To avoid non-specific attraction we add free biotin to the solution. Due to high diffusivity and concentration, biotin would bind, before free DNA strands, to any free grafting site on the colloids surface.

The experiments are carried out in a quasi-2D environment in order to allow optical imaging of high density solutions. The sample chambers are designed with a wedge-like structure, with an area of 18×18 mm and thickness varying between 0 and 150 μm. This which allows us to optimize the imaging of each sample by choosing the region of the sample with optimal thickness. The chambers are sealed to avoid any evaporation. For the imaging we use a Leica TCS SP5 inverted confocal microscope equipped with a HCX PLAPO CS 100× 1.4 oil immersion objective.

We functionalize streptavidin coated polystyrene colloids (Microparticles GmbH, Berlin, Germany) with DNA strands (Integrated DNA Technologies BVBA, Leuven, Belgium), to provide

## Appendix E. Appendix: Materials and experimental setup.

---

the correct selective interactions among species. Double strand DNA (dsDNA), 20 nm in length, acts as rigid spacer (see main text) and is prepared beforehand by hybridizing each of the four single strands:

A: biotin-5'-TTT TTG AGG AGG AAA GAG AGA AAG AAG GAG AGG AGA AGG GAG AAA AGA GAG AGG GAA  
AGA GGG AAT TTT TAT CCC GGC C-3'

A': biotin-5'-TTT TTG AGG AGG AAA GAG AGA AAG AAG GAG AGG AGA AGG GAG AAA AGA GAG AGG GAA  
AGA GGG AAT TTT TGG CCG GGA T-3'

B: biotin-5'-TTT TTG AGG AGG AAA GAG AGA AAG AAG GAG AGG AGA AGG GAG AAA AGA GAG AGG GAA  
AGA GGG AAT TTT TCG CAG CAC C-3'

B': biotin-5'-TTT TTG AGG AGG AAA GAG AGA AAG AAG GAG AGG AGA AGG GAG AAA AGA GAG AGG GAA  
AGA GGG AAT TTT TGG TGC TGC G-3'

with the single strand:

C : 5'-TTC CCT CTT TCC CTC TCT CTT TTC TCC CTT CTC CTC TCC TTC TTT CTC TCT TTC CTC CTC-3'.

The hybridization is carried out in 10mM TRIS-EDTA buffer solution (TE, Sigma Aldrich) in four different tubes. Each of the tubes is heated up to 80°C for 2 hours and then slowly cooled down overnight in order to avoid kinetic traps such as hairpins.

The colloids are green-fluorescent (G) and red-fluorescent (R) and have a diameter of 0.5  $\mu\text{m}$ . R and G colloidal particles are sonicated for 15 minutes, then dispersed in TE buffer solution containing 5000 MW biotinylated poly-ethylene glycol (biotin-PEG, Laysan Bio Inc., Arab, USA) and the functionalizing mixtures of either A-A' or B-B'. The concentration of DNA is tuned to obtain a 5 $\times$  excess compared to the binding capacity of the colloids. The DNA/PEG concentration ratio in the solution is kept to 50/3. Since biotin-PEG is much more diffusive than the DNA constructs, we expect the DNA/PEG ratio on the surface of the colloids to be close to 7/3. The samples are left at 45°C for 2 hours to allow for grafting. The chosen temperature is above the  $T_m$  of the complementary strands to avoid hybridization during the coating process. Afterwards, each of the samples is spun for 2 minutes at 13k rpm to pellet the particles and remove the excess solution containing unbound DNA and biotin-PEG, then the colloids are redispersed in clean TE buffer at 45°C. The washing procedure is repeated 3 times, then the colloids are spun again and resuspended in density matched TE buffer with additional 20 mM NaCl. This buffer is prepared beforehand by dissolving 4.46 g sucrose and 0.11 g NaCl to 100 ml of 10 mM TE buffer. The final concentration of the colloidal solution at this stage is  $\approx$ 10%.

With the above procedure we can naturally define the species according to their DNA coating: AA' or BB'. We refer to them as G and R for brevity but the reader should keep in mind that different coating can be associated to different fluorescence labels R or G without changing the physical properties of the system (See Fig.E.3 and discussion below).

The experiments are carried out in wedge-shaped glass chambers sealed with ultraviolet curing

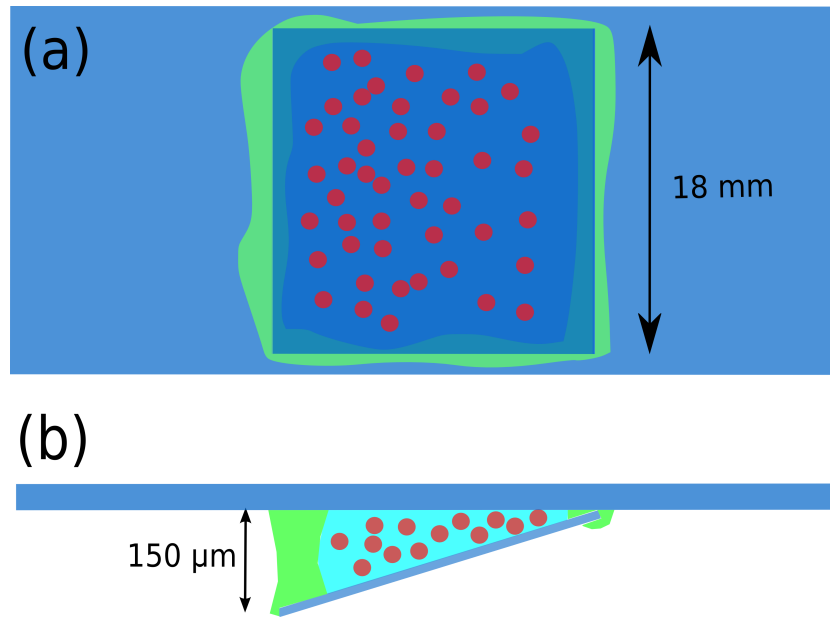


Figure E.1: (a) Schematic bottom-view and (b) side view of a sample chamber.

glue (Norland Optical Adhesive, Norland Products Inc. Cranbury, USA) and two-components epoxy glue. The chambers are made of a thick glass support (a microscope slide) to which a microscope coverslip ( $18\text{ mm} \times 18\text{ mm} \times 150\text{ }\mu\text{m}$ ) is attached using ultraviolet curing glue to form a wedge-shaped chamber with a thickness between 0 and  $150\text{ }\mu\text{m}$ . Microscope slides and coverslips are washed beforehand in strong surfactant solution at high temperature, sonicated and rinsed in double-distilled water and 3M NaOH solution to remove any surface impurity. We choose to work with wedge-shaped chambers to obtain quasi-2D samples: within each sample, this geometry allows us to find the thickest possible region that allows good quality imaging. A schematic of the bottom view and the side view of a chamber is shown in Fig. E.1 (a) and (b) respectively.

The solutions are prepared by mixing equal quantities of R and G colloidal suspensions into an empty tube and adding  $1\text{ }\mu\text{l}$  of 0.2mM biotin solution prepared by dissolving dry biotin powder (Sigma-Aldrich) in density matched TE buffer. The chambers are plasma-cleaned (Diener Electronic Femto) to avoid the colloids to stick to their walls, and then filled with the colloidal solution and sealed with the two-component epoxy glue to protect the samples from evaporation.

R and G colloids, the empty tube and the chamber are heated up to  $60^\circ\text{C}$  beforehand, so to make the sample stay in the gas phase during all the manipulations and avoid the shearing of colloidal aggregates that could compromise the quality of the coating. After sealing the chamber, the samples are quickly cooled down to RT. Large and inhomogeneous aggregates form. At this stage, the samples are heated up and equilibrated at  $T > T_m$ , above the melting temperature. Afterwards they are cooled down until the BiGel phase is formed. This procedure follows rigorously the quenching protocol adopted for the simulations. The thermal processing is performed while monitoring the samples with a Nikon Elcipse Ti-E inverted

## Appendix E. Appendix: Materials and experimental setup.

---

optical-microscope with a Nikon CFI60 Plan Fluor 40× 0.75 NA dry objective. Once the BiGel structures are formed, the samples are moved to a Leica TCS SP5 microscope equipped with a HCX PL APO CS 100X 1.4 oil immersion objective for confocal imaging. The adsorption/emission wavelengths of G and R dyes are respectively 492/519 nm and 519/589 nm, respectively. Excitation at the exact frequencies of the dyes is achieved by using a white laser with tunable emission. Imperfections of the fluorescent dyes have been noticed, with G colloids fluorescing at the wavelength of the red emission under both red and green excitation. The effect is shown for single colloids in Fig. E.4 (a)-(c). To distinguish the R species, thus, we had to remove the unwanted red fluorescence of G colloids under red light. This is made by subtracting the image obtained under green light. In Fig. E.4 we show how this canceling method works for distinguishing the R colloids. Moreover, to make sure that the red fluorescence of the green aggregates is due only to unwanted red fluorescence of the G colloids, and not to R colloids embedded in the G aggregates (i.e. an incomplete demixing) we repeated all the experiments after exchanging DNA coatings between the two species, i.e. by testing both the combinations G-AA' / R-BB' and R-AA' / G-BB'. As shown in Fig. E.3, upon exchanging the DNA coatings, the fluorescence contamination is not inverted, i.e. G aggregates still fluoresce red but R aggregates do not fluoresce green. Since colloidal aggregation behavior is solely determined by the DNA coating and not by the fluorescent dye, this demonstrates that the only cause for the red fluorescence of G aggregates is the unwanted overlap of the spectra, and not an incomplete demixing.



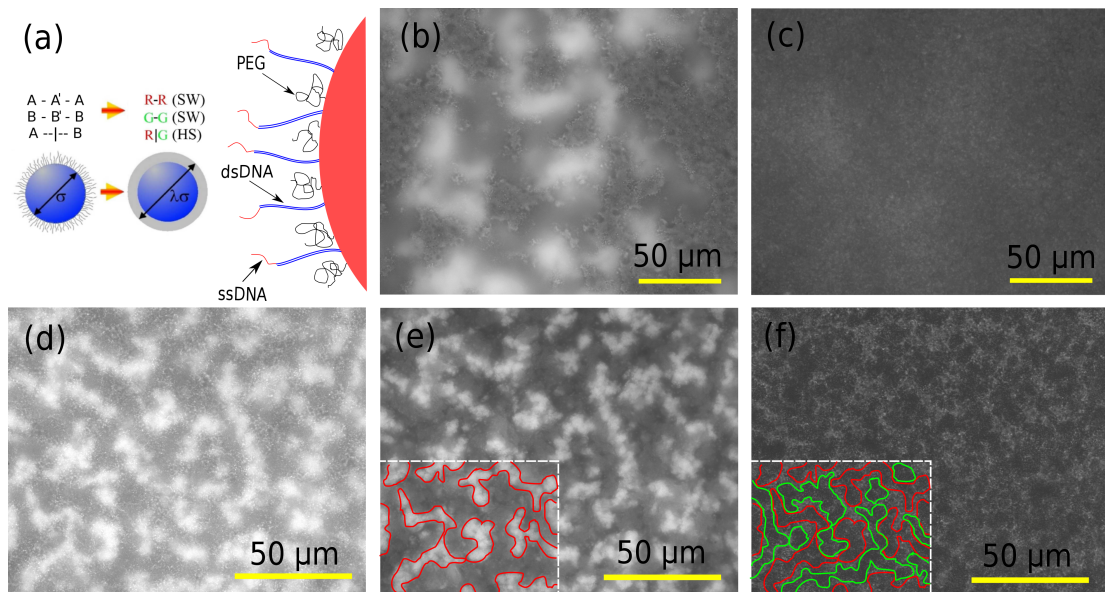


Figure E.2: **(a)** A schematic of the surface coating of the colloids, highlighting the correspondence between theoretical model and experimental realization of inter-particle interactions. **(b)** BF / FL optical microscopy image of a sample at RT before annealing. **(c)** BF / FL image at  $T \approx 50^\circ\text{C}$ . **(d)** BF / FL, **(e)** FL only and **(f)** BF only images of the same region of a sample at RT after annealing. Red and green lines in panels (e) and (f) are guides for the eye highlighting fluorescent and non-fluorescent aggregates respectively..

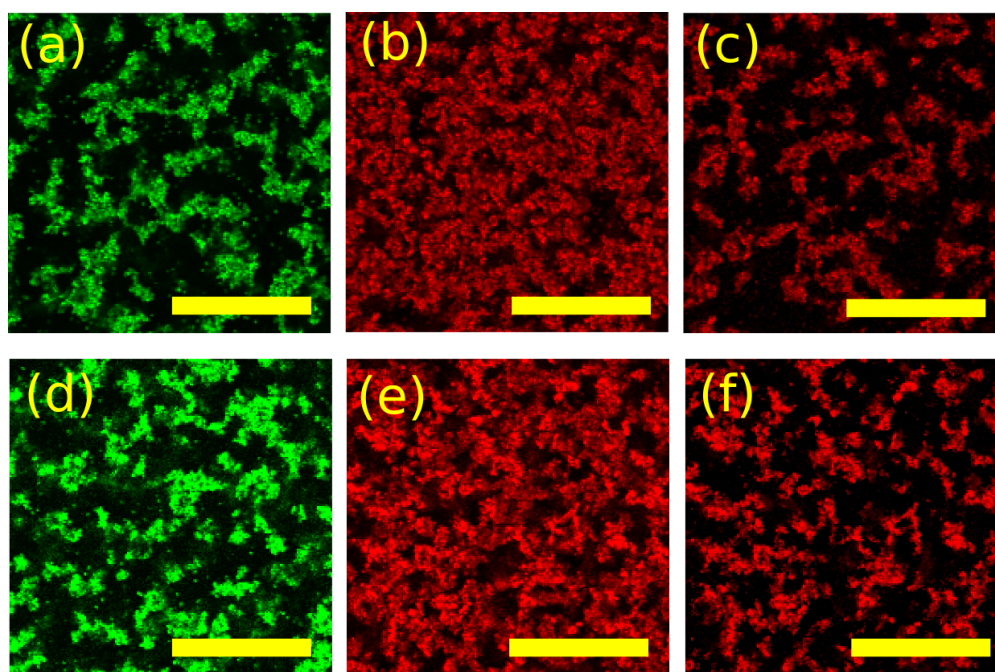


Figure E.3: (a) Green fluorescent, (b) original red fluorescent and (c) subtraction of (a) from (b) confocal images, for a sample with DNA coating BB' on red colloids and AA' on green colloids. (d) green fluorescent, (e) original red fluorescent and (f) subtraction of (e) from (f) confocal images, for a sample with DNA coating AA' on red colloids and BB' on green colloids. By comparing panels (a),(b),(c) and panels (d),(e),(f) it is clear that with both combinations of DNA coatings green aggregates fluoresce red but red aggregates do not fluoresce green. Scale bars are  $25 \mu\text{m}$ .

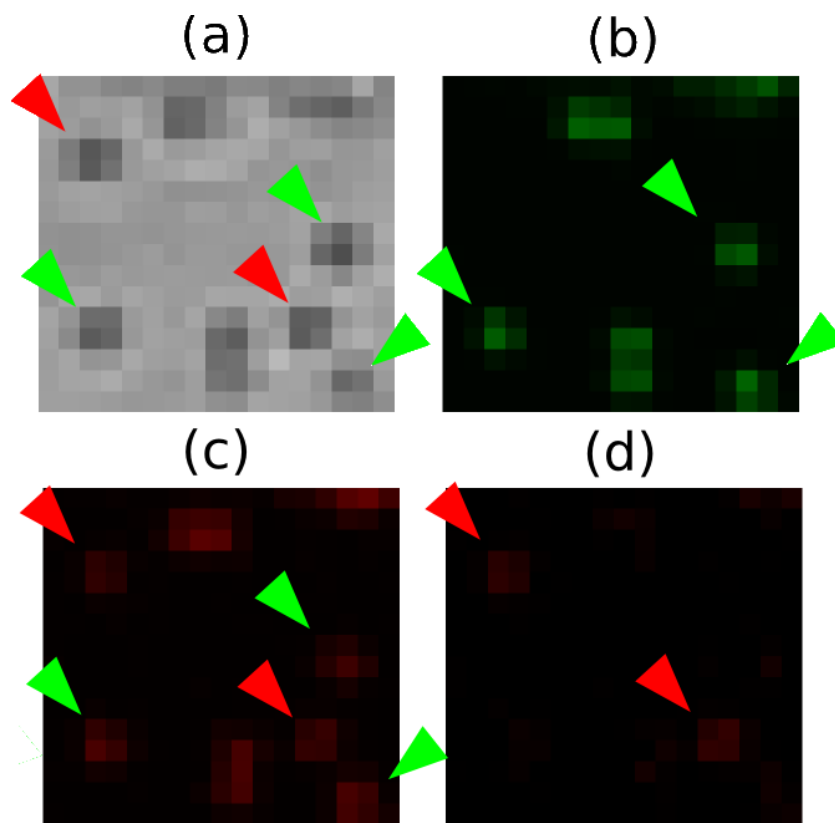


Figure E.4: (a) Zoom of a bright field image containing 5 single colloids immobilized on a glass surface. Single colloids are pointed by arrows. Features not pointed by arrows are colloidal doublets or small aggregates. (b) Fluorescence of the same region under green excitation. Only 3 of the 5 single colloids fluoresce green. (c) Fluorescence image of the same region under red excitation, all the single colloids, including green ones, fluoresce red. (d) Image resulting from the subtraction of (d) and (c). Only red colloids (i.e. colloids not emitting under green excitation) survive to the subtraction. The width of each image image is  $5.1 \mu\text{m}$ .



## Bibliography

- D. G. A. L. Aarts. Capillary length in a fluid-fluid demixed colloid-polymer mixture. *J. Phys. Chem. B*, 109(15):7407–7411, Mar. 2005. ISSN 1520-6106. doi: 10.1021/jp044312q. URL <http://dx.doi.org/10.1021/jp044312q>.
- D. G. A. L. Aarts. The interface in demixed colloid-polymer systems: wetting, waves and droplets. *Soft Matter*, 3(1):19–23, 2007. ISSN 1744-683X. URL <http://dx.doi.org/10.1039/B608479F>.
- D. G. A. L. Aarts and H. N. W. Lekkerkerker. Confocal scanning laser microscopy on fluid-fluid demixing colloid-polymer mixtures. *Journal of Physics: Condensed Matter*, 16(38):S4231–, 2004. ISSN 0953-8984. URL <http://stacks.iop.org/0953-8984/16/i=38/a=035>.
- D. G. A. L. Aarts, M. Schmidt, and H. N. W. Lekkerkerker. Direct visual observation of thermal capillary waves. *Science*, 304(5672):847–850, 2004. doi: 10.1126/science.1097116. URL <http://www.sciencemag.org/content/304/5672/847.abstract>.
- D. G. A. L. Aarts, R. P. A. Dullens, and H. N. W. Lekkerkerker. Interfacial dynamics in demixing systems with ultralow interfacial tension. *New Journal of Physics*, 7(1):40–, 2005. ISSN 1367-2630. URL <http://stacks.iop.org/1367-2630/7/i=1/a=040>.
- T. Abete. *A statistical mechanical approach to the study of gels and colloidal systems*. PhD thesis, Università degli Studi di Napoli Federico II, 2006. URL [http://www.fedoa.unina.it/1415/1/Abete\\_Fisica\\_Fondamentale\\_ed\\_Applicata.pdf](http://www.fedoa.unina.it/1415/1/Abete_Fisica_Fondamentale_ed_Applicata.pdf).
- Z. Akdeniz, P. Vignolo, P. Capuzzi, and M. Tosi. Boson-fermion demixing and collapse in low dimensions, 2006-06-01. ISSN 1054-660X. URL <http://dx.doi.org/10.1134/S1054660X06060144>.
- F. A. Aldaye, A. L. Palmer, and H. F. Sleiman. Assembling materials with dna as the guide. *Science*, 321(5897):1795–1799, 2008. doi: 10.1126/science.1154533. URL <http://www.sciencemag.org/content/321/5897/1795.abstract>.
- B. J. Alder and T. E. Wainwright. Phase transition for a hard sphere system. *J. Chem. Phys.*, 27(5):1208–1209, Nov. 1957. URL <http://dx.doi.org/10.1063/1.1743957>.

## Bibliography

---

- A. P. Alivisatos, K. P. Johnsson, X. Peng, T. E. Wilson, C. J. Loweth, M. P. Bruchez, and P. G. Schultz. Organization of 'nanocrystal molecules' using dna. *Nature*, 382(6592):609–611, Aug. 1996. URL <http://dx.doi.org/10.1038/382609a0>.
- C. Allain, M. Cloitre, and M. Wafra. Aggregation and sedimentation in colloidal suspensions. *Phys. Rev. Lett.*, 74(8):1478–1481, Feb. 1995. URL <http://link.aps.org/doi/10.1103/PhysRevLett.74.1478>.
- V. Ambegaokar, B. I. Halperin, and J. S. Langer. Hopping conductivity in disordered systems. *Phys. Rev. B*, 4(8):2612–2620, Oct. 1971. URL <http://link.aps.org/doi/10.1103/PhysRevB.4.2612>.
- G. Ambrosetti, C. Grimaldi, I. Balberg, T. Maeder, A. Danani, and P. Ryser. Solution of the tunneling-percolation problem in the nanocomposite regime. *Phys. Rev. B*, 81(15):155434–, Apr. 2010. URL <http://link.aps.org/doi/10.1103/PhysRevB.81.155434>.
- A. Amirjanov and K. Sobolev. Fractal properties of apollonian packing of spherical particles. *Modelling and Simulation in Materials Science and Engineering*, 14(4):789–, 2006. ISSN 0965-0393. URL <http://stacks.iop.org/0965-0393/14/i=4/a=018>.
- V. J. Anderson and H. N. W. Lekkerkerker. Insights into phase transition kinetics from colloid science. *Nature*, 416(6883):811–815, Apr. 2002. ISSN 0028-0836. URL <http://dx.doi.org/10.1038/416811a>.
- J. Andrade, Jos   S., H. J. Herrmann, R. F. S. Andrade, and L. R. da Silva. Apollonian networks: Simultaneously scale-free, small world, euclidean, space filling, and with matching graphs. *Phys. Rev. Lett.*, 94(1):018702–, Jan. 2005. URL <http://link.aps.org/doi/10.1103/PhysRevLett.94.018702>.
- S. Angioletti-Uberti, B. M. Mognetti, and D. Frenkel. Re-entrant melting as a design principle for dna-coated colloids. *Nat Mater*, 11(6):518–522, June 2012. ISSN 1476-1122. URL <http://dx.doi.org/10.1038/nmat3314>.
- S. V. Anishchik and N. N. Medvedev. Three-dimensional apollonian packing as a model for dense granular systems. *Phys. Rev. Lett.*, 75(23):4314–4317, Dec. 1995. URL <http://link.aps.org/doi/10.1103/PhysRevLett.75.4314>.
- S. Asakura and F. Oosawa. On interaction between two bodies immersed in a solution of macromolecules. *J. Chem. Phys.*, 22(7):1255–1256, July 1954. URL <http://dx.doi.org/10.1063/1.1740347>.
- T. Aste and D. Weaire. *The Pursuit of Perfect Packing, Second Edition*. Taylor & Francis, 2008. URL <http://books.google.ch/books?id=d8bZDWcSdzMC>.
- A. E. Bailey, W. C. K. Poon, R. J. Christianson, A. B. Schofield, U. Gasser, V. Prasad, S. Manley, P. N. Segre, L. Cipelletti, W. V. Meyer, M. P. Doherty, S. Sankaran, A. L. Jankovsky, W. L. Shiley, J. P. Bowen, J. C. Eggers, C. Kurta, J. Lorik, T., P. N. Pusey, and D. A. Weitz. Spinodal decomposition

- in a model colloid-polymer mixture in microgravity. *Phys. Rev. Lett.*, 99(20):205701–, Nov. 2007. URL <http://link.aps.org/doi/10.1103/PhysRevLett.99.205701>.
- A. Banerjee, R. Rawat, K. Mukherjee, and P. Chaddah. Excess specific heat and evidence of zero-point entropy in magnetic glassy state of half-doped manganites. *Phys. Rev. B*, 79(21):212403–, June 2009. URL <http://link.aps.org/doi/10.1103/PhysRevB.79.212403>.
- P. R. Banerjee, A. Pande, J. Patrosz, G. M. Thurston, and J. Pande. Cataract-associated mutant e107a of human  $\gamma$ d-crystallin shows increased attraction to  $\alpha$ -crystallin and enhanced light scattering. *Proceedings of the National Academy of Sciences*, 108(2):574–579, 2011. doi: 10.1073/pnas.1014653107. URL <http://www.pnas.org/content/108/2/574.abstract>.
- R. M. Baram, H. J. Herrmann, and N. Rivier. Space-filling bearings in three dimensions. *Phys. Rev. Lett.*, 92(4):044301–, Jan. 2004. URL <http://link.aps.org/doi/10.1103/PhysRevLett.92.044301>.
- B. Barbooy and R. Tenne. Distribution functions and equations of state of sticky hard sphere fluids in the percus-yevick approximation. *Chemical Physics*, 38(3):369–387, May 1979. ISSN 0301-0104. doi: 10.1016/0301-0104(79)89011-4. URL <http://www.sciencedirect.com/science/article/pii/0301010479890114>.
- J. A. Barker and D. Henderson. Perturbation theory and equation of state for fluids: The square-well potential. *J. Chem. Phys.*, 47(8):2856–2861, Oct. 1967. URL <http://dx.doi.org/10.1063/1.1712308>.
- R. J. Baxter. Percus–yevick equation for hard spheres with surface adhesion. *J. Chem. Phys.*, 49(6):2770–2774, Sept. 1968. URL <http://dx.doi.org/10.1063/1.1670482>.
- M. Belushkin and G. Gompper. Twist grain boundaries in cubic surfactant phases. *J. Chem. Phys.*, 130(13):134712–10, Apr. 2009. URL <http://dx.doi.org/10.1063/1.3096987>.
- H. J. C. Berendsen, J. P. M. Postma, W. F. van Gunsteren, A. DiNola, and J. R. Haak. Molecular dynamics with coupling to an external bath. *J. Chem. Phys.*, 81(8):3684–3690, Oct. 1984. URL <http://dx.doi.org/10.1063/1.448118>.
- J. Bergenholtz, W. C. K. Poon, and M. Fuchs. Gelation in model colloid-polymer mixtures. *Langmuir*, 19(10):4493–4503, Apr. 2003. ISSN 0743-7463. doi: 10.1021/la0340089. URL <http://dx.doi.org/10.1021/la0340089>.
- A. B. Bhatia and D. E. Thornton. Structural aspects of the electrical resistivity of binary alloys. *Phys. Rev. B*, 2(8):3004–3012, Oct. 1970. URL <http://link.aps.org/doi/10.1103/PhysRevB.2.3004>.
- P. L. Biancaniello, A. J. Kim, and J. C. Crocker. Colloidal interactions and self-assembly using dna hybridization. *Phys. Rev. Lett.*, 94(5):058302–, Feb. 2005. URL <http://link.aps.org/doi/10.1103/PhysRevLett.94.058302>.

## Bibliography

---

- E. Bianchi, J. Largo, P. Tartaglia, E. Zaccarelli, and F. Sciortino. Phase diagram of patchy colloids: Towards empty liquids. *Phys. Rev. Lett.*, 97(16):168301–, Oct. 2006. URL <http://link.aps.org/doi/10.1103/PhysRevLett.97.168301>.
- J. Bibette, T. G. Mason, H. Gang, and D. A. Weitz. Kinetically induced ordering in gelation of emulsions. *Phys. Rev. Lett.*, 69(6):981–984, Aug. 1992. URL <http://link.aps.org/doi/10.1103/PhysRevLett.69.981>.
- R. Blaak, M. A. Miller, and J.-P. Hansen. Reversible gelation and dynamical arrest of dipolar colloids. *EPL (Europhysics Letters)*, 78(2):26002–, 2007. ISSN 0295-5075. URL <http://stacks.iop.org/0295-5075/78/i=2/a=26002>.
- D. R. Bland. The theory of linear viscoelasticity, 1960. URL [http://sfx.ethz.ch:9003/sfx\\_epf?sid=google&auinit=DR&aulast=Bland&title=The%20theory%20of%20linear%20viscoelasticity&genre=book&date=1960](http://sfx.ethz.ch:9003/sfx_epf?sid=google&auinit=DR&aulast=Bland&title=The%20theory%20of%20linear%20viscoelasticity&genre=book&date=1960).
- M. Borkovec, W. De Paris, and R. Peikert. The fractal dimension of the apollonian sphere packing. *Fractals*, 02(04):521–526, Dec. 1994. ISSN 0218-348X. doi: 10.1142/S0218348X94000739. URL <http://dx.doi.org/10.1142/S0218348X94000739>.
- M. Born. *Atom Physics*. Hafner, 1962. URL [http://books.google.ch/books?id=\\_FFyuAAACAAJ](http://books.google.ch/books?id=_FFyuAAACAAJ).
- T. Boublik. Hard-sphere equation of state. *J. Chem. Phys.*, 53(1):471–472, July 1970. URL <http://dx.doi.org/10.1063/1.1673824>.
- D. W. Boyd. Osculatory packing of a 3 dimensional sphere. *Canadian Journal of Mathematics-journal Canadien De Mathematiques*, 25(2):303–322, 1973. doi: 10.4153/CJM-1973-030-5.
- M. L. Broide, Y. Garrabos, and D. Beysens. Nonfractal colloidal aggregation. *Phys. Rev. E*, 47(5):3768–3771, May 1993. URL <http://link.aps.org/doi/10.1103/PhysRevE.47.3768>.
- W. D. Brown and R. C. Ball. Computer simulation of chemically limited aggregation. *Journal of Physics A: Mathematical and General*, 18(9):L517–, 1985. ISSN 0305-4470. URL <http://stacks.iop.org/0305-4470/18/i=9/a=006>.
- R. Bruinsma. Elasticity and excitations of minimal crystals. *J. Phys. II France*, 2(3):425–451, 1992. URL <http://dx.doi.org/10.1051/jp2:1992142>.
- S. Brunetti, D. Roux, A. M. Bellocq, G. Fourche, and P. Bothorel. Micellar interactions in water-in-oil microemulsions. 2. light scattering determination of the second virial coefficient. *J. Phys. Chem.*, 87(6):1028–1034, Mar. 1983. ISSN 0022-3654. doi: 10.1021/j100229a022. URL <http://dx.doi.org/10.1021/j100229a022>.
- M. F. Butler and M. Heppenstall-Butler. Phase separation in gelatin/dextran and gelatin/maltodextrin mixtures. *Food Hydrocolloids*, 17(6):815–830, Nov. 2003. ISSN 0268-005X. doi: 10.1016/S0268-005X(03)00103-6. URL <http://www.sciencedirect.com/science/article/pii/S0268005X03001036>.



- P. B. Canham. The minimum energy of bending as a possible explanation of the biconcave shape of the human red blood cell, 1970. ISSN 0022-5193. URL [http://sfx.ethz.ch/sfx\\_epf?sid=Elsevier%3AScopus&\\_service\\_type=getFullTxt&issn=00225193&isbn=&volume=26&issue=1&spage=61&epage=76%2CIN7-IN8%2C77-81&pages=61-76%2CIN7-IN8%2C77-81&artnum=&date=1970&id=doi%3A&title=Journal%20of%20Theoretical%20Biology&atitle=The%20minimum%20energy%20of%20bending%20as%20a%20possible%20explanation%20of%20the%20biconcave%20shape%20of%20the%20human%20red%20blood%20cell&aufirst=P.B.&aunit=P.B.&aunit1=P&aust=Canham](http://sfx.ethz.ch/sfx_epf?sid=Elsevier%3AScopus&_service_type=getFullTxt&issn=00225193&isbn=&volume=26&issue=1&spage=61&epage=76%2CIN7-IN8%2C77-81&pages=61-76%2CIN7-IN8%2C77-81&artnum=&date=1970&id=doi%3A&title=Journal%20of%20Theoretical%20Biology&atitle=The%20minimum%20energy%20of%20bending%20as%20a%20possible%20explanation%20of%20the%20biconcave%20shape%20of%20the%20human%20red%20blood%20cell&aufirst=P.B.&aunit=P.B.&aunit1=P&aust=Canham).
- X. Cao, H. Cummins, and J. Morris. Hydrodynamic and interparticle potential effects on aggregation of colloidal particles. *Journal of Colloid and Interface Science*, 368(1):86–96, Feb. 2012. ISSN 0021-9797. doi: 10.1016/j.jcis.2011.11.050. URL <http://www.sciencedirect.com/science/article/pii/S0021979711014263>.
- F. Cardinaux, T. Gibaud, A. Stradner, and P. Schurtenberger. Interplay between spinodal decomposition and glass formation in proteins exhibiting short-range attractions. *Phys. Rev. Lett.*, 99(11):118301–, Sept. 2007. URL <http://link.aps.org/doi/10.1103/PhysRevLett.99.118301>.
- N. F. Carnahan and K. E. Starling. Equation of state for nonattracting rigid spheres. *J. Chem. Phys.*, 51(2):635–636, July 1969. URL <http://dx.doi.org/10.1063/1.1672048>.
- M. Carpineti and M. Giglio. Spinodal-type dynamics in fractal aggregation of colloidal clusters. *Phys. Rev. Lett.*, 68(22):3327–3330, June 1992. URL <http://link.aps.org/doi/10.1103/PhysRevLett.68.3327>.
- M. Carpineti, F. Ferri, M. Giglio, E. Paganini, and U. Perini. Salt-induced fast aggregation of polystyrene latex. *Phys. Rev. A*, 42(12):7347–7354, Dec. 1990. URL <http://link.aps.org/doi/10.1103/PhysRevA.42.7347>.
- B. L. Carvalho, P. Tong, J. S. Huang, T. A. Witten, and L. J. Fetters. Adsorption of end-functionalized polymers on colloidal spheres. *Macromolecules*, 26(17):4632–4639, Aug. 1993. ISSN 0024-9297. doi: 10.1021/ma00069a033. URL <http://dx.doi.org/10.1021/ma00069a033>.
- X. S. Chen and F. Forstmann. The demixing and gas–liquid instability of a binary yukawa fluid. *J. Chem. Phys.*, 97(5):3696–3703, Sept. 1992. URL <http://dx.doi.org/10.1063/1.462951>.
- Z. Cheng, J. Zhu, P. M. Chaikin, S.-E. Phan, and W. B. Russel. Nature of the divergence in low shear viscosity of colloidal hard-sphere dispersions. *Phys. Rev. E*, 65(4):041405–, Apr. 2002. URL <http://link.aps.org/doi/10.1103/PhysRevE.65.041405>.
- L. Cipelletti and L. Ramos. Slow dynamics in glassy soft matter. *Journal of Physics: Condensed Matter*, 17(6):R253–, 2005. ISSN 0953-8984. URL <http://stacks.iop.org/0953-8984/17/i=6/a=R01>.

## Bibliography

---

- L. Cipelletti, S. Manley, R. C. Ball, and D. A. Weitz. Universal aging features in the restructuring of fractal colloidal gels. *Phys. Rev. Lett.*, 84(10):2275–2278, Mar. 2000. URL <http://link.aps.org/doi/10.1103/PhysRevLett.84.2275>.
- A. Coniglio, T. Abete, A. de Candia, E. D. Gado, and A. Fierro. Dynamical heterogeneities: from glasses to gels. *Journal of Physics: Condensed Matter*, 20(49):494239–, 2008. ISSN 0953-8984. URL <http://stacks.iop.org/0953-8984/20/i=49/a=494239>.
- K. A. Dawson, G. Foffi, F. Sciortino, P. Tartaglia, and E. Zaccarelli. Mode-coupling theory of colloids with short-range attractions. *Journal of Physics: Condensed Matter*, 13(41):9113–, 2001. ISSN 0953-8984. URL <http://stacks.iop.org/0953-8984/13/i=41/a=305>.
- P. De Gennes. On a relation between percolation theory and the elasticity of gels. *J. Physique Lett.*, 37(1):1–2, 1976. URL <http://dx.doi.org/10.1051/jphyslet:019760037010100>.
- P. G. De Gennes. C. r. acad. sci. paris, 1978. URL [http://sfx.ethz.ch:9003/sfx\\_epf?sid=IOPP%3Aajnl\\_ref&genre=bookitem&date=1978&aulast=De&aufirst=Gennes%20P.%20G.&volume=286&spage=131&title=C.%20R.%20Acad.%20Sci.%20Paris](http://sfx.ethz.ch:9003/sfx_epf?sid=IOPP%3Aajnl_ref&genre=bookitem&date=1978&aulast=De&aufirst=Gennes%20P.%20G.&volume=286&spage=131&title=C.%20R.%20Acad.%20Sci.%20Paris).
- H. De Hek and A. Vrij. Interactions in mixtures of colloidal silica spheres and polystyrene molecules in cyclohexane: I. phase separations. *Journal of Colloid and Interface Science*, 84(2):409–422, Dec. 1981. ISSN 0021-9797. doi: 10.1016/0021-9797(81)90232-0. URL <http://www.sciencedirect.com/science/article/pii/0021979781902320>.
- E. H. A. de Hoog, W. K. Kegel, A. van Blaaderen, and H. N. W. Lekkerkerker. Direct observation of crystallization and aggregation in a phase-separating colloid-polymer suspension. *Phys. Rev. E*, 64(2):021407–, July 2001. URL <http://link.aps.org/doi/10.1103/PhysRevE.64.021407>.
- D. de las Heras, J. M. Tavares, and M. M. Telo da Gama. Bicontinuous and mixed gels in binary mixtures of patchy colloidal particles. *Soft Matter*, 8(6):1785–1794, 2012. ISSN 1744-683X. URL <http://dx.doi.org/10.1039/C1SM06948A>.
- C. De Michele. Optimizing event-driven simulations. *Computer Physics Communications*, 182(9):1846–1850, Sept. 2011. ISSN 0010-4655. doi: 10.1016/j.cpc.2010.11.012. URL <http://www.sciencedirect.com/science/article/pii/S0010465510004583>.
- C. De Michele, S. Gabrielli, P. Tartaglia, and F. Sciortino. Dynamics in the presence of attractive patchy interactions. *J. Phys. Chem. B*, 110(15):8064–8079, Mar. 2006. ISSN 1520-6106. doi: 10.1021/jp056380y. URL <http://dx.doi.org/10.1021/jp056380y>.
- C. De Michele, E. Del Gado, and D. Leporini. Scaling between structural relaxation and particle caging in a model colloidal gel. *Soft Matter*, 7(8):4025–4031, 2011. ISSN 1744-683X. URL <http://dx.doi.org/10.1039/C0SM00941E>.
- P. Debye, H. R. Anderson, Jr., and H. Brumberger. Scattering by an inhomogeneous solid. ii. the correlation function and its application. *J. Appl. Phys.*, 28(6):679–683, June 1957. URL <http://dx.doi.org/10.1063/1.1722830>.

- E. Del Gado. Aggregation of model gels with directional interactions. *Journal of Physics: Condensed Matter*, 22(10):104117–, 2010. ISSN 0953-8984. URL <http://stacks.iop.org/0953-8984/22/i=10/a=104117>.
- E. Del Gado and W. Kob. A microscopic model for colloidal gels with directional effective interactions: network induced glassy dynamics. *Soft Matter*, 6(7):1547–1558, 2010. ISSN 1744-683X. URL <http://dx.doi.org/10.1039/B916813C>.
- G. W. Delaney, S. Hutzler, and T. Aste. Relation between grain shape and fractal properties in random apollonian packing with grain rotation. *Phys. Rev. Lett.*, 101(12):120602–, Sept. 2008. URL <http://link.aps.org/doi/10.1103/PhysRevLett.101.120602>.
- J. Dhont. *An Introduction to Dynamics of Colloids*. Elsevier, 1996a. URL <http://books.google.ch/books?id=mmArTF5SJ9oC>.
- J. K. G. Dhont. Spinodal decomposition of colloids in the initial and intermediate stages. *J. Chem. Phys.*, 105(12):5112–5125, Sept. 1996b. URL <http://dx.doi.org/10.1063/1.472355>.
- E. Dickinson. *An Introduction to Food Colloids*. Oxford University Press, 1992. URL <http://books.google.ch/books?id=ppdkQgAACA AJ>.
- M. Dijkstra and D. Frenkel. Evidence for entropy-driven demixing in hard-core fluids. *Phys. Rev. Lett.*, 72(2):298–300, Jan. 1994. URL <http://link.aps.org/doi/10.1103/PhysRevLett.72.298>.
- A. D. Dinsmore and D. A. Weitz. Direct imaging of three-dimensional structure and topology of colloidal gels. *Journal of Physics: Condensed Matter*, 14(33):7581–, 2002. ISSN 0953-8984. URL <http://stacks.iop.org/0953-8984/14/i=33/a=303>.
- A. D. Dinsmore, E. R. Weeks, V. Prasad, A. C. Levitt, and D. A. Weitz. Three-dimensional confocal microscopy of colloids. *Appl. Opt.*, 40(24):4152–4159, Aug. 2001. URL <http://ao.osa.org/abstract.cfm?URI=ao-40-24-4152>.
- N. M. Dixit and C. F. Zukoski. Competition between crystallization and gelation: A local description. *Phys. Rev. E*, 67(6):061501–, June 2003. URL <http://link.aps.org/doi/10.1103/PhysRevE.67.061501>.
- P. S. Dodds and J. S. Weitz. Packing-limited growth. *Phys. Rev. E*, 65(5):056108–, May 2002. URL <http://link.aps.org/doi/10.1103/PhysRevE.65.056108>.
- P. S. Dodds and J. S. Weitz. Packing-limited growth of irregular objects. *Phys. Rev. E*, 67(1):016117–, Jan. 2003. URL <http://link.aps.org/doi/10.1103/PhysRevE.67.016117>.
- A. Donev. *Jammed Packings of Hard Particles*. Princeton University, 2006. URL <http://books.google.ch/books?id=-Qk1HQAACA AJ>.
- J. Donnet. *Carbon Black: Science and Technology, Second Edition*. Taylor & Francis, 1993. URL <http://books.google.ch/books?id=SPpx6MkRYwMC>.

## Bibliography

---

- E. Donth. *The Glass Transition: Relaxation Dynamics in Liquids and Disordered Materials*. Springer, 2001. URL <http://books.google.ch/books?id=8p425FjPKzAC>.
- N. Dorsaz. *A colloidal approach to eye lens protein mixtures : relevance for cataract formation*. PhD thesis, EPFL, Doctoral school Physics, 2009. URL <http://library.epfl.ch/theses/?nr=4375>.
- N. Dorsaz, G. M. Thurston, A. Stradner, P. Schurtenberger, and G. Foffi. Colloidal characterization and thermodynamic stability of binary eye lens protein mixtures. *J. Phys. Chem. B*, 113(6):1693–1709, Dec. 2008. ISSN 1520-6106. doi: 10.1021/jp807103f. URL <http://dx.doi.org/10.1021/jp807103f>.
- N. Dorsaz, G. M. Thurston, A. Stradner, P. Schurtenberger, and G. Foffi. Phase separation in binary eye lens protein mixtures. *Soft Matter*, 7(5):1763–1776, 2011. ISSN 1744-683X. URL <http://dx.doi.org/10.1039/C0SM00156B>.
- J. P. K. Doye and C. P. Massen. Self-similar disk packings as model spatial scale-free networks. *Phys. Rev. E*, 71(1):016128–, Jan. 2005. URL <http://link.aps.org/doi/10.1103/PhysRevE.71.016128>.
- R. Dreyfus, M. E. Leunissen, R. Sha, A. V. Tkachenko, N. C. Seeman, D. J. Pine, and P. M. Chaikin. Simple quantitative model for the reversible association of dna coated colloids. *Phys. Rev. Lett.*, 102(4):048301–, Jan. 2009. URL <http://link.aps.org/doi/10.1103/PhysRevLett.102.048301>.
- R. Dreyfus, M. E. Leunissen, R. Sha, A. Tkachenko, N. C. Seeman, D. J. Pine, and P. M. Chaikin. Aggregation-disaggregation transition of dna-coated colloids: Experiments and theory. *Phys. Rev. E*, 81(4):041404–, Apr. 2010. URL <http://link.aps.org/doi/10.1103/PhysRevE.81.041404>.
- M. Dubois and B. Cabane. Light-scattering study of the sol-gel transition in silicon tetraethoxide. *Macromolecules*, 22(5):2526–2533, May 1989. ISSN 0024-9297. doi: 10.1021/ma00195a090. URL <http://dx.doi.org/10.1021/ma00195a090>.
- E. Duguet, A. Desert, A. Perro, and S. Ravaine. Design and elaboration of colloidal molecules: an overview. *Chem. Soc. Rev.*, 40(2):941–960, 2011. ISSN 0306-0012. URL <http://dx.doi.org/10.1039/C0CS00048E>.
- J. Earnshaw and D. Robinson. Inter-cluster scaling in two-dimensional colloidal aggregation. *Physica A: Statistical Mechanics and its Applications*, 214(1):23–51, 1995. URL <http://www.scopus.com/inward/record.url?eid=2-s2.0-0002294129&partnerID=40&md5=9466be4797ca6ec8e65705fb8f998e41>.
- T. Eckert and E. Bartsch. Re-entrant glass transition in a colloid-polymer mixture with depletion attractions. *Phys. Rev. Lett.*, 89(12):125701–, Aug. 2002. URL <http://link.aps.org/doi/10.1103/PhysRevLett.89.125701>.

- D. H. Everett. *Manual of Symbols and Terminology for Physicochemical Quantities and Units, Appendix II: Definitions, Terminology and Symbols in Colloid and Surface Chemistry*. London Butterworths, 1972.
- R. S. Farr and E. Griffiths. Estimate for the fractal dimension of the apollonian gasket in  $d$  dimensions. *Phys. Rev. E*, 81(6):061403–, June 2010. URL <http://link.aps.org/doi/10.1103/PhysRevE.81.061403>.
- U. Feldkamp and C. M. Niemeyer. Rational design of dna nanoarchitectures. *Angewandte Chemie International Edition*, 45(12):1856–1876, 2006. ISSN 1521-3773. URL <http://dx.doi.org/10.1002/anie.200502358>.
- S. Feng, B. I. Halperin, and P. N. Sen. Transport properties of continuum systems near the percolation threshold. *Phys. Rev. B*, 35(1):197–214, Jan. 1987. URL <http://link.aps.org/doi/10.1103/PhysRevB.35.197>.
- L. Finegold. Cell membrane fluidity: Molecular modeling of particle aggregations seen in electron microscopy. *Biochimica et Biophysica Acta (BBA) - Biomembranes*, 448(2):393–398, Oct. 1976. ISSN 0005-2736. doi: 10.1016/0005-2736(76)90252-2. URL <http://www.sciencedirect.com/science/article/pii/0005273676902522>.
- D. Fiocco, G. Pastore, and G. Foffi. Effective forces in square well and square shoulder fluids. *J. Phys. Chem. B*, 114(37):12085–12095, Aug. 2010. ISSN 1520-6106. doi: 10.1021/jp105145x. URL <http://dx.doi.org/10.1021/jp105145x>.
- A. Fizazi, J. Moulton, K. Pakbaz, S. D. D. V. Rughooputh, P. Smith, and A. J. Heeger. Percolation on a self-assembled network: Decoration of polyethylene gels with conducting polymer. *Phys. Rev. Lett.*, 64(18):2180–2183, Apr. 1990. URL <http://link.aps.org/doi/10.1103/PhysRevLett.64.2180>.
- G. Foffi and F. Sciortino. Extended law of corresponding states in short-range square wells: A potential energy landscape study. *Phys. Rev. E*, 74(5):050401–, Nov. 2006. URL <http://link.aps.org/doi/10.1103/PhysRevE.74.050401>.
- G. Foffi, G. D. McCullagh, A. Lawlor, E. Zaccarelli, K. A. Dawson, F. Sciortino, P. Tartaglia, D. Pini, and G. Stell. Phase equilibria and glass transition in colloidal systems with short-ranged attractive interactions: Application to protein crystallization. *Phys. Rev. E*, 65(3):031407–, Mar. 2002. URL <http://link.aps.org/doi/10.1103/PhysRevE.65.031407>.
- G. Foffi, W. G tze, F. Sciortino, P. Tartaglia, and T. Voigtmann.  $\alpha$ -relaxation processes in binary hard-sphere mixtures. *Phys. Rev. E*, 69(1):011505–, Jan. 2004. URL <http://link.aps.org/doi/10.1103/PhysRevE.69.011505>.
- G. Foffi, C. De Michele, F. Sciortino, and P. Tartaglia. Arrested phase separation in a short-ranged attractive colloidal system: A numerical study. *J. Chem. Phys.*, 122(22):224903–13, June 2005a. URL <http://dx.doi.org/10.1063/1.1924704>.

## Bibliography

---

- G. Foffi, C. D. Michele, F. Sciortino, and P. Tartaglia. Scaling of dynamics with the range of interaction in short-range attractive colloids. *Phys. Rev. Lett.*, 94(7):078301–, Feb. 2005b. URL <http://link.aps.org/doi/10.1103/PhysRevLett.94.078301>.
- S. R. Forrest and J. T. A. Witten. Long-range correlations in smoke-particle aggregates. *Journal of Physics A: Mathematical and General*, 12(5):L109–, 1979. ISSN 0305-4470. URL <http://stacks.iop.org/0305-4470/12/i=5/a=008>.
- D. Frenkel and B. Smit. *Understanding Molecular Simulation: From Algorithms to Applications*. Academic Press, 2002. URL <http://books.google.sh/books?id=XmyO2oRUg0cC>.
- J. Fröhlich and D. Ruelle. *Scaling and Self-Similarity in Physics*. Birkhauser, Boston, MA, 1983.
- A. Furukawa and H. Tanaka. Key role of hydrodynamic interactions in colloidal gelation. *Phys. Rev. Lett.*, 104(24):245702–, June 2010. URL <http://link.aps.org/doi/10.1103/PhysRevLett.104.245702>.
- H. Furukawa. Dynamics-scaling theory for phase-separating unmixing mixtures: Growth rates of droplets and scaling properties of autocorrelation functions. *Physica A: Statistical Mechanics and its Applications*, 123(2-3):497–515, Feb. 1984. ISSN 0378-4371. doi: 10.1016/0378-4371(84)90168-7. URL <http://www.sciencedirect.com/science/article/pii/0378437184901687>.
- H. Furukawa. A dynamic scaling assumption for phase separation. *Advances in Physics*, 34(6):703–750, Jan. 1985. ISSN 0001-8732. doi: 10.1080/00018738500101841. URL <http://www.tandfonline.com/doi/abs/10.1080/00018738500101841>.
- H. Furukawa. Multi-time scaling for phase separation. *J. Phys. Soc. Jpn.*, 58:216, 1989. URL <http://jpsj.ipap.jp/link?JPSJ/58/216/>.
- E. D. Gado, A. Fierro, L. d. Arcangelis, and A. Coniglio. Slow dynamics in gelation phenomena: From chemical gels to colloidal glasses. *Phys. Rev. E*, 69(5):051103–, May 2004. URL <http://link.aps.org/doi/10.1103/PhysRevE.69.051103>.
- A. Gast, C. Hall, and W. Russel. Polymer-induced phase separations in nonaqueous colloidal suspensions. *Journal of Colloid and Interface Science*, 96(1):251–267, Nov. 1983. ISSN 0021-9797. doi: 10.1016/0021-9797(83)90027-9. URL <http://www.sciencedirect.com/science/article/pii/0021979783900279>.
- D. Gazzillo and A. Giacometti. Analytic solutions for baxter's model of sticky hard sphere fluids within closures different from the percus–yevick approximation. *J. Chem. Phys.*, 120(10):4742–4754, Mar. 2004. URL <http://dx.doi.org/10.1063/1.1645781>.
- N. Geerts and E. Eiser. Dna-functionalized colloids: Physical properties and applications. *Soft Matter*, 6(19):4647–4660, 2010. ISSN 1744-683X. URL <http://dx.doi.org/10.1039/C001603A>.

- N. Geerts, T. Schmatko, and E. Eiser. Clustering versus percolation in the assembly of colloids coated with long dna. *Langmuir*, 24(9):5118–5123, Mar. 2008. ISSN 0743-7463. doi: 10.1021/la7036789. URL <http://dx.doi.org/10.1021/la7036789>.
- T. Gibaud and P. Schurtenberger. A closer look at arrested spinodal decomposition in protein solutions. *Journal of Physics Condensed Matter*, 21(32):-, 2009. URL <http://www.scopus.com/inward/record.url?eid=2-s2.0-70349117731&partnerID=40&md5=f80bf7b7e819c2a2f13406e3ece359d6>.
- T. Gibaud, F. Cardinaux, J. Bergenholtz, A. Stradner, and P. Schurtenberger. Phase separation and dynamical arrest for particles interacting with mixed potentials-the case of globular proteins revisited. *Soft Matter*, 7(3):857–860, 2011. ISSN 1744-683X. URL <http://dx.doi.org/10.1039/C0SM01175D>.
- T. Gibaud, N. Mahmoudi, J. Oberdisse, P. Lindner, J. S. Pedersen, C. L. P. Oliveira, A. Stradner, and P. Schurtenberger. New routes to food gels and glasses. *Faraday Discuss.*, pages –, 2012. ISSN 1359-6640. URL <http://dx.doi.org/10.1039/C2FD20048A>.
- O. Glatter. Scattering studies on colloids of biological interest (amphiphilic systems): Trends in colloid and interface science v, 1991. ISSN 978-3-7985-0885-9. URL <http://dx.doi.org/10.1007/BFb0115932>.
- S. C. Glotzer. Some assembly required. *Science*, 306(5695):419–420, 2004. doi: 10.1126/science.1099988. URL <http://www.sciencemag.org/content/306/5695/419.short>.
- S. C. Glotzer and M. J. Solomon. Anisotropy of building blocks and their assembly into complex structures. *Nat Mater*, 6(7):557–562, Aug. 2007. ISSN 1476-1122. URL <http://dx.doi.org/10.1038/nmat1949>.
- G. Gompper and S. Zschocke. Elastic properties of interfaces in a ginzburg-landau theory of swollen micelles, droplet crystals and lamellar phases. *EPL (Europhysics Letters)*, 16(8):731–, 1991. ISSN 0295-5075. URL <http://stacks.iop.org/0295-5075/16/i=8/a=005>.
- G. Gompper and S. Zschocke. Ginzburg-landau theory of oil-water-surfactant mixtures. *Phys. Rev. A*, 46(8):4836–4851, Oct. 1992. URL <http://link.aps.org/doi/10.1103/PhysRevA.46.4836>.
- G. Gompper, J. Dhont, and D. Richter. A unified view of soft matter systems? (editorial), 2008. ISSN 1292-8941. URL <http://dx.doi.org/10.1140/epje/i2008-10328-1>.
- A. E. González and G. Ramírez-Santiago. Spatial ordering and structure factor scaling in the simulations of colloid aggregation. *Phys. Rev. Lett.*, 74(7):1238–1241, Feb. 1995. URL <http://link.aps.org/doi/10.1103/PhysRevLett.74.1238>.
- A. Goyal, C. K. Hall, and O. D. Velev. Bicontinuous gels formed by self-assembly of dipolar colloid particles. *Soft Matter*, 6(3):480–484, 2010. ISSN 1744-683X. URL <http://dx.doi.org/10.1039/B907873H>.

## Bibliography

---

- M. C. Grant and W. B. Russel. Volume-fraction dependence of elastic moduli and transition temperatures for colloidal silica gels. *Phys. Rev. E*, 47(4):2606–2614, Apr. 1993. URL <http://link.aps.org/doi/10.1103/PhysRevE.47.2606>.
- A. L. Greer. Metallic glasses. *Science*, 267(5206):1947–1953, 1995. doi: 10.1126/science.267.5206.1947. URL <http://www.sciencemag.org/content/267/5206/1947.abstract>.
- H. Gu, J. Chao, S.-J. Xiao, and N. C. Seeman. Dynamic patterning programmed by dna tiles captured on a dna origami substrate. *Nat Nano*, 4(4):245–248, Apr. 2009. ISSN 1748-3387. URL <http://dx.doi.org/10.1038/nnano.2009.5>.
- M. Gunton J.D., San Miguel and P. Sahni. *Phase Transitions and Critical Phenomena*, volume 8. Academic Press, 1983.
- J. Gurland. An estimate of contact and continuity of dispersions in opaque samples. *Transactions of the Metallurgical Society of Aime*, 236(5):642–&, 1966.
- T. C. Hales. The sphere packing problem. *Journal of Computational and Applied Mathematics*, 44(1):41–76, Dec. 1992. ISSN 0377-0427. doi: 10.1016/0377-0427(92)90052-Y. URL <http://www.sciencedirect.com/science/article/pii/037704279290052Y>.
- J. Hansen and I. McDonald. *Theory of Simple Liquids*. Elsevier Academic Press, 2006. URL <http://books.google.ch/books?id=Uhm87WZBnxEC>.
- J. P. Hansen and I. R. McDonald. *Theory of Simple Liquids*. Academic Press: London, 1986.
- J.-P. Hansen and L. Verlet. Phase transitions of the lennard-jones system. *Phys. Rev.*, 184(1):151–161, Aug. 1969. URL <http://link.aps.org/doi/10.1103/PhysRev.184.151>.
- A. Hasmy, E. Anglaret, M. Foret, J. Pelous, and R. Jullien. Small-angle neutron-scattering investigation of long-range correlations in silica aerogels: Simulations and experiments. *Phys. Rev. B*, 50(9):6006–6016, Sept. 1994. URL <http://link.aps.org/doi/10.1103/PhysRevB.50.6006>.
- M. Haw, W. Poon, and P. Pusey. Structure factors from cluster-cluster aggregation simulation at high concentration. *Physica A: Statistical Mechanics and its Applications*, 208(1):8–17, 1994. URL <http://www.scopus.com/inward/record.url?eid=2-s2.0-0002759681&partnerID=40&md5=6cff7abb62f79660dfc4ea76887796fc>.
- M. Haw, M. Sievwright, W. Poon, and P. Pusey. Structure and characteristic length scales in cluster-cluster aggregation simulation. *Physica A: Statistical Mechanics and its Applications*, 217(3-4):231–260, 1995. URL <http://www.scopus.com/inward/record.url?eid=2-s2.0-58149319810&partnerID=40&md5=b1f2e7434a02892f34ca0b7bd096c8a2>.
- W. Helfrich. Elastic properties of lipid bilayers - theory and possible experiments. *Zeitschrift Fur Naturforschung C-a Journal of Biosciences*, C 28(11-1):693–703, 1973.



- T. Hellweg, S. Schemmel, G. Rother, A. Brücklet, H. Eckerlebe, and G. Findenegg. De-mixing dynamics of a binary liquid system in a controlled-pore glass, 2003. ISSN 1292-8941. URL <http://dx.doi.org/10.1140/epjed/e2003-01-001-9>.
- D. Henderson and E. W. Grundke. Direct correlation function: Hard sphere fluid. *J. Chem. Phys.*, 63(2):601–607, July 1975. URL <http://dx.doi.org/10.1063/1.431378>.
- H. J. Herrmann and M. Kolb. Irreversible aggregation of clusters at high density. *Journal of Physics A: Mathematical and General*, 19(16):L1027–, 1986. ISSN 0305-4470. URL <http://stacks.iop.org/0305-4470/19/i=16/a=014>.
- H. J. Herrmann, D. Stauffer, and D. P. Landau. Computer simulation of a model for irreversible gelation. *Journal of Physics A: Mathematical and General*, 16(6):1221–, 1983. ISSN 0305-4470. URL <http://stacks.iop.org/0305-4470/16/i=6/a=017>.
- E. M. Herzig. *Bijel - a novel composite material from colloids on liquid-liquid interfaces*. PhD thesis, University of Edinburgh, 2008. URL <http://www.era-test.lib.ed.ac.uk/handle/123456789/2580>.
- H. Hirano. *Leibniz's Cultural Pluralism And Natural Law*. Hosei University, Tokyo, 2010.
- J. K. Hoffer and D. N. Sinha. Dynamics of binary phase separation in liquid  $^3\text{-}^4\text{He}$  mixtures. *Phys. Rev. A*, 33(3):1918–1939, Mar. 1986. URL <http://link.aps.org/doi/10.1103/PhysRevA.33.1918>.
- R. Hunter. *Foundations of Colloid Science*. Number v. 2. Oxford University Press, 1986. URL <http://books.google.ch/books?id=Nw1KuAAACAAJ>.
- P. I. Hurtado, L. Berthier, and W. Kob. Heterogeneous diffusion in a reversible gel. *Phys. Rev. Lett.*, 98(13):135503–, Mar. 2007. URL <http://link.aps.org/doi/10.1103/PhysRevLett.98.135503>.
- S. M. Ilett, A. Orrock, W. C. K. Poon, and P. N. Pusey. Phase behavior of a model colloid-polymer mixture. *Phys. Rev. E*, 51(2):1344–1352, Feb. 1995. URL <http://link.aps.org/doi/10.1103/PhysRevE.51.1344>.
- T. S. Ingebrigtsen, T. B. Schröder, and J. C. Dyre. What is a simple liquid? *Phys. Rev. X*, 2(1):011011–, Mar. 2012. URL <http://link.aps.org/doi/10.1103/PhysRevX.2.011011>.
- A. M. Jackson, J. W. Myerson, and F. Stellacci. Spontaneous assembly of subnanometre-ordered domains in the ligand shell of monolayer-protected nanoparticles. *Nat Mater*, 3(5):330–336, May 2004. ISSN 1476-1122. URL <http://dx.doi.org/10.1038/nmat1116>.
- N. Johner. *On the origin of transport non-universality and piezoresistivity in segregated conductor-insulator composites and application to thick-film resistors*. PhD thesis, EPFL, 2009.

## Bibliography

---

- N. Johner, C. Grimaldi, I. Balberg, and P. Ryser. Transport exponent in a three-dimensional continuum tunneling-percolation model. *Phys. Rev. B*, 77(17):174204–, May 2008. URL <http://link.aps.org/doi/10.1103/PhysRevB.77.174204>.
- R. Jullien and M. Kolb. Hierarchical model for chemically limited cluster-cluster aggregation. *Journal of Physics A: Mathematical and General*, 17(12):L639–, 1984. ISSN 0305-4470. URL <http://stacks.iop.org/0305-4470/17/i=12/a=003>.
- A. R. Kansal, S. Torquato, and F. H. Stillinger. Computer generation of dense polydisperse sphere packings. *J. Chem. Phys.*, 117(18):8212–8218, Nov. 2002. URL <http://dx.doi.org/10.1063/1.1511510>.
- E. Kasner and F. Supnick. The apollonian packing of circles. *Proceedings of the National Academy of Sciences*, 29(11):378–384, 1943. URL <http://www.pnas.org/content/29/11/378.short>.
- S. Katano and M. Iizumi. Crossover phenomenon in dynamical scaling of phase separation in fe-cr alloy. *Phys. Rev. Lett.*, 52(10):835–838, Mar. 1984. URL <http://link.aps.org/doi/10.1103/PhysRevLett.52.835>.
- W. Kinzel and G. Reents. *Physics by computer: programming physical problems using Mathematica and C*. Number v. 1. Springer, 1998. URL <http://books.google.ch/books?id=UApBAQAIAAJ>.
- S. Kirkpatrick. Percolation and conduction. *Rev. Mod. Phys.*, 45(4):574–588, Oct. 1973. URL <http://link.aps.org/doi/10.1103/RevModPhys.45.574>.
- J. G. Kirkwood. Statistical mechanics of fluid mixtures. *J. Chem. Phys.*, 3(5):300–313, May 1935. URL <http://dx.doi.org/10.1063/1.1749657>.
- J. Kofinger, N. B. Wilding, and G. Kahl. Phase behavior of a symmetrical binary fluid mixture. *J. Chem. Phys.*, 125(23):234503–14, Dec. 2006. URL <http://dx.doi.org/10.1063/1.2393241>.
- M. Kolb and H. J. Herrmann. The sol-gel transition modelled by irreversible aggregation of clusters. *Journal of Physics A: Mathematical and General*, 18(8):L435–, 1985. ISSN 0305-4470. URL <http://stacks.iop.org/0305-4470/18/i=8/a=007>.
- M. Kolb, R. Botet, and R. Jullien. Scaling of kinetically growing clusters. *Phys. Rev. Lett.*, 51(13):1123–1126, Sept. 1983. URL <http://link.aps.org/doi/10.1103/PhysRevLett.51.1123>.
- W. P. Krekelberg, J. Mittal, V. Ganesan, and T. M. Truskett. How short-range attractions impact the structural order, self-diffusivity, and viscosity of a fluid. *J. Chem. Phys.*, 127(4):044502–8, July 2007. URL <http://dx.doi.org/10.1063/1.2753154>.
- A. M. Kulkarni, N. M. Dixit, and C. F. Zukoski. Ergodic and non-ergodic phase transitions in globular protein suspensions. *Faraday Discuss.*, 123:37–50, 2003. ISSN 1359-6640. URL <http://dx.doi.org/10.1039/B204453F>.

- A. Lakhtakia. *Speculat. Sci. Technol.*, 18:153–156, 1995.
- F. Lancon, L. Billard, J. Laugier, and A. Chamberod. Simulation of a reproducible model of metallic glasses by hardsphere relaxation. *Journal of Physics F: Metal Physics*, 12(2):259–, 1982. ISSN 0305-4608. URL <http://stacks.iop.org/0305-4608/12/i=2/a=005>.
- J. S. Langer. *Solids far from Equilibrium*. Cambridge University Press, 1992.
- J. Largo, M. A. Miller, and F. Sciortino. The vanishing limit of the square-well fluid: The adhesive hard-sphere model as a reference system. *J. Chem. Phys.*, 128(13):134513–5, Apr. 2008. URL <http://dx.doi.org/10.1063/1.2883696>.
- M. Laurati, G. Petekidis, N. Koumakis, F. Cardinaux, A. B. Schofield, J. M. Brader, M. Fuchs, and S. U. Egelhaaf. Structure, dynamics, and rheology of colloid-polymer mixtures: From liquids to gels. *J. Chem. Phys.*, 130(13):134907–14, Apr. 2009. URL <http://dx.doi.org/10.1063/1.3103889>.
- J. L. Lebowitz. Exact solution of generalized percus-yevick equation for a mixture of hard spheres. *Phys. Rev.*, 133(4A):A895–A899, Feb. 1964. URL <http://link.aps.org/doi/10.1103/PhysRev.133.A895>.
- J. A. Leegwater, H. van Beijeren, and J. P. J. Michels. Linear kinetic theory of the square-well fluid. *Journal of Physics: Condensed Matter*, 1(1):237–, 1989. ISSN 0953-8984. URL <http://stacks.iop.org/0953-8984/1/i=1/a=020>.
- H. N. W. Lekkerkerker, W. C.-K. Poon, P. N. Pusey, A. Stroobants, and P. B. Warren. Phase behaviour of colloid + polymer mixtures. *EPL (Europhysics Letters)*, 20(6):559–, 1992. ISSN 0295-5075. URL <http://stacks.iop.org/0295-5075/20/i=6/a=015>.
- J. Leszczynski. *Handbook of Computational Chemistry*. Springer, 2012. URL [http://books.google.ch/books?id=30VIVBtE\\_bYC](http://books.google.ch/books?id=30VIVBtE_bYC).
- M. E. Leunissen and D. Frenkel. Numerical study of dna-functionalized microparticles and nanoparticles: Explicit pair potentials and their implications for phase behavior. *J. Chem. Phys.*, 134(8):084702–18, Feb. 2011. URL <http://dx.doi.org/10.1063/1.3557794>.
- M. E. Leunissen, R. Dreyfus, F. C. Cheong, D. G. Grier, R. Sha, N. C. Seeman, and P. M. Chaikin. Switchable self-protected attractions in dna-functionalized colloids. *Nat Mater*, 8(7):590–595, July 2009. ISSN 1476-1122. URL <http://dx.doi.org/10.1038/nmat2471>.
- C. N. Likos. Effective interactions in soft condensed matter physics. *Physics Reports*, 348(4-5):267–439, July 2001. ISSN 0370-1573. doi: 10.1016/S0370-1573(00)00141-1. URL <http://www.sciencedirect.com/science/article/pii/S0370157300001411>.
- C. Lin and H. Yan. Dna nanotechnology: A cascade of activity. *Nat Nano*, 4(4):211–212, Apr. 2009. ISSN 1748-3387. URL <http://dx.doi.org/10.1038/nnano.2009.66>.

## Bibliography

---

- M. Y. Lin, H. M. Lindsay, D. A. Weitz, R. C. Ball, R. Klein, and P. Meakin. Universal reaction-limited colloid aggregation. *Phys. Rev. A*, 41(4):2005–2020, Feb. 1990. URL <http://link.aps.org/doi/10.1103/PhysRevA.41.2005>.
- F. Lo Verso, C. N. Likos, C. Mayer, and L. Reatto. Effect of attraction on the dynamical arrest of soft colloids. *Molecular Physics*, 104(22-24):3523–3534, Nov. 2006. ISSN 0026-8976. doi: 10.1080/00268970600976733. URL <http://dx.doi.org/10.1080/00268970600976733>.
- P. J. Lu, J. C. Conrad, H. M. Wyss, A. B. Schofield, and D. A. Weitz. Fluids of clusters in attractive colloids. *Phys. Rev. Lett.*, 96(2):028306–, Jan. 2006. URL <http://link.aps.org/doi/10.1103/PhysRevLett.96.028306>.
- P. J. Lu, P. A. Sims, H. Oki, J. B. Macarthur, and D. A. Weitz. Target-locking acquisition with real-time confocal (tarc) microscopy. *Opt. Express*, 15(14):8702–8712, July 2007. URL <http://www.opticsexpress.org/abstract.cfm?URI=oe-15-14-8702>.
- P. J. Lu, E. Zaccarelli, F. Ciulla, A. B. Schofield, F. Sciortino, and D. A. Weitz. Gelation of particles with short-range attraction. *NATURE*, 453(7194):499–U4, MAY 22 2008. ISSN 0028-0836. doi: 10.1038/nature06931.
- B. D. Lubachevsky and F. H. Stillinger. Geometric properties of random disk packings, 1990. ISSN 0022-4715. URL <http://dx.doi.org/10.1007/BF01025983>.
- B. D. Lubachevsky, F. H. Stillinger, and E. N. Pinson. Disks vs. spheres: Contrasting properties of random packings, 1991. ISSN 0022-4715. URL <http://dx.doi.org/10.1007/BF01048304>.
- A. Malijevsky, S. B. Yuste, and A. Santos. How “sticky” are short-range square-well fluids? *J. Chem. Phys.*, 125(7):074507–12, Aug. 2006. URL <http://dx.doi.org/10.1063/1.2244549>.
- F. Mallamace, P. Gambadauro, N. Micali, P. Tartaglia, C. Liao, and S.-H. Chen. Kinetic glass transition in a micellar system with short-range attractive interaction. *Phys. Rev. Lett.*, 84(23):5431–5434, June 2000. URL <http://link.aps.org/doi/10.1103/PhysRevLett.84.5431>.
- Y. Mamunya, V. Davydenko, P. Pissis, and E. Lebedev. Electrical and thermal conductivity of polymers filled with metal powders. *European Polymer Journal*, 38(9):1887–1897, Sept. 2002. ISSN 0014-3057. doi: 10.1016/S0014-3057(02)00064-2. URL <http://www.sciencedirect.com/science/article/pii/S0014305702000642>.
- B. B. Mandelbrot. *The fractal geometry of nature*. WH Freeman and Co., New York, 1983.
- S. Manley, L. Cipelletti, V. Trappe, A. E. Bailey, R. J. Christianson, U. Gasser, V. Prasad, P. N. Segre, M. P. Doherty, S. Sankaran, A. L. Jankovsky, B. Shiley, J. Bowen, J. Eggers, C. Kurta, T. Lorik, and D. A. Weitz. Limits to gelation in colloidal aggregation. *Phys. Rev. Lett.*, 93(10):108302–, Sept. 2004. URL <http://link.aps.org/doi/10.1103/PhysRevLett.93.108302>.
- S. Manley, H. M. Wyss, K. Miyazaki, J. C. Conrad, V. Trappe, L. J. Kaufman, D. R. Reichman, and D. A. Weitz. Glasslike arrest in spinodal decomposition as a route to colloidal gelation. *Phys.*

- Rev. Lett.*, 95(23):238302–, Dec. 2005. URL <http://link.aps.org/doi/10.1103/PhysRevLett.95.238302>.
- S. Manna. Space filling tiling by random packing of discs. *Physica A: Statistical Mechanics and its Applications*, 187(3-4):373–377, Sept. 1992. ISSN 0378-4371. doi: 10.1016/0378-4371(92)90001-7. URL <http://www.sciencedirect.com/science/article/pii/0378437192900017>.
- S. S. Manna and H. J. Herrmann. Precise determination of the fractal dimensions of apollonian packing and space-filling bearings. *Journal of Physics A: Mathematical and General*, 24(9):L481–, 1991. ISSN 0305-4470. URL <http://stacks.iop.org/0305-4470/24/i=9/a=006>.
- G. A. Mansoori, N. F. Carnahan, K. E. Starling, and T. W. Leland, Jr. Equilibrium thermodynamic properties of the mixture of hard spheres. *J. Chem. Phys.*, 54(4):1523–1525, Feb. 1971. URL <http://dx.doi.org/10.1063/1.1675048>.
- D. W. Marr and A. P. Gast. On the solid–fluid interface of adhesive spheres. *J. Chem. Phys.*, 99(3):2024–2031, Aug. 1993. URL <http://dx.doi.org/10.1063/1.465265>.
- J. E. Martin, J. Wilcoxon, and D. Adolf. Critical exponents for the sol-gel transition. *Phys. Rev. A*, 36(4):1803–1810, Aug. 1987. URL <http://link.aps.org/doi/10.1103/PhysRevA.36.1803>.
- F. Martínez-López, M. Cabrerizo-Vílchez, and R. Hidalgo-Álvarez. An improved method to estimate the fractal dimension of physical fractals based on the hausdorff definition. *Physica A: Statistical Mechanics and its Applications*, 298(3-4):387–399, Sept. 2001a. ISSN 0378-4371. doi: 10.1016/S0378-4371(01)00255-2. URL <http://www.sciencedirect.com/science/article/pii/S0378437101002552>.
- F. Martínez-López, M. A. Cabrerizo-Vílchez, and R. Hidalgo-Álvarez. On the self-similarity of fractal colloidal aggregates in two dimensions. *Journal of Physics A: Mathematical and General*, 34(36):7393–, 2001b. ISSN 0305-4470. URL <http://stacks.iop.org/0305-4470/34/i=36/a=318>.
- F. Martínez-López, M. Cabrerizo-Vílchez, and R. Hidalgo-Álvarez. A study of the different methods usually employed to compute the fractal dimension. *Physica A: Statistical Mechanics and its Applications*, 311(3-4):411–428, Aug. 2002. ISSN 0378-4371. doi: 10.1016/S0378-4371(02)00819-1. URL <http://www.sciencedirect.com/science/article/pii/S0378437102008191>.
- J. Mattsson, H. M. Wyss, A. Fernandez-Nieves, K. Miyazaki, Z. Hu, D. R. Reichman, and D. A. Weitz. Soft colloids make strong glasses. *Nature*, 462(7269):83–86, Nov. 2009. ISSN 0028-0836. URL <http://dx.doi.org/10.1038/nature08457>.
- P. Meakin. Formation of fractal clusters and networks by irreversible diffusion-limited aggregation. *Phys. Rev. Lett.*, 51(13):1119–1122, Sept. 1983. URL <http://link.aps.org/doi/10.1103/PhysRevLett.51.1119>.
- M. Menyhard, A. Sulyok, K. Pentek, and A. Zeltser. Demixing in spin valve structures: an auger depth profiling study. *Thin Solid Films*, 366(1-2):129–134, May 2000. ISSN 0040-6090. doi:

## Bibliography

---

- 10.1016/S0040-6090(00)00715-X. URL <http://www.sciencedirect.com/science/article/pii/S004060900000715X>.
- R. Mezzenga, P. Schurtenberger, A. Burbidge, and M. Michel. Understanding foods as soft materials. *Nat Mater*, 4(10):729–740, Oct. 2005. ISSN 1476-1122. URL <http://dx.doi.org/10.1038/nmat1496>.
- S. Miljanic, L. Frkanec, T. Biljan, Z. Meic, and M. Zinic. Surface-enhanced raman scattering on colloid gels originated from low molecular weight gelator. *J. Raman Spectrosc.*, 39(12):1799–1804, 2008. ISSN 1097-4555. URL <http://dx.doi.org/10.1002/jrs.2039>.
- M. A. Miller and D. Frenkel. Competition of percolation and phase separation in a fluid of adhesive hard spheres. *Phys. Rev. Lett.*, 90(13):135702–, Apr. 2003. URL <http://link.aps.org/doi/10.1103/PhysRevLett.90.135702>.
- M. A. Miller, R. Blaak, and J.-P. Hansen. Topological characteristics of model gels. *Journal of Physics: Condensed Matter*, 22(10):104109–, 2010. ISSN 0953-8984. URL <http://stacks.iop.org/0953-8984/22/i=10/a=104109>.
- C. A. Mirkin, R. L. Letsinger, R. C. Mucic, and J. J. Storhoff. A dna-based method for rationally assembling nanoparticles into macroscopic materials. *Nature*, 382(6592):607–609, Aug. 1996. URL <http://dx.doi.org/10.1038/382607a0>.
- B. M. Mognetti, P. Varilly, S. Angioletti-Uberti, F. J. Martinez-Veracoechea, J. Dobnikar, M. E. Leunissen, and D. Frenkel. Predicting dna-mediated colloidal pair interactions. *Proceedings of the National Academy of Sciences*, 109(7):E378–E379, 2012. doi: 10.1073/pnas.1119991109. URL <http://www.pnas.org/content/109/7/E378.short>.
- A. Moncho-Jordá, A. A. Louis, P. G. Bolhuis, and R. Roth. The asakura-oosawa model in the protein limit: the role of many-body interactions. *Journal of Physics: Condensed Matter*, 15(48):S3429–, 2003. ISSN 0953-8984. URL <http://stacks.iop.org/0953-8984/15/i=48/a=004>.
- K. J. Mutch, J. S. van Duijneveldt, and J. Eastoe. Colloid-polymer mixtures in the protein limit. *Soft Matter*, 3(2):155–167, 2007. ISSN 1744-683X. URL <http://dx.doi.org/10.1039/B611137H>.
- A. Nabok, J. Massey, S. Buttle, and A. Ray. Study of electron tunnelling through thin polymer films using a mercury probe technique. *Circuits, Devices and Systems, IEE Proceedings -*, 151(5):461–465, 2004. ISSN 1350-2409.
- D. H. Napper. Polymeric stabilization of colloidal dispersions, 1983. URL [http://sfx.ethz.ch:9003/sfx\\_epf?sid=google&auunit=DH&aulast=Napper&title=Polymeric%20stabilization%20of%20colloidal%20dispersions&genre=book&date=1983](http://sfx.ethz.ch:9003/sfx_epf?sid=google&auunit=DH&aulast=Napper&title=Polymeric%20stabilization%20of%20colloidal%20dispersions&genre=book&date=1983).
- B. Nigro, C. Grimaldi, M. A. Miller, P. Ryser, and T. Schilling. Tunneling conductivity in composites of attractive colloids. *J. Chem. Phys.*, 136(16):164903–9, Apr. 2012. URL <http://dx.doi.org/10.1063/1.4705307>.

- M. G. Noro and D. Frenkel. Extended corresponding-states behavior for particles with variable range attractions. *J. Chem. Phys.*, 113(8):2941–2944, Aug. 2000. URL <http://dx.doi.org/10.1063/1.1288684>.
- D. Nykypanchuk, M. M. Maye, D. van der Lelie, and O. Gang. Dna-guided crystallization of colloidal nanoparticles. *Nature*, 451(7178):549–552, Jan. 2008. ISSN 0028-0836. URL <http://dx.doi.org/10.1038/nature06560>.
- S. Y. Park, A. K. R. Lytton-Jean, B. Lee, S. Weigand, G. C. Schatz, and C. A. Mirkin. Dna-programmable nanoparticle crystallization. *Nature*, 451(7178):553–556, Jan. 2008. ISSN 0028-0836. URL <http://dx.doi.org/10.1038/nature06508>.
- K. N. Pham, A. M. Puertas, J. Bergenholtz, S. U. Egelhaaf, A. Moussaoui, P. N. Pusey, A. B. Schofield, M. E. Cates, M. Fuchs, and W. C. K. Poon. Multiple glassy states in a simple model system. *Science*, 296(5565):104–106, Apr. 2002. URL <http://www.sciencemag.org/content/296/5565/104.abstract>.
- R. Piazza. Interactions in protein solutions near crystallisation: a colloid physics approach. *Journal of Crystal Growth*, 196(2-4):415–423, Jan. 1999. ISSN 0022-0248. doi: 10.1016/S0022-0248(98)00867-7. URL <http://www.sciencedirect.com/science/article/pii/S0022024898008677>.
- P. Pincus. Colloid stabilization with grafted polyelectrolytes. *Macromolecules*, 24(10):2912–2919, May 1991. ISSN 0024-9297. doi: 10.1021/ma00010a043. URL <http://dx.doi.org/10.1021/ma00010a043>.
- Y. Pineiro, M. A. Lopez-Quintela, J. Rivas, and D. Leisner. Percolation threshold and scattering power law of gelatin gels. *Phys. Rev. E*, 79(4):041409–, Apr. 2009. URL <http://link.aps.org/doi/10.1103/PhysRevE.79.041409>.
- A. V. Pinheiro, D. Han, W. M. Shih, and H. Yan. Challenges and opportunities for structural dna nanotechnology. *Nat Nano*, 6(12):763–772, Dec. 2011. ISSN 1748-3387. URL <http://dx.doi.org/10.1038/nnano.2011.187>.
- D. Pini, M. Tau, A. Parola, and L. Reatto. Phase diagram of symmetric binary mixtures at equimolar and nonequimolar concentrations: A systematic investigation. *Phys. Rev. E*, 67(4):046116–, Apr. 2003. URL <http://link.aps.org/doi/10.1103/PhysRevE.67.046116>.
- M. Pollak. A percolation treatment of dc hopping conduction. *Journal of Non-Crystalline Solids*, 11(1):1–24, July 1972. ISSN 0022-3093. doi: 10.1016/0022-3093(72)90304-3. URL <http://www.sciencedirect.com/science/article/pii/0022309372903043>.
- W. Poon and M. Haw. Mesoscopic structure formation in colloidal aggregation and gelation. *Advances in Colloid and Interface Science*, 73(0):71–126, Oct. 1997. ISSN 0001-8686. doi: 10.1016/S0001-8686(97)90003-8. URL <http://www.sciencedirect.com/science/article/pii/S0001868697900038>.

## Bibliography

---

- W. Poon, S. Ilett, and P. Pusey. Phase behaviour of colloid-polymer mixtures, 1994. ISSN 0392-6737. URL <http://dx.doi.org/10.1007/BF02458793>.
- W. C. Poon. Phase separation, aggregation and gelation in colloid-polymer mixtures and related systems. *Current Opinion in Colloid & Interface Science*, 3(6):593–599, Dec. 1998. ISSN 1359-0294. doi: 10.1016/S1359-0294(98)80085-X. URL <http://www.sciencedirect.com/science/article/pii/S135902949880085X>.
- W. C. K. Poon. The physics of a model colloidal-polymer mixture. *Journal of Physics: Condensed Matter*, 14(33):R859–, 2002. ISSN 0953-8984. URL <http://stacks.iop.org/0953-8984/14/i=33/a=201>.
- W. C. K. Poon, J. S. Selfe, M. B. Robertson, S. M. Ilett, A. D. Pirie, and P. N. Pusey. An experimental study of a model colloid-polymer mixture. *J. Phys. II France*, 3(7): 1075–1086, 1993. URL <http://dx.doi.org/10.1051/jp2:1993184>
- W. C. K. Poon, A. D. Pirie, and P. N. Pusey. Gelation in colloid-polymer mixtures. *Faraday Discuss.*, 101:65–76, 1995. ISSN 1359-6640. URL <http://dx.doi.org/10.1039/FD9950100065>.
- S. Popinet. GTS: GNU Triangulated Surface library. <http://gts.sourceforge.net/>, 2000–2010.
- G. Porod. Die rontgenkleinwinkelstreuung von dichtgepackten kolloiden systemen .1. *Kolloid-zeitschrift and Zeitschrift Fur Polymere*, 124(2):83–114, 1951. doi: 10.1007/BF01512792.
- G. Porod. Die rontgenkleinwinkelstreuung von dichtgepackten kolloiden systemen .2. *Kolloid-zeitschrift and Zeitschrift Fur Polymere*, 125(1):51–57, 1952. doi: 10.1007/BF01519615.
- P. Poulin, J. Bibette, and D. Weitz. From colloidal aggregation to spinodal decomposition in sticky emulsions, Jan. 1999. ISSN 1434-6028. URL <http://dx.doi.org/10.1007/s100510050614>.
- V. Prasad, D. Semwogerere, and E. R. Weeks. Confocal microscopy of colloids. *Journal of Physics: Condensed Matter*, 19(11):113102–, 2007. ISSN 0953-8984. URL <http://stacks.iop.org/0953-8984/19/i=11/a=113102>.
- P. Pusey, A. Pirie, and W. Poon. Dynamics of colloid-polymer mixtures. *Physica A: Statistical Mechanics and its Applications*, 201(1-3):322–331, 1993. URL



- <http://www.scopus.com/inward/record.url?eid=2-s2.0-43949164935&partnerID=40&md5=22650480e5a934db0e7794f6f3610661>.
- P. N. Pusey and W. van Megen. Phase behaviour of concentrated suspensions of nearly hard colloidal spheres. *Nature*, 320(6060):340–342, Mar. 1986. URL <http://dx.doi.org/10.1038/320340a0>.
- P. N. Pusey, W. van Megen, P. Bartlett, B. J. Ackerson, J. G. Rarity, and S. M. Underwood. Structure of crystals of hard colloidal spheres. *Phys. Rev. Lett.*, 63(25):2753–2756, Dec. 1989. URL <http://link.aps.org/doi/10.1103/PhysRevLett.63.2753>.
- A. Rahman and F. H. Stillinger. Molecular dynamics study of liquid water. *J. Chem. Phys.*, 55(7):3336–3359, Oct. 1971. URL <http://dx.doi.org/10.1063/1.1676585>.
- S. Ramakrishnan and C. F. Zukoski. Characterizing nanoparticle interactions: Linking models to experiments. *J. Chem. Phys.*, 113(3):1237–1248, July 2000. URL <http://dx.doi.org/10.1063/1.481901>.
- S. Ramakrishnan, M. Fuchs, K. S. Schweizer, and C. F. Zukoski. Entropy driven phase transitions in colloid–polymer suspensions: Tests of depletion theories. *J. Chem. Phys.*, 116(5):2201–2212, Feb. 2002. URL <http://dx.doi.org/10.1063/1.1426413>.
- D. C. Rapaport. The art of computer simulations, 1997. URL [http://sfx.ethz.ch:9003/sfx\\_epf?sid=IOPP%3Ajnl\\_ref&genre=bookitem&date=1997&aulast=Rapaport&aufirst=D%20C&title=The%20Art%20of%20Computer%20Simulations](http://sfx.ethz.ch:9003/sfx_epf?sid=IOPP%3Ajnl_ref&genre=bookitem&date=1997&aulast=Rapaport&aufirst=D%20C&title=The%20Art%20of%20Computer%20Simulations).
- D. C. Rapaport. The event-driven approach to n-body simulation. *Prog. Theor. Phys. Supplement*, 178(178):5–14, 2009. ISSN 03759687. URL <http://ci.nii.ac.jp/naid/110007225706/en/>.
- W. B. Rogers and J. C. Crocker. Direct measurements of dna-mediated colloidal interactions and their quantitative modeling. *Proceedings of the National Academy of Sciences*, 2011. doi: 10.1073/pnas.1109853108. URL <http://www.pnas.org/content/early/2011/09/01/1109853108.abstract>.
- O. Ronsin, C. Caroli, and T. Baumberger. Interplay between shear loading and structural aging in a physical gelatin gel. *Phys. Rev. Lett.*, 103(13):138302–, Sept. 2009. URL <http://link.aps.org/doi/10.1103/PhysRevLett.103.138302>.
- D. Rosenbaum and C. Zukoski. Protein interactions and crystallization. *Journal of Crystal Growth*, 169(4):752–758, Dec. 1996. ISSN 0022-0248. doi: 10.1016/S0022-0248(96)00455-1. URL <http://www.sciencedirect.com/science/article/pii/S0022024896004551>.
- D. Rosenbaum, P. C. Zamora, and C. F. Zukoski. Phase behavior of small attractive colloidal particles. *Phys. Rev. Lett.*, 76(1):150–153, Jan. 1996. URL <http://link.aps.org/doi/10.1103/PhysRevLett.76.150>.
- M. N. Rosenbluth and A. W. Rosenbluth. Further results on monte carlo equations of state. *J. Chem. Phys.*, 22(5):881–884, May 1954. URL <http://dx.doi.org/10.1063/1.1740207>.

## Bibliography

---

- P. W. K. Rothemund. Folding dna to create nanoscale shapes and patterns. *Nature*, 440(7082): 297–302, Mar. 2006. ISSN 0028-0836. URL <http://dx.doi.org/10.1038/nature04586>.
- P. Rouw, A. Woutersen, B. Ackerson, and C. De Kruif. Adhesive hard sphere dispersions. v. observation of spinodal decomposition in a colloidal dispersion. *Physica A: Statistical Mechanics and its Applications*, 156(3):876–898, 1989. URL <http://www.scopus.com/inward/record.url?eid=2-s2.0-0001008902&partnerID=40&md5=17541ead2b1edf079717f3203a2ca639>.
- C. P. Royall and A. Malins. The role of quench rate in colloidal gels. *Faraday Discuss.*, pages –, 2012. ISSN 1359-6640. URL <http://dx.doi.org/10.1039/C2FD20041D>.
- W. Russel, D. Saville, and W. Schowalter. *Colloidal Dispersions*. Cambridge University Press, 1992. URL <http://books.google.ch/books?id=3shp8Kl6YoUC>.
- B. Ruzicka, E. Zaccarelli, L. Zulian, R. Angelini, M. Sztucki, A. MoussaĆEd, T. Narayanan, and E. Sciortino. Observation of empty liquids and equilibrium gels in a colloidal clay. *Nat Mater*, 10(1):56–60, Jan. 2011. ISSN 1476-1122. URL <http://dx.doi.org/10.1038/nmat2921>.
- S. Sacanna, W. T. M. Irvine, P. M. Chaikin, and D. J. Pine. Lock and key colloids. *Nature*, 464(7288):575–578, Mar. 2010. ISSN 0028-0836. URL <http://dx.doi.org/10.1038/nature08906>.
- S. Safran. *Statistical Thermodynamics Of Surfaces, Interfaces, And Membranes*. Westview Press, 2003. URL <http://books.google.ch/books?id=AadFAfZtd1sC>.
- I. Schenker, F. T. Filser, T. Aste, and L. J. Gauckler. Microstructures and mechanical properties of dense particle gels: Microstructural characterisation. *Journal of the European Ceramic Society*, 28(7):1443–1449, 2008. ISSN 0955-2219. doi: 10.1016/j.jeurceramsoc.2007.12.007. URL <http://www.sciencedirect.com/science/article/pii/S0955221907006152>.
- M. Schmidt and W. Burchard. Critical exponents in polymers: a sol-gel study of anionically prepared styrene-divinylbenzene copolymers. *Macromolecules*, 14(2):370–376, Mar. 1981. ISSN 0024-9297. doi: 10.1021/ma50003a027. URL <http://dx.doi.org/10.1021/ma50003a027>.
- D. V. Schroeder. An introduction to thermal physics, 1999. URL [http://sfx.ethz.ch:9003/sfx\\_epf?sid=IOPP%3Ajl\\_ref&genre=bookitem&date=1999&aulast=Schroeder&aufirst=D%20V&title=An%20Introduction%20to%20Thermal%20Physics](http://sfx.ethz.ch:9003/sfx_epf?sid=IOPP%3Ajl_ref&genre=bookitem&date=1999&aulast=Schroeder&aufirst=D%20V&title=An%20Introduction%20to%20Thermal%20Physics).
- F. Sciortino. Disordered materials: One liquid, two glasses. *Nat Mater*, 1(3):145–146, Nov. 2002. ISSN 1476-1122. URL <http://dx.doi.org/10.1038/nmat752>.
- F. Sciortino and P. Tartaglia. Structure factor scaling during irreversible cluster-cluster aggregation. *Phys. Rev. Lett.*, 74(2):282–285, Jan. 1995. URL <http://link.aps.org/doi/10.1103/PhysRevLett.74.282>.
- F. Sciortino, A. Belloni, and P. Tartaglia. Cluster-cluster correlation during irreversible diffusion-limited aggregation, 1994-08-01. ISSN 0392-6737. URL <http://dx.doi.org/10.1007/BF02458796>.

- F. Sciortino, A. Belloni, and P. Tartaglia. Irreversible diffusion-limited cluster aggregation: The behavior of the scattered intensity. *Phys. Rev. E*, 52(4):4068–4079, Oct. 1995. URL <http://link.aps.org/doi/10.1103/PhysRevE.52.4068>.
- N. C. Seeman. Dna in a material world. *Nature*, 421(6921):427–431, Jan. 2003. ISSN 0028-0836. URL <http://dx.doi.org/10.1038/nature01406>.
- P. N. Segré, V. Prasad, A. B. Schofield, and D. A. Weitz. Glasslike kinetic arrest at the colloidal-gelation transition. *Phys. Rev. Lett.*, 86(26):6042–6045, June 2001. URL <http://link.aps.org/doi/10.1103/PhysRevLett.86.6042>.
- W. Shih, J. Liu, W.-H. Shih, and I. Aksay. Aggregation of colloidal particles with a finite interparticle attraction energy. *Journal of Statistical Physics*, 62(5-6):961–984, 1991. URL <http://www.scopus.com/inward/record.url?eid=2-s2.0-0000594131&partnerID=40&md5=129af08a2c1eaa2b1b3a3c8b3b82d5ad>.
- F. Simmel. Three-dimensional nanoconstruction with dna. *Angewandte Chemie International Edition*, 47(32):5884–5887, 2008. ISSN 1521-3773. URL <http://dx.doi.org/10.1002/anie.200801982>.
- S. K. Sinha, E. B. Sirota, S. Garoff, and H. B. Stanley. X-ray and neutron scattering from rough surfaces. *Phys. Rev. B*, 38(4):2297–2311, Aug. 1988. URL <http://link.aps.org/doi/10.1103/PhysRevB.38.2297>.
- W. R. Smith, D. J. Henderson, P. J. Leonard, J. A. Barker, and E. W. Grundke. Fortran codes for the correlation functions of hard sphere fluids. *Molecular Physics*, 106(1):3–7, Jan. 2008. ISSN 0026-8976. doi: 10.1080/00268970701628423. URL <http://dx.doi.org/10.1080/00268970701628423>.
- F. Soddy. The kiss precise. *Nature*, 137:1021, 1936. doi: 10.1038/1371021a0. URL <http://www.nature.com/nature/journal/v137/n3477/pdf/1371021a0.pdf>.
- K. G. Soga, J. R. Melrose, and R. C. Ball. Continuum percolation and depletion flocculation. *J. Chem. Phys.*, 108(14):6026–6032, Apr. 1998. URL <http://dx.doi.org/10.1063/1.476015>.
- C. M. Sorensen and G. C. Roberts. The prefactor of fractal aggregates. *Journal of Colloid and Interface Science*, 186(2):447–452, Feb. 1997. ISSN 0021-9797. doi: 10.1006/jcis.1996.4664. URL <http://www.sciencedirect.com/science/article/pii/S0021979796946640>.
- H. Stanley. *Introduction to Phase Transitions and Critical Phenomena*. Oxford University Press, USA, 1987.
- D. Stauffer. Theory and experiment at the sol-gel phase transition. *Physica A: Statistical Mechanics and its Applications*, 106(1-2):177–188, Mar. 1981. ISSN 0378-4371. doi: 10.1016/0378-4371(81)90218-1. URL <http://www.sciencedirect.com/science/article/pii/0378437181902181>.

## Bibliography

---

- D. Stauffer and A. Aharony. *Introduction To Percolation Theory*. Taylor & Francis, 1994. URL <http://books.google.ch/books?id=v66pllej5QC>.
- D. Stauffer, A. Coniglio, and M. Adam. Gelation and critical phenomena: Polymer networks, 1982. ISSN 978-3-540-11471-0. URL [http://dx.doi.org/10.1007/3-540-11471-8\\_4](http://dx.doi.org/10.1007/3-540-11471-8_4).
- G. Stell. Sticky spheres and related systems, 1991. ISSN 0022-4715. URL <http://dx.doi.org/10.1007/BF01030007>.
- D. N. Sutherland. A theoretical model of floc structure. *Journal of Colloid and Interface Science*, 25(3):373–380, Nov. 1967. ISSN 0021-9797. doi: 10.1016/0021-9797(67)90043-4. URL <http://www.sciencedirect.com/science/article/pii/0021979767900434>.
- R. H. Swendsen. Dynamics of random sequential adsorption. *Phys. Rev. A*, 24(1):504–508, July 1981. URL <http://link.aps.org/doi/10.1103/PhysRevA.24.504>.
- J. Talbot, P. Schaaf, and G. Tarjus. Random sequential addition of hard spheres. *Molecular Physics*, 72(6):1397–1406, Apr. 1991. ISSN 0026-8976. doi: 10.1080/00268979100100981. URL <http://dx.doi.org/10.1080/00268979100100981>.
- A. K. Thakre, W. K. den Otter, and W. J. Briels. Domain formation and growth in spinodal decomposition of a binary fluid by molecular dynamics simulations. *Phys. Rev. E*, 77(1):011503–, Jan. 2008. URL <http://link.aps.org/doi/10.1103/PhysRevE.77.011503>.
- L. Tisza. *Generalized thermodynamics*. M.I.T. Press, 1977. URL <http://books.google.ch/books?id=Opt6AAAAIAAJ>.
- S. Torquato, T. M. Truskett, and P. G. Debenedetti. Is random close packing of spheres well defined? *Phys. Rev. Lett.*, 84(10):2064–2067, Mar. 2000. URL <http://link.aps.org/doi/10.1103/PhysRevLett.84.2064>.
- V. Trappe and P. Sandkühler. Colloidal gels — low-density disordered solid-like states. *Current Opinion in Colloid & Interface Science*, 8(6):494–500, Apr. 2004. ISSN 1359-0294. doi: 10.1016/j.cocis.2004.01.002. URL <http://www.sciencedirect.com/science/article/pii/S1359029404000032>.
- V. Trappe, V. Prasad, L. Cipelletti, P. N. Segre, and D. A. Weitz. Jamming phase diagram for attractive particles. *Nature*, 411(6839):772–775, June 2001. ISSN 0028-0836. URL <http://dx.doi.org/10.1038/35081021>.
- S. Y. Trofimov, E. L. F. Nies, and M. A. J. Michels. Thermodynamic consistency in dissipative particle dynamics simulations of strongly nonideal liquids and liquid mixtures. *J. Chem. Phys.*, 117(20):9383–9394, Nov. 2002. URL <http://dx.doi.org/10.1063/1.1515774>.
- R. Tuinier, J. Rieger, and C. de Kruif. Depletion-induced phase separation in colloid-polymer mixtures. *Advances in Colloid and Interface Science*, 103(1):1–31, Mar. 2003. ISSN 0001-8686. doi: 10.1016/S0001-8686(02)00081-7. URL <http://www.sciencedirect.com/science/article/pii/S0001868602000817>.

- C. P. Ursenbach and G. N. Patey. Stability of binary mixtures: Supersaturation limits of aqueous alkali halide solutions. *J. Chem. Phys.*, 100(5):3827–3842, Mar. 1994. URL <http://dx.doi.org/10.1063/1.466372>.
- M.-P. Valignat, O. Theodoly, J. C. Crocker, W. B. Russel, and P. M. Chaikin. Reversible self-assembly and directed assembly of dna-linked micrometer-sized colloids. *Proceedings of the National Academy of Sciences of the United States of America*, 102(12):4225–4229, 2005. doi: 10.1073/pnas.0500507102. URL <http://www.pnas.org/content/102/12/4225.abstract>.
- F. Valle, M. Favre, P. De Los Rios, A. Rosa, and G. Dietler. Scaling exponents and probability distributions of dna end-to-end distance. *Phys. Rev. Lett.*, 95(15):158105–, Oct. 2005. URL <http://link.aps.org/doi/10.1103/PhysRevLett.95.158105>.
- A. van Blaaderen and P. Wiltzius. Real-space structure of colloidal hard-sphere glasses. *Science*, 270(5239):1177–1179, 1995. doi: 10.1126/science.270.5239.1177. URL <http://www.sciencemag.org/content/270/5239/1177.abstract>.
- K. van Gruijthuisen, V. Herle, R. Tuinier, P. Schurtenberger, and A. Stradner. Origin of suppressed demixing in casein/xanthan mixtures. *Soft Matter*, 8(5):1547–1555, 2012. ISSN 1744-683X. URL <http://dx.doi.org/10.1039/C1SM06761C>.
- L. Van Hove. Correlations in space and time and born approximation scattering in systems of interacting particles. *Phys. Rev.*, 95(1):249–262, July 1954. URL <http://link.aps.org/doi/10.1103/PhysRev.95.249>.
- P. Varadan and M. J. Solomon. Direct visualization of long-range heterogeneous structure in dense colloidal gels. *Langmuir*, 19(3):509–512, Oct. 2002. ISSN 0743-7463. doi: 10.1021/la026303j. URL <http://dx.doi.org/10.1021/la026303j>.
- P. Varilly, S. Angioletti-Uberti, B. M. Mognetti, and D. Frenkel. A general theory of dna-mediated and other valence-limited interactions, 2012. URL <http://arxiv.org/abs/1205.6921v3>. arXiv:1205.6921v3 [cond-mat.soft].
- H. Verduin and J. Dhont. Phase diagram of a model adhesive hard-sphere dispersion. *Journal of Colloid And Interface Science*, 172(2):425–437, 1995. URL <http://www.scopus.com/inward/record.url?eid=2-s2.0-0000659037&partnerID=40&md5=6205c3fb4e08fe951f282d87454052ef>.
- N. A. Verhaegh, D. Asnaghi, H. N. Lekkerkerker, M. Giglio, and L. Cipelletti. Transient gelation by spinodal decomposition in colloid-polymer mixtures. *Physica A: Statistical Mechanics and its Applications*, 242(1-2):104–118, Aug. 1997. ISSN 0378-4371. doi: 10.1016/S0378-4371(97)00184-2. URL <http://www.sciencedirect.com/science/article/pii/S0378437197001842>.
- N. A. Verhaegh, D. Asnaghi, and H. N. Lekkerkerker. Transient gels in colloid-polymer mixtures studied with fluorescence confocal scanning laser microscopy. *Physica A: Statistical Mechanics and its Applications*, 264(1-2):64–74, Feb. 1999. ISSN 0378-4371. doi:

## Bibliography

---

- 10.1016/S0378-4371(98)00420-8. URL <http://www.sciencedirect.com/science/article/pii/S0378437198004208>.
- L. Verlet and J.-J. Weis. Equilibrium theory of simple liquids. *Phys. Rev. A*, 5(2):939–952, Feb. 1972. URL <http://link.aps.org/doi/10.1103/PhysRevA.5.939>.
- B. Vincent, P. Luckham, and F. Waite. The effect of free polymer on the stability of sterically stabilized dispersions. *Journal of Colloid and Interface Science*, 73(2):508–521, Feb. 1980. ISSN 0021-9797. doi: 10.1016/0021-9797(80)90097-1. URL <http://www.sciencedirect.com/science/article/pii/0021979780900971>.
- A. Vrij. Polymers at interfaces and interactions in colloidal dispersions. *Pure and Applied Chemistry*, 48(4):471–483, 1976. doi: 10.1351/pac197648040471.
- A. Walther and A. H. E. Muller. Janus particles. *Soft Matter*, 4(4):663–668, 2008. ISSN 1744-683X. URL <http://dx.doi.org/10.1039/B718131K>.
- Q. Wang, L. Wang, M. S. Detamore, and C. Berklund. Biodegradable colloidal gels as moldable tissue engineering scaffolds. *Adv. Mater.*, 20(2):236–239, 2008. ISSN 1521-4095. URL <http://dx.doi.org/10.1002/adma.200702099>.
- Q. Wang, J. Wang, Q. Lu, M. S. Detamore, and C. Berklund. Injectable plga based colloidal gels for zero-order dexamethasone release in cranial defects. *Biomaterials*, 31(18):4980–4986, June 2010. ISSN 0142-9612. doi: 10.1016/j.biomaterials.2010.02.052. URL <http://www.sciencedirect.com/science/article/pii/S014296121000298X>.
- A. Ward and A. Courts. *The Science and Technology of Gelatin*. Academic Press, London (England), 1977.
- E. R. Weeks, J. C. Crocker, A. C. Levitt, A. Schofield, and D. A. Weitz. Three-dimensional direct imaging of structural relaxation near the colloidal glass transition. *Science*, 287(5453):627–631, 2000. doi: 10.1126/science.287.5453.627. URL <http://www.sciencemag.org/content/287/5453/627.abstract>.
- D. A. Weitz and M. Oliveria. Fractal structures formed by kinetic aggregation of aqueous gold colloids. *Phys. Rev. Lett.*, 52(16):1433–1436, Apr. 1984. URL <http://link.aps.org/doi/10.1103/PhysRevLett.52.1433>.
- R. Wessel and R. C. Ball. Fractal aggregates and gels in shear flow. *Phys. Rev. A*, 46(6):R3008–R3011, Sept. 1992. URL <http://link.aps.org/doi/10.1103/PhysRevA.46.R3008>.
- G. Whitesides, J. Mathias, and C. Seto. Molecular self-assembly and nanochemistry: a chemical strategy for the synthesis of nanostructures. *Science*, 254(5036):1312–1319, 1991. doi: 10.1126/science.1962191. URL <http://www.sciencemag.org/content/254/5036/1312.abstract>.
- J. K. Whitmer and E. Luijten. Influence of hydrodynamics on cluster formation in colloid-polymer mixtures. *J. Phys. Chem. B*, 115(22):7294–7300, May 2011. ISSN 1520-6106. doi: 10.1021/jp111388m. URL <http://dx.doi.org/10.1021/jp111388m>.

- R. S. Whitney and W. Burchard. Molecular size and gel formation in branched poly(methyl methacrylate) copolymers. *Makromol. Chem.*, 181(4):869–890, 1980. ISSN 0025-116X. URL <http://dx.doi.org/10.1002/macp.1980.021810409>.
- N. B. Wilding, F. Schmid, and P. Nielaba. Liquid-vapor phase behavior of a symmetrical binary fluid mixture. *Phys. Rev. E*, 58(2):2201–2212, Aug. 1998. URL <http://link.aps.org/doi/10.1103/PhysRevE.58.2201>.
- G. Williams. *Chaos Theory Tamed*. Taylor & Francis, 1997. URL <http://books.google.ch/books?id=0bH1Dvo3YJQC>.
- O. I. Wilner, Y. Weizmann, R. Gill, O. Lioubashevski, R. Freeman, and I. Willner. Enzyme cascades activated on topologically programmed dna scaffolds. *Nat Nano*, 4(4):249–254, Apr. 2009. ISSN 1748-3387. URL <http://dx.doi.org/10.1038/nnano.2009.50>.
- P. Wiltzius, F. S. Bates, and W. R. Heffner. Spinodal decomposition in isotopic polymer mixtures. *Phys. Rev. Lett.*, 60(15):1538–1541, Apr. 1988. URL <http://link.aps.org/doi/10.1103/PhysRevLett.60.1538>.
- J. Witten, T. A. and L. M. Sander. Diffusion-limited aggregation, a kinetic critical phenomenon. *Phys. Rev. Lett.*, 47(19):1400–1403, Nov. 1981. URL <http://link.aps.org/doi/10.1103/PhysRevLett.47.1400>.
- W. W. Wood and J. D. Jacobson. Preliminary results from a recalculation of the monte carlo equation of state of hard spheres. *J. Chem. Phys.*, 27(5):1207–1208, Nov. 1957. URL <http://dx.doi.org/10.1063/1.1743956>.
- H. Wu, M. Lattuada, P. Sandkühler, J. Sefcik, and M. Morbidelli. Role of sedimentation and buoyancy on the kinetics of diffusion limited colloidal aggregation. *Langmuir*, 19(26):10710–10718, Nov. 2003. ISSN 0743-7463. doi: 10.1021/la034970m. URL <http://dx.doi.org/10.1021/la034970m>.
- H. M. Wyss, E. V. Tervoort, and L. J. Gauckler. Mechanics and microstructures of concentrated particle gels. *Journal of the American Ceramic Society*, 88(9):2337–2348, 2005. ISSN 1551-2916. URL <http://dx.doi.org/10.1111/j.1551-2916.2005.00622.x>.
- X. Ye, T. Narayanan, P. Tong, J. S. Huang, M. Y. Lin, B. L. Carvalho, and L. J. Fetters. Depletion interactions in colloid-polymer mixtures. *Phys. Rev. E*, 54(6):6500–6510, Dec. 1996. URL <http://link.aps.org/doi/10.1103/PhysRevE.54.6500>.
- A. Yethiraj and A. van Blaaderen. A colloidal model system with an interaction tunable from hard sphere to soft and dipolar. *Nature*, 421(6922):513–517, Jan. 2003. ISSN 0028-0836. URL <http://dx.doi.org/10.1038/nature01328>.
- S. Yip and T. Rubia. *Scientific Modeling and Simulations*. Springer, 2009. URL <http://books.google.ch/books?id=cXh29CUn-qYC>.

## Bibliography

---

- E. Zaccarelli. Colloidal gels: equilibrium and non-equilibrium routes. *Journal of Physics: Condensed Matter*, 19(32):323101–, 2007. ISSN 0953-8984. URL <http://stacks.iop.org/0953-8984/19/i=32/a=323101>.
- E. Zaccarelli, G. Foffi, K. A. Dawson, F. Sciortino, and P. Tartaglia. Mechanical properties of a model of attractive colloidal solutions. *Phys. Rev. E*, 63(3):031501–, Feb. 2001. URL <http://link.aps.org/doi/10.1103/PhysRevE.63.031501>.
- E. Zaccarelli, F. Sciortino, S. Buldyrev, and P. Tartaglia. Short-ranged attractive colloids: What is the gel state? In A. Coniglio, A. Fierro, H. J. Herrmann, H. J. H. Mario Nicodemi, Antonio Coniglio, Annalisa Fierro, and M. Nicodemi, editors, *Unifying Concepts in Granular Media and Glasses*, pages 181–194. Elsevier, Amsterdam, 2004. doi: 10.1016/B978-044451607-7/50015-7. URL <http://www.sciencedirect.com/science/article/pii/B9780444516077500157>.
- E. Zaccarelli, S. V. Buldyrev, E. La Nave, A. J. Moreno, I. Saika-Voivod, F. Sciortino, and P. Tartaglia. Model for reversible colloidal gelation. *Phys. Rev. Lett.*, 94(21):218301–, June 2005. URL <http://link.aps.org/doi/10.1103/PhysRevLett.94.218301>.
- E. Zaccarelli, I. Saika-Voivod, S. V. Buldyrev, A. J. Moreno, P. Tartaglia, and F. Sciortino. Gel to glass transition in simulation of a valence-limited colloidal system. *J. Chem. Phys.*, 124(12):124908–14, Mar. 2006. URL <http://dx.doi.org/10.1063/1.2177241>.
- E. Zaccarelli, P. J. Lu, E. Ciulla, D. A. Weitz, and F. Sciortino. Gelation as arrested phase separation in short-ranged attractive colloid-polymer mixtures. *Journal of Physics: Condensed Matter*, 20(49):494242–, 2008. ISSN 0953-8984. URL <http://stacks.iop.org/0953-8984/20/i=49/a=494242>.
- A. Zaccone and E. Del Gado. On mean coordination and structural heterogeneity in model amorphous solids. *J. Chem. Phys.*, 132(2):024906–5, Jan. 2010. URL <http://dx.doi.org/10.1063/1.3284786>.
- Y. Zweifel, C. J. G. Plummer, and H.-H. Kausch. A microscopic investigation of conducting filled polymers, 1998-04-01. ISSN 0022-2461. URL <http://dx.doi.org/10.1023/A:1004316229497>.



# CURRICULUM VITAE

Ch. de Fontenay 13  
CH-1007 Lausanne

francesco.varrato@gmail.com  
Born on August 17<sup>th</sup> 1980, Italy



[Languages: **Italian** (native), **French** (B2/C1), **English** (B2/C1)]

## EDUCATION

---

2008-2012	EPFL (CH), Inst. of Theoretical Physics	PhD
2006-2008	Pisa University (IT), Physics Department	Physics of Matter, MSc (107/110)
2000-2005	Pisa University (IT), Physics Department	Theoretical Physics, BSc (105/110)
1994-1999	C.di Sangro High School (IT), Science edu.	Secondary school Certif. (100/100)

## POSTFORMATION

---

<b>Assistant:</b>	<i>Physique générale I</i> [FR] and <i>II</i> [FR]	(profs. B.Baldereschi and D.Pavuna)
<b>Examiner:</b>	<i>Stat. phys. of bio-macromolecules</i> [EN/FR], <i>Stat. Phys. III</i> [EN/FR]	(prof. P.De Los Rios)
<b>Classes:</b>	<ul style="list-style-type: none"><li>• “<i>The polymer physics of DNA</i>” (prof. B.Duplantier)</li><li>• “<i>Mechanics of Proteins and Enzymes</i>” (prof. C.Micheletti)</li><li>• “<i>Conformational transitions in polymers</i>” (prof. E.Orlandini)</li><li>• “<i>Dynamics of Biomacromolecules</i>” (prof. R.Winkler)</li></ul>	
<b>Schools:</b>	<ul style="list-style-type: none"><li>• WARSAW SCHOOL OF STATISTICAL PHYSICS (Kazimierz, PL)</li><li>• INTERNATIONAL SCHOOL OF PHYSICS “ENRICO FERMI” (Varenna, IT)</li><li>• PREMIÈRE ÉCOLE DES HOUCHES DE PHYSIQUE NUMÉRIQUE (Les Houches, FR)</li></ul>	

## PROFESSIONAL ACTIVITIES

---

2008-2012	RESEARCH (EPFL) IN COLLOIDAL GELS AND FRACTAL PACKINGS With duties of teaching assistant (mechanics and thermodynamics)
2007	TEMPORARY R&D JOB FOR ISTI-CNR Semantic database tagging ( <i>Ist. Scienza e Tecn.dell’Informazione</i> , Pisa)
2000-2006	SEASONAL SHOPKEEPER EXPERIENCE Summer/winter (household electrical appliances shop)

## TALKS / POSTERS

---

- Daan Frenkel research group (Cambridge University, UK): “*Apollonian Packing, Bigels*”
- Swiss Soft Days conference (Nestlé Research Center, CH): “*Arrested demixing: from gels to bigels*”
- International School of Phys. “E.Fermi” (Varenna, IT): “*Apollonian Packing and Physical Fractals*”

## PUBLICATIONS

---

<b>Molecular Physics:</b>	“ <i>Apollonian packings as physical fractals</i> ”
<b>P.N.A.S.:</b>	“ <i>Arrested demixing opens route to bigels</i> ”
<b>Phys.Rev.B</b> (in submission):	“ <i>Enhanced tunneling conductivity induced by gelation of attractive colloids</i> ”